

Université de Montréal

NOCICEPTOR NEURONS CONTROL CANCER IMMUNOSURVEILLANCE

Par
Maryam Ahmadi

Département de pharmacologie et physiologie
Faculté de Médecine

Thèse présentée en vue de l'obtention du grade de Philosophie doctorat (Ph.D.) en physiologie moléculaire,
cellulaire et intégrative – option générale

Mars, 2023

© Maryam Ahmadi, 2023

Cette thèse intitulée

NOCICEPTOR NEURONS CONTROL CANCER IMMUNOSURVEILLANCE

Présentée par

Maryam Ahmadi

A été évaluée par un jury composé de

Dr. Maja Krajinovic
Président-rapporteur

Dr. Sébastien Talbot
Directeur de recherche

Dr. Moutih Rafei
Co-directeur

Dr. Jonathan Brouillette
Membre du jury

Dr. Reza Sharif-Naeini
Examineur externe

Dr. Houman Savoji
Représentant du Doye

Résumé

Les interactions neuro-immunitaires entre les systèmes sensoriels et immunitaires ont été abondamment étudiées; cependant, leur rôle dans la régulation des cancers est encore mal connu. Les interactions croisées entre les cytokines, les facteurs de croissance et les neuropeptides peuvent promouvoir la progression des tumeurs. Les neuropeptides libérés par les nocicepteurs peuvent affecter la polarisation, la chimiotaxie et l'activité du système immunitaire acquis. Étant donné que les neurones sensoriels libèrent localement des neuropeptides qui modulent l'activité des lymphocytes, nous faisons l'hypothèse que les nocicepteurs sécrètent des neuropeptides qui induisent l'épuisement des cellules T CD8 et la croissance tumorale. L'épuisement des lymphocytes T CD8 est un phénomène observé dans le cadre d'infections chroniques et de cancers. Elle est définie comme une perte de la fonction effectrice des lymphocytes T CD8 (diminution de la production d'IFN- γ , de TNF- α et d'IL-2) ainsi qu'une expression élevée de récepteurs inhibiteurs tels que PD-1 (protéine 1 de mort cellulaire programmée), LAG-3 (gène 3 d'activation des lymphocytes) et TIM-3 (protéine 3 d'immunoglobuline des lymphocytes T et de contenant du domaine mucine).

Nous avons utilisé le modèle murin de mélanome pour tester cette hypothèse et avons observé que les cellules malignes de cancer de la peau B16F10 interagissent avec les nocicepteurs pour promouvoir la croissance des neurites, la sensibilité aux ligands activateurs et la libération de neuropeptides. En conséquence, le peptide lié au gène de la calcitonine (CGRP), qui est libéré par les nocicepteurs, augmente directement l'épuisement des cellules T CD8 et réduit leur capacité à éliminer les cellules du mélanome. L'ablation génétique des neurones sensoriels, leur inhibition pharmacologique ou le blocage du récepteur au CGRP (RAMP1) suffisent à limiter l'épuisement des lymphocytes infiltrés dans la tumeur et la croissance tumorale. De plus, l'injection de CGRP recombinant dans des souris dépourvues de neurones sensoriels réduit l'épuisement des cellules T CD8. Les cellules T CD8 RAMP1^{-/-} montrent aussi moins d'épuisement que leurs homologues sauvages lorsqu'elles sont co-transplantées dans des souris immunodéficientes Rag1^{-/-} portant une tumeur.

En résumé, réduire la libération de CGRP en bloquant localement les nocicepteurs associés à la tumeur limite les effets immunomodulateurs de CGRP sur les cellules T cytotoxiques CD8 et représente une stratégie d'intérêt pour protéger l'immunité antitumorale.

Mots-clés: Neurones sensoriels, l'épuisement des cellules T CD8, CGRP, RAMP1

Abstract

Neuroimmune crosstalk between the nervous and the immune systems has been widely studied; however, their modulating roles are largely unknown in cancer. Bilateral interactions of cytokines, growth factors and neuropeptides may support tumor progression. Nociceptor-released neuropeptides can affect polarization, chemotaxis and adaptive immune system activity. Since sensory neurons locally release neuropeptides that modulate the activities of lymphocytes, we hypothesized that nociceptors might secrete neuropeptides leading to CD8⁺ T-cell exhaustion and tumor growth. CD8 T cell exhaustion is a phenomenon observed in the context of chronic infections and cancer. It is defined as loss of effector function of CD8 T cells (decreasing the production of IFN- γ , TNF- α , and IL-2) as well as high expression of inhibitory receptors such as PD-1 (programmed cell death protein 1), LAG-3 (lymphocyte-activation gene 3), and TIM-3 (T-cell immunoglobulin and mucin domain-containing protein 3). We used the mouse model of melanoma cancer to test this hypothesis and found that malignant B16F10 skin cancer cells interacted with nociceptors to expand neurite outgrowth, responsiveness to noxious ligands, and neuropeptide release. Consecutively, neuropeptide calcitonin gene-related peptide (CGRP), which is released by nociceptors, directly increased the exhaustion of cytotoxic CD8⁺ T cells and reduced their ability to eliminate melanoma cells. Genetic ablation of sensory neurons, local pharmacological silencing, and antagonism of the CGRP receptor (RAMP1) were all able to limit the exhaustion of tumor-infiltrating lymphocytes (TIL) and tumor growth. Moreover, treatment with recombinant CGRP in sensory neuron-depleted mice reduced the exhaustion of CD8⁺ T cells. Compared with wild-type cells, RAMP1^{-/-} CD8⁺ T cells were rescued to go under exhaustion when co-transplanted into tumor-bearing Rag1^{-/-} deficient mice. In summary, reducing CGRP release by local silencing of tumor-associated nociceptors, limits the immunomodulatory effects of CGRP on cytotoxic CD8⁺ T cells and represents an ideal strategy to protect anti-tumor immunity.

Keywords: Nociceptor neurons, T cell exhaustion, CGRP, RAMP1

Table of Contents

RÉSUMÉ.....	I
ABSTRACT	II
TABLE OF CONTENTS.....	III
TABLE OF FIGURES	VI
ABBREVIATIONS.....	VII
ACKNOWLEDGMENT	IX
CHAPTER 1: INTRODUCTION	1
1. BACKGROUND.....	2
1.1. MELANOMA	2
1.2. CANCER IMMUNOSURVEILLANCE	2
1.2.1. <i>The evidences of cancer immunosurveillance in animal models</i>	5
1.2.2. <i>Cancer immunosurveillance evidence in human</i>	5
1.3. ADAPTIVE IMMUNITY IN CANCER.....	5
1.3.1. <i>CD8⁺ T cells</i>	5
1.3.2. <i>CD4⁺ T cells</i>	7
1.3.3. <i>B cells</i>	7
1.4. INNATE IMMUNITY IN CANCER	8
1.4.1. <i>Natural killer cells</i>	8
1.4.2. <i>Neutrophils</i>	8
1.5. <i>T cell exhaustion</i>	8
1.6. SEVERAL MEDIATORS IN TME DRIVE T CELLS EXHAUSTION	10
1.6.1. <i>Myeloid drive suppressor cells (MDSC)</i>	11
1.6.2. <i>Tumor-associated macrophages (TAMs)</i>	11
1.6.3. <i>Cancer-associated fibroblasts (CAFs)</i>	11
1.7. INHIBITORY RECEPTORS	12
1.7.1. <i>Programmed cell death-1 (PD-1)</i>	12
1.7.2. <i>Lymphocyte activation gene 3 (LAG-3)</i>	13
1.7.3. <i>T cell immunoglobulin and mucin domain 3 (TIM-3)</i>	13
1.7.4. <i>Cytotoxic T-lymphocyte-associated protein 4 (CTLA-4)</i>	13

1.7.5. <i>T cell immunoreceptor with Ig and TIM domains (TIGIT)</i>	13
1.8. <i>Cancer immunotherapy</i>	15
1.8.1. <i>Immune checkpoint inhibitor therapy</i>	15
1.8.2. <i>Targeting inhibitory cells</i>	15
1.8.3. <i>CAR T cell therapy</i>	15
1.8.4. <i>Neoantigen T cell therapy</i>	16
1.8.5. <i>Cytokine therapy</i>	16
1.8.6. <i>Challenges and future directions of cancer immunotherapy</i>	16
1.9. PERIPHERAL NERVOUS SYSTEM (PNS)	17
1.9.1. <i>Nociceptor neurons</i>	17
1.9.2. <i>Neurogenic inflammation</i>	19
1.9.3. <i>Peripheral nervous system with immune system crosstalk</i>	19
1.9.5. <i>Bone marrow innervation</i>	21
1.9.6. <i>Lymph nodes (LNs) innervation</i>	21
1.9.7. <i>Spleen innervation</i>	21
1.10. REGULATION OF IMMUNE CELLS BY NEUROTRANSMITTERS	22
1.10.1. <i>Neurotransmitters of autonomic nervous system</i>	22
1.10.2. <i>Neurotransmitters of sensory nerves</i>	22
1.11. NERVE-CANCER CROSSTALK	23
1.11.1. <i>Neuron-cancer interaction mediates tumor progression</i>	23
1.11.2. <i>Cancer drives axonogenesis</i>	26
1.11.3. <i>Cancer promotes neurogenesis</i>	26
1.11.4. <i>Tumor cells induce neural reprogramming</i>	28
1.11.5. <i>Perineural invasion in cancer (PNI)</i>	30
1.11.6. <i>Tumor-associated neurons repress intra-tumoral immune cells</i>	30
1.11.7. <i>Autonomic neurotransmitters modulate tumor progression</i>	30
1.11.8. <i>Sensory neuron activity supports tumor development</i>	31
Chapter 2: Rationale, hypothesis, and research objectives	32
AUTHORS CONTRIBUTION	33
CHAPTER 3: DISCUSSION	67
3.1. TUMOR CELLS COMMUNICATE WITH SENSORY NEURONS	67
3.2. CANCER CELLS SENSITIZE SENSORY NEURONS	67
3.3. ACTIVATION OF TUMOR-ASSOCIATED NERVES MODULATES PAIN	68
3.4. NOCICEPTOR NEURONS MODULATE CD8+ T CELL EXHAUSTION	68
3.5. TUMOR-INNERVATING NOCICEPTORS PROMOTE CANCER PROGRESSION	69

3.6. HUMAN MELANOMA TUMOR BIOPSIES ARE INNERVATED BY TRPV1+ SENSORY NEURONS.....	70
3.7. NEUROPEPTIDES DRIVE CARCINOGENESIS IN HUMAN.....	70
3.8. COMBINATION OF NERVE AND IMMUNOTHERAPY AS A THERAPEUTIC APPROACH FOR CANCER ...	71
3.9. SIMILAR FINDINGS.....	71
3.10. LIMITATIONS.....	72
3.11. FUTURE DIRECTIONS.....	72
3.12. CONCLUSION.....	73
4. BIBLIOGRAPHY.....	74

Table of figures

Figure 1. Cancer immunoediting represses immune system responses4

Figure 2 T-cell activation requires three signals.....7

Figure 3. T cell exhaustion.....9

Figure 4. Several cells and components control CD8⁺ T cell exhaustion in TME...10

Figure 5. Co-expression of inhibitory receptors on T cells induces T cell exhaustion.....14

Figure 6. TRPV1 channel structure18

Figure 7. Immune system and nervous system crosstalk to detect danger.20

Figure 8. Interaction of sensory nerves with immune cells in the skin.....24

Figure 9. Nerve-cancer communication in tumor microenvironment25

Figure 10. Nerve innervation in prostate cancer27

Figure 11. Axonogenesis, neurogenesis and remodeling induced by tumor cells in TME29

Abbreviations

ARG1:	Arginase 1
Bregs:	B Regulatory Cells
Calcr1:	Calcitonin-receptor-like receptor
CAR:	Chimeric Antigen Receptor
CCL-1:	Chemokine (C-C motif) Ligand 1
CCL-2:	Chemokine (C-C motif) Ligand 2
CD:	Cluster of Differentiation
CGRP:	Calcitonin Gene-Related Peptide
CNS:	Central Nervous System
CTLA-4:	Cytotoxic T Lymphocyte-associated Antigen 4
CXCL-1:	C-X-C Motif Chemokine Ligand 1
CXCL-2:	C-X-C Motif Chemokine Ligand 2
CXCL-8:	Chemokine C-X-C Motif Ligand 8
DCs:	Dendritic cells
DMEM:	Dulbecco/Vogt Modified Eagle's Minimal Essential Medium
DRG:	Dorsal Root Ganglion
DTA:	Diphtheria Toxin
ELISA:	Enzyme-linked Immunosorbent Assay
EOMES:	Eomesodermin
ERK :	Extracellular Signal-Regulated Kinases
FACS:	Fluorescence-Activated Cell Sorting
FAS-L:	Fas Ligand
Foxp3:	Forkhead box P3
GABA:	G-aminobutyric Acid
Gata3:	GATA binding protein 3
GDNF:	Glial cell line-Derived Neurotrophic Factor
GFR- α 1:	GDNF family receptor alpha 1
GM-CSF:	Granulocyte Macrophage Colony-Stimulating Factor
GNZB:	Granzyme B
GPCRs:	G protein-Coupled Receptors
HGSOC:	High-Grade Serous Ovarian Carcinoma
HNSCC:	Head and Neck Squamous Cell Carcinoma
HSCs :	Hematopoietic Stem Cells
IB4:	Isolectin B4
ICIs:	Immune Checkpoint Inhibitors
IDO:	Indoleamine 2,3-Dioxygenase
IFN- γ :	Interferon- γ
Ig:	Immunoglobulin
iDISCO:	Immunolabeling-enabled Imaging of Solvent-Cleared Organs
IL:	Interleukin
IL-10:	Interleukin-10
IL-2:	Interleukin-2
IL-12:	Interleukin-12
IL-18:	Interleukin-18
ILC-2:	Innate Lymphoid Cell
INOS:	Inducible Nitric Oxide Synthase
KO:	Knock-Out
LAG-3:	Lymphocyte-Activation Gene 3
LN:	Lymph nodes
MDSC:	Myeloid-Derived Suppressor Cells
MHC:	Major Histocompatibility Complex
MAPK:	Mitogen-Activated Protein Kinase
Nav1.8:	Sodium Voltage 1.8
NE:	Norepinephrine

NFAT:	Nuclear Factor of Activated T cells
NF- κ B:	Nuclear Factor- κ B
NGF:	Nerve Growth Factor
NK cell:	Natural Killer cell
NO:	Nitric Oxide
NPY:	Neuropeptide Y
NR4A1:	Nuclear Receptor Subfamily 4 Group A Member 1
OCSCC :	Oral Cavity Squamous Cell Carcinoma
PD-1 :	Program cell Death
PDAC:	Pancreatic Ductal Adenocarcinoma
PD-L1:	Programmed Death-Ligand 1
PD-L2:	Programmed Death-Ligand 2
PGE2:	Prostaglandin E2
PI3K:	Phosphatidylinositide 3-kinase
Piezo:	Piezo type mechanosensitive ion channel component
PMA:	Phorbol 12-Myristate 13-Acetate
PNI:	Perineural Invasion
PKA:	Protein Kinase A
P2X3:	Purinergic receptor
PNS:	Peripheral Nervous System
RAG:	Recombination Activating Gene
RAMP1:	Receptor Activity Modifying Protein 1
ROS:	Reactive Oxygen Species
SLPI:	Secretory Leukocyte Protease Inhibitor
SNAP-25:	Synaptosomal-Associated Protein
SP:	Substance P
STAT1:	Signal Transducers and Activators of Transcription 1
STAT5:	Signal Transducers and Activators of Transcription 5
TAFs:	Tumor-Associated Fibroblasts
TAMs:	Tumour-Associated Macrophages
T-bet:	T-box expressed in T cells
TCR:	T Cell Receptor
TFs:	Transcription Factors
TGF- β :	Transforming Growth Factor- β
TH:	Tyrosine Hydroxylase
Th1:	T helper 1
Th17:	T helper 17
Th2 cells:	T helper type 2 cells
TIGIT:	T cell Immunoreceptor with Ig and ITIM domains
TIL:	Tumor-Infiltrating Lymphocyte
TIM-3 :	T cell immunoglobulin domain mucin domain-containing protein 3
TLR:	Toll-Like Receptor
TME:	Tumor Microenvironment
TNF:	Tumor Necrosis Factor
TNF- α :	Tumor Necrosis Factor- α
TOX:	Thymocyte selection-associated HMG BOX
Tregs:	Regulatory T cells
Trks:	Tyrosine-receptor kinases
TRP:	Transient Receptor Potential
TRPA1:	Transient Receptor Potential Ankyrin subfamily, member 1
TRPV1:	Transient Receptor Potential Vanilloid subfamily, member 1
UV:	Ultraviolet
VEGF:	Vascular Endothelial Growth Factor
VIP:	Vasoactive Intestinal Peptide

Acknowledgment

I would like to express my deep gratitude to my PhD supervisor Dr. Sébastien Talbot for all his incredible support and mentoring as well as the confidence he had in me during my PhD. His expertise, advice and positive attitude helped me improve my knowledge in several aspects. I have had the opportunity to learn a lot of techniques, and contribute in several interesting, exciting and varied projects, and to work in a very dynamic and passionate lab environment.

I would also like to acknowledge my jury members: Dr. Maja Krajinovic, Dr. Jonathan Brouillette, Dr. Reza Sharif-Naeini and Dr. Houman Savoji for accepting to take part as my committee. Also, I would like to thank my laboratory colleagues who without their contribution and supports, this research would not have been possible; many and special thanks to Dr. Mohammad Balood and Dr. Abdelilah Majdoubi who trained me the flow cytometry and helped me with performing the experiments. I would also like to thank Tuany Eichwald, Theo Crosson, Ali Ahmadi, Dr. Katiane Roversi, Dr. Karine Roversi, Jo-Chiao Wang, Alissa Dory, Dr. Aminreza Nikpour, and Dr. Sara Nikoofal as well as all past and present members of Dr. Talbot lab for sharing their expertise.

I would like to thank all other scientific collaborators including Dr. Moutih Rafei for advising with the experiments and Dr. Paola Vermeer for providing us the patient samples. Many thanks to all collaborators of flow cytometry and genetic platform including Armelle Le Campion, Annie Gosselin, Angelique Bellemarre-Pelletier, Raphaëlle Lambert, and Patric Gendron.

A very special thanks to my husband Dr. Hamed Khakpour and my sister Dr. Mina Ahmadi for their love and all supports and many thanks to my parents for their presence and encouragements. Finally, I would like to acknowledge the financial supports I received from Fonds de recherche du Québec-Société et Culture (FRQS) and Université de Montréal (FESP).

Chapter 1: Introduction

Cancer is a leading cause of death worldwide¹, and with an aging population, its rate is expected to rise. Malignant cells form within tissues, divide and grow faster than their progenitors over time resulting in less responsiveness to several signals which control cell growth and death². Given the fact that various abnormalities of tumor cells must force them as the early targets for apoptosis; however, abnormal cells are able to escape programmed cell death². In this regard, tumors can be classified into metastatic and nonmetastatic groups³. Conventionally, metastasis has been observed in later stages of cancer progression⁴. During metastasis, cancer cells, by passing into the blood circulation or lymphatic system and neurons via perineural invasion can escape from the primary tumor site and migrate or colonize distant tissues⁵.

Both primary and metastatic tumor microenvironments (TME) compose of extracellular matrix, endothelial cells, resident mesenchymal support cells, inflammatory immune cells and components of the nervous system. Dynamic communication between tumors and other cells or components of TME shapes and supports the proliferation, survival and invasion of cancer cells⁶. In addition, as evidenced by several studies, angiogenesis and neurogenesis are also the main procedures that contribute to the progression and metastasis of malignant cells in TME⁶.

The immune system protects the body against detrimental invaders and eliminates transformed cells. However, some of the transformed cells may escape the elimination and develop tumors in the body by recruiting immunosuppressive leukocytes that shape a tumor microenvironment to suppress anti-tumor immune responses⁷. By developing different mechanisms, tumors are able to evade destruction by the immune system. Tumors mainly limit antigen recognition by downregulating the expression of major histocompatibility complex (MHC) peptides on their surface and upregulating inhibitory ligands. Engagement of the inhibitory ligands with their cognate receptors on T cells suppresses the cytotoxic functions of T cells⁷.

In addition to the immune system, the nervous system has been validated to detect and respond to environmental threats, achieved by specialized receptors on the surface of both systems. This neuro-immune crosstalk happens in both central nervous system (CNS) and peripheral nervous system (PNS)⁸. The peripheral nervous system is composed of autonomic and somatic branches. The autonomic nervous system maintains internal homeostasis through the sympathetic and parasympathetic branches. The somatic nervous system divides into the sensory and somatosensory fibers, which innervate most tissues. The sensory fibers regulate the immune responses by releasing several neurotransmitters and neuropeptides and by transferring glial cells across the axons, which enable glial cells to produce several cytokines and growth factors.

These peripheral glial cells -Schwann cells- play an important immunomodulatory role under critical situations, including cancer^{8,9,10}. Schwann cells also participate in tumor processes, including tumor invasion, migration, immune exclusion, and cancer pain^{ref}. Communication of tumor-Schwann cells-nerve play a major role in immunosuppressive TME by communicating with myeloid-derived suppressor cells (MDSCs), dendritic cells (DCs), mast cells, and other immune cell types. This interaction induces the activation of immune cells and facilitates the migration and invasion of tumor cells¹¹. Intra-tumoral nerve fibers actively secrete neuropeptides and neuromodulators such as substance P (SP) and calcitonin gene-related peptide (CGRP) in the tumor microenvironment to stimulate cancer growth and metastasis^{12,13,14}. Conversely, the presence of nerves in the tumor primes the secretion of neurotrophic growth factors such as nerve growth factor (NGF) by cancer cells leading to axonogenesis of nerves. These factors, in turn, influence immune cells and endothelial cells resulting in the inhibition of anti-tumor immune responses or inducing neoangiogenesis, which supports tumor proliferation and survival.

Since the tumor-stimulating effects of nerves are well appreciated, the interaction of different mediators in TME might provide crucial targets to improve anti-tumor immunity. This thesis explores the mechanisms underlying the interaction between sensory nerves and cancer growth. Sensory nerves induce the overexpression of several inhibitory molecules on T cells, this phenomenon is termed T cell exhaustion, which attenuates the immune responses in the cancer microenvironment. We investigate whether the

absence of sensory neurons, either by genetic approaches or pharmacology, can facilitate anti-tumor immunity, limit tumor growth and increase the overall survival rate in cancers.

1. Background

1.1. Melanoma

Melanoma is the most aggressive skin cancer type that initiates from transformed melanocytes. The chance of survival rate for melanoma patients in stage IV of the disease is around 10%, and the incidence of melanoma is rapidly increasing across the world¹⁵. The incidence and mortality rate of melanoma vary worldwide depending on genetic disposition and access to early diagnosis and primary care. Depending on several risk factors including age, melanoma varies between genders. In younger individuals, melanoma is more commonly reported in females. However, in older individuals, the incidence of melanoma enhances more rapidly in males¹⁶. There are different types of melanoma that might be developed in the skin, eyes, or in internal tissues such as throat. Multiple risk factors have been specified for transforming healthy cells into malignant melanocytes, including genetic alterations and environmental factors such as ultraviolet (UV) exposure^{17,18}. Cutaneous melanoma is a heterogeneous disorder with a high tumor mutational load. These mutations contribute to the rapid proliferation and migration of transformed melanocytes into the dermis layer of the skin resulting in the metastatic spread of melanoma cells to distant organs.

Numerous mutated genes have been pointed out as main contributors to several signaling pathways in melanoma carcinogenesis. Among different signaling pathways, the mitogen-activated protein kinase (MAPK) pathway is the most frequently activated signaling pathway in cancer which assist in the rapid proliferation of malignant cells¹⁹. Mutated components such as *BRAF* and *NRAS* drive hyperactivation of MAPK cascade. Almost 50% of melanoma cases carry V600E mutation in *BRAF*. *BRAF* (v-raf murine sarcoma viral oncogene homolog B1) is a serine/threonine kinase protein that is involved in transferring the signals in MAPK signaling. MAPK signaling also acts as the main regulator of *NRAS* that controls the proliferation, differentiation and survival of the cells. Activated *NRAS* (neuroblastoma RAS viral oncogene homolog) protein triggers the subsequent activation of receptor tyrosine kinase (RTK) to amplify the downstream activity of *RAF* signaling. *NRAS* mutation is detected in around 25% of melanoma patients^{19,20,21,22}. Several neoantigens, derived from somatic mutations, can be recognized by the host immune system resulting in anti-tumor responses²³. In melanoma, cancer cells communicate with immune components to suppress anti-tumor immunity²⁴.

1.2. Cancer Immunosurveillance

The immune system applies three major strategies to fight against tumors. First, by eradicating or suppressing viral infections, the immune system shields the host from virus-induced cancers²⁵; Second, by resolving an inflammatory environment, following the elimination of infection; Third, through tumor-specific antigens recognition, which selectively destroys tumor cells.

The idea of cancer immunosurveillance which was proposed by Thomas (1959) and Burnt (1970), argues that the immune system is able to detect and eliminate carcinogenic cells^{25,26}. Despite the cancer immunosurveillance mechanisms in action, malignant cells are still developed and metastasized because of the concept of tumor immunoediting^{25,27}.

Cancer immunoediting is a procedure in which the immune system acts to control and shape the tumor under three consecutive stages which are entitled "elimination, equilibrium and escape". Each phase requires a number of immune effector cells and different cytokines. In course of the elimination phase, both innate and adaptive immune cells cooperate to detect and eliminate transformed cells which are hidden from cell-intrinsic mechanisms of tumor suppression²⁸.

A portion of tumor cells may not be completely eliminated, and they undergo the temporary phase of equilibrium. During equilibrium stage, cancer cells may either stay dormant or continue to develop more transformations which may stimulate and express tumor-specific antigens. In this phase, despite the

constant pressure by the immune system to control tumor development, the immune response may fail to completely destroy the tumors. As this process continues, it results in the selection of resistant tumor cells and establishes an immunosuppressive microenvironment. These immunoedited tumors can pass into the escape phase, where the immune system is no longer capable of suppressing tumor growth, and consequently leads to aggressive tumor progression^{25,28,29} **(Figure 1)**.

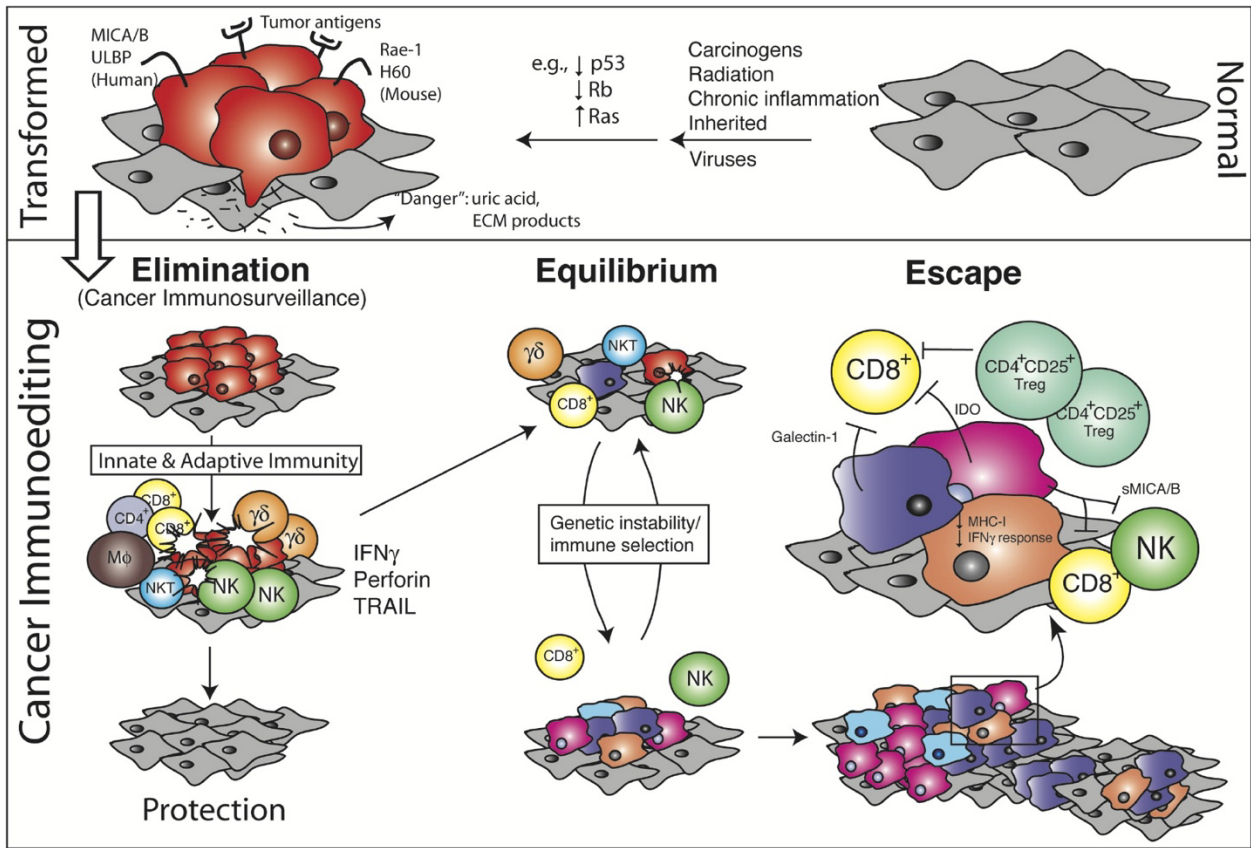


Figure 1. Cancer immunoevasion represses immune system responses. The immune system recognizes and destroys transformed cells while they are hidden from intrinsic tumor suppressors (elimination stage). Cancer immunoevasion is classified into three main steps: elimination phase, where tumor cells are killed by immune cells; equilibrium, where cancer cells grow and develop suppressive pathways to attenuate immune responses; escape phase, where immune-resistant tumor cells start to grow progressively³⁰.

1.2.1. The evidences of cancer immunosurveillance in animal models

T lymphocytes are the major mediators for resolving tumor cells. However, in tumors with a high level of mutations, such as melanoma, tumor cells are able to evade immune responses by secreting immunosuppressive cytokines and overexpression of inhibitory ligands on their surface in the tumor microenvironment³¹. The anti-tumor function of adaptive immune cells has been proven by different approaches, such as the use of preclinical gene-targeted models.

Recombination activating gene-2 (RAG2-knockout) mice, immunodeficient mice with no mature B and T lymphocytes, led to the progression of intestine and lung adenocarcinomas³¹. Interestingly, the rate of tumor growth was even higher when RAG2-knockout mice were deficient for STAT1 (signal transducer and activator of transcription 1), which is a key signaling pathway activated by type I and type II interferons (IFN) in carcinogenesis. Activation of STAT1 can perform antitumor effects by increasing immune responses against tumor cells. When stimulated by interferons, STAT1 can enhance the expression of different immune-related genes, including genes encoding MHC molecules and cytokines^{31,32}. These data propose that innate and adaptive immune cells, as well as IFN signaling, are the major components for the inhibition of tumor growth³¹. In addition, mice lacking IFN- γ were found to promote T cell lymphomas, and mice deficient for both IFN- γ and perforin developed B cell abnormality³³. Perforin is a pore-forming molecule produced by cytotoxic T lymphocyte and natural killer cells that facilitates apoptosis of target cells³⁴. Despite the important roles of IL-12 and IL-18 in IFN- γ signaling, it was found that mice lacking IL-12 or IL-18 have no significant impact on tumor development compared to their wild-type counterparts^{25,33}.

Using $\alpha\beta$ T cell^{-/-} mice (deficient mice for T cell receptor (TCR) β -chain), the impact of $\alpha\beta$ T cells in regulating tumor progression was determined as fibrosarcoma development was faster in mice lacking $\alpha\beta$ T cell³⁵. The use of other preclinical models with the lack of crucial immune mediators not only proved the influence of immune system in the regulation of tumors but also proposed the contribution of both innate and adaptive immune compartments in cancer immune surveillance. Specifically, genetic depletion of natural killer (NK) cells, NKT cells, $\alpha\beta$ T cells, as well as IFN- γ or IL-12, all result in the vulnerability of the host to the tumors³⁵.

Overall, different immune cell types such as NK cells, NKT cells, $\alpha\beta$ T cells, as well as some effector components and cytokines such as perforin and IFN- γ have been shown to involve in the elimination and immunoediting processes.

1.2.2. Cancer immunosurveillance evidence in human

In addition to mice, cancer immunosurveillance has been evidenced in humans. Immunodeficient and immunosuppressed humans presented a higher risk of developing cancer³⁶. Moreover, several malignancies arise following chronic inflammations, such as viral infections. Higher rates of lymphoma and sarcoma have been observed in transplanted patients³⁶. AIDS patients and infected patients with the herpes virus and papillomavirus have been viewed to elevate the frequency of malignancies³⁷. Thus, a higher incidence of cancer in immunodeficient patients represents an important role of the immune system in cancer immunosurveillance. Additionally, the rate of malignant melanoma has been reported to increase as a consequence of organ transplantation^{27,38}. Furthermore, the prevalence of lung cancer was higher in cardiac transplant patients³⁹. Beside all supporting epidemiological evidences, another convincing investigation supported the positive correlation between the level of infiltrated T lymphocytes (TILs) and elevated patient survival in cutaneous melanoma^{40,41}. In summary, the evidences observed in both murine and human provide powerful support for cancer immunosurveillance.

1.3. Adaptive immunity in cancer

1.3.1. CD8⁺ T cells

The natural immune responses depend on the cooperation and interplay between innate and adaptive immune systems. Unlike innate immunity, the adaptive immune system consists of fewer types of cells to

perform its tasks, including B and T lymphocytes. Both B and T cells are derived from hematopoietic stem cells in the bone marrow. T cell progenitors then migrate to the thymus and mature there before entering secondary lymphoid organs such as lymph nodes (LNs). The initiation of T cell responses in the lymph nodes involves the encounter of these cells with antigen-presenting cells (APC) such as dendritic cells (DCs)^{42,42,43}. Depending on the different immunological settings, T lymphocytes obtain effector phenotype to function as an anti-tumor immunity. Naïve T cells also require multiple contact dependent and contact independent signals for proper differentiation. During initial infection, some effector signals are needed for proper CD8⁺ T cell differentiation. They include the interaction of TCR/peptide-MHC I (signal 1), co-stimulatory signals induced by CD28 binding to CD80/86 on APC (signal 2), and production of cytokines such as IL-12 (signal 3)^{44,45}. Thus, naïve CD8⁺ T cells are primed by three main signals and differentiated into activated T cells (**Figure 2**).

Following clearance of antigen or infection, a subpopulation of these effector CD8⁺ T cells differentiates into long-lived memory T cells capable of producing several cytokines and effector T cells. However, in chronic infection and high inflammation, by increasing the antigen level or viral load, the effector T lymphocyte responses amplify, and they enter into the inflammation site or tumor environment to clear the infection or cancer cells. These functional cytotoxic CD8⁺ T cells apply different mechanisms to eliminate target cells, including the release of cytolytic cytokines such as granzyme B and perforin. Perforin makes pores in the plasma membrane of the infected or tumor cells allowing the passage of granzyme B cytokine to trigger apoptosis of target cells. Another mechanism is mediated by the interaction of the Fas ligand on the surface of cytotoxic T lymphocytes and its receptor Fas on the surface of tumor cells resulting in apoptosis of target cells. In addition, secreted cytokines by cytotoxic T lymphocytes (IFN- γ and tumor necrosis factor alpha (TNF- α)) can induce indirect tumor cell death⁴⁶. Therefore, CD8⁺ T cells are considered the first arm of defense in adaptive T cell immunity.

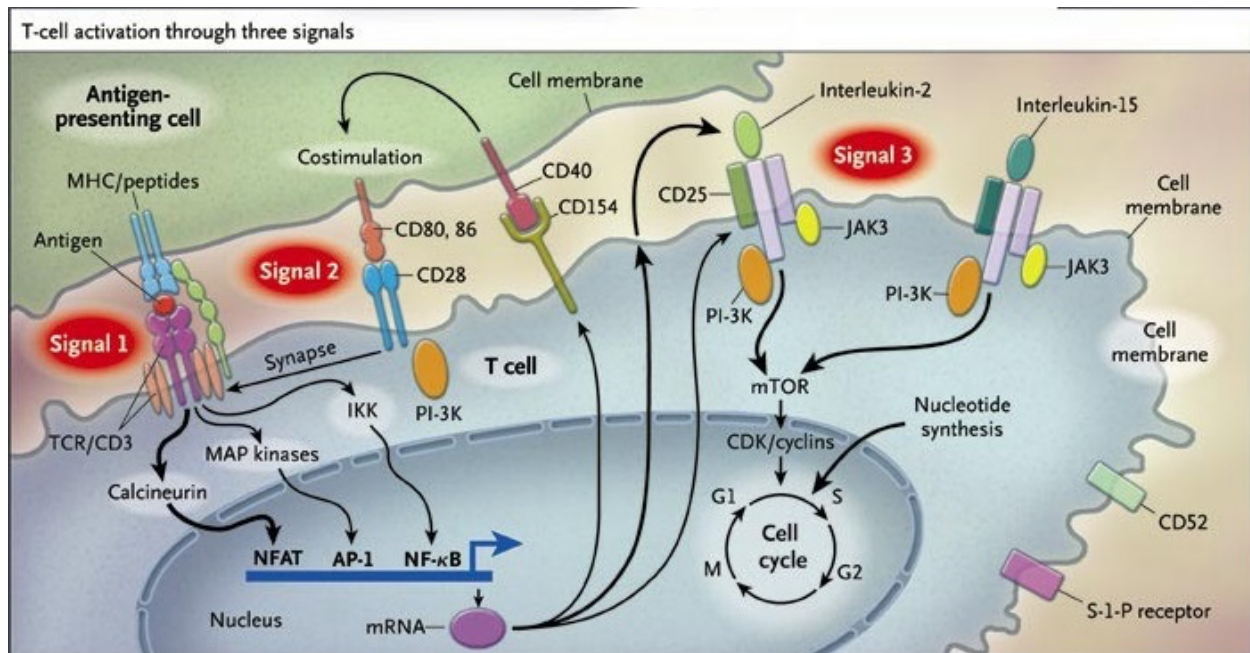


Figure 2. T-cell activation requires three signals. The initial signal is triggered by TCR recognition of antigen-MHC complex. The second signal, mainly defined as co-stimulation, is equipped by interaction of co-stimulatory molecules (e.g., CD28) on the surface of T cells with CD80/CD86 on APCs. The third signal is delivered through cytokines (e.g., IL-2) that stimulates T cell proliferation⁴⁵.

1.3.2. CD4⁺ T cells

CD4⁺ T cells are considered as the second line of defense in adaptive T cell immunity. In response to different signals, often in the form of cytokines and interactions with APCs, CD4⁺ T cells are able to differentiate into several functional subtypes, such as T-helpers (Th1, Th2 and Th17) to allocate help to effector immune cells and regulatory T cells (Tregs). CD4⁺ T cells mediate anti-tumor immunity by modulating the function of CD8⁺ cytotoxic T cells and B cells and through the release of effector cytokines, such as IFN- γ and TNF- α ^{47,48}. CD4⁺ T cells can directly target the transformed cells either by eliminating them through the cytolytic mechanisms or by indirect modulating effect on the tumor microenvironment. Activated CD4⁺ T cells produce IL-2 to induce CD8⁺ T cells activation, which express IL-2 receptor (CD25) to drive the differentiation and proliferation of these cells. In addition, CD4⁺ T cells help CD8⁺ T cell responses using cross-presenting tumor antigen of DCs which stimulates the activating signals for CD8⁺ T cells^{49,50,51,52}. Engagement of CD40 ligand on activated CD4⁺ T cells with CD40 receptor on DCs allows for induction and maintaining functional pro-inflammatory DCs and initiates type 1 immunity. Furthermore, CD4⁺ T cells activate humoral anti-tumor responses by assisting through CD40 ligand binding to CD40 receptor on B cells which differentiate them into mature B cells to produce specific antibodies for tumor antigens^{53,54}.

1.3.3. B cells

B cells are the main humoral immune cells and a type of adaptive immune system that has an important role in anti-tumor immunity⁵⁵. B cells are able to infiltrate within the tumor tissues and differentiate into different subtypes after they are primed by several components in the tumor microenvironment. Different

subgroups of B cells perform the dual function in tumor immunity through antigen presentation, producing antibodies and releasing cytokines^{56,57}.

Regulatory B cells (Bregs) are a subpopulation of tumor-infiltrating B cells with an active role in tumor immunosuppression. They not only have a direct impact on tumor cells but also indirectly regulate the immunity of the tumors by modulating the role of other immune cell types, such as CD4⁺ T cells and Tregs inside the tumor. Breg cells are involved in tumor progression and metastasis by producing mainly IL-10 to stimulate DCs. Activated DCs then upregulate IL-4 production and downregulate the IL-12 synthesis. This inhibitory mechanism suppresses the differentiation of CD4⁺ T cells into Th1 and Th17 and shifts the differentiation of naïve CD4⁺ T cells mostly into Treg cells^{58,59,60}.

1.4. Innate immunity in cancer

1.4.1. Natural killer cells

Natural killer cells (NK) belong to the innate immune system that presents strong cytolytic functions against transformed cells. Activated NK cells regulate the activity of other innate and adaptive immune compartments via the release of cytokines such as IFN- γ , TNF- α , granulocyte macrophage colony stimulating factor (GM-CSF) and several chemokines ((C-C motif) ligand: CCL-1, CCL-2 and CXCL-8)⁶¹. The activation and effector activity of NK cells depend on the signals that originate from activating or inhibitory receptors.

In normal condition, NK cells express MHC I ligands on their surface, which after binding to inhibitory receptors, mediate the self-tolerance of NK cells. However, malignant cells downregulate the expression of MHC I molecules to reduce the inhibitory signals in the NK cells. Cancer cells, on the other hand, increase the expression of inhibitory ligands. The interaction between those ligands and their receptors on NK cells, eliminate target cells through the direct cytotoxic function of NK cells or indirectly via the release of pro-inflammatory cytokines^{62,63}.

1.4.2. Neutrophils

Neutrophils are another myeloid cell type, which play important roles in solid tumors. Despite their immune defence activity, neutrophils have been observed to be involved in tumor progression and metastasis. Their recruitment to the TME is mediated by several factors, such as cytokines, chemokines, and growth factors that are released from tumor cells^{64,65}. Several studies using animal cancer models reported that transforming growth factor beta (TGF- β , an immunosuppressive cytokine) induces the production of neutrophils with pro-tumoral phenotypes, whereas IFN- β induces the generation of neutrophils with anti-tumor properties^{66,67}. In addition, protease cathepsin C released by breast cancer cells has been observed to generate a signalling cascade in murine models that facilitate neutrophil recruitment to the lung metastatic niche⁶⁸.

1.5. T cell exhaustion

The term T cell exhaustion was preliminary recognized in a chronic lymphocytic choriomeningitis virus (LCMV) infection model⁶⁹. Activated cytotoxic CD8⁺ T cells apply their anti-tumor activity using cytolytic components such as granzymes and through inflammatory cytokines such as IFN- γ and TNF- α in the tumor microenvironment^{42,70}. However, under chronic antigen stimulation in the tumor site, cytotoxic CD8⁺ T cells start to decrease the secretion of effector cytokines and increase the co-expression of inhibitory checkpoint receptors such as program cell death (PD-1), lymphocyte-activation gene 3 (LAG-3), T cell immunoglobulin domain mucin domain-containing protein 3 (TIM-3) and cytotoxic T lymphocyte-associated antigen-4 (CTLA4)^{71,72}. The engagement of immune checkpoint receptors on T cells with their cognate ligands on the surface of target cells transmits the negative signals to T cells. These signals attenuate the effector function of T cells and induce their apoptosis. Therefore, this phenomenon which is associated with the reduced cytotoxic activity of T cells, is termed T cell exhaustion^{72,73} (**Figure 3**).

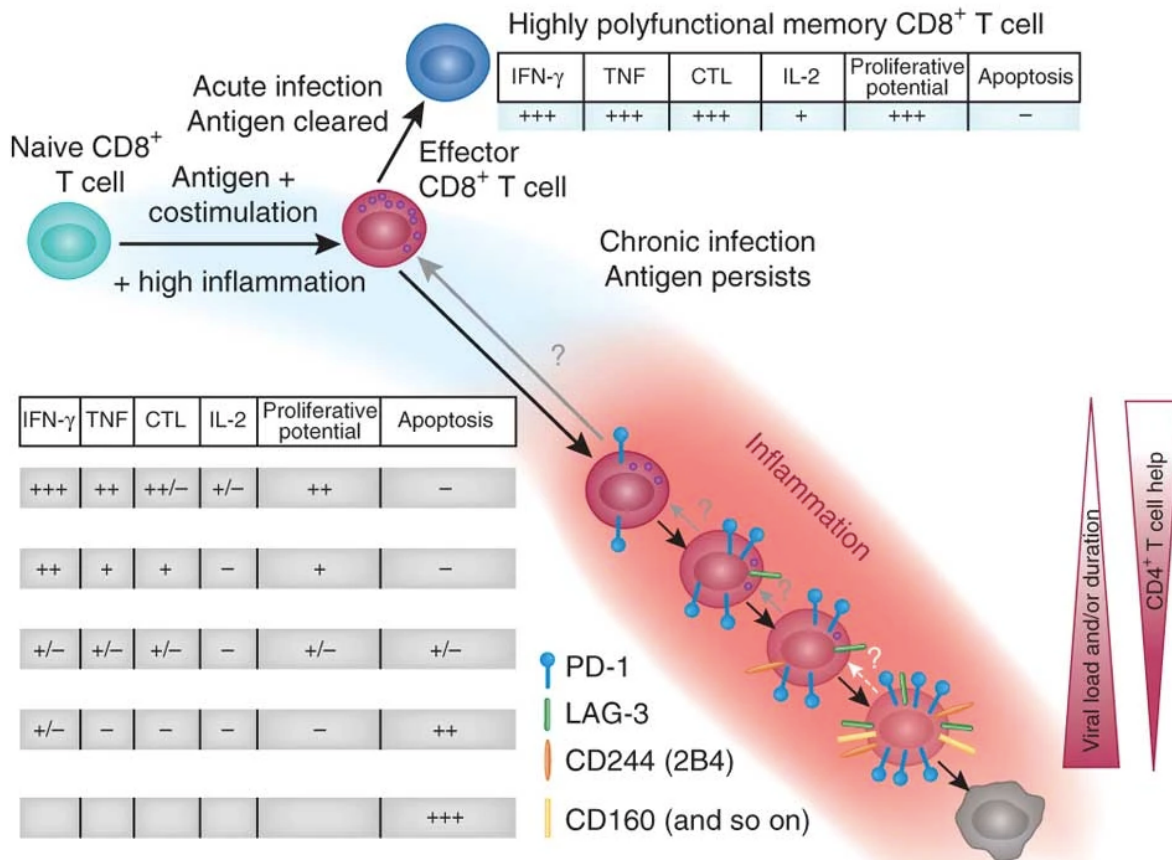


Figure 3. T cell exhaustion. During an infection, naïve CD8⁺ T lymphocytes encounter antigens and differentiate into effector CD8⁺ T cells capable of producing different types of cytokines, including TNF- α , IFN- γ and IL-2. However, in chronic infection, along with increased antigen or viral load, T cells go under stages of dysfunction by decreasing cytokines expression and enhancing the co-expression of various inhibitory receptors such as PD-1, LAG-3 and TIM-3 on their surface. This step by which T cells lose their effector properties is known as T cell exhaustion⁶⁹.

1.6. Several mediators in TME drive T cells exhaustion

The anti-tumor effect of CD8⁺ T cells is related to their differentiation and infiltration within the tumor⁷⁴. The tumor microenvironment contains different components and signals, such as tumor cells, inflammatory cells and cytokines which shape an immunosuppressive network around the tumor to mediate T cell dysfunction. These factors are the main drivers of T cell exhaustion in cancer. In the TME, there are a large number of tumor antigens that contribute to the exhaustion of T cells^{75,76}. Furthermore, the abundance of immunosuppressive cells and components such as Tregs, MDSCs, tumor-associated macrophages (TAM), tumor-associated fibroblasts (TAFs), TGF- β in TME is associated with T cell exhaustion and tumor progression^{77,78} (**Figure 4**).

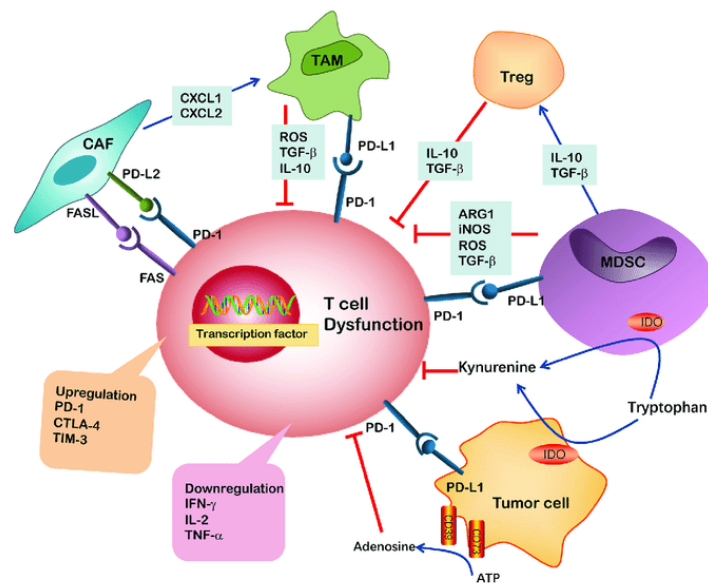


Figure 4. Several cells and components control CD8⁺ T cell exhaustion in TME. Immunosuppressive components, including TGF- β , ARG1 and iNOS are released by MDSCs and TAMs to trigger CD8⁺ T cell dysfunction. Cancer cells and MDSCs inhibit the proliferation of CD8⁺ T cells via IDO hydrolyzation. Kynurenine is another component of TME that limits anti-tumor T cell functions. In addition, MDSCs release immunosuppressive cytokines such as IL-10 and TGF- β to mediate Tregs activation. The overexpression of PD-L1 on MDSCs, TAMs, as well as cancer cells, support CD8⁺ T cell exhaustion. CAFs also release CXCL-1 and CXCL-2 chemokines that trigger polarization of M2 macrophages in TME. CAFs also produce FAS ligand that binds to FAS receptor on T cells to block CD8⁺ T cells anti-tumor immunity⁷⁹.

1.6.1. Myeloid drive suppressor cells (MDSC)

MDSCs are a population of myeloid cells with the immunosuppressive activity which are present in the pathological conditions. Based on their origin, MDSCs are classified into two major subtypes: granulocytic/polymorphonuclear MDSCs (PMN-MDSCs) and monocytic MDSCs (M-MDSCs)^{79,80}. Recruitment of MDSCs in the tumor site assist with the inhibition of T cell function by overexpression of inducible nitric oxide synthase (iNOS). Produced nitric oxide (NO) from iNOS, suppresses T cell proliferation via direct inhibition of Jak/STAT5 pathway or indirect prohibition of antigen presentation from DCs as well.

Moreover, overexpression of reactive oxygen species (ROS) in MDSCs, decreases the synthesis T cell receptor chains^{81,82,83}. MDSCs also interfere trafficking of T cells to the target site by increasing the production of metalloproteinase 17 (ADAM17) that cleaves the ectodomain of L selectin and decreases L-selectin on CD8⁺ T cells. MDSCs are able to inhibit the proliferation of T cells through depletion of essential amino acids, which are necessary for T cell activation. Furthermore, the Indoleamine 2,3-dioxygenase (IDO) is produced by both cancer cells and MDSCs that catabolizes tryptophan to kynurenine. Depletion of essential amino acid tryptophan and production of kynurenine blocks the proliferation and expansion of cytotoxic T cells⁸³.

1.6.2. Tumor-associated macrophages (TAMs)

Macrophages are another cell type that are present in the environment of solid tumors. When these cells infiltrate within TME, they are termed tumor-associated macrophages (TAMs) and contribute to tumor growth by producing and releasing inflammatory cytokines and growth factors⁸⁴. Depending on the type of stimulation they receive, TAMs polarize to M1 and M2 macrophages^{85,86}. M1-like TAMs are designed to have antitumor properties by releasing pro-inflammatory cytokines (e.g., IFN- γ , TNF- α and IL-12), which effectively destroy malignant cells. Cytokines released by other immune cell types in TME, such as IFN- γ and granulocyte-macrophage colony stimulating-factors (GM-CSF), can stimulate M1-like macrophages. Activated M1-macrophages, in turn, present antigens to T cells and activate them. At the same time, cytokines released by activated M1-macrophages and T cells modulate the activity of NK cells to reduce the production of matrix metalloproteinases (MMP-9) and Vascular Endothelial Growth Factor (VEGF) in the tumor area, which promotes anti-tumor immunity.

In contrast, M2-like macrophages, through several inhibitory mechanisms, contribute to immunosuppressive activities in TME and support the formation of tumor-associated fibroblasts⁷⁹. They are also responsible for promoting angiogenesis in TME^{85,87,88}. Both M2-like TAMs and malignant cells produce MMP-9 and VEGF that can contribute to the malignant growth of cancer cells and metastasis^{89,90}. Furthermore, these cells increase the expression of PD-L1 on the surface of monocytes. PD-L1/PD-1 interaction on CD8⁺ T cells, suppress the anti-tumor CD8⁺ T cell responses and induce T cell exhaustion. Moreover, immunosuppressive cytokines and components produced by TAMs, such as IL-10 and TGF- β can induce the exhaustion of tumor-infiltrated CD8⁺ T cells. TAMs can directly hamper the cytotoxicity of CD8⁺ T cells by depletion of L-arginine and tryptophan amino acids in TME^{91,90}.

1.6.3. Cancer-associated fibroblasts (CAFs)

Cancer-associated fibroblasts are the most abundant stromal subtypes that negatively regulate TME by releasing suppressive mediators of T cell immune responses. CAFs release chemokines such as CXCL-1 and CXCL-2, which induce infiltration of myeloid cells in vicinity of the tumor. CAFs activation also helps the infiltration of MDSCs and Tregs in the target site, which further suppresses anti-tumor responses. Furthermore, they apply direct immunosuppressive effect on T cell responses underlying mechanisms which amplify PD-1/PD-L2 and FAS/FASL interaction on CD8 T cells and CAFs^{79,92}. The presence of several cytokines released by activated immune cells (e.g., IL-1 β) can facilitate the transformation of healthy fibroblasts into CAFs to orchestrate anti-tumor immunity^{93,94}.

1.6.4. Other mediators

The tumor microenvironment consists of several inflammation-related factors such as immunosuppressive cytokines, which not only upregulate the expression of inhibitory molecules on T cells, but also trigger oncogenic signaling pathways and modulate the production of inhibitory ligands. IL-6 induces T cell exhaustion by transcription regulation of IL-6/STAT3/PD-1^{95,96}. Other pro-inflammatory cytokines, such as IL-10 and TGF- β released by immunosuppressive cells in TME, also upregulate PD-1 expression on T cells resulting in T cell exhaustion^{96,97,98,99}. In addition, it has been reported in prostate cancer that Notch receptor overexpression on T cell surface activates Notch signaling that induces T cell exhaustion by controlling the Nuclear factor of activated T cells (NFAT) transcription factor^{100,101}. A variety of transcription factors such as NR4A1, TOX, Eomes, T-bet and BATF have been shown to involve in PD-1 overexpression and T cell dysfunction¹⁰².

For example, NR4A1 overexpression prevents the differentiation of effector T lymphocytes, while deletion of NR4A1 promotes T cell growth and anti-tumor activity. Furthermore, in NR4A1^{-/-} mice, PD-1 and TIM-3 expression on T cells declined compared to the intact mice^{102,103}. Transcription factor TOX was recently reported as a key modulator of T cell exhaustion during chronic infection¹⁰⁴. Deletion of TOX limited CD8⁺ T cell exhaustion and boosted anti-tumor effect of CD8⁺ T cells¹⁰⁴. BATF expression of CD8⁺ T cells was also found to contribute to lower T cell differentiation and cytokine production during HIV infection¹⁰⁵.

Together, all these outcomes show that TME contains several mediators and components that create an immunosuppressive environment that restricts anti-tumor T cell activity by inducing T cell exhaustion.

1.7. Inhibitory receptors

1.7.1. Programmed cell death-1 (PD-1)

Antigen presenting cells present antigen to CD8⁺ T cells using MHC-I molecules to activate CD8⁺ T cells. Activated CD8⁺ T cells are then transferred into the inflammation site to implicate anti-tumor activity. On the other hand, malignant cells apply multiple approaches to escape from T cell-mediated immunity. One such technique is through the upregulation of immune checkpoints on T lymphocytes to repress the cytotoxic functions of these cells¹⁰⁶ (**Figure 5**).

PD-1 is one of the immune checkpoint receptors produced by activated innate and adaptive immune cells including tumor-infiltrating CD8⁺ T cells that play a critical role in the regulation of inflammation¹⁰⁷. In turn, tumor cells express PD-L1 on their surface, which can bind to PD-1 on T cells. This interaction activates PD-1 signaling on CD8⁺ T cells and provides tumor immune escape. Due to continuous antigen encounter, tumor-infiltrating CD8⁺ T cells markedly overexpress PD-1 and decrease cytokine production leading to T cell dysfunction^{108,91}.

PD-1 binding to PD-L1 (expressed by tumor cells) induces phosphorylation of ITIMs in the intracellular domain of PD-1 that recruits tyrosine acid phosphatases SHP1 and SHP2 to attenuate PI3K/AKT/Ras/MAPK/ERK signaling pathway and consequently leads to T cell dysfunction^{109,110}. Furthermore, PD-1 directly impacts on T cell receptor signaling by blocking the activity of cyclin-dependent kinases (CDKs), which suppresses cell cycle development. PD-1 also attenuates TCR expression by downregulation of casein kinase II (CK2)^{110,111,112}. CR-C and CR-B are highly conserved regions in *Pdcd1* promoter which are mandated for *Pdcd1* gene transcription. Upon antigen encounter, these regions are demethylated, causing PD-1 expression^{113,114}. In some studies, PD-1 has been documented as a T cell activation marker. However, in chronic inflammatory conditions such as TME, sustained PD-1 expression by antigen-specific T lymphocytes associates with terminal exhaustion of T cells^{115,116,109}. Also, the absence of PD-1 was found to protect CD8⁺ T cells from undergoing exhaustion¹⁰⁹.

1.7.2. Lymphocyte activation gene 3 (LAG-3)

LAG-3 (CD223) is another inhibitory molecule that is expressed by activated T cells, B cells and NK cells. Similar to PD-1, LAG-3 is also overexpressed on exhausted tumor-infiltrating lymphocytes (TILs)¹¹⁷. This protein generally binds to MHC-II molecules on APC or cancer cells. LAG-3 is able to interact with other ligands such as Galectin-3, lymph node endothelial cell C-type lectin (LSECTIN), and fibrinogen-like protein 1 (FGL1)¹¹⁸. Even though the mechanisms behind LAG-3 signaling are not fully understood, LAG-3 has been demonstrated to negatively modulate immune responses-mediated by T cells and boost the suppressive functions of regulatory T cells. Co-expression of LAG-3 with other inhibitory receptors has been found to assist cytotoxic CD8⁺ T cell exhaustion in cancer^{119,120}. After ligand binding, LAG-3 blocks TCR signaling and limits the activation of transcription factors, including NFAT, which results in a decreased proliferation and cytokine production of cytotoxic CD8⁺ T cells. IL-2 and IL-17 have been found to promote the expression of LAG-3 on activated T cells^{121,122}.

1.7.3. T cell immunoglobulin and mucin domain 3 (TIM-3)

TIM-3 is an inhibitory receptor expressed by exhausted T cells in the tumor microenvironment, which was first found in IFN- γ -producing Th1 and Tc1 cells^{123,124}. Upon binding with its ligands galectin-9 and HMGB1, TIM-3 evokes T cell dysfunction and apoptosis^{125,126}. The exact intracellular mechanisms of TIM-3 have not been fully understood. However, TIM-3 interaction with its ligands on the surface of target cells results in dephosphorylation of Lck and downregulation of ZAP70/LAT/PLC γ 1/Ca⁺⁺ TCR signaling pathway, which attenuates the proliferation of TILs¹²⁷. Co-expression of TIM-3 and PD-1 has been reported to correlate with the inhibition of anti-tumor responses of tumor-infiltrating T cells. TIM-3 expression also involves the development of Tregs and MDSCs in tumor tissues¹²³. In breast cancer, TIM-3 expression by CD8⁺ and CD4⁺ T cells has been reported to correlate with lymph node metastasis via TIM-3-mediated immune escape^{128,122}.

1.7.4. Cytotoxic T-lymphocyte-associated protein 4 (CTLA-4)

CTLA-4 is an inhibitory receptor which is upregulated on activated T cells. It engages with B7-1 (CD80) and B7-2 (CD86) ligands (similar ligands as CD28) on APCs to block the delivery of positive signals induced by CD28. Additionally, CTLA-4 prevents T cell activation by decreasing IL-2 synthesis and impairing cell cycle^{129,130}. CTLA-4/CD80/86 interaction also induces the expression of indoleamine-2,3-dioxygenase (IDO) by APCs and promotes Tregs function¹³¹.

1.7.5. T cell immunoreceptor with Ig and TIM domains (TIGIT)

TIGIT is characterized as an inhibitory receptor which is expressed by several activated lymphocytes¹³². Upon binding TIGIT to its ligands CD155 and CD112 on dendritic cells, TIGIT indirectly targets the transfer of co-inhibitory signals, which suppress effector functions of cytotoxic CD8⁺ T cells. Furthermore, TIGIT interaction with CD155 on DCs augments IL-10 secretion and declines pro-inflammatory cytokine production. TIGIT-CD155 signaling through ITIM domain of TIGIT exerts NK cell dysfunction^{132,133}. TIGIT overexpression on a subset of Tregs is associated with inhibition of Th1 and Th17 T cell responses^{134,135}.

Together, inhibitory receptors such as PD-1, LAG-3, TIM-3, CTLA-4 and TIGIT play an important role in the control of T cell immunity. The co-expression of these inhibitory molecules on T cells has been shown to dampen effector responses of T cells and correlate with T cell exhaustion.

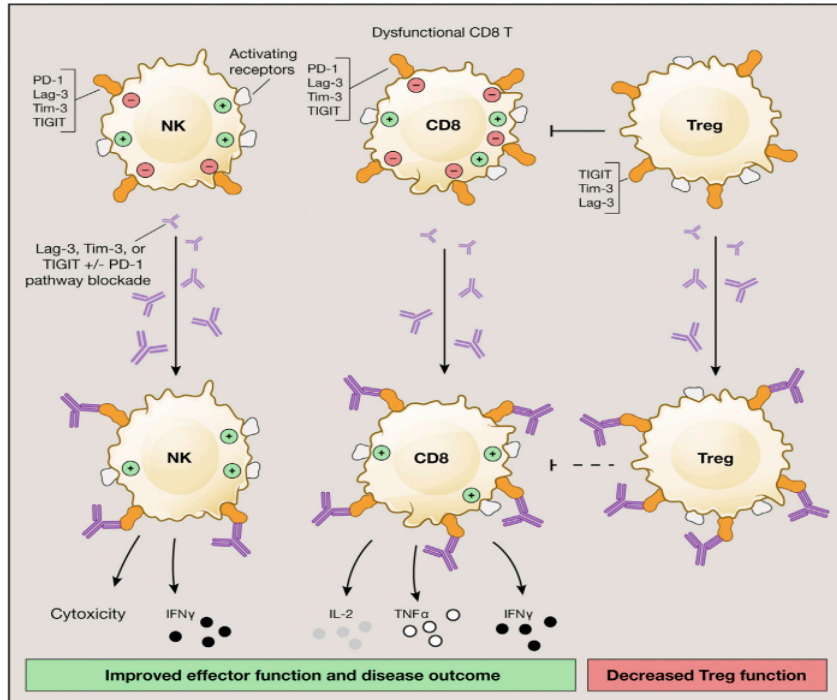


Figure 5. Co-expression of inhibitory receptors on T cells induces T cell exhaustion. PD-1, LAG-3 and TIM-3 co-expression on activated T lymphocytes is correlated with dysfunction or exhaustion of T cells in chronic viral infection and cancer¹²².

1.8. Cancer immunotherapy

The aim of cancer immunotherapy is to control the host immune system, which detects and destroys malignant cells and most likely limits the development of different cancer types. The main part of cancer immunotherapy response is the recognition of tumor-associated neoantigens by T cell receptors. However, massive variations in neoantigens as well as antigen-presenting molecules, are the main obstacles in solid tumors. Therefore, tumor-infiltrating lymphocytes are considered the major targets for cancer immunotherapy. Multiple types of immunotherapy approaches are applied to treat cancer¹³⁶.

1.8.1. Immune checkpoint inhibitor therapy

There are several negative regulatory molecules on activated T cells that function as checkpoint molecules to regulate immune responses and control the hyperactivation of immune cells. However, tumor cells apply different strategies to escape from the immune system. Expression of different ligands by tumors (e.g., PD-L1), which bind to immune checkpoint inhibitors (e.g., CTLA-4, PD-1, LAG-3 and TIM-3) on T cells is one mechanism by which cancer cells target anti-tumor activity¹³⁷.

Immune checkpoint blockade is a validated and important therapy to rescue anti-tumor T cell responses by targeting these checkpoint receptors. Ipilimumab was the first antibody authorized by FDA to block CTLA-4 receptor. Following that, several monoclonal antibodies have been successfully developed to target PD-1 (nivolumab and pembrolizumab) and PD-L1 (durvalumab and avelumab). These monoclonal antibodies showed strong and long-lasting anti-tumor effects on different types of cancers, including melanoma, breast cancer, renal cell carcinoma, and colorectal cancer^{138,139,140}. Similar to PD-1 blockade therapeutic effects, anti-PD-L1 antibodies have been verified for the treatment of several cancer types. Combination blockade of LAG-3 and PD-1 therapy are certified to effectively improve the survival rate of patients with metastatic melanoma¹⁴¹. Similarly, several monoclonal antibodies against TIM-3 in combination with anti-PD1 therapy showed promising effects in patients' survival^{142,143}.

1.8.2. Targeting inhibitory cells

The tumor microenvironment produces several soluble factors that target normal myeloid differentiation and transform them into immunosuppressive cells. This environment facilitates tumor cell growth and limits the efficacy of tumor immunotherapy. MDSCs are a subset of cells with immunosuppressive effects that impair the efficacy of anti-tumor strategies such as immunotherapy¹⁴⁴. Therefore, these cells are regarded as potential therapeutic targets for cancer immunotherapy. It has been evidenced that vitamin D and trans-retinoic acid (ATRA) treatment lead to immature differentiation of myeloid cells and attenuate immunosuppressive activity of these cells in head and neck squamous cell carcinoma (HNSCC) and renal cell tumors^{145,146,147}. Similar to MDSCs, regulatory T cells can be another important target to improve the efficacy of immunotherapy. Blocking the suppressive activity of Tregs using antibodies against or by targeting small molecule antagonists in combination with immune checkpoint blockade can protect the anti-tumor immunity^{148,149}.

1.8.3. CAR T cell therapy

Chimeric antigen receptor (CAR) T cells are synthetic receptors that are designed to detect and destroy tumor cells expressing cognate antigens^{150,151}. In this technology, T lymphocytes are isolated from circulation and designed to express CARs. T cells expressing CARs identify and bind to tumor cells independent of a MHC interaction¹⁵². Subsequent to *in vitro* proliferation, the modified cells are reinfused into the patients to induce anti-tumor immune responses^{152,153}. These modifications of T cells allow for better proliferation and improve CAR T cell survival. Modified T cells also produce cytokines such as IL-12 that promote T cell viability and activate other immune cells to eliminate tumors¹⁵⁴⁻¹⁵⁵. CAR T cells have been applied to various solid tumors, including glioblastoma¹⁵⁶, sarcoma¹⁵⁷, gastrointestinal track tumors¹⁵⁸, and B cell abnormalities^{159,160} with promising responses¹⁶¹.

However, the immunosuppressive effect of TME induces the exhaustion phenotype of CAR T cells and limits their infiltration to the tumor site and metabolic starvation. These issues negatively contribute to less efficiency of CAR T cells. Recent generation of CAR T cells with “exhaustion-resistant” phenotype have presented high anti-tumor efficacy and durable survival^{154,162,163}. CAR T cells with genetic ablation of inhibitory receptors such as PD-1 and CTLA-4 have demonstrated higher anti-tumor activity^{155,164,165}. In addition, overexpression of TOX and NR4A transcription factors have been reported to involve in T cell exhaustion. Thus, TOX and NR4A deficient CAR T cells could limit exhaustion by promoting cytokine production and declining the expression of inhibitory receptors^{166,167}.

1.8.4. Neoantigen T cell therapy

Neoantigens generated from somatic mutations are expressed on malignant cells that inhibit T lymphocytes anti-tumor responses. Hence, they can be an ideal target for cancer immunotherapy, either as a vaccine or cell therapy¹⁶⁸. For instance, dendritic cell vaccines modulated neoantigen-specific T cell responses, which were previously undetected neoantigens in patients with advanced melanoma¹⁶⁹. More studies have revealed that neoantigens were also associated with immune checkpoint antagonism responses in lung cancer and melanoma^{168,170,171}. In addition, clonal neoantigen therapy has been found to correlate with the improvement in immune checkpoint blockade responses¹⁷².

1.8.5 Cytokine therapy

Upon normal immune responses, cytokines can directly impact immunity by increasing or blocking the activity of immune system components¹⁷³. Therefore, another type of immunotherapy involves systemic inoculation of certain cytokines to boost cancer immunity. IFN- γ treatment has been recognized to improve anti-cancer immune responses through several strategies, including activation of DCs and enhancement of antigen presentation, increase of Th1 responses and elevation of cytotoxic functions of NK cells^{174,175}. Similar to IFN- γ , IL-2 has been shown to promote anti-tumor activity of the immune system via elevating the cytotoxic functions of tumor-infiltrating T cells and NK cells¹⁷³.

In summary, cancer immunotherapy advances aim to support the immune system and harness tumor development. Despite all efforts made by researchers, there are still some challenges that limit the efficacy of immunotherapy techniques.

1.8.6. Challenges and future directions of cancer immunotherapy

Cancer immunotherapy can be broadly described as an effective approach for promoting the immune system to fight against cancer cells. Current advances in cancer immunotherapy, including immune checkpoint blockade, tumor vaccination and CAR T cell therapy, have obviously altered the outlook of cancer treatment. Despite all advancements for treating patients with certain types of cancers, the majority of cancer patients are still non-responsive to these treatment approaches^{174,176}. There are multiple directions to improve the response rate to cancer immunotherapy, including recognition of more specific immune checkpoint inhibitors, biomarkers and mechanisms¹⁷⁷. In addition, promoting anti-tumor immunity via targeting immune checkpoint inhibitors may impair the normal mechanisms involved in the regulation of autoimmune disorders. Inhibiting these immune checkpoint proteins can also be associated with some side effects^{178,179}. Therefore, due to all challenges facing cancer immunotherapy, there is a necessity to concentrate on crucial questions in both research and clinical investigation areas.

1.9. Peripheral Nervous System (PNS)

Peripheral nervous system (PNS) refers to components of the nervous system that reside outside of the brain and spinal cord that innervates the skin and other organs, including lung and gut. The PNS is originated from neural crest stem cells which migrate to distant parts. PNS is classified into the autonomic nervous system and somatic nervous system. The somatic nervous system consists of two main subtypes, including afferent (sensory) nerves that convey the electrical signals from the periphery towards the central nervous system (brain and spinal cord) for integration and efferent (motor) neurons that carry electrical signals from central nervous system to the periphery^{180,181}. The cell bodies of visceral sensory nerves are located in dorsal root ganglia (DRG).

1.9.1. Nociceptor neurons

Nociceptors are a subgroup of sensory neurons that act as a line of defense to detect environmental danger, specifically through ligand- and voltage-gated ion channel receptors. These receptors include transient receptor potential cation channels (TRP) and voltage-gated sodium channels (Nav1.8), which are expressed in the nerve terminals. The danger signal receptors enable nociceptor sensory neurons to detect and respond to thermal, chemical and mechanical stimuli¹⁸².

Activated sensory neurons transfer electrical information from the axon terminals in the periphery to the cell body and then to the central axon branch, which ends in the spinal cord and brain stem^{183,184,185}. Sensory neurons are classified as C fibers, A β and A δ fibers. C afferent nerves are unmyelinated, slow-conducting fibers that are mainly sensitive to capsaicin and are accompanied by thermal pain sensitivity. A β and A δ are myelinated fibers that are faster conductors and A δ nerves are mostly associated with mechanical pain sensitivity^{186,187}. In addition to these classifications, C fibers can be categorized as peptidergic and non-peptidergic nerves¹⁸⁸. Peptidergic C fibers secrete neuropeptides, including SP and CGRP and express tropomyosin receptor kinase A (TrkA), which can bind to nerve growth factor. However, non-peptidergic C fibers are determined to bind to isolectin B4 (IB4) and they can express several receptors, including GFR- α and the purinergic receptor P2X3^{189,190,191}.

Upon activation of C fibers, they highly overexpress ion channels on their surface. Phosphorylation of these ion channels can consequently mediate some alterations in the membrane properties, such as enhancing action potential firing and increasing the sensitivity to thermal and mechanical stimulators¹⁹².

Compared to other transducers, Nav1.8 voltage-gated sodium channels on nociceptors can markedly generate action potential firing and they are mandated for nociceptors depolarization leading to pain signaling^{192,193}. Mechanosensation is mediated by Piezo2 ion channel. TRP ion channels are also critical mediators of pain and mechanical sensation. Transient receptor potential ankyrin 1 (TRPA1) nociceptors are characterized to mediate chemical and mechanical pain sensitivity and can be activated by allyl isothiocyanates^{194,195}.

Transient receptor potential vanilloid 1 (TRPV1) is expressed by both sensory C and A δ fibers. TRPV1 nociceptors are also necessary for the mediation of pain hypersensitivity and can be activated by exogenous stimulators such as heat (>43 °C) and capsaicin (chili peppers components), as well as endogenous modulators including acidic pH, prostaglandins E2 (PGE2), serotonin (5-HT), Histamine, ATP and NGF which are products of tissue injury, inflammation, and tumor progression^{196,197,198,199,200}. Activation of the TRPV1 channel leads to the influx of cations (Ca⁺⁺ and Na⁺) into nociceptor neurons (depolarization state) and secretion of pro-inflammatory neuropeptides, such as calcitonin-gene-related peptides (CGRP) and substance P (SP), which can drive neurogenic inflammation^{201,202,203,204,205} (**Figure 6**).

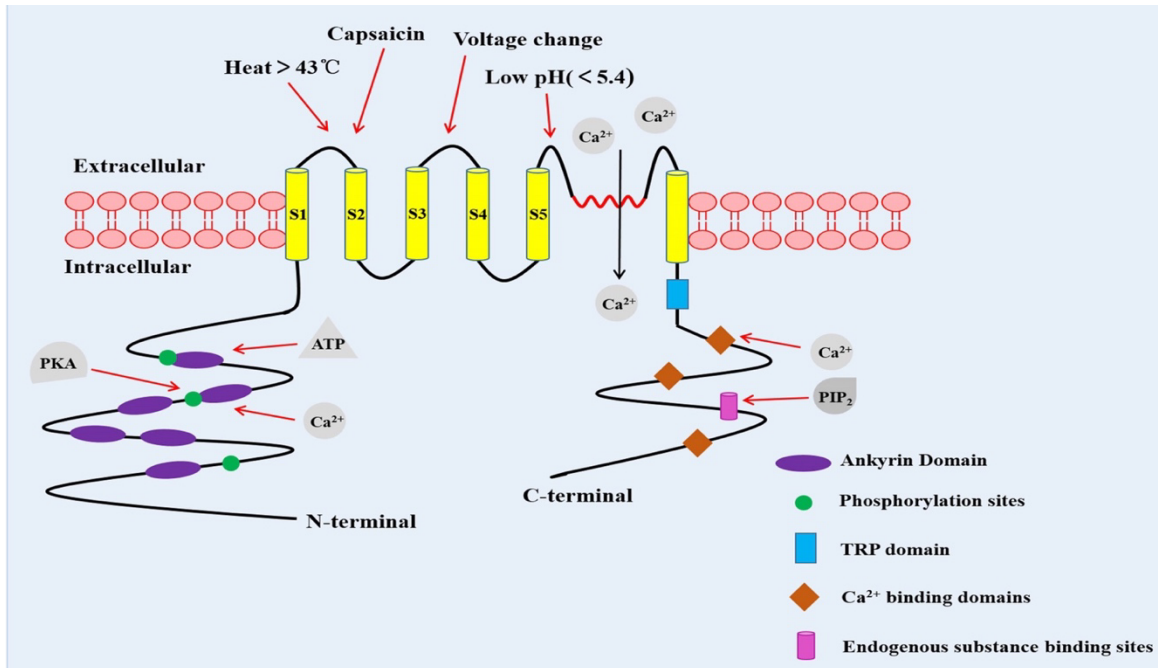


Figure 6. TRPV1 channel structure. TRPV1 is a protein consist of six transmembrane subunits. There is a pore-forming hydrophobic group between fifth and sixth transmembrane subunits. Activation of TRPV1 by a variety of stimuli such as heat, capsaicin and H⁺ induces the influx of extracellular Ca⁺⁺ ions inside the neurons that modulates neuronal activity²⁰⁶.

1.9.2. Neurogenic inflammation

The “neurogenic inflammation” term has described the notion of sensory nerve presence in inflammation. The neurogenic inflammation was proposed in 1874 when Goltz reported the existence of vasodilator fibers in sciatic nerve in the dogs²⁰⁷. This idea was also confirmed by another evidence demonstrating that stimulation of dorsal root in the dogs led to an enhanced blood circulation around the skin densely innervated with sensory neurons²⁰⁸. In 1967, Jancsó pointed that upon stimulation of sensory nerves by damaging stimuli, action potential is generated and conveyed to the CNS to begin reflexes (withdrawal) or sensations (pain, itch)²⁰⁹. After transmission of electrical signals to the CNS, they are transferred back to the axon terminals in the periphery. This leads to the activation of voltage-gated calcium channels, enhances cytoplasmic calcium and triggers the local release of neuropeptides, including SP and CGRP. Released neuropeptides, in turn, modulate the activity of local immune cells and affect vascular smooth muscle cells. They all result in inflammation which is determined by four major signs: redness, swelling, heat and pain. Accordingly, the process by which neuropeptides-released nociceptors induce inflammatory symptoms is known as “neurogenic inflammation”^{210,211,212}.

1.9.3. Peripheral nervous system with immune system crosstalk

The peripheral nervous system and immune system preserve vast communication, including nerve innervation of lymphoid organs. Neurotransmitters and neuropeptides released by the peripheral nervous system directly regulate immune activity²¹³. Conversely, immune cells express receptors for several types of neurotransmitters (e.g., acetylcholine and catecholamine) and neuropeptides such as CGRP and SP^{214,215}. Immune cells also produce cytokines that make these neurons more sensitive. Nociceptor sensory neurons are able to notify CNS about the detection of harmful stimuli in both synaptic terminals in the CNS and in peripheral nerve terminals. This leads to the modulation of immune responses in the periphery and is essential for the maintenance of physiological homeostasis^{216,211} (**Figure 7**).

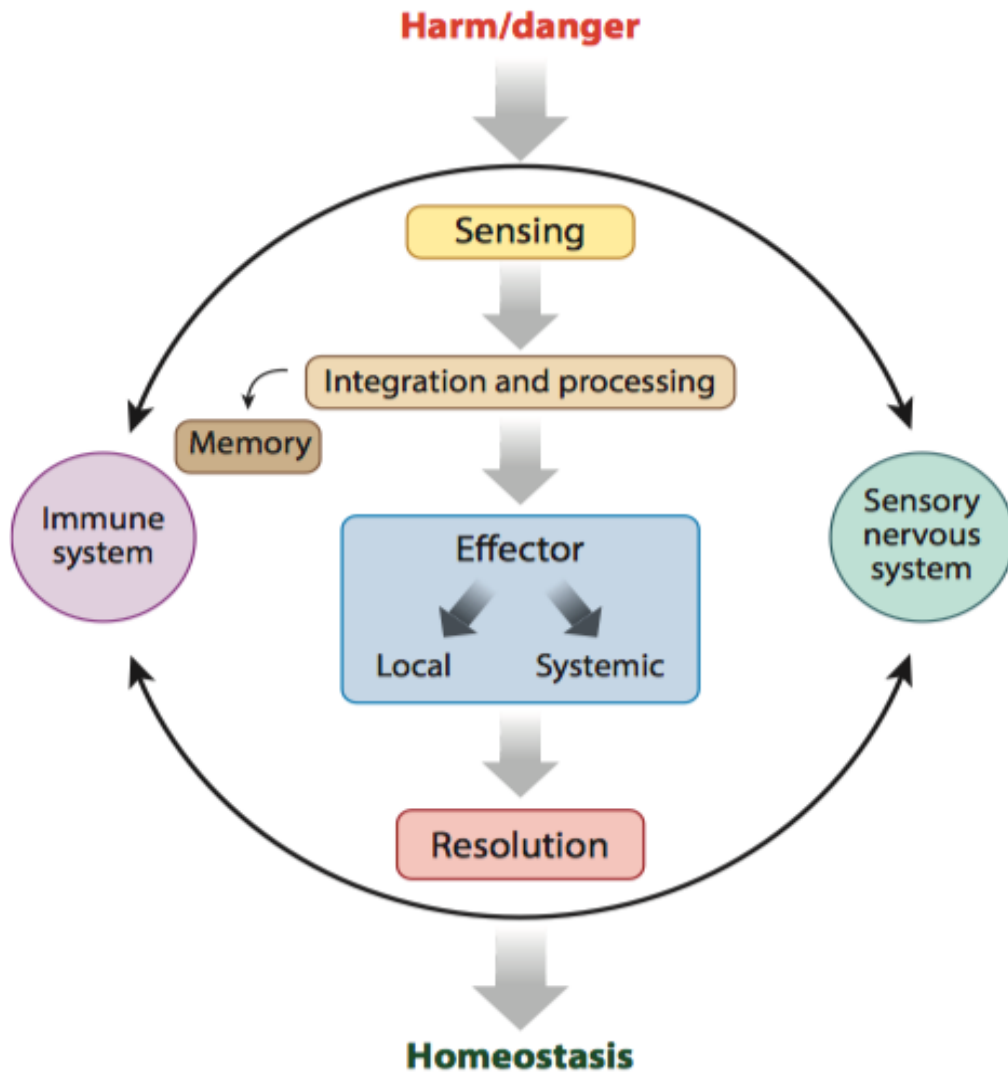


Figure 7. Immune system and nervous system crosstalk to detect danger. Both systems detect and respond to internal and external damaging stimuli through the expression of various receptors. The signals are combined and processed to produce effector responses and memory leading to the elimination of the threats and maintaining homeostasis²¹¹.

1.9.4. Innervation of lymphoid organs

Several studies have revealed the bidirectional crosstalk between the peripheral nervous system and primary (bone marrow and thymus) or secondary (spleen and lymph node) lymphoid organs. For instance, peptidergic sensory fibers have been observed to innervate lymphoid organs and barrier tissues^{217,218,219,220}. However, the type of innervation and nerve density as well as resident cell types are different between organs. Sensory neurons innervation of specific tissues may affect different immune responses^{221,222}. Mechanisms underlying and outcomes of neuro-immune communications are still poorly understood. But in several evidences, the interaction of PNS (sympathetic, parasympathetic and sensory nerves) and the immune system happens through the local secretion of neuromodulators such as neuropeptides, neurotransmitters, and growth factors.

1.9.5. Bone marrow innervation

Immune cells originate from hematopoietic stem cells (HSCs) and the process of immune cells development mainly happens in the bone marrow and thymus²²³. Bone marrow innervation by the autonomic nervous system orchestrates the progression of innate and adaptive immune cells²²⁴. Bone marrow innervation was described by Calvo in 1968 when he suggested the idea that autonomic and sensory fibers regulate the activity of bone marrow²²⁵. Sympathetic nerves are the main group of neurons in the bone marrow and the periosteal part of bone is highly innervated by these neurons²²⁶.

Sensory and sympathetic nerves do not provide direct synapse with the target cells in the bone. The direct effect of these nerves on bone marrow is provided by the presence of axons in the vicinity of target cells and through the local secretion of neurotransmitters and neuropeptides^{227,228}. Sympathetic fibers that express tyrosine hydroxylase (TH) were found in the vicinity of bone marrow adipocytes²²⁹. In addition to TH-expressing sympathetic nerves, CGRP-producing sensory axons were found in the bone marrow adipocytes^{230,231}.

1.9.6. Lymph nodes (LNs) innervation

LNs are a part of secondary lymphoid organs where the local adaptive immune responses against harmful stimuli initiates. Compared to other lymphoid organs, source of LN innervation has been less investigated, however it is probably to be region specific. Several investigations have reported the innervation of LNs by noradrenergic and peptidergic fibers²¹⁸. Sympathetic nerves which are located around blood vessels travel to the subcapsular plexus of LNs and then these nerves enter into T cell zones^{232,233}. The secretion of norepinephrine in LNs is necessary for antigen presentation and activation of T lymphocytes as well as their efflux into circulation²³⁴. In the absence of norepinephrine, cytotoxic T cell activation is also limited^{215,235}.

Furthermore, sensory nerve fibers that produce SP and CGRP, have been discovered in the close proximity of lymphocytes in LNs while there is no evidence for the presence of cholinergic fibers in LNs²³⁶. Huang et al. have shown that LNs are innervated with a specific neuronal population with strong enrichment of peptidergic nociceptor fibers. Using combination of several approaches including immunolabeling, single-cell genomics and optogenetic techniques, they determined that there is a bilateral neuro-immune correlation in LNs²²⁰. In addition, it has been recently reported that the depletion of nociceptor sensory nerves in mouse model using diphtheria toxin fragment A (DTA), contributes to antigen preservation via peripheral LNs. This data reflect that regulation of lymphatic trafficking may be one of the major mechanisms by which sensory fibers can locally control immune responses in LNs^{237,220}.

1.9.7. Spleen innervation

Spleen is densely innervated by autonomic fibers through the splenic nerve which contains sympathetic nerves from superior mesenteric-celiac ganglion. Postganglionic nerve endings innervate the spleen along with blood vessels which provide an essential network in the white pulp^{238,239,240}. Nerves ending in the splenic parafollicular regions are detected close to the T and B lymphocytes and macrophages. The

splenic sympathetic innervation mainly acts through norepinephrine which has been termed the inflammatory reflex. The splenic inflammatory reflex is regulated by noradrenergic and cholinergic neuronal networks which accordingly leads to inhibition of splenic macrophages²⁴¹.

Neuropeptide production by sensory and sympathetic fibers are also associated with splenic immune modulation. Neuropeptide Y (NPY) regulates the development of effector T and B cells²⁴². VIP has been found to decrease the production of pro-inflammatory cytokines by T cells and macrophages. VIP also triggers the activation of DCs which contribute in generation of regulatory T cells (Tregs)^{243,244}. Substance P-producing sensory neurons in the spleen modulate proliferation of lymphocytes through increasing the level of IFN- γ , IL-2 and IL-4. CGRP-expressing sensory neurons act on DCs, T cells and macrophages in order to control inflammation^{245,246,247,233}. Collectively, these outcomes provide supports for innervation of lymphoid tissues by autonomic and sensory fibers. This bidirectional communication can regulate immune system responses in several pathophysiological disorders.

1.10. Regulation of immune cells by neurotransmitters

1.10.1. Neurotransmitters of autonomic nervous system

Norepinephrine (NE) secretion level is increased by activated sympathetic nerves. NE engages with β 2-adrenergic receptors (β 2ARs) which are the most expressed receptors on immune cells^{248,249}. Additionally, stimulation of β 2ARs on the surface of natural killer T (NKT) cells has been viewed to enhance IL-10 and inhibit IFN- γ production by these cells which results in systemic immune activity in a model of stroke^{249,250}. Moreover, in mouse model of allergic airway, NE has been found to negatively control innate lymphoid cell 2 (ILC-2) proliferation and Th2 cytokines production (IL-13) via β 2AR²⁵¹. In contrast, during mouse cytomegalovirus infection (MCMV), splenic NK cells have been shown to elevate β 2AR production using IL-12 and STAT4 signaling pathways.

The depletion of β 2AR was associated with limited proliferation of NK cells and their effector functions²⁵². In animal tumor model, catecholamine-producing nerves have been viewed to overexpress β 2AR on myeloid-derived suppressor cells (MDSCs). This effect was correlated with the development and survival of MDSCs within tumors and other tissues²⁵³. Activation of dopaminergic neurons enhance the activity of peritoneal myeloid cells and IFN- γ -expressing T cells in lymph node during *Escherichia coli* infection²⁵⁴. Stimulation of cholinergic nerves in the spleen has been demonstrated to trigger β 2AR signaling as well as nicotinic α -7 acetylcholine-receptor on myeloid cells to limit the expression of TNF- α ²⁵⁵.

1.10.2. Neurotransmitters of sensory nerves

CGRP is a neuropeptide released by sensory neurons which involved in nociception and pain sensation. During inflammatory responses, the frequency of local and systemic CGRP is quickly upregulated. CGRP acts normally through its receptors which are expressed by wide variety of immune cell subsets: receptor activity-modifying protein 1 (RAMP1), RAMP2, RAMP3, and its co-receptor calcitonin receptor-like receptor (CLR)^{207,256}. In murine model of lung infection, CGRP has been found to repress immune responses through the restriction of neutrophil and $\gamma\delta$ -T cells infiltration in the inflammation site and via limiting the activity of these cells²⁵⁷.

Furthermore, CGRP can control adaptive immunity by affecting the activity of antigen-presenting cells. It was reported that the treatment of Langerhans cells with CGRP weakens their ability to stimulate the proliferation of mouse T cells^{258,259}. Several lines of evidence have shown that CGRP dampens the production of inflammatory mediators including TNF- α and IL-1 β as well as CCL-4 by phagocytes and DCs treated with inactivated bacteria or toll-like receptor (TLR) agonists²⁶⁰. CGRP also declines the production of IFN- γ by CD4 T cells while it elevates the production of IL-4²⁶¹. Additional studies revealed that CGRP signaling promotes intracellular cAMP level and triggers protein kinase A (PKA). cAMP-PKA signaling works as an inhibitory pathway in immune cells and it involves in anti-inflammatory responses to hamper self-tissue damage²⁶².

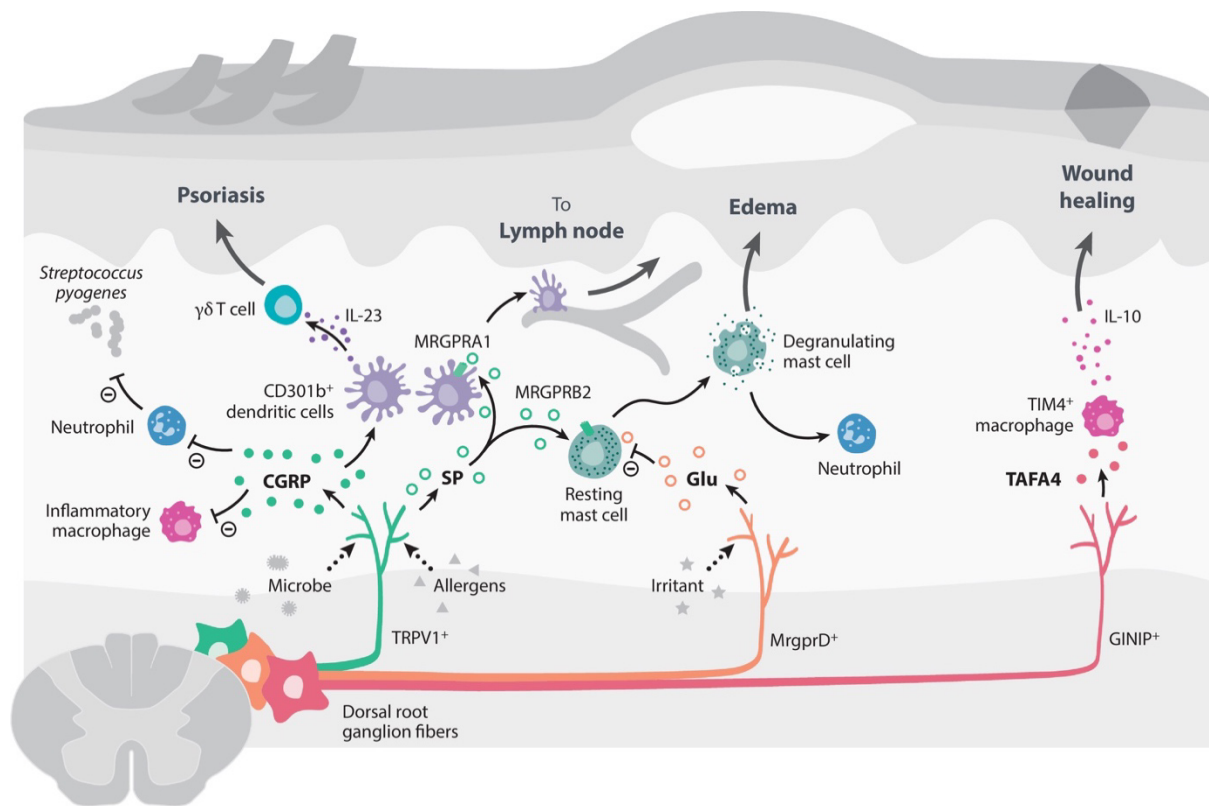
Substance P is secreted by activated TRPV1⁺Nav1.8⁺ sensory neurons and controls the function of innate and adoptive immune cells through different intracellular signaling pathways. The important function of SP lies in its capacity to induce the production of numerous cytokines by different immune cells including pro-inflammatory (IL-1 β) and immunomodulatory (IL-10) cytokines. Cytokines (IL-12, IL-18 and TNF- α) in turn, promote the effect of substance P by upregulating the expression of its receptor neurokinine-1 (NK1R) on T cells. In a murine model of atopic dermatitis, harmful stimuli induces the release of SP to activate type-2 skin inflammation through the activation of mast cells and their degranulation^{263,264,265} **(Figure 8)**.

Altogether, these findings suggest that neuromodulators notably act to control immune responses, and it would be interesting to further explore how and what type of these mediators are involved in modulation of anti-tumor immune responses.

1.11. Nerve-cancer crosstalk

1.11.1. Neuron-cancer interaction mediates tumor progression

The participation of nerves in pathogenesis has been remarkably noted in several studies. Nerves have been viewed to infiltrate into tumor microenvironment and communicate with other components resulting in progression and invasion of cancer cells. In addition, an enhanced nerve density was found to positively correlate with more aggressive disease as shown for melanoma, prostate, colon and rectum, pancreas, breast and lung^{180,266}. The interaction between nerve and cancer is described by two principal aspects: 1) cancer cells can release neurotrophic factors such as NGF and brain-derived neurotrophic factor (BDNF), neurotransmitters (Ach and glutamate) as well as axon guidance molecules (CX3CL1 and EphA2) to contribute in nerves infiltration or cancer invasion; 2) nerves in turn release neuroactive molecules which engage with their receptors on tumor cells and assist with the proliferation and metastasis of cancer cells^{180, 267} **(Figure 9)**.



Klein Wolterink RGJ, et al. 2022
Annu. Rev. Neurosci. 45:339–60

Figure 8. Interaction of sensory nerves with immune cells in the skin. Skin is highly innervated with DRG sensory fibers which have been found to interact with skin-resident and infiltrated immune cells. Noxious stimuli activate these fibers to release CGRP and SP. CGRP can suppress the activity of inflammatory macrophages to block TNF- α production. It also declines the infiltration of neutrophils in the infection site. In addition, CGRP acts on skin-resident DCs to release IL-23 which consequently modulates the activity of $\gamma\delta$ -T cells. SP triggers MRGPRA1 on the surface of DCs to induce their migration to draining lymph nodes and drive Th2 responses. Moreover, SP mediates mast cell degranulation²⁶⁵.

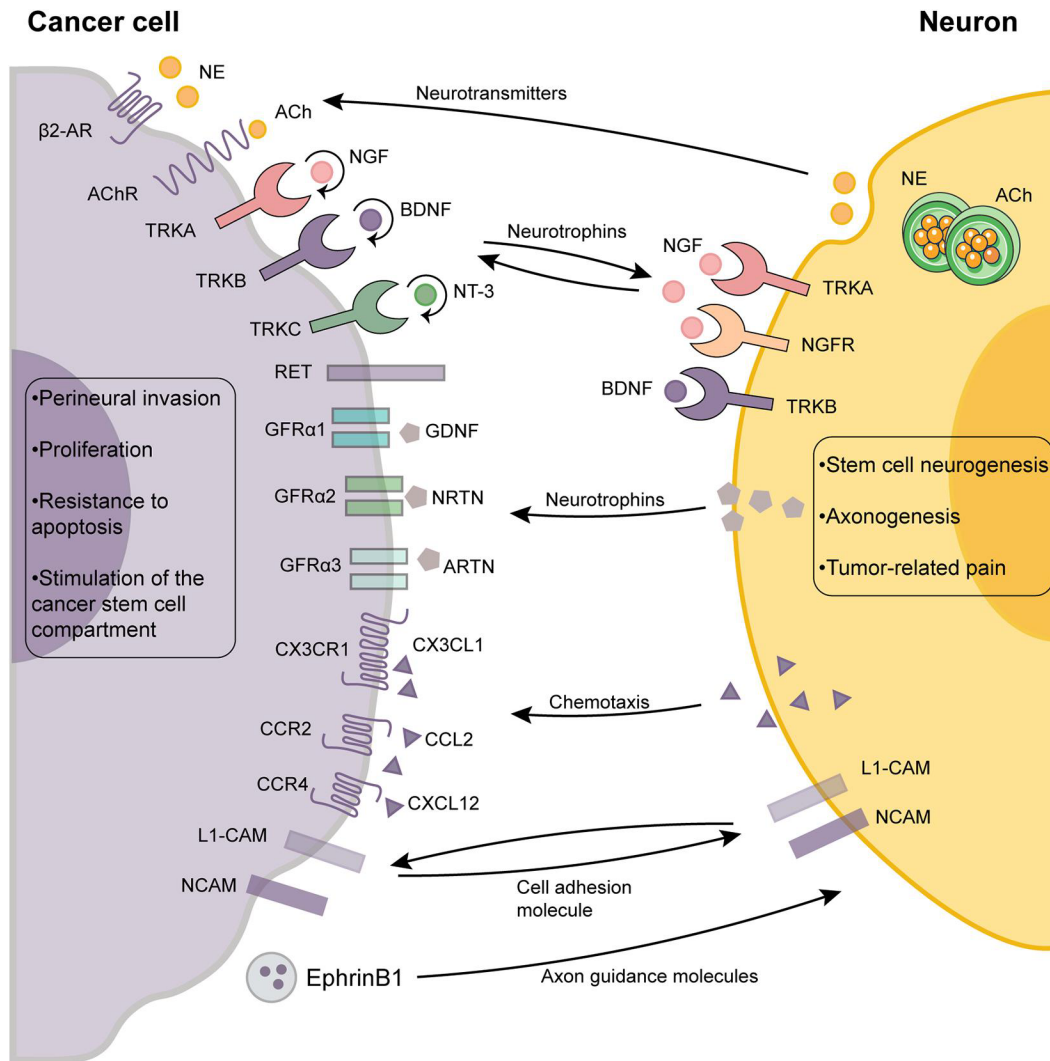


Figure 9. Nerve-cancer communication in tumor microenvironment. Bilateral interaction between cancer cells and neurons is importantly associated with neurogenesis, axonogenesis as well as perineural invasion. Autocrine effect of tumor cells also supports tumor development and dissemination²⁶⁷.

1.11.2. Cancer drives axonogenesis

Cancer-released neurotrophins promote axonogenesis through activation of tyrosine kinase receptors (TrkA) on nerve terminals resulting in tumor progression²⁶⁸. DRG neuron co-culture with prostate cancer cells showed the differentiation and extension of nerves toward cancer cells as well as migration of tumor cells to the neurons²⁶⁹. Similar to neurotrophic factors, axon guidance molecules released by tumor cells contribute to axonogenesis^{270,271}. For example, semaphoring 4 (an axon guidance molecule) has been viewed to play an important role in promoting axonogenesis in prostate cancer²⁷².

In addition to nerve fibers, tumor cells also express wide variety of receptors including TrkA, TRKB and NGF receptors to encounter with several nerve factors and trigger downstream pathways^{273,274}. The neurotransmitter ACh has been reported to function as an autocrine growth factor to stimulate the proliferation of lung tumors by modulating mitogen-activated protein kinase and AKT signaling. Ach also triggers the adhesion, migration and invasion of tumor cells^{275,276,277}.

Interaction through chemical synapses between nerves and cancer cells usually mediated by two neighboring cells that communicate via neurotransmitters such as glutamate²⁷⁸. This form of communication requires presynaptic nerves and postsynaptic cancer cells as confirmed by electron microscopy^{279,280}. Altogether, nerves interact with the tumor cells by forming functional synapses to promote tumor development.

1.11.3. Cancer promotes neurogenesis

In addition to involvement in axonogenesis, Ayala et al. revealed the role of cancer cells in neurogenesis. Neurogenesis is a procedure by which tumor cells respond to nerve regeneration and recruit the axons within the tumor site. In contrast to neurons of central nervous system, peripheral nerves are able to regenerate following an injury^{275,281}. In prostate tumor, high density of nerves in the ganglion represents neurogenesis phenomenon which is associated with cancer progression²⁸². This process is probably cancer specific. In normal prostate tissue, sympathetic fibers have been shown to regenerate themselves after damage which might be a consequence of axonogenesis, with no proof of neurogenesis.

However, in prostate cancer, the infiltration of new autonomic nerves within the tumor supports the establishment and development of tumors using activation of β -adrenergic and toxicological cholinergic pathways development^{283,284,285} (**Figure 10**). Furthermore, cancer cells can generate new neurons from cancer stem cells (CSCs). In 2017, Lu et al. showed that cancer stem cells harvested from gastric and colorectal carcinoma patients, can generate neurons that contribute to tumor development and neurogenesis²⁸⁶. In addition to sympathetic and parasympathetic innervation, sensory nerves also contributed to tumor development.

For example, in pancreatic cancer microenvironment, the release of neurotrophic factors leads to increased sensory innervation²⁸⁷. In the aggressive stages of pancreatic cancer, tumor cells can travel to the ganglia of sensory nerves and spinal cord reflecting the participation of these neurons in different stages of pancreatic cancer^{275,288}.

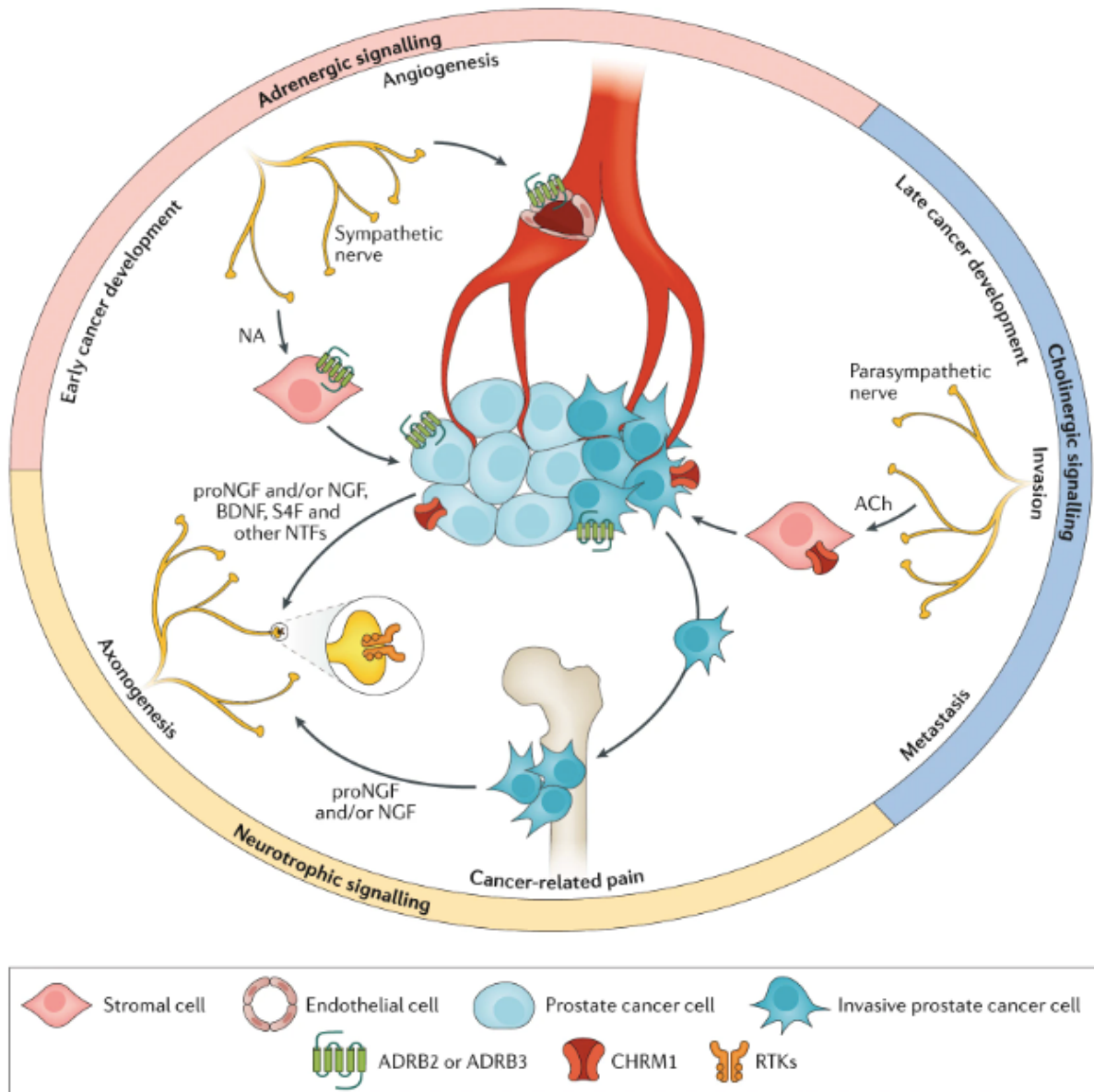


Figure 10. Nerve innervation in prostate cancer. Peripheral nerves infiltrate in the early stages of prostate cancer which results in tumor initiation. Autonomic nerve development happens in the prostate TME in response to neurotrophic factors and axon guidance molecules produced by prostate cancer cells. Following cancer metastasis to bone, NGF released by tumor cells can mediate cancer-related pain by sending the signals to nociceptor sensory neurons²⁸⁹.

1.11.4. Tumor cells induce neural reprogramming

Amit et al. proposed that extracellular vesicles released by tumor cells can contribute to neuronal reprogramming and cancer-related axonogenesis²⁹⁰. The authors observed that p53-knockout or mutant murine oropharyngeal squamous cell carcinomas (OPSCC) secrete exosomes that increase axonogenesis of DRG sensory neurons^{290,291,292,293}. The release of exosomes is relying on RAB-27 GTPase which is a key protein for EVs secretion. Upon stimulation of PC12 cells with derived exosomes from OPSCC, neurite outgrowth is significantly increased. Analysis of miRNA profiles of exosomes revealed that the differentially expressed genes are identified with morphogenesis, neuronal development and synaptic transportation²⁷⁰.

The density of tyrosine hydroxylase expressing nerves (TH⁺ adrenergic fibers) is significantly enhanced in TP53-mutant or depleted OPSCC compared to their wild-type counterparts, whereas there is no significant change in the parasympathetic nerves density²⁹⁰. The analysis also disclosed that the absence of miR-34a in vesicles extracted from p53-knockout OCSCC induces transcriptional reprogramming of tumor-associated sensory fibers and transdifferentiated them to adrenergic nerves and increases tumor development in murine model of OCSCC²⁹⁰. Overall, these findings proposed a new pathway by which tumor cells can prime the nerve density and initiate adrenergic neurogenesis (**Figure 11**).

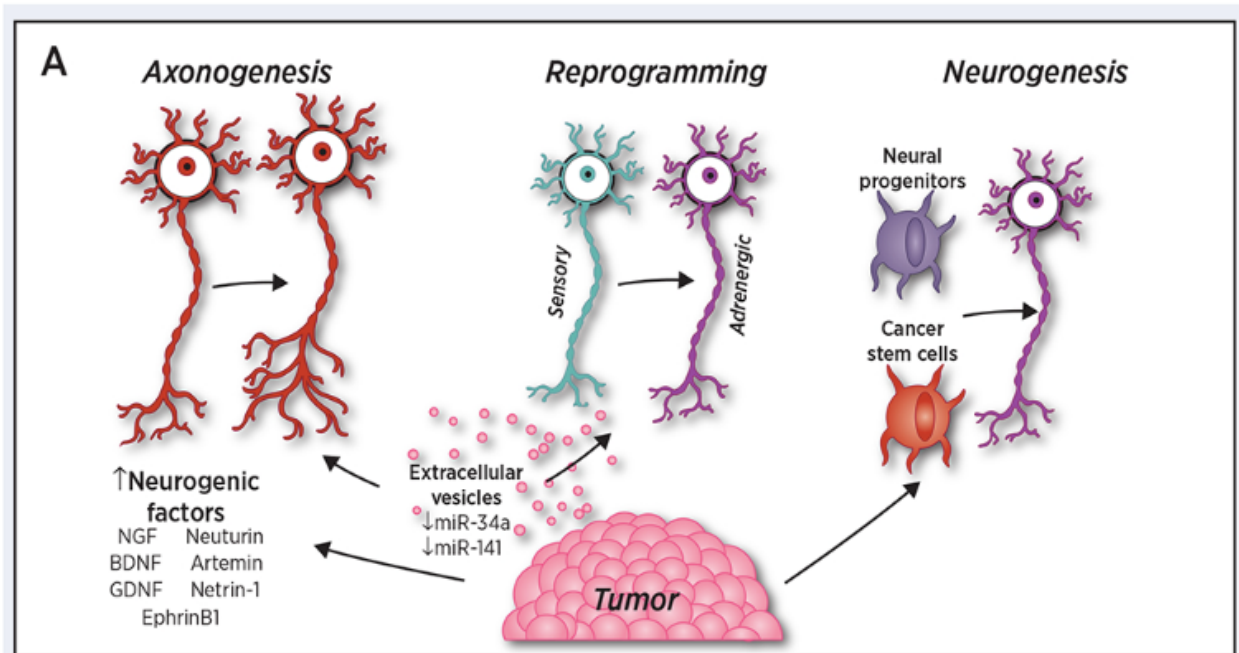


Figure 11. Axonogenesis, neurogenesis and remodeling induced by tumor cells in TME. Neurotrophic factors released by tumor cells, including GDNF, BDNF, NGF, Artemin, Neurturin, EphrinB1, and Netrin-1 induce axonogenesis. Extracellular vesicles with decreased levels of miR-34a and miR-121 induce the transformation of sensory nerves into adrenergic fibers. Cancer cells also mediate the migration of neural progenitor cells from the brain into the tumor tissue via the bloodstream. Furthermore, cancer produces new neurons from cancer stem cells in TME²⁹⁴.

1.11.5. Perineural invasion in cancer (PNI)

Solid tumors disseminate by different processes including direct invasion of neighboring tissues, invasion through vascular and lymphatic vessels as well as dissemination along nerves (PNI)²⁹⁵. Perineural invasion has been detected in several malignancies including head and neck, prostate, pancreas and colon cancers²⁹⁶. In PNI, tumor cells disseminate passively throughout the connective tissues that shield the nerves. During invasion, cancer cells contribute to structural nerve damage that in turn increases neural regeneration. It is conceivable that injured nerves release several growth factors that further develop cancer cell proliferation. On the other hand, increased level of growth factors by nerves may happen independent of neuronal injury²⁹⁷. Destruction of perineurium space by invading tumor cells provides a torrent of inflammation and repairs processes which favor cancer cell survival, proliferation and invasion^{298,282,299,300,296}.

1.11.6. Tumor-associated neurons repress intra-tumoral immune cells

Infiltration and activation of lymphocytes in the tumor vicinity are critical for preventing tumor growth³⁰¹. However, beside their direct effects on tumor progression, cancer-associated nerves (CANs) interact with the infiltrated immune cells in TEM, to contribute to tumor progression via inflammation³⁰². Neuroendocrine and neuronal pathways are associated with the regulation of immune responses, as most of their molecular signals and receptors originate from the same superfamily.

In breast cancer, it has been reported that sympathetic and parasympathetic nerve density upregulates the expression of immune checkpoint molecules such as PD-1 and FOXP3 in CD8⁺ and regulatory T cells³⁰³. Both denervation of sympathetic nerves or parasympathetic stimulation have been reported to decline the expression of immune checkpoints in a tumor-specific and nerve-type specific manner in murine breast cancer models.

These results unveils the opposite impacts of sympathetic nerves and parasympathetic fibers in breast cancer as well as the nerves contribution in immune checkpoint therapy³⁰³. Moreover, the infiltration of tumor associated macrophages (TAM) is controlled by sympathetic and parasympathetic nerves in TME.

Adrenergic signaling in pancreatic cancer has been shown to contribute to tumor development and poor survival by recruitment of TAM in the tumor site. However, cholinergic signaling showed the opposite effects²⁸⁵. Altogether, these findings propose that neurons can control tumor development by affecting on the immune cells.

1.11.7. Autonomic neurotransmitters modulate tumor progression

Neurotransmitters produced by peripheral and autonomic fibers are considered as the key modulators of tumor microenvironment. In addition to regulating immune responses, neurotransmitters can directly affect tumor progression. Based on their structure, neurotransmitters are classified into different groups: 1) amino acids, including acetylcholine (ACh) and glutamate; 2) biogenic amines, such as dopamine, norepinephrine (NE) and epinephrine (E); 3) peptidergic neuropeptides such as SP and CGRP³⁰⁴. Interaction of neurotransmitters with their receptors on tumor cells can activate several processes related to tumor progression.

Catecholamines, including E and NE, released by sympathetic fibers act through α - and β -adrenergic receptors on tumor cells that support proliferation, survival, invasion, and metastasis of tumor cells. NE can modulate the metabolism of endothelial cells, limit oxidative phosphorylation, and elevate angiogenesis to assist cancer development^{305,306}. One of the main mechanisms by which E and NE contribute to tumor growth is through the activation of β -adrenergic receptor.

This consequently upregulates the expression of vascular endothelial growth factor (VEGF), metalloproteases 2 (MMP2) and MMP9, which mediate angiogenesis and metastasis of breast, ovarian and lung cancer³⁰⁷. Conversely, dopamine is able to suppress signaling pathways by VEGF receptor and reduce tumor development in a mouse model of colon cancer³⁰⁷.

1.11.8. Sensory neuron activity supports tumor development

Neuropeptides released by sensory fibers can also contribute to tumor progression. SP neuropeptide mainly acts through neurokinin-1 (NK-1) receptor and their interaction is widely involved in the proliferation, survival, invasion, and metastasis of several cancer types, including melanoma, colon, pancreatic, gastric, and lung carcinoma^{308,309}. Several studies showed that pharmacological blockade of NK1 receptor is associated with anti-tumor effects^{310,309}.

NPY is another neuropeptide released by the sensory nerve which not only contributes to tumor growth and dissemination but also potentially assists with metastasis and resistance of cancer cells to chemotherapy³¹¹.

Given the vast research efforts on deciphering the pathways by which neuropeptides and neurotransmitters regulate oncogenic processes, there is still a need to uncover more exact mechanisms. Indeed, the available evidence support the strong potential of neuropeptides and their receptors as therapeutic targets in oncology.

Chapter 2: Rationale, hypothesis, and research objectives

Nervous and immune systems mostly function in an integrated and coordinated fashion to protect the host from possible threats and maintain homeostasis. However, the modulating roles of these systems are largely unknown in cancer. These systems communicate through cell surface G protein-coupled receptors (GPCRs) and receptor tyrosine kinases, that allow them to respond to the signals each one produces. Furthermore, they reciprocally communicate through neuropeptides, cytokines, and growth factors, which unexpectedly cooperate with pathogenesis. As an example of sensory neurons regulation of the immune system, it has been shown that bacteria can directly activate peripheral sensory neurons that induce pain. Skin nociceptors, in turn, locally release neuropeptides which restrict the activation of immune cells, suggesting the capacity of bacteria to modulate nociceptor neuron functions to decline immune defences and facilitate their survival. Nociceptor-released neuropeptides can also influence polarization, chemotaxis and adaptive immune system function. Since skin nociceptors locally secrete neuropeptides, which dampen immune cell activation, **we hypothesized that tumor-innervating nociceptors might release neuropeptides resulting in CD8⁺ T cell exhaustion and tumor growth.** Since the skin is richly innervated with nociceptors, we used the mouse model of melanoma cancer to test this hypothesis.

We aimed to: i) define the impacts of B16F10 melanoma cancer cells on nociceptor neuron function; ii) determine the impact of nociceptor-released neuropeptides on cytotoxic T lymphocyte; iii) assess the role of nociceptor neurons in controlling *in vivo* anti-tumor responses.

We found that malignant B16F10 skin cancer cells communicate with nociceptors to increase neurite outgrowth, responsiveness to noxious ligands, and neuropeptide release. Consecutively, neuropeptide calcitonin gene-related peptide (CGRP), which is released by nociceptors, directly enhanced the exhaustion of cytotoxic CD8⁺ T cells and reduced their ability to eliminate melanoma cells. Moreover, treatment of sensory neuron-depleted mice with recombinant CGRP rescued the exhaustion of CD8⁺ T cells. Genetic ablation of TRPV1 neurons, local pharmacological silencing or blocking the secretion of neuropeptides, and application of CGRP receptor (RAMP1) antagonist, all diminished the exhaustion of tumor infiltrating CD8⁺ T cells as well as tumor growth.

Furthermore, compared with wild-type cells, RAMP1^{-/-} CD8⁺ T cells were rescued from exhaustion when co-transplanted into tumor-bearing Rag1^{-/-} deficient mice. Together, decreasing CGRP release by local silencing of tumor-associated nociceptors, limits the immunomodulatory effects of CGRP on cytotoxic CD8⁺ T cells and represents an ideal strategy to protect anti-tumor immunity.

Authors contribution

Mohammad Balood, Maryam Ahmadi, Tuany Eichwald, Jacques Thibodeau, Moutih Rafei, Clifford J. Woolf, and Sebastien Talbot designed the study.

Maryam Ahmadi, Mohammad Balood, Tuany Eichwald, Ali Ahmadi, Abdelilah Majdoubi, Karine Roversi, Katiane Roversi and Sebastien Talbot conducted the experiments.

Maryam Ahmadi, Mohammad Balood, Paola D. Vermeer, Clifford J. Woolf and Sebastien Talbot wrote the manuscript with input from all authors.

Maryam Ahmadi performed the experiments in Figs. 1d,e, 2a,b, 3a–c, 4a–d and 5a and Extended Data Figs. 4a–c,e, 5a–e,h–j, 6l–n, 7g,o,p, 8g,j,k,s,t and 10e,g.

Mohammad Balood performed the experiments in Figs. 1d,e, 2a,b, 3a,b,d,e,h, 4a,b,e and 5a–c and Extended Data Figs. 4e, 5a–e, 6a–g,k,q, 7a–f,h–n, 8a–e,l–r, 9 and 10a–f,h–w.

Tuany Eichwald performed the experiments in Fig. 2c–f and Extended Data Fig. 5f–j and did the in silico analysis for Fig. 5d,e and Extended Data Figs. 1a–d, 3 and 11.

Ali Ahmadi performed the experiments in Fig. 3g,h and Extended Data Figs. 6o and 9.

Abdelilah Majdoubi performed the experiments in Fig. 3f.

Karine Roversi performed the experiments in Fig. 3a and Extended Data Fig. 6c–g,p.

Katiane Roversi performed the experiments in Fig. 3a.

Siyi Huang generated Fig. 1a.

Anthony C. Restaino performed the experiments in Extended Data Figs. 2a–g.

Nociceptor neurons affect cancer immunosurveillance


<https://doi.org/10.1038/s41586-022-05374-w>

Received: 9 June 2021

Accepted: 21 September 2022

Published online: 2 November 2022

Open access

 Check for updates

Mohammad Balood^{1,2,13}, Maryam Ahmadi^{1,13}, Tuany Eichwald^{1,3}, Ali Ahmadi¹, Abdelilah Majdoubi⁴, Karine Roversi¹, Katiane Roversi¹, Christopher T. Lucido⁵, Anthony C. Restaino⁵, Siyi Huang⁶, Lexiang Ji⁶, Kai-Chih Huang⁶, Elise Semerena¹, Sini C. Thomas¹, Alexandro E. Trevino^{7,8}, Hannah Merrison^{7,8}, Alexandre Parrin^{7,8}, Benjamin Doyle^{7,8}, Daniel W. Vermeer⁵, William C. Spanos⁵, Caitlin S. Williamson⁵, Corey R. Seehus^{7,8}, Simmie L. Foster⁹, Hongyue Dai⁶, Chengyi J. Shu⁶, Manu Rangachari², Jacques Thibodeau⁴, Sonia V. Del Rincon¹⁰, Ronny Drapkin¹¹, Moutih Rafei¹, Nader Ghasemlou¹², Paola D. Vermeer⁵, Clifford J. Woolf^{7,8} & Sebastien Talbot^{1,12}✉

Solid tumours are innervated by nerve fibres that arise from the autonomic and sensory peripheral nervous systems^{1–5}. Whether the neo-innervation of tumours by pain-initiating sensory neurons affects cancer immunosurveillance remains unclear. Here we show that melanoma cells interact with nociceptor neurons, leading to increases in their neurite outgrowth, responsiveness to noxious ligands and neuropeptide release. Calcitonin gene-related peptide (CGRP)—one such nociceptor-produced neuropeptide—directly increases the exhaustion of cytotoxic CD8⁺ T cells, which limits their capacity to eliminate melanoma. Genetic ablation of the TRPV1 lineage, local pharmacological silencing of nociceptors and antagonism of the CGRP receptor RAMP1 all reduced the exhaustion of tumour-infiltrating leukocytes and decreased the growth of tumours, nearly tripling the survival rate of mice that were inoculated with B16F10 melanoma cells. Conversely, CD8⁺ T cell exhaustion was rescued in sensory-neuron-depleted mice that were treated with local recombinant CGRP. As compared with wild-type CD8⁺ T cells, *Ramp1*^{-/-} CD8⁺ T cells were protected against exhaustion when co-transplanted into tumour-bearing *Rag1*-deficient mice. Single-cell RNA sequencing of biopsies from patients with melanoma revealed that intratumoral *RAMP1*-expressing CD8⁺ T cells were more exhausted than their *RAMP1*-negative counterparts, whereas overexpression of *RAMP1* correlated with a poorer clinical prognosis. Overall, our results suggest that reducing the release of CGRP from tumour-innervating nociceptors could be a strategy to improve anti-tumour immunity by eliminating the immunomodulatory effects of CGRP on cytotoxic CD8⁺ T cells.

Cytotoxic T cells express a variety of receptors, including PD-1 (programmed cell death protein 1), LAG3 (lymphocyte activation gene-3 protein) and TIM3 (T cell immunoglobulin and mucin domain-containing protein 3)^{6–8}, which inhibit the function of T cells after being activated by their cognate ligands. These checkpoint receptors ensure that immune responses to damage or infection are kept in check, thus preventing overly intense responses that might damage healthy cells⁹. Tumour cells express ligands for these immune checkpoints, which, when activated, block the cytolytic functions of T cells, thereby favouring the survival of cancer cells^{9,10}.

In prostate cancer, doublecortin-expressing neural progenitors initiate autonomic adrenergic neurogenesis³, which facilitates the development and dissemination of tumours². In head and neck tumours, a loss of TP53 drives the reprogramming of tumour-innervating sensory nerves into adrenergic neurons that promote tumour growth¹. The presence of such neo-innervation in cancer, together with the diverse actions of neuropeptides on immune cells^{11–18}, led us to examine whether the local release of neuropeptides from activated nociceptors could favour cancer growth by suppressing immune surveillance.

¹Département de Pharmacologie et Physiologie, Université de Montréal, Montréal, Quebec, Canada. ²Département de Médecine Moléculaire, Faculté de Médecine, Université Laval, Québec, Quebec, Canada. ³Departamento de Bioquímica, Universidade Federal de Santa Catarina, Florianópolis, Brazil. ⁴Département de Microbiologie, Infectiologie et Immunologie, Université de Montréal, Montréal, Quebec, Canada. ⁵Cancer Biology and Immunotherapies, Sanford Research, Sioux Falls, SD, USA. ⁶Cygnal Therapeutics, Cambridge, MA, USA. ⁷F.M. Kirby Neurobiology Center, Boston Children's Hospital, Boston, MA, USA. ⁸Department of Neurobiology, Harvard Medical School, Boston, MA, USA. ⁹Depression Clinical Research Program, Massachusetts General Hospital, Boston, MA, USA. ¹⁰Department of Oncology, McGill University, Montréal, Quebec, Canada. ¹¹Penn Ovarian Cancer Research Center, Perelman School of Medicine, University of Pennsylvania, Philadelphia, PA, USA. ¹²Department of Biomedical and Molecular Sciences, Queen's University, Kingston, Ontario, Canada. ¹³These authors contributed equally: Mohammad Balood, Maryam Ahmadi. ✉e-mail: sebastien.talbot@queensu.ca

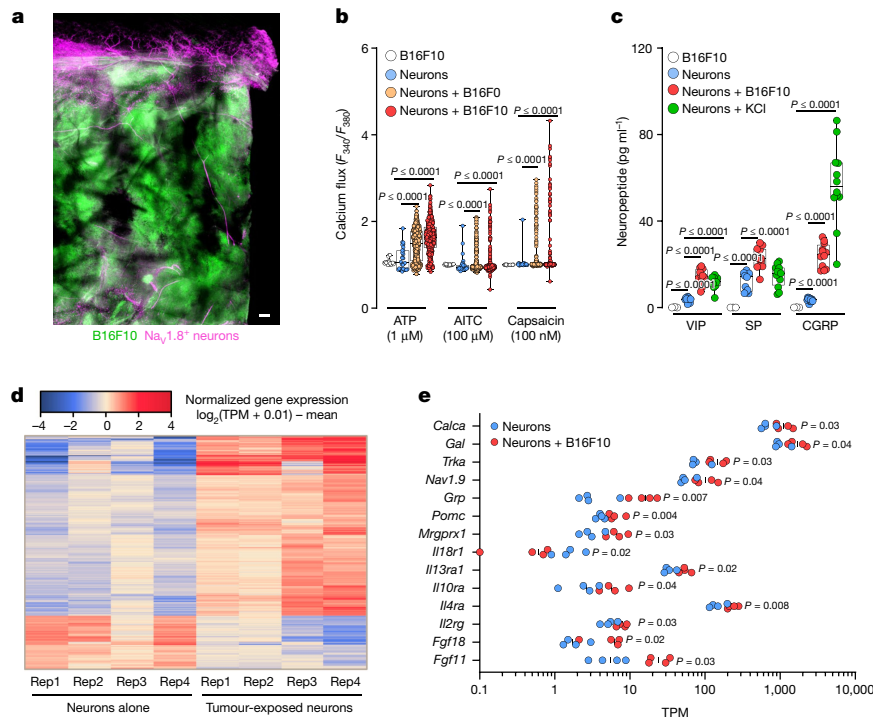


Fig. 1 | Melanoma cells sensitize nociceptors. **a**, Nociceptor (*Nav1.8^{Cre}::tdTomato^{fl/wt}*; magenta) reporter mice were inoculated in the hindpaw with B16F10-eGFP cancer cells (i.d., 2×10^5 cells; green). Representative image of $Na_v1.8^+$ nerve fibres (magenta) innervating B16F10-eGFP-inoculated mouse skin after 22 days. Scale bar, 200 μ m. **b**, In co-culture, B16F0 or B16F10 cells sensitize the response of nociceptors to capsaicin (100 nM), allyl isothiocyanate (AITC, 100 μ M) and ATP (1 μ M), as measured by calcium flux. A low concentration of the ligands induces a minimal response in control neurons, whereas B16F10 cells show marginal sensitivity to ATP. **c**, Dorsal root ganglion (DRG) neurons co-cultured (96 h) with B16F10 cells release substance P (SP), vasoactive intestinal peptide (VIP) and CGRP. B16F10 cells alone do not release neuropeptides. Stimulation with KCl (40 mM; 30 min) induced a significant release of neuropeptides from cultured neurons. **d, e**, Naive DRG neurons (*Trpv1^{Cre}::Cheriff-eGFP^{fl/wt}*) were cultured alone or in combination with B16F10-mCherry-OVA cells. After 48 h, the cells were collected, FACS purified and RNA sequenced. Hierarchical

clustering of DEGs from the sorted neurons shows distinct groups of transcripts enriched in cancer-exposed TRPV1⁺ neurons (**d**), including *Calca* (the gene encoding CGRP; **e**). Data are shown as a representative image (**a**), as box-and-whisker plots (running from minimal to maximal values; the box extends from 25th to 75th percentile and the middle line indicates the median), for which individual data points are given (**b, c**), as a heat map showing normalized gene expression ($\log_2(0.01 + \text{transcripts per million reads (TPM)}) - \text{mean}$) (**d**) or as a scatter dot plot with medians (**e**). Experiments were independently repeated two (**a**) or three (**b, c**) times with similar results. The sequencing experiment was not repeated (**d, e**). *n* as follows: **a**: *n* = 4; **b**: neurons (29 neurons from 10 mice), B16F10 (16 cells from 10 dishes), neurons + B16F0 (387 neurons from 12 mice), neurons + B16F10 (409 neurons from 12 mice); **c**: neurons (*n* = 12), neurons + B16F10 (*n* = 12), neurons + KCl (*n* = 12), B16F10 (*n* = 3); **d, e**: *n* = 4 per group. *P* values were determined by one-way ANOVA with post-hoc Bonferroni (**b, c**) or two-sided unpaired Student's *t*-test (**e**).

Melanomas are innervated

Although the expression of genes of neuronal origin is not detected by RNA-sequencing approaches in human malignant cells or immune cells (Extended Data Fig. 1a–c), we observed a significant increase in their expression in biopsies from patients with melanoma^{19–22} (Extended Data Fig. 1d). As these clinical data suggested increased innervation of melanomas, we tested for the presence of nociceptor neurons by assessing TRPV1⁺ neurons in biopsies from patients with melanoma. TRPV1 immunolabelling was increased by around twofold in the tumour compared to adjacent healthy tissue in each of the ten biopsies examined. The numbers of tumour-infiltrating lymphocytes (TILs) correlated ($R^2 = 0.63$) with increased TRPV1 immunolabelling (Extended Data Fig. 2). These data indicate that melanomas are innervated by sensory neurons and that these neurons may affect the intratumoral numbers of immune cells.

To investigate this in more detail, we inoculated a GFP-expressing melanoma (B16F10-eGFP) cell line into *Nav1.8^{Cre}::tdTomato^{fl/wt}* mice (*Nav1.8* is also known as *Scn10a*). Twenty-two days after implantation, we found abundant $Na_v1.8^+$ nociceptor neurons around and within the tumour (Fig. 1a). RNA sequencing of samples from B16F10-bearing mice revealed that malignant and melanoma-infiltrating immune cells had

no detectable levels of neuronal markers (*Nav1.8* or *Trpv1*), indicating that the $Na_v1.8$ signal could be ascribed to tumour-infiltrating nerves (Extended Data Fig. 3). We next used an in vitro co-culture approach to assess whether malignant cells modulate the function of nociceptor neurons. When co-cultured, TRPV1⁺ nociceptors directly extended neurites towards the B16F10-eGFP melanoma cells, and the average length of neurites increased, whereas the overall neuronal arborization or branching decreased (Extended Data Fig. 4a–c). Together, these data indicate that nociceptor outgrowth is enhanced when in proximity to melanoma cells and that skin sensory neuron collaterals sprout directly into the tumour bed. Such tumour neo-innervation may be akin to cancer's neoangiogenesis.

Melanoma cells sensitize nociceptors

Given that melanoma promotes axonogenesis, leading to tumour innervation (Fig. 1a and Extended Data Fig. 2), we examined whether this physical proximity allows melanomas to modulate the sensitivity of the nociceptor. As nociceptor neurons detect signals from the local environment, we measured changes in calcium flux in response to sub-threshold concentrations of various noxious ligands. When nociceptors were cultured without melanoma cells, few responded

to the ligands at the concentrations selected. However, the number of responsive neurons increased when they were co-cultured with B16F10 cells (Fig. 1b). Similarly, the amplitude of calcium flux responses to the ligands was greater in lumbar DRG neurons (L3–L5) that were collected ipsilateral to a 14-day tumour inoculation in mice, as compared to those collected from mice that were injected with non-tumorigenic keratinocytes (Extended Data Fig. 4d). Signals released from melanoma, therefore, heighten nociceptor sensitivity.

We next tested whether this neuronal hypersensitivity would lead to an increased release of immunomodulatory neuropeptides. In contrast to B16F10 cells alone, DRG neurons co-cultured with B16F10 cells (5×10^4 cells, 96 h) actively release CGRP in the medium (Fig. 1c). These data prompted us to test whether exposure to melanoma alters the transcriptome of nociceptor neurons. To do so, we cultured naive DRG neurons (*Trpv1^{cre}::CheRiff-eGFP^{R/WT}*) alone or in combination with B16F10-mCherry-OVA cells. After 48 h, TRPV1⁺ nociceptors were purified by fluorescence-activated cell sorting (FACS) and RNA sequenced. Differentially expressed genes (DEGs) were calculated, and *Calca*—the gene that encodes CGRP—and the NGF receptor *Trka* (also known as *Ntrk1*) were found to be overexpressed in nociceptors that were exposed to cancer (Fig. 1d–e and Extended Data Fig. 4e). Overexpression of *Trka* may help to drive melanoma-induced hypersensitivity to pain, whereas CGRP, when released from activated nociceptors, may immunomodulate TILs.

To identify the mechanism through which melanoma sensitizes nociceptor neurons, we used a co-culture system designed to mimic the interactions that take place in the melanoma microenvironment. Type 1 (T₁)—stimulated (ex-vivo-activated by CD3 and CD28, IL-12 and anti-IL-4 for 48 h) OVA-specific cytotoxic CD8⁺ T cells (OT-I mice), naive DRG neurons (*Trpv1^{cre}::CheRiff-eGFP^{R/WT}*) and B16F10-mCherry-OVA melanoma cancer cells were cultured alone or in combination. After 48 h, the cells were collected, purified by FACS and RNA sequenced, and DEGs were calculated. Among others, we found that *Slpi* (secretory leukocyte protease inhibitor) was overexpressed in the melanoma cancer cells when co-cultured with either DRG neurons (around 3.6-fold) or OVA-specific cytotoxic CD8⁺ T cells (around 270-fold), and when exposed to both populations (around 150-fold) (Fig. 2a,b and Extended Data Fig. 5a–e). We also found that B16F10-mCherry-OVA cells, when co-cultured with naive DRG neurons and OVA-specific cytotoxic CD8⁺ T cells, increased the secretion of SLPI into the culture medium, with this effect being maximal after 48 h (around 200-fold; Fig. 2c).

In addition to protecting epithelial cells from the activity of serine proteases, SLPI enhances the regeneration of transected retinal ganglion cell axons²³ and the proliferation of neural stem cells²⁴. Although these data provide evidence of the effect of SLPI on neurons, its role in nociception is unclear. To address this, we measured whether SLPI directly activates cultured DRG neurons using calcium microscopy. We found that SLPI (0.01–10 ng ml⁻¹) activates around 20% of DRG neurons and that—consistent with these neurons being nociceptors—SLPI-sensitive neurons were mostly small (with a mean area of 151 μm²) capsaicin-responsive (around 90%) neurons (Fig. 2d,e and Extended Data Fig. 5f–i). Given that SLPI triggered calcium influx, we investigated whether this is the means by which B16F10 cells drive the release of CGRP from neurons (Fig. 1c). SLPI, when used at a concentration similar to that secreted by melanoma cells (Fig. 2c), induced the release of CGRP from cultured naive DRG neurons (Fig. 2f). Finally, we sought to test whether SLPI can drive pain hypersensitivity in vivo. When administered into the right hindpaw of naive mice, SLPI generated transient thermal hypersensitivity (Extended Data Fig. 5j).

Melanoma-secreted SLPI acts on nociceptors to trigger calcium influx, neuropeptide release and thermal hypersensitivity, which indicates that these sensory neurons detect and react to the presence of cancer cells. Whether this gives the malignant cells a functional advantage over the host cells remains unknown. To assess this, we implanted B16F10-mCherry-OVA cells (intradermally (i.d.), 2×10^5 cells) into the hindpaw of eight-week-old

male and female mice. We found that mice with larger tumours had a higher proportion of intratumoral PD-1⁺LAG3⁺TIM3⁺ CD8⁺ T cells and greater hypersensitivity to thermal pain (not shown). Notably, heightened sensitivity to thermal pain positively correlated ($n = 60$; $R^2 = 0.55$, $P < 0.0001$) with increased frequency in intratumoral PD-1⁺LAG3⁺TIM3⁺ CD8⁺ T cells (Fig. 3a; measured on day 13 after implantation).

Melanoma-innervating nociceptors control tumour growth

The expression of adrenergic and cholinergic axon markers in tumours correlates with poor clinical outcome². Gastric tumour denervation limits growth and patients who have undergone vagotomy have lower rates of mortality from intestinal cancer^{16,25,26}. To investigate the nature of the three-way interaction between cancer, nociceptors and CD8⁺ T cells, we next used a syngeneic mouse model of triple-negative melanoma, which is an established model of immunosurveillance⁹. B16F10-mCherry-OVA cells were inoculated (i.d., 5×10^5 cells) into eight-week-old male and female nociceptor-ablated (*Trpv1^{cre}::DTA^{R/WT}*) or intact (littermate control; *Trpv1^{WT}::DTA^{R/WT}*) mice. In nociceptor-ablated male and female mice, the median length of survival increased by 2.5-fold (evaluated until day 22; Fig. 3b). In another set of mice that were analysed 16 days after tumour inoculation, we found that genetic ablation of nociceptors reduced tumour growth (Fig. 3c). In addition, nociceptor-ablated mice showed an increase in the total number and relative frequency of cytotoxic (IFN γ ⁺, TNF⁺ or IL-2⁺) tumour-infiltrating CD8⁺ T cells, but a reduced proportion of PD-1⁺LAG3⁺TIM3⁺ CD8⁺ T cells (Fig. 3d,e and Extended Data Fig. 6a,b).

Up to this point, our data suggest that nociceptor neurons are an upstream driver of intratumoral PD-1⁺LAG3⁺TIM3⁺ CD8⁺ T cells. To assess whether this is indeed the case, we mapped out the kinetics of thermal pain hypersensitivity, increased frequency in intratumoral PD-1⁺LAG3⁺TIM3⁺ CD8⁺ T cells and tumour growth. When compared to their baseline threshold and to that of sensory-neuron-ablated mice (*Trpv1^{cre}::DTA^{R/WT}*; $n = 19$), eight-week-old littermate control mice (*Trpv1^{WT}::DTA^{R/WT}*; $n = 96$) that were inoculated with B16F10-mCherry-OVA (left hindpaw, i.d., 2×10^5 cells) showed significant thermal hypersensitivity on day 7, an effect that peaked on day 21 (Extended Data Fig. 6c). In these mice, the intratumoral frequency of PD-1⁺LAG3⁺TIM3⁺ (Extended Data Fig. 6d) or IFN γ ⁺ (Extended Data Fig. 6e) CD8⁺ T cells was significantly increased 12 days after tumour inoculation and peaked on day 19. Finally, B16F10-mCherry-OVA tumour volume peaked on day 22 (Extended Data Fig. 6f). Altogether, these data show that thermal hypersensitivity precedes any significant exhaustion of intratumoral CD8⁺ T cells by around five days and that pain hypersensitivity develops before the tumour is measurable using a digital caliper (Extended Data Fig. 6g).

Blocking the activity of immune checkpoint proteins releases a cancer-cell-induced ‘brake’ on the immune system, thereby increasing its ability to eliminate tumours^{6–10}. Immune checkpoint inhibitors (ICIs), including those that target PD-L1, improve clinical outcomes in patients with metastatic melanoma⁸; however, the efficacy of ICIs varies considerably among patients, half of whom will not benefit²⁷. We set out to assess whether the presence (*Trpv1^{WT}::DTA^{R/WT}*) or absence (*Trpv1^{cre}::DTA^{R/WT}*) of tumour-innervating nociceptor neurons would affect responsiveness to treatment with anti-PD-L1. Anti-PD-L1 (intraperitoneally (i.p.), days 7, 10, 13 and 16) was given either to mice whose tumour cells (B16F10-mCherry-OVA, i.d., 5×10^5 cells) were inoculated on the same day, or to mice with established tumours (around 85 mm³; achieved by inoculating *Trpv1^{cre}::DTA^{R/WT}* around 3 days before). In both scenarios, ablation of nociceptors increased the anti-PD-L1-mediated reduction in tumours and the infiltration of tumour-specific CD8⁺ T cells (Extended Data Fig. 6h–k).

To test whether the reduction in tumour growth that was observed in the absence of nociceptor neurons depends on their action on

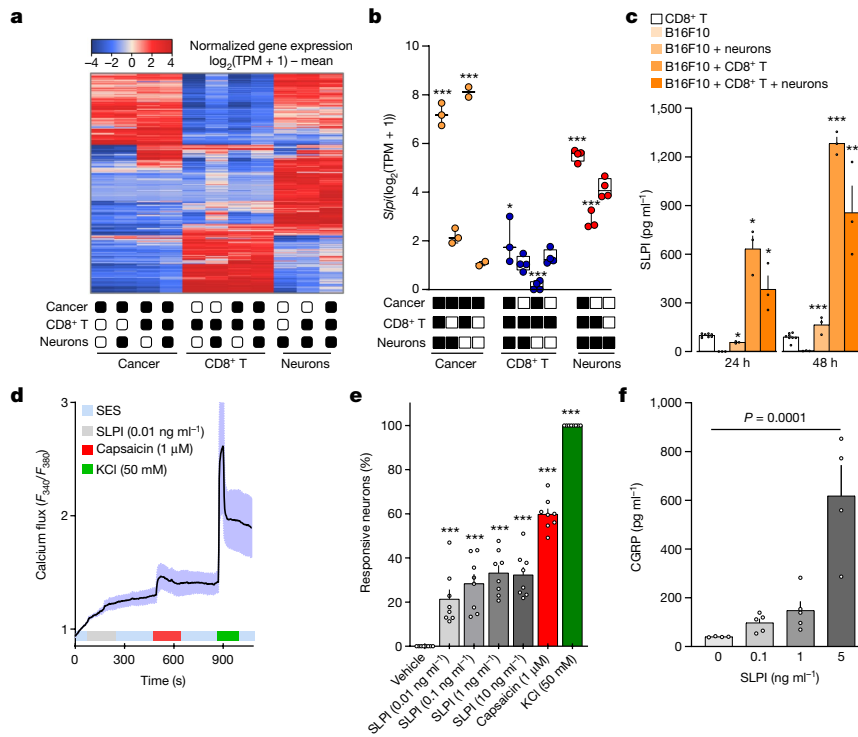


Fig. 2 | Cancer-secreted SLPI drives the release of CGRP by nociceptor neurons. **a–c**, Naive DRG neurons (*Trpv1^{cre}::CheRiff-eGFP^{fl/wt}*), B16F10-mCherry-OVA cells and OVA-specific cytotoxic CD8⁺ T cells were cultured alone or in combination. After 48 h, the cells were collected, FACS purified and RNA sequenced. **a**, Hierarchical clustering of sorted neuron molecular profiles depicts distinct groups of transcripts enriched in each group. **b**, DEGs were calculated, and *Slpi* was found to be overexpressed in cancer cells when co-cultured with OVA-specific cytotoxic CD8⁺ T cells, DRG neurons or both populations. **c**, SLPI is secreted by B16F10-mCherry-OVA cells when co-cultured (24 h or 48 h) with naive DRG neurons and OVA-specific cytotoxic CD8⁺ T cells, with a maximal effect after 48 h. **d–f**, Using calcium microscopy, we found that

SLPI (10 pg ml⁻¹–10 ng ml⁻¹) activated around 20% of cultured naive DRG neurons (**d,e**). Activation of cultured neurons (3 h) with SLPI also leads to significant release of CGRP (**f**). Data are shown as a heat map showing normalized gene expression ($\log_2(1 + \text{TPM}) - \text{mean}$) (**a**), as box-and-whiskers plots (as defined in Fig. 1b,c) (**b**) or as mean \pm s.e.m. (**c–f**). *n* as follows: **a,b**: *n* = 2–4 per groups; **c**: *n* = 3 for all groups except CD8⁺ T cells (*n* = 8); **d**: *n* = 17; **e**: *n* = 8 per group; **f**: 0 ng ml⁻¹ (*n* = 4), 0.1 ng ml⁻¹ (*n* = 5), 1 ng ml⁻¹ (*n* = 5), 5 ng ml⁻¹ (*n* = 4). Experiments in **c–f** were independently repeated three times with similar results. The sequencing experiment was not repeated (**a,b**). *P* values were determined by one-way ANOVA with post-hoc Bonferroni (**b,e,f**) or two-sided unpaired Student's *t*-test (**c**). **P* \leq 0.05, ***P* \leq 0.01, and ****P* \leq 0.001.

immune cells, we compared the respective effects of nociceptors on the growth of an immunogenic and a non-immunogenic isogenic melanoma model. YUMMER1.7 is a highly immunogenic derivative of the *Braf^{V600E}Cdkn2a^{-/-}Pten^{-/-}* cell line modified by ultraviolet (UV) exposure, and provides a clinically relevant model of melanoma²⁸. As in the case of B16F10-OVA, ablation of nociceptors decreased the growth of tumours (Extended Data Fig. 6l) and reduced their frequency in intratumoral PD-1⁺LAG3⁺TIM3⁺ CD8 T cells, while increasing their number and cytotoxic potential (IFN γ ⁺ or TNF⁺; not shown). By contrast, YUMM1.7 (the parental and non-immunogenic²⁹ counterpart of YUMMER1.7) showed similar tumour growth (Extended Data Fig. 6m) and a similar frequency of intratumoral PD-1⁺LAG3⁺TIM3⁺ CD8⁺ T cells in both the presence and the absence of nociceptors (not shown).

Next, we assessed whether these differences were due to nociceptor neurons directly modulating intratumoral T cells. We observed no major changes in tumour growth between nociceptor-intact and nociceptor-ablated mice after systemic depletion of CD8⁺ (Fig. 3f) or CD3⁺ (Extended Data Fig. 6n) T cells. Although chemoablation of nociceptor neurons with resiniferatoxin (RTX) reduced tumour growth in B16F10-inoculated wild-type mice (Extended Data Fig. 6o), we found that naive OT-ICD8⁺ T cells enhanced tumour shrinkage when transplanted in RTX-exposed *Rag1^{-/-}* mice (Fig. 3g). In doing so, the chemoablation of nociceptor neurons shielded the naive OT-ICD8⁺ T cells from undergoing exhaustion (Fig. 3h). These data imply that the

slower tumour growth found in *Trpv1^{cre}::DTA^{fl/wt}* and RTX-exposed mice depends on the modulation of CD8⁺ T cells by nociceptors.

Optogenetic activation of skin nociceptor neurons triggers the antidromic release of neuropeptides that mediate anticipatory immunity against microorganisms³⁰ and potentiate skin immunity³¹. We used transdermal illumination to stimulate tumour-innervating Na_v1.8⁺ channelrhodopsin-expressing neurons (*Nav1.8^{cre}::ChR2^{fl/wt}*). Daily stimulation with blue light enhanced the growth of B16F10 when exposure began in mice bearing visible (around 20 mm³) or well-established (around 200 mm³) tumours (Extended Data Fig. 6p). This increase in tumour volume was also linked to an increase in the intratumoral levels of CGRP, confirming the engagement of pain-transmitting neurons (Extended Data Fig. 6q). Laser exposure had no effect on tumour growth in light-insensitive mice (*Nav1.8^{wt}::ChR2^{fl/wt}*; not shown).

The neonatal or embryonic ablation of neuronal subsets may lead to compensatory changes. To circumvent this possibility, we silenced neurons using botulinum neurotoxin A (BoNT/A), a neurotoxic protein produced by *Clostridium botulinum*, which acts by cleaving SNAP25 (ref. 32). BoNT/A causes a long-lasting (20 days) abolition of neurotransmitter release from skin-innervating neurons³³. BoNT/A reduces tumour growth in prostate cancer² and blocks nociceptor-mediated modulation of neutrophils during skin infection³³. BoNT/A does not affect the function of cultured B16F10 or CD8⁺ T cells in vitro (Extended Data Fig. 7a–f). When BoNT/A (25 pg μ l⁻¹, 50 μ l, five i.d. sites) was administered one and three days before the B16F10-OVA cell inoculation, it reduced

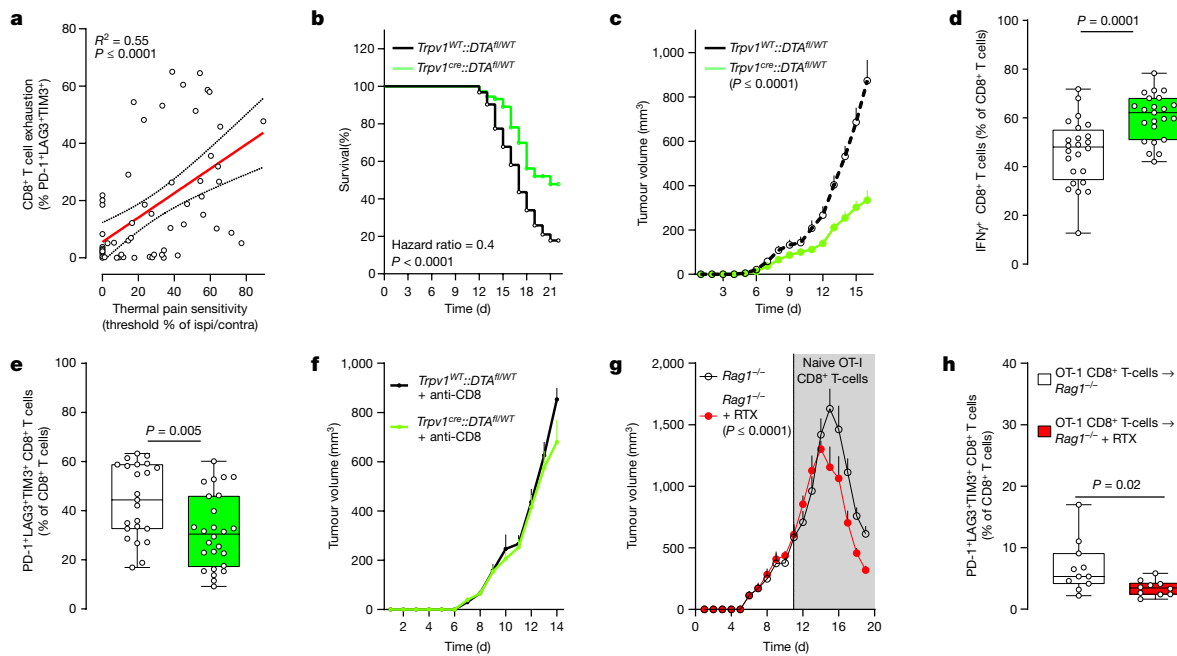


Fig. 3 | Genetic ablation of nociceptors safeguards anti-tumour immunity. **a**, Orthotopic B16F10-mCherry-OVA cells (2×10^5 cells, i.d.) were injected into the left hindpaw of wild-type mice. As measured on day 13 after tumour inoculation, intratumoral CD8⁺ T cell exhaustion positively correlated with thermal hypersensitivity ($R^2 = 0.55$, $P \leq 0.0001$). The thermal pain hypersensitivity represents the withdrawal latency ratio of the ipsilateral paw (tumour-inoculated) to the contralateral paw. **b**, Orthotopic B16F10-mCherry-OVA (5×10^5 cells, i.d.) were inoculated into the flank of eight-week-old male and female mice with sensory neurons intact (*Trpv1*^{WT}::*DTA*^{fl/WT}) or ablated (*Trpv1*^{Cre}::*DTA*^{fl/WT}). The median length of survival was increased by around 250% in nociceptor-ablated mice (measured until 22 days after inoculation). **c–f**, Sixteen days after tumour inoculation, sensory-neuron-ablated mice have reduced tumour growth (**c**) and increased tumour infiltration of IFN γ ⁺ CD8⁺ T cells (**d**), and the proportion of PD-1⁺LAG3⁺TIM3⁺ CD8⁺ T cells is decreased (**e**). This reduction in B16F10-mCherry-OVA (5×10^5 cells, i.d.) tumour volume was absent in nociceptor-ablated mice whose CD8⁺ T cells were systemically depleted (**f**; assessed until day 14; anti-CD8, 200 μ g per mouse, i.p., every 3 days). **g, h**, To chemically

deplete their nociceptor neurons, *Rag1*^{-/-} mice were injected with RTX. Twenty-eight days later, the mice were inoculated with B16F10-mCherry-OVA (5×10^5 cells, i.d.). RTX-injected mice that were adoptively transferred with naive OVA-specific CD8⁺ T cells (i.v., 1×10^6 cells, when tumour reached around 500 mm³) showed reduced tumour growth (**g**; assessed until day 19) and exhaustion (**h**) compared to vehicle-exposed *Rag1*^{-/-} mice. Data are shown as a linear regression analysis \pm s.e. (**a**), as a Mantel–Cox regression (**b**), as mean \pm s.e.m. (**c, f, g**) or as box-and-whisker plots (as defined in Fig. 1b,c), for which individual data points are given (**d, e, h**). *n* as follows: **a**: *n* = 60; **b**: intact (*n* = 62), ablated (*n* = 73); **c**: intact (*n* = 20), ablated (*n* = 25); **d**: intact (*n* = 24), ablated (*n* = 23); **e**: intact (*n* = 23), ablated (*n* = 26); **f**: intact + anti-CD8 (*n* = 10), ablated + anti-CD8 (*n* = 8); **g**: vehicle (*n* = 12), RTX (*n* = 10); **h**: vehicle (*n* = 11), RTX (*n* = 10). Experiments were independently repeated two (**a, f–h**) or six (**b–e**) times with similar results. *P* values were determined by simple linear regression analysis (**a**), Mantel–Cox regression (**b**), two-way ANOVA with post-hoc Bonferroni (**c, f, g**) or two-sided unpaired Student's *t*-test (**d, e, h**).

subsequent tumour growth and preserved the cytotoxic potential of intratumoral CD8⁺ T cells (Extended Data Fig. 7g–n; as measured 18 days after inoculation). Pre-treatment with BoNT/A also reduced the growth of YUMMER1.7 tumours and enhanced anti-PD-L1-mediated tumour regression (Extended Data Fig. 7o,p). When administered to mice with established tumours (around 200 mm³), BoNT/A had limited efficacy (Extended Data Fig. 7g–n). BoNT/A also did not affect tumour growth when given to mice in which TRPV1⁺ nociceptor neurons were genetically ablated (Extended Data Fig. 7o), which suggests that its anti-tumour effectiveness depends on the presence of tumour-innervating nociceptor neurons.

We next tested the anti-tumour efficacy of a proven nociceptor-selective silencing strategy³⁴. This protocol uses large-pore ion channels (TRPV1) as cell-specific drug-entry ports to deliver QX-314—a charged and membrane-impermeable form of lidocaine—to block voltage-gated sodium (Na_v) channels. During inflammation, similar to what we observed in tumour microenvironments, these large-pore ion channels open, which allows QX-314 to permeate the neurons and results in a long-lasting electrical blockade¹⁷. Although QX-314 did not affect cultured B16F10-mCherry-OVA cells or CD8⁺ T cell function in vitro (Extended Data Fig. 8a–f), we confirmed that it silences tumour-innervating nociceptors in vivo, as shown by reduced B16F10-induced release of CGRP

and pain hypersensitivity (Extended Data Fig. 8g–i). We found that vehicle-exposed B16F10-mCherry-OVA-bearing mice succumbed at a 2.7-fold higher rate ($P \leq 0.02$) than QX-314-exposed mice (Extended Data Fig. 8j; measured until day 19). As observed 17 days after tumour inoculation, QX-314-mediated silencing of sensory neurons (0.3%; daily i.d., surrounding the tumour) reduced melanoma growth and limited the exhaustion of intratumoral CD8⁺ T cells (Extended Data Fig. 8k–n). Nociceptor silencing also increased the intratumoral numbers of CD8⁺ T cells and preserved their cytotoxic potential (IFN γ ⁺ or TNF⁺) as well as their proliferative capacity (IL-2⁺; Extended Data Fig. 8o–r). Similar to what was observed in nociceptor-ablated mice (Extended Data Fig. 6j–j), silencing tumour-innervating neurons with QX-314 enhanced anti-PD-L1-mediated tumour regression (Extended Data Fig. 8s,t). When administered to mice with an established (around 200 mm³) B16F10-mCherry-OVA tumour, QX-314 still reduced tumour growth and preserved the anti-tumour capacity of CD8⁺ T cells (Extended Data Fig. 8k–r), suggesting that it could be used as a therapeutic agent in cancer.

CGRP attenuates the activity of RAMP1⁺ CD8⁺ T cells

In breast cancer, tumour-specific sympathetic denervation downregulates the expression of PD-L1, PD-1 and FOXP3 in TILs¹⁵. Human and

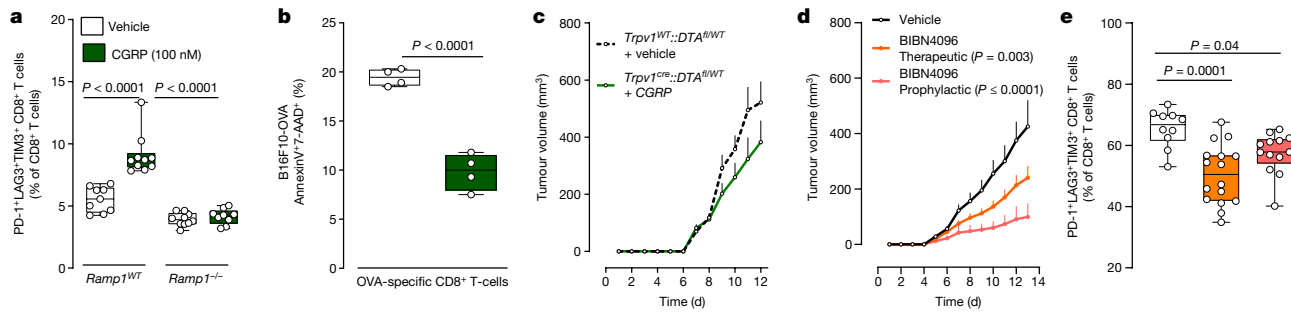


Fig. 4 | CGRP modulates the activation of CD8⁺ T cells. **a, b**, Splenocyte CD8⁺ T cells from wild-type (**a**), *Ramp1*^{-/-} (**a**) or naive OT-I (**b**) mice were cultured under T_{H1}-stimulating conditions (ex-vivo-activated by CD3 and CD28, IL-12 and anti-IL4) for 48 h to generate cytotoxic CD8⁺ T cells. In the presence of IL-2 (10 ng ml⁻¹), the cells were stimulated with CGRP (100 nM; challenged once every two days) for 96 h. Wild-type cytotoxic CD8⁺ T cells showed an increased proportion of PD-1⁺LAG3⁺TIM3⁺ cells; this effect was absent when treating cytotoxic CD8⁺ T cells that were collected from *Ramp1*^{-/-} mice (**a**). In co-culture (48 h), CGRP (100 nM; once daily) also reduced the ability of OT-I cytotoxic CD8⁺ T cells (4 × 10⁵ cells) to eliminate B16F10-mCherry-OVA cancer cells (**b**). **c**, Orthotopic B16F10-mCherry-OVA cells (5 × 10⁵ cells, i.d.) were inoculated into eight-week-old female mice with sensory neurons intact or ablated. In nociceptor-ablated mice, peritumour recombinant CGRP injection (100 nM, i.d., once daily) rescues B16F10 growth (assessed until day 12). **d, e**, Orthotopic B16F10-mCherry-OVA cells (5 × 10⁵ cells, i.d.) were inoculated into eight-week-old male and female mice. Starting one day after inoculation (defined as prophylactic),

the RAMP1 antagonist BIBN4096 (5 mg kg⁻¹) was administered systemically (i.p.) once every two days. In another group of mice, BIBN4096 (5 mg kg⁻¹, i.p., every two days) injections were started once the tumour reached a volume of around 200 mm³ (defined as therapeutic). Prophylactic or therapeutic BIBN4096 treatments decreased tumour growth (**d**) and reduced the proportion of intratumoural PD-1⁺LAG3⁺TIM3⁺ CD8⁺ T cells (**e**; assessed until day 13). Data are shown as box-and-whisker plots (as defined in Fig. 1b, c), for which individual data points are given (**a, b, e**), or as mean ± s.e.m. (**c, d**). *n* as follows: **a**: *Ramp1*^{WT} CD8⁺ + vehicle (*n* = 9), *Ramp1*^{WT} CD8⁺ + CGRP (*n* = 10), *Ramp1*^{-/-} CD8⁺ + vehicle (*n* = 10), *Ramp1*^{-/-} CD8⁺ + CGRP (*n* = 9); **b**: *n* = 4 per group; **c**: intact + vehicle (*n* = 15), ablated + CGRP (*n* = 11); **d**: vehicle (*n* = 13), BIBN prophylactic (*n* = 16), BIBN therapeutic (*n* = 18); **e**: vehicle (*n* = 10), BIBN prophylactic (*n* = 13), BIBN therapeutic (*n* = 16). Experiments were independently repeated three times with similar results. *P* values were determined by one-way ANOVA with post-hoc Bonferroni (**a, e**), two-sided unpaired Student's *t*-test (**b**) or two-way ANOVA with post-hoc Bonferroni (**c, d**).

mouse cytotoxic CD8⁺ T cells express multiple neuropeptide receptors (10 or more), including the CGRP receptor RAMP1 (Extended Data Figs. 1b and 3b). Given that nociceptors readily interact with CD8⁺ T cells in culture and that the neuropeptides they release block anti-bacterial immunity^{33,35–37}, we aimed to test whether these mediators drive the expression of immune checkpoint receptors in CD8⁺ T cells. First, splenocyte-isolated CD8⁺ T cells were cultured under type 1 (T_{H1}) CD8⁺ T cell-stimulating conditions for two days and then co-cultured with DRG neurons for an additional four days. We found that nociceptor stimulation with capsaicin increased the proportion of PD-1⁺LAG3⁺TIM3⁺-expressing CD8⁺ T cells but decreased the levels of IFNγ⁺, TNF⁺ and IL-2⁺. Capsaicin had no measurable effect on CD8⁺ T cells in the absence of DRG neurons (Extended Data Fig. 9a, b). When T_{H1}-activated CD8⁺ T cells were exposed to fresh conditioned medium (1:2 dilution) collected from KCl (50 mM)-stimulated DRG neurons, this treatment increased the proportion of PD-1⁺LAG3⁺TIM3⁺ cytotoxic CD8⁺ T cells and reduced that of IFNγ⁺ cells (Extended Data Fig. 9c, d; measured after four days of co-culture). These effects were prevented when the cytotoxic CD8⁺ T cells were challenged (1:2 dilution) with fresh KCl-induced conditioned medium from BoNT/A-silenced neurons (50 pg per 200 μl) or when they were co-exposed to the RAMP1 blocker CGRP_{8–37} (2 μg ml⁻¹; Extended Data Fig. 9c, d). To confirm that nociceptor-released neuropeptides drive T cell exhaustion, we exposed T_{H1}-activated CD8⁺ T cells to CGRP. CGRP-treated cells expressing wild-type RAMP1 showed increased exhaustion and limited cytotoxic potential. These effects were absent in CGRP-exposed CD8⁺ T cells that were collected from CGRP-receptor-knockout (*Ramp1*^{-/-}) mice (Fig. 4a and Extended Data Fig. 9e, f).

We then assessed whether neuropeptides released by nociceptor neurons blunt the anti-tumour responses of cytotoxic CD8⁺ T cells through exhaustion. OT-I cytotoxic T cells induced robust apoptosis of cultured B16F10-mCherry-OVA cells (AnnexinV7-AAD⁺ B16F10-mCherry-OVA; Extended Data Fig. 9g–i). However, this apoptosis of B16F10-mCherry-OVA cells was decreased when the T cells were exposed to capsaicin- or KCl-stimulated neuron-derived conditioned medium, or when the cells were stimulated with CGRP (Fig. 4b and Extended Data Fig. 9g–i). OT-I

cytotoxic T cells did not eliminate cultured B16F10-mCherry-OVA when co-exposed to KCl-induced neuron-conditioned medium supplemented with the RAMP1 blocker CGRP_{8–37} (2 μg ml⁻¹; Extended Data Fig. 9h). When taken together with previous evidence that CGRP limits the activity of CD8⁺ T cells^{12,38}, our data suggest that, through the CGRP–RAMP1 axis, nociceptors lead to the functional exhaustion of CD8⁺ T cells, as defined by a simultaneous loss of expression of cytotoxic molecules (that is, IFNγ and TNF) and proliferative capacity (IL-2), increased co-expression of several exhaustion markers (PD-1⁺LAG3⁺TIM3⁺) and a reduced capacity to eliminate malignant cells.

Nociceptor-produced neuropeptides reduce immunity against bacteria³⁷ and fungi³⁹, and promote cytotoxic CD8⁺ T cell exhaustion (Fig. 4a, b and Extended Data Fig. 9). Given that nociceptor-released CGRP is increased when cultured with B16F10 cells (Fig. 1c) or exposed to SLPI (Fig. 2f), and that tumour-infiltrating nociceptor neurons over-express *Calca* (Fig. 1d, e), we next sought to test whether the intratumoural levels of CGRP correlate with CD8⁺ T cell exhaustion. To do this we used an *Nav1.8*^{Cre} driver to ablate most mechano- and thermosensitive nociceptors with diphtheria toxin (*Nav1.8*^{Cre::DTA}^{fl/WT})^{17,37}. When compared with melanoma-bearing littermate controls (*Nav1.8*^{WT::DTA}^{fl/WT}), the ablation of Na_v1.8⁺ sensory neurons preserved the functionality of intratumoural CD8⁺ T cells (Extended Data Fig. 10a–d). In both groups of mice, the proportion of intratumoural CGRP directly correlated with the frequency of PD-1⁺LAG3⁺TIM3⁺ CD8⁺ T cells (Extended Data Fig. 10e).

We then set out to rescue CGRP levels (by daily intratumoural injection) in sensory-neuron-ablated mice and measured the effect on tumour growth and TIL exhaustion. At 11 days after inoculation, CGRP-treated sensory-neuron-ablated mice (*Trpv1*^{Cre::DTA}^{fl/WT}) showed similar tumour growth and CD8⁺ T cell exhaustion to that of nociceptor-intact mice (Fig. 4c and Extended Data Fig. 10f). Next, we treated tumour-bearing mice with the selective RAMP1 antagonist BIBN4096 (5 mg kg⁻¹, i.p., once every two days). The latter was previously found to block neuro-immune interactions during microorganism infections and rescues host anti-bacterial activity³⁵. BIBN4096-exposed mice succumb at a rate 2.6-fold lower (*P* ≤ 0.02) than that of vehicle-exposed B16F10-bearing mice (Extended Data Fig. 10g; measured until day 19). As measured

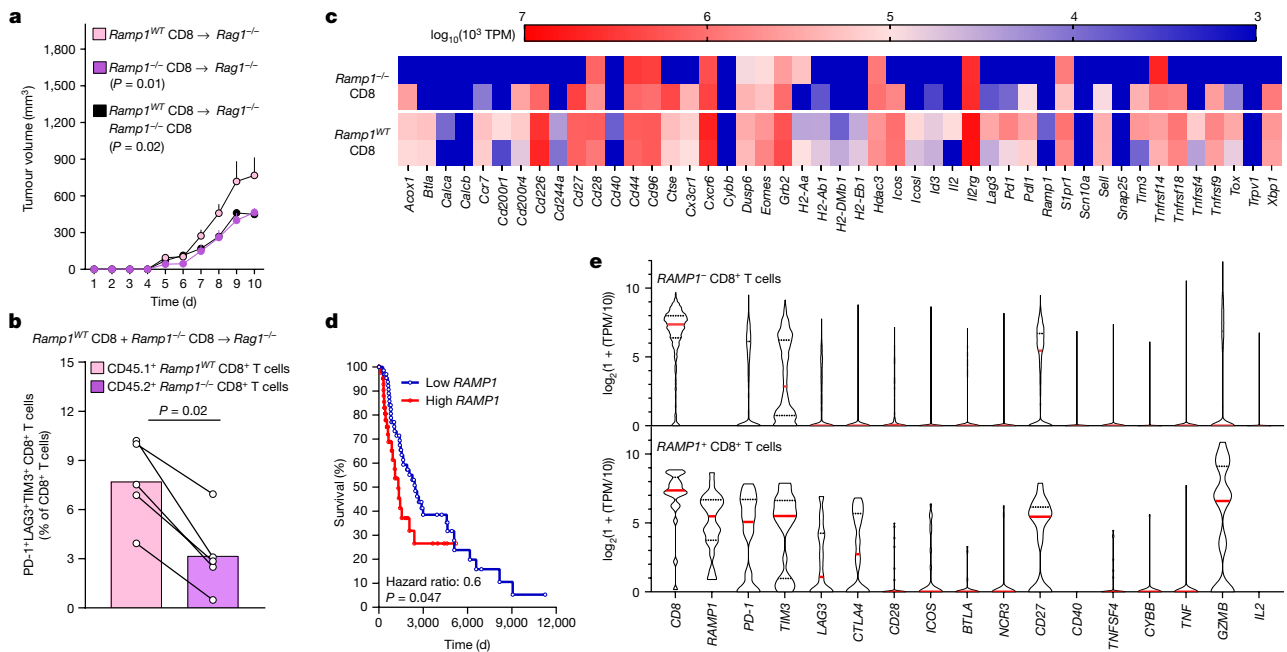


Fig. 5 | CGRP attenuates the anti-tumour immunity of RAMP1⁺ CD8⁺ T cells. **a–c.** Splenocyte CD8⁺ T cells were FACS purified from *Ramp1*^{WT} (CD45.1⁺) or *Ramp1*^{-/-} (CD45.2⁺) mice, expanded and stimulated (CD3 and CD28 + IL-2) in vitro. Eight-week-old female *Rag1*^{-/-} mice were transplanted (i.v., 2.5×10^6 cells) with activated *Ramp1*^{-/-} or *Ramp1*^{WT} CD8⁺ T cells or a 1:1 mix of *Ramp1*^{-/-} and *Ramp1*^{WT} CD8⁺ T cells. One week after transplantation, the mice were inoculated with B16F10-mCherry-OVA cells (5×10^5 cells, i.d.). Ten days after B16F10 inoculation, we observed greater tumour growth (a) in *Ramp1*^{WT} transplanted mice. Intratumoral *Ramp1*^{-/-} (CD45.2⁺) and *Ramp1*^{WT} (CD45.1⁺) CD8⁺ T cells were FACS purified, immunophenotyped (b) and RNA sequenced (c). *Ramp1*^{-/-} CD8⁺ T cells showed a lower proportion of PD-1⁺LAG3⁺TIM3⁺ CD8⁺ T cells (b) as well as reduced transcript expression of exhaustion markers (c). **d.** In silico analysis of The Cancer Genome Atlas (TCGA) data⁴⁰ was used to correlate the survival rate of 459 patients with melanoma with the relative

RAMP1 expression (primary biopsy bulk RNA sequencing). In comparison to patients with low *RAMP1* expression, higher *RAMP1* levels correlate with decreased patient survival. **e.** In silico analysis of single-cell RNA sequencing of human melanoma⁴¹ reveals that intratumoral *RAMP1*-expressing CD8⁺ T cells strongly overexpress several immune checkpoint receptors (*PD-1* (also known as *PDCDI*), *TIM3*, *LAG3*, *CTLA4*) in comparison to *Ramp1*-negative CD8⁺ T cells. Data are shown as mean \pm s.e.m. (a), slopegraph (b), as a heat map showing normalized gene expression ($\log_{10}(10^3 \times \text{TPM})$) (c), as a Mantel–Cox regression (d) or as a violin plot (e). *n* as follows: **a–c:** *n* = 5 per group; **d:** high (*n* = 45), low (*n* = 68); **e:** *RAMP1*⁺ CD8⁺ (*n* = 1,732), *RAMP1*⁻ CD8⁺ (*n* = 25). Experiments were independently repeated two (a, b) times with similar results. The sequencing experiment was not repeated (c). *P* values were determined by two-way ANOVA with post-hoc Bonferroni (a), two-sided unpaired Student's *t*-test (b) or Mantel–Cox regression (d).

on day 13, BIBN4096 (5 mg kg⁻¹, i.p., every other day) reduced B16F10 growth, tumour weight and frequency of PD-1⁺LAG3⁺TIM3⁺ CD8⁺ T cells (Fig. 4d–e and Extended Data Fig. 10h–m). As BIBN4096 showed no effect when administered to nociceptor-ablated mice and did not affect cultured B16F10 cells or CD8⁺ T cell function in vitro (Extended Data Fig. 10n–t), we conclude that the anti-tumour property of BIBN4096 relies on the presence of active nociceptor neurons.

To directly address whether RAMP1 is the main driver of CD8⁺ T cell exhaustion, we transplanted *Rag1*^{-/-} mice with *Ramp1*^{-/-} or *Ramp1* wild-type (*Ramp1*^{WT}) CD8⁺ T cells (intravenously (i.v.), 2.5×10^6) or a 1:1 mixture of both. Although we retrieved similar numbers of CD8⁺ T cells across all three groups (Extended Data Fig. 10u), limited B16F10-OVA tumour growth (Fig. 5a) was found in mice that received the *Ramp1*^{-/-} CD8⁺ T cells—which are not responsive to CGRP. The relative proportion of intratumoral PD-1⁺LAG3⁺TIM3⁺ CD8⁺ T cells was also lower in *Ramp1*^{-/-} transplanted *Rag1*^{-/-} mice (Extended Data Fig. 10v). In *Rag1*^{-/-} mice co-transplanted with RAMP1-expressing and -non-expressing CD8⁺ T cells, we found that within the same tumour, the relative proportion of intratumoral PD-1⁺LAG3⁺TIM3⁺ CD8⁺ T cells was lower in *Ramp1*^{-/-} CD8⁺ T cells (Fig. 5b and Extended Data Fig. 10w). Next, we RNA sequenced FACS-purified *Ramp1*^{WT} and *Ramp1*^{-/-} CD8⁺ T cells from these tumours. Compared to their *Ramp1*^{WT} counterparts, we found that intratumoral *Ramp1*^{-/-} CD8⁺ T cells expressed fewer pro-exhaustion transcription factors (*Tox* and *Eomes*) and markers (*Pdcd1* (encoding PD-1), *Lag3* and *Tim3* (also known as *Havcr2*); Fig. 5c). Overall, CGRP-unresponsive *Ramp1*^{-/-} CD8⁺ T cells are

protected against undergoing nociceptor-induced exhaustion, which safeguards their anti-tumour responses.

When compared with benign nevi, patient melanomas showed increased expression of *Calca* (Extended Data Fig. 1d). Along with other markers of nociceptor neurons, overexpression of *RAMP1* in these biopsies⁴⁰ correlates (*P* \leq 0.05) with reduced patient survival (Fig. 5d and Extended Data Fig. 11a–l). Whether RAMP1 does this by affecting intratumoral CD8⁺ T cell exhaustion is unknown. To answer this, we analysed two independent unbiased single-cell RNA-sequencing datasets of human melanomas^{41,42}, and found that around 1.5% of tumour-infiltrating CD8⁺ T cells expressed *RAMP1*. The melanoma-infiltrating *RAMP1*⁺ CD8⁺ T cells of the patients overexpressed the immune checkpoint receptors *PD-1* (also known as *PDCDI*), *TIM3* (*HAVCR2*), *LAG3*, *CTLA4* and *CD27* (Fig. 5e and Extended Data Fig. 11m). This analysis also revealed that tumour-infiltrating CD8⁺ cells collected from patients who were resistant to ICI markedly overexpressed *RAMP1* (Extended Data Fig. 11n–p). Such an expression profile resembles the functional exhaustion of effector CD8⁺ T cells and suggests that the CGRP receptor RAMP1 influences CD8⁺ T cell exhaustion and the clinical response to ICI in patients with melanoma.

Overall, the genetic ablation of nociceptor neurons decreases the growth of B16F10 tumours by preventing CD8⁺ T cells from undergoing exhaustion, whereas exogenous administration of CGRP has the opposite effect. These effects are restricted to immunogenic tumours and are not present in the absence of CD8⁺ T cells. Similar to the pre-clinical

modelling in mice, human data imply that RAMP1-expressing CD8⁺ T cells are more prone to exhaustion and are associated with lower responsiveness to ICIs.

Tumour-innervating nociceptors dampen the immune response to melanoma by upregulating multiple immune checkpoint receptors on cytotoxic CD8⁺ T cells. Blocking the CGRP–RAMP1 axis attenuates this immunomodulatory action of the nervous system on CD8⁺ T cells, thereby safeguarding the anti-tumour immunity of the host (Extended Data Fig. 12) and providing potential therapeutic opportunities by interrupting pro-cancerous neuro–immune links.

Online content

Any methods, additional references, Nature Research reporting summaries, source data, extended data, supplementary information, acknowledgements, peer review information; details of author contributions and competing interests; and statements of data and code availability are available at <https://doi.org/10.1038/s41586-022-05374-w>.

- Amit, M. et al. Loss of p53 drives neuron reprogramming in head and neck cancer. *Nature* **578**, 449–454 (2020).
- Magnon, C. et al. Autonomic nerve development contributes to prostate cancer progression. *Science* **341**, 1236361 (2013).
- Mauffrey, P. et al. Progenitors from the central nervous system drive neurogenesis in cancer. *Nature* **569**, 672–678 (2019).
- Zahalka, A. H. et al. Adrenergic nerves activate an angio-metabolic switch in prostate cancer. *Science* **358**, 321–326 (2017).
- Zahalka, A. H. & Frenette, P. S. Nerves in cancer. *Nat. Rev. Cancer* **20**, 143–157 (2020).
- Chambers, C. A., Kuhns, M. S., Egen, J. G. & Allison, J. P. CTLA-4-mediated inhibition in regulation of T cell responses: mechanisms and manipulation in tumor immunotherapy. *Annu. Rev. Immunol.* **19**, 565–594 (2001).
- Das, M., Zhu, C. & Kuchroo, V. K. Tim-3 and its role in regulating anti-tumor immunity. *Immunol. Rev.* **276**, 97–111 (2017).
- Topalian, S. L. et al. Safety, activity, and immune correlates of anti-PD-1 antibody in cancer. *N. Engl. J. Med.* **366**, 2443–2454 (2012).
- Baumeister, S. H., Freeman, G. J., Dranoff, G. & Sharpe, A. H. Coinhibitory pathways in immunotherapy for cancer. *Annu. Rev. Immunol.* **34**, 539–573 (2016).
- Dougan, M. & Dranoff, G. Immune therapy for cancer. *Annu. Rev. Immunol.* **27**, 83–117 (2009).
- Donnelly, C. R. et al. STING controls nociception via type I interferon signalling in sensory neurons. *Nature* **591**, 275–280 (2021).
- McIlvried, L. A., Atherton, M. A., Horan, N. L., Goch, T. N. & Scheff, N. N. Sensory neurotransmitter calcitonin gene-related peptide modulates tumor growth and lymphocyte infiltration in oral squamous cell carcinoma. *Adv. Biol.* **6**, e2200019 (2022).
- Wang, K. et al. STING suppresses bone cancer pain via immune and neuronal modulation. *Nat. Commun.* **12**, 4558 (2021).
- Chen, G. et al. PD-L1 inhibits acute and chronic pain by suppressing nociceptive neuron activity via PD-1. *Nat. Neurosci.* **20**, 917–926 (2017).
- Kamiya, A. et al. Genetic manipulation of autonomic nerve fiber innervation and activity and its effect on breast cancer progression. *Nat. Neurosci.* **22**, 1289–1305 (2019).
- Saloman, J. L. et al. Ablation of sensory neurons in a genetic model of pancreatic ductal adenocarcinoma slows initiation and progression of cancer. *Proc. Natl Acad. Sci. USA* **113**, 3078–3083 (2016).
- Talbot, S. et al. Silencing nociceptor neurons reduces allergic airway inflammation. *Neuron* **87**, 341–354 (2015).
- Anderson, P. & Gonzalez-Rey, E. Vasoactive intestinal peptide induces cell cycle arrest and regulatory functions in human T cells at multiple levels. *Mol. Cell. Biol.* **30**, 2537–2551 (2010).
- Haqq, C. et al. The gene expression signatures of melanoma progression. *Proc. Natl Acad. Sci. USA* **102**, 6092–6097 (2005).
- Harlin, H. et al. Chemokine expression in melanoma metastases associated with CD8⁺ T-cell recruitment. *Cancer Res.* **69**, 3077–3085 (2009).
- Riker, A. I. et al. The gene expression profiles of primary and metastatic melanoma yields a transition point of tumor progression and metastasis. *BMC Med. Genom.* **1**, 13 (2008).
- Talantov, D. et al. Novel genes associated with malignant melanoma but not benign melanocytic lesions. *Clin. Cancer Res.* **11**, 7234–7242 (2005).
- Hannila, S. S. et al. Secretory leukocyte protease inhibitor reverses inhibition by CNS myelin, promotes regeneration in the optic nerve, and suppresses expression of the transforming growth factor- β signaling protein Smad2. *J. Neurosci.* **33**, 5138–5151 (2013).
- Mueller, A. M. et al. Novel role for SLP1 in MOG-induced EAE revealed by spinal cord expression analysis. *J. Neuroinflammation* **5**, 20 (2008).
- Boilly, B., Faulkner, S., Jobling, P. & Hondermarck, H. Nerve dependence: from regeneration to cancer. *Cancer Cell* **31**, 342–354 (2017).
- Zhao, C. M. et al. Denervation suppresses gastric tumorigenesis. *Sci. Transl. Med.* **6**, 250ra115 (2014).
- Larkin, J. et al. Five-year survival with combined nivolumab and ipilimumab in advanced melanoma. *N. Engl. J. Med.* **381**, 1535–1546 (2019).
- Wang, J. et al. UV-induced somatic mutations elicit a functional T cell response in the YUMMER1.7 mouse melanoma model. *Pigment Cell Melanoma Res.* **30**, 428–435 (2017).
- Meeth, K., Wang, J. X., Micevic, G., Damsky, W. & Bosenberg, M. W. The YUMM lines: a series of congenic mouse melanoma cell lines with defined genetic alterations. *Pigment Cell Melanoma Res.* **29**, 590–597 (2016).
- Cohen, J. A. et al. Cutaneous TRPV1⁺ neurons trigger protective innate type 17 anticipatory immunity. *Cell* **178**, 919–932 (2019).
- Michoud, F. et al. Epineural optogenetic activation of nociceptors initiates and amplifies inflammation. *Nat. Biotechnol.* **39**, 179–185 (2021).
- Pellet, S., Tepp, W. H., Whitmarsh, R. C., Bradshaw, M. & Johnson, E. A. In vivo onset and duration of action varies for botulinum neurotoxin A subtypes 1–5. *Toxicon* **107**, 37–42 (2015).
- Pinho-Ribeiro, F. A. et al. Blocking neuronal signaling to immune cells treats streptococcal invasive infection. *Cell* **173**, 1083–1097 (2018).
- Binshtok, A. M., Bean, B. P. & Woolf, C. J. Inhibition of nociceptors by TRPV1-mediated entry of impermeant sodium channel blockers. *Nature* **449**, 607–610 (2007).
- Baral, P. et al. Nociceptor sensory neurons suppress neutrophil and $\gamma\delta$ T cell responses in bacterial lung infections and lethal pneumonia. *Nat. Med.* **24**, 417–426 (2018).
- Yissachar, N. et al. An intestinal organ culture system uncovers a role for the nervous system in microbe–immune crosstalk. *Cell* **168**, 1135–1148 (2017).
- Chiu, I. M. et al. Bacteria activate sensory neurons that modulate pain and inflammation. *Nature* **501**, 52–57 (2013).
- Ding, W., Stohl, L. L., Wagner, J. A. & Granstein, R. D. Calcitonin gene-related peptide biases Langerhans cells toward Th2-type immunity. *J. Immunol.* **181**, 6020–6026 (2008).
- Kashem, S. W. et al. Nociceptive sensory fibers drive interleukin-23 production from CD301b⁺ Dermal dendritic cells and drive protective cutaneous immunity. *Immunity* **43**, 515–526 (2015).
- The Cancer Genome Atlas Research Network et al. The Cancer Genome Atlas Pan-Cancer analysis project. *Nat. Genet.* **45**, 1113–1120 (2013).
- Jerby-Arnon, L. et al. A cancer cell program promotes T Cell exclusion and resistance to checkpoint blockade. *Cell* **175**, 984–997 (2018).
- Tirosh, I. et al. Dissecting the multicellular ecosystem of metastatic melanoma by single-cell RNA-seq. *Science* **352**, 189–196 (2016).

Publisher's note Springer Nature remains neutral with regard to jurisdictional claims in published maps and institutional affiliations.



Open Access This article is licensed under a Creative Commons Attribution 4.0 International License, which permits use, sharing, adaptation, distribution and reproduction in any medium or format, as long as you give appropriate credit to the original author(s) and the source, provide a link to the Creative Commons license, and indicate if changes were made. The images or other third party material in this article are included in the article's Creative Commons license, unless indicated otherwise in a credit line to the material. If material is not included in the article's Creative Commons license and your intended use is not permitted by statutory regulation or exceeds the permitted use, you will need to obtain permission directly from the copyright holder. To view a copy of this license, visit <http://creativecommons.org/licenses/by/4.0/>.

© The Author(s) 2022

Methods

Secondary use of biopsies as research specimens

The ten melanoma samples used in this study were collected by Sanford Health and classified by a board-certified pathologist. Their secondary use as research specimens (fully de-identified formalin-fixed, paraffin-embedded (FFPE) blocks) was approved under Sanford Health IRB protocol 640 (titled 'Understanding and improving cancer treatment of solid tumours'). As part of this Institutional Review Board (IRB)-approved retrospective tissue analysis, and in accordance with the US Department of Health and Human Services (HHS) secretary's advisory committee on human research protections, no patient consent was necessary as these secondary use specimens were free of linkers or identifiers and posed no more than minimal risk to the human individuals.

Immunohistochemistry and scoring

In compliance with all the relevant ethical regulations and as approved by Sanford Health IRB protocol 640, ten fully de-identified FFPE melanoma blocks were randomly selected for secondary use as research specimens. The notes of a board-certified pathologist on these specimens are provided in Supplementary Table 1. The specimens were stained using a BenchMark XT slide staining system (Ventana Medical Systems). The Ventana iView DAB detection kit was used as the chromogen, and slides were counterstained with haematoxylin and anti-TRPV1 (Alomone Labs, ACC-030; 1:100). Haematoxylin and eosin (H&E) staining followed standard procedures. TRPV1 immunohistochemistry-stained specimens were analysed on an Olympus BX51 bright-field microscope. Sections were viewed under 20 \times magnification. Five random fields per sample for both tumour and adjacent normal tissue were analysed and scored on a scale from 0 to 3. Scores were averaged. A score of 0 indicates no appreciated nerve fibres in the evaluated field; +1 indicates sparse nerve fibres; +2 indicates 5–20 nerve fibres; +3 indicates more than 20 nerve fibres.

IACUC approval

The Institutional Animal Care and Use Committee (IACUC) of Boston Children's Hospital and of the Université de Montréal (Comité de Déontologie de l'Expérimentation sur les Animaux; #21046; 21047) approved all animal procedures.

Housing of mice

Mice were housed in standard environmental conditions (12-h light-dark cycle; 23 °C; food and water ad libitum) at facilities accredited by the Canadian Council of Animal Care (Université de Montréal) or the Association for Assessment and Accreditation of Laboratory Animal Care (Boston Children's Hospital).

IACUC end-points

As per our IACUC-approved protocol, the following end-points were used in all of the experiments and were not exceeded. Along with excessive body weight loss (maximum of 10%), the end-points include excessive tumour volume (10% of the mouse's body weight; around 17 mm \times 17 mm), skin ulceration, necrosis, bleeding, infection and self-inflicted injury, prostration, lethargy, unresponsiveness to stimulation and/or lack of grooming.

Mouse lines

Six-to-twenty-week-old male and female C57BL6J (Jax, 000664); CD45.1⁺ C57BL6J (Jax, 002014), *Ramp1*^{-/-} (Jax, 031560), *Rag1*^{-/-} (Jax, 002216), OT-1 (Jax, 003831)⁴³, *Trpv1*^{cre} (Jax, 017769)⁴⁴, *ChR2*^{fl/fl} (Jax, 012567)⁴⁵, *tdTomato*^{fl/fl} (Jax, 007908)⁴⁶, *DTA*^{fl/fl} (Jax, 009669)⁴⁷ or *DTA*^{fl/fl} (Jax, 010527), *QuasAr2-dark mOrange2-CheRiff-eGFP*^{fl/fl} (referred to in the text as *CheRiff-eGFP*^{fl/fl}; Jax, 028678)⁴⁸ mice were purchased from the Jackson Laboratory. *Nav1.8*^{cre} mice⁴⁹ were supplied by R. Kuner and

J. Wood. Excluding CD45.1⁺ mice, all other lines were backcrossed for more than six generations on a C57BL6/J background (H-2Kb). Although Capecchi's *DTA*^{fl/fl} (Jax, 010527) was created on a mixed C57BL6J/129 background, both haplotypes are H-2Kb. All these mice are therefore fully compatible with being transplanted with B16F10-derived cells (C57BL6/J background (H-2Kb)).

We used the Cre-*lox* toolbox to engineer the various mice lines used (*Trpv1*^{cre}::*DTA*^{fl/WT}, *Trpv1*^{cre}::*CheRiff-eGFP*^{fl/WT}, *Trpv1*^{cre}::*tdTomato*^{fl/WT}, *Nav1.8*^{cre}::*DTA*^{fl/WT}, *Nav1.8*^{cre}::*tdTomato*^{fl/WT}, *Nav1.8*^{cre}::*ChR2*^{fl/WT} and littermate control) by crossing heterozygote Cre mice with homozygous *loxP* mice. Mice of both sexes were used for these crosses. All Cre driver lines used were viable and fertile, and abnormal phenotypes were not detected. Offspring were tail-clipped and tissue was used to assess the presence of the transgene by standard PCR, as described by The Jackson Laboratory or the donating investigators. Offspring of both sexes were used at 6–20 weeks of age.

Cell lines

B16F0⁵⁰ (ATCC, CRL-6322), B16F10⁵¹ (ATCC, CRL-6475), B16F10-mCherry-OVA⁵² (M. F. Krummel, UCSF), B16F10-eGFP (Iman, CL053), YUMM1.7²⁹ (ATCC, CRL-3362), and non-tumorigenic keratinocytes (CellInTEC, MPEK-BL6100) were cultured in complete Dulbecco's modified Eagle's medium high glucose (DMEM; Corning, 10-013-CV) supplemented with 10% fetal bovine serum (FBS; Seradigm, 3100) and 1% penicillin-streptomycin (Corning, MT-3001-Cl), and maintained at 37 °C in a humidified incubator with 5% CO₂. YUMMER1.7²⁸ (M. Bosenberg, Yale University) cells were cultured in DMEM F12 (Gibco, 11320033) supplemented with 10% FBS, 1% penicillin-streptomycin (Corning, MT-3001-Cl) and MEM nonessential amino acids (Corning, 25-025Cl), and maintained at 37 °C in a humidified incubator with 5% CO₂.

All the cell lines tested negative for mycoplasma, and none are listed by the International Cell Line Authentication Committee registry (v.11). Non-commercial cell lines (B16F10-OVA, B16F10-OVA-mCherry and B16F10-eGFP) were authenticated using antibodies (against OVA, eGFP and mCherry) and/or imaging as well as morphology and growth properties. Commercial cell lines were not further authenticated.

Cancer inoculation and volume measurement

Cancer cells were resuspended in phosphate buffered saline (PBS; Corning, 21040CV) and injected into the mouse's skin in the right flank (5 \times 10⁵ cells, i.d., 100 μ l) or hindpaw (2 \times 10⁵ cells, i.d., 50 μ l). Growth was assessed daily using a handheld digital caliper and tumour volume was determined by the formula ($L \times W^2 \times 0.52$) (ref. ⁵³), in which L = length and W = width.

BoNT/A

BoNT/A³⁵ (List Biological Labs, 130B) was injected (25 pg μ l⁻¹, i.d., five neighbouring sites injected with 20 μ l) into the skin three days and one day before tumour inoculation (defined as prophylactic). BoNT/A (25 pg μ l⁻¹; i.d., five neighbouring sites injected with 20 μ l) was injected around the tumour one day and three days after the tumour reached a volume of around 200 mm³ (defined as therapeutic) in other groups of C57BL/6J mice.

QX-314

Starting one day after tumour inoculation (defined as prophylactic), QX-314 (ref. ³⁴; Tocris, 2313; 0.3%) was injected (i.d., 100 μ l) daily at five points around the tumour. In another group of mice, QX-314 daily injection started once the tumour reached a volume of around 200 mm³ (defined as therapeutic).

BIBN4096

Starting one day after tumour inoculation, BIBN4096 (ref. ³³; Tocris, 4561; 5 mg kg⁻¹) was administered systemically (i.p., 50 μ l) on alternate days to eight-week-old male and female mice (defined as prophylactic).

Article

In another group of mice, BIBN4096 (5 mg kg⁻¹) was administered systemically (i.p., 50 µl) on alternate days once the tumour reached a volume of around 200 mm³ (defined as therapeutic).

RTX

RTX (ref. 33; Alomone Labs, R-400) was injected (subcutaneously; s.c.) in three dosages (30, 70 and 100 µg kg⁻¹) into the right flank of *Rag1*^{-/-} and C57BL/6J mice of around three weeks of age. Denervation was confirmed 28 days after RTX by an absence of pain withdrawal reflex (paw flinching) when exposed to heat (see 'Thermal hypersensitivity' for details on the test).

Survival

In specific groups of mice, orthotopic B16F10-mCherry-OVA (5 × 10⁵ cells, i.d.) cells were administered to intact and nociceptor-ablated mice and survival was measured until day 22 and determined by the tumour reaching a volume of 1,000 mm³ or greater, or according to the ethical end-points described above. In B16F10-mCherry-OVA-inoculated mice treated with QX-314 or BIBN4096, survival was measured until day 19 and determined by the tumour reaching a volume of 800 mm³ or greater, or according to the ethical end-points described above. As the survival analysis of vehicle-injected, QX-314-treated and BIBN4096-treated mice was performed simultaneously, the same group of vehicle-injected mice is shown in the respective panels for QX-314 and BIBN4096.

iDISCO imaging

Whole-mount immunohistochemistry of tumours was performed using an iDISCO protocol^{54,55} with methanol pre-treatment optimized for tumours. In brief, adult mice (eight weeks old) were perfused with 25 ml of PBS (HyClone) and 25 ml of 4% paraformaldehyde (PFA; Sigma) sequentially at room temperature. Tumours were post-fixed with 4% PFA for 6 h at 4 °C. For methanol pre-treatment, fixed tumours were washed sequentially in 50% methanol (in PBS) for 1 h and 100% methanol for 1 h, and then bleached in 5% H₂O₂ in 20% DMSO and methanol overnight at 4 °C. Tumours were subsequently rehydrated in 100% methanol for 1 h twice, 20% DMSO and methanol for 1 h twice, 50% methanol in PBS for 1 h, PBS for 1 h twice and PBS and 0.2% Triton X-100 for 1 h twice at room temperature. Tumours were then left in PBS, 0.2% Triton X-100, 20% DMSO and 0.3 M glycine (Sigma) overnight at room temperature and blocked in PBS, 0.2% Triton X-100, 10% DMSO, 6% donkey serum (Jackson ImmunoResearch) and anti-CD16/CD32 (Fc block; Bio X Cell) overnight at room temperature. Tumours were subsequently washed in PBS, 0.2% Tween-20 and 10 mg ml⁻¹ heparin (PTwH; Sigma) for 1 h twice at room temperature before incubation with antibody mix (GFP (Aves Labs) at 1:500, mCherry (OriGene) at 1:500, in PTwH, 5% DMSO, 3% donkey serum and Fc block 1:100 for four days at room temperature). Tumours were extensively washed in PTwH at least six times over the course of one day at room temperature. Tumours were further incubated with a secondary panel of species-specific anti-IgG (H+L) Alexa Fluor 488 or 546-conjugated antibodies (Invitrogen or Jackson ImmunoResearch), all at 1:500, in PTwH, 5% DMSO, 3% donkey serum and Fc block 1:100 for three more days at room temperature. Tumours were washed in the same way as after primary antibody incubation for one day. Immunolabelled tumours were then processed for clearing, which included sequential incubation with 50% methanol for 1 h at room temperature, 100% methanol for 1 h three times at room temperature, and a mixture of one part benzyl alcohol (Sigma):two parts benzyl benzoates (Sigma) overnight at 4 °C. For tdTomato and GFP immunolabelling, mCherry and GFP antibodies were preabsorbed against tumours from *tdTomato*^{-/-} mice overnight at room temperature before use. Cleared whole-mount tissues were imaged in BABB between two cover glasses using Olympus FV3000 confocal imaging system.

Tumour and tumour-draining lymph node digestion

Mice were euthanized when the tumour reached a volume of 800–1,500 mm³ (refs. 50,51,56). Tumours and their draining lymph nodes were collected. Tumours were enzymatically digested in DMEM + 5% FBS (Seradigm, 3100) + 2 mg ml⁻¹ collagenase D (Sigma, 11088866001) + 1 mg ml⁻¹ collagenase IV (Sigma, C5138-1G) + 40 µg ml⁻¹ DNase I (Sigma, 10104159001) under constant shaking (40 min, 37 °C). The cell suspension was centrifuged at 400g for 5 min. The pellet was resuspended in 70% Percoll gradient (GE Healthcare), overlaid with 40% Percoll and centrifuged at 500g for 20 min at room temperature with acceleration and deceleration at 1. The cells were aspirated from the Percoll interface and passed through a 70-µm cell strainer. Tumour-draining lymph nodes were dissected in PBS + 5% FBS, mechanically dissociated using a plunger, strained (70 µm) and washed with PBS.

Immunophenotyping

Single cells were resuspended in FACS buffer (PBS, 2% fetal calf serum and EDTA), and stained with ZombieAqua (15 min, room temperature; BioLegend, 423102) or a Viability Dye eFluor 780 (15 min, 4 °C; eBioscience, 65-0865-14). The cells were washed and Fc-blocked (0.5 mg ml⁻¹, 15 min, 4 °C; BD Biosciences, 553141). Finally, the cells were stained (30 min, 4 °C) with one of anti-CD45-BV421 (1:100, BioLegend, 103134), anti-CD45.1-BV421 (1:100, BioLegend, 110732), anti-CD45.2-BV650 (1:100, BioLegend, 109836), anti-CD45-Alexa Fluor 700 (1:100, BioLegend, 103128), anti-CD11b-APC/Cy7 (1:100, BioLegend, 101226), anti-CD8-AF700 (1:100, BioLegend, 100730), anti-CD8-BV421 (1:100, BioLegend, 100753), anti-CD8-PerCP/Cyanine5.5 (1:100, BioLegend, 100734), anti-CD8-Pacific Blue (1:100, BioLegend, 100725), anti-CD4-PerCP/Cyanine5.5 (1:100, BioLegend, 100540), anti-CD4-FITC (1:100, BioLegend, 100406), anti-PD-1-PE-Cy7 (1:100, BioLegend, 109110), anti-LAG3-PE (1:100, BioLegend, 125208), anti-LAG3-PerCP/Cyanine5.5 (1:100, BioLegend, 125212) or anti-TIM3-APC (1:100, BioLegend, 119706), washed and analysed using a LSRFortessa or FACSCanto II (Becton Dickinson). Antigen-specific CD8⁺ T cells were stained with H-2Kb/OVA257-264 (15 min, 37 °C; NIH tetramer core facility), washed and stained with surface markers. Cytokine expression was analysed after *in vitro* stimulation (PMA-ionomycin; see 'Intracellular cytokine staining').

Intracellular cytokine staining

Cells were stimulated (3 h) with phorbol-12-myristate 13-acetate (PMA; 50 ng ml⁻¹, Sigma-Aldrich, P1585), ionomycin (1 µg ml⁻¹, Sigma-Aldrich, I3909) and Golgi Stop (1:100, BD Biosciences, 554724). The cells were then fixed and permeabilized (1:100, BD Biosciences, 554714) and stained with anti-IFNγ-APC (1:100, BioLegend, 505810), anti-IFNγ-FITC (1:100, BioLegend, 505806), anti-TNF-BV510 (1:100, BioLegend, 506339), anti-TNF-BV5711 (1:100, BioLegend, 506349), anti-TNF-PE (1:100, BioLegend, 506306), anti-IL2-Pecy7 (1:100, BioLegend, 503832), anti-IL2-Pacific Blue (1:100, BioLegend, 503820), anti-IL2-BV510 (1:100, BioLegend, 503833), and analysed using a LSRFortessa or FACSCanto II (Becton Dickinson).

In vivo depletion of CD3 or CD8

Anti-mouse CD3 (200 µg per mouse, Bio X Cell, BE0001-1) or anti-mouse CD8 (200 µg per mouse, Bio X Cell, BP0061) were injected (i.p.) three days before B16F10-mCherry-OVA inoculation (5 × 10⁵ cells; i.d.) and continued every three days. Blood samples were taken twice weekly to confirm depletion, and tumour growth was measured daily.

In vivo CGRP rescue experiment

Trpv1-ablated mice were injected (i.d.) once daily with recombinant CGRP (100 nM) at five points around the tumour (treatment began once the tumour was visible), and tumour growth was measured daily by a handheld digital caliper. Mice were euthanized, and tumour-infiltrating

CD8⁺ cell exhaustion was immunophenotyped by flow cytometry using an LSRFortessa or a FACSCanto II (Becton Dickinson).

Anti-PD-L1 treatment

Orthotopic B16F10-mCherry-OVA cells (5×10^5 cells, i.d.) were inoculated into eight-week-old male and female sensory-neuron-intact or -ablated mice. On days 7, 10, 13 and 16 after tumour inoculations, the mice were treated with anti-PD-L1^{14,57} (Bio X Cell, BE0101, 6 mg kg⁻¹; i.p., 50 μ l) or isotype control. Nineteen days after tumour inoculation, the effect of anti-PD-L1 on tumour growth was analysed and TIL exhaustion was immunophenotyped using an LSRFortessa or a FACSCanto II (Becton Dickinson).

Anti-PD-L1 treatment in mice with similar tumour sizes

Orthotopic B16F10-mCherry-OVA cells (5×10^5 cells; i.d.) were injected into a cohort of nociceptor neuron-ablated mice three days before nociceptor-intact mice were injected. Mice from each group with a similar tumour size (around 85 mm³) were selected and exposed to anti-PD-L1^{14,57} (Bio X Cell, BE0101, 6 mg kg⁻¹, i.p., 50 μ l) or isotype control once every three days for a total of nine days. The effect of anti-PD-L1 treatment on tumour growth was analysed until day 18.

One and three days before tumour inoculation, the skin of eight-week-old male and female mice was injected with BoNT/A (25 pg μ l⁻¹, i.d., five neighbouring sites injected with 20 μ l) or vehicle. One day after the last injection, orthotopic B16F10-mCherry-OVA cells (5×10^5 cells, i.d.) were inoculated into the area pre-exposed to BoNT/A. On days 7, 10, 13 and 16 after tumour inoculation, the mice were exposed to anti-PD-L1 (6 mg kg⁻¹, i.p.) or isotype control. Eighteen days after tumour inoculation, we found that neuron silencing using BoNT/A potentiated anti-PD-L1-mediated tumour reduction.

Orthotopic B16F10-mCherry-OVA (5×10^5 cells, i.d.) were injected into mice treated with QX-314 (0.3%, i.d.) two to three days before being given to vehicle-exposed mice. Mice from each group with a similar tumour size (around 100 mm³) were selected and exposed to anti-PD-L1¹⁴ (Bio X Cell, BE0101, 6 mg kg⁻¹, i.p.) or isotype control once every three days for a total of nine days. Eighteen days after tumour inoculation, the effect of anti-PD-L1 on tumour growth was analysed, and TIL exhaustion was immunophenotyped using an LSRFortessa or a FACSCanto II (Becton Dickinson).

Adoptive transfer of *Ramp1*^{WT} or *Ramp1*^{-/-} CD8 T cells

Total CD8⁺ T cells were isolated from the spleen of wild-type (CD45.1⁺) or *Ramp1*^{-/-} (CD45.2⁺) mice, expanded and stimulated *in vitro* using a mouse T cell Activation/Expansion Kit (Miltenyi Biotec, #130-093-627). CD8⁺ cells from *Ramp1*^{-/-} and *Ramp1*^{WT} were injected separately or 1:1 mix through tail vein of *Rag1*^{-/-} mice. One week after, the mice were inoculated with B16F10-mCherry-OVA cancer cells (5×10^5 cells; i.d.), and tumour growth was measured daily using a handheld digital caliper. On day 10, tumours were collected and *Ramp1*^{-/-} (CD45.2⁺) and *Ramp1*^{WT} (CD45.1⁺) CD8⁺ T cells were immunophenotyped using a FACSCanto II (Becton Dickinson) or FACS purified using a FACSARIA IIu cell sorter (Becton Dickinson).

RNA sequencing of adoptive transferred *Ramp1*^{WT} or *Ramp1*^{-/-} CD8 T cells

For FACS-purified cells, *Ramp1*^{-/-} and *Ramp1*^{WT} CD8⁺ T cell RNA-sequencing libraries were constructed using KAPA Hyperprep RNA (1 \times 75 bp) following the manufacturer's instructions. Nextseq500 (0.5 Flowcell High Output; 200 M defragments; 75 cycles single-end read) sequencing was performed on site at the Institute for Research in Immunology and Cancer (IRIC) genomic centre. Sequences were trimmed for sequencing adapters and low-quality 3' bases using Trimmomatic v.0.35 and aligned to the reference mouse genome version GRCm38 (gene annotation from Gencode v.M23, based on Ensembl 98) using STAR v.2.5.1b (ref.⁵⁸). Gene expression levels were obtained both as a read count

directly from STAR and computed using RSEM to obtain normalized gene and transcript level expression, in TPM values, for these stranded RNA libraries. DESeq2 v.1.18.1 (ref.⁵⁹) was then used to normalize gene read counts. Individual cell data are shown as a log₁₀ of (TPM \times 1,000). These data have been deposited in the National Center for Biotechnology Information (NCBI)'s Gene Expression Omnibus (GEO)⁶⁰ (GSE205863).

Adoptive T cell transfer in mice treated with RTX

CD8⁺ T cells were isolated from OT-I mice spleens and magnet sorted (StemCell; 19858). Naive CD8⁺ T cells (CD8⁺CD44^{low}CD62L^{hi}) cells were then purified by FACS using an FACSARIA IIu cell sorter (Becton Dickinson) and injected (1×10^6 cells, i.v., tail vein) into vehicle- or RTX-exposed *Rag1*^{-/-} mice.

Mechanical hypersensitivity

B16F10-mCherry-OVA (2×10^5 cells, i.d.) or non-cancerous keratinocytes (MPEK-BL6; 2×10^5 cells, i.d.) were inoculated intradermally in the left hindpaw of the mice. On alternate days, mechanical sensitivity was evaluated using von Frey filaments (Ugo Basile, 52-37450-275). To do so, the mice were placed in a test cage with a wire mesh floor and allowed to acclimatize (three consecutive days: 1 h per session). Von Frey filaments of increasing size (0.008–2 g) were applied to the plantar surface and the response rate was evaluated using the up-down test paradigm⁶¹.

Thermal hypersensitivity

To measure thermal sensitivity, the mice were placed on a glass plate of a Hargreaves's apparatus (Ugo Basile)⁶² and stimulated using radiant heat (infrared beam). The infrared beam intensity was set at 44 and calibrated to result in a withdrawal time of around 12 seconds in acclimatized wild-type mice. An automatic cut-off was set to 25 s to avoid tissue damage. The radiant heat source was applied to the dorsal surface of the hindpaw and latency was measured as the time for the mouse to lift, lick or withdraw the paw⁶².

Before any treatment, the mice were allowed to acclimatize in the apparatus (minimum of three consecutive days: 1 h per session) and three baseline measurements were taken on the following day. In some instances, B16F10-mCherry-OVA (2×10^5 cells; i.d.) or non-cancerous keratinocytes (MPEK-BL6; 2×10^5 cells; i.d.) were inoculated intradermally to the mouse's left hindpaw and thermal pain hypersensitivity was measured on alternate days (10:00). In other instances, SLPI (1 μ g per 20 μ l) or saline (20 μ l) were injected in the left and right hindpaw, respectively, and thermal hypersensitivity was measured in both hindpaws at 1, 3 and 6 h after treatment.

Kinetics of pain and intratumoral CD8 T cell exhaustion

We implanted B16F10-mCherry-OVA (2×10^5 cells, i.d.) in several groups of littermate control (*Trpv1*^{WT}::*DTA*^{R/WT}; $n = 96$) and nociceptor-ablated (*Trpv1*^{cre}::*DTA*^{R/WT}; $n = 18$) mice. We then evaluated the level of thermal hypersensitivity (daily), tumour size (handheld digital caliper), and intratumoral CD8⁺ T cell exhaustion (flow cytometry) at the time of euthanasia (days 1, 4, 7, 8, 12, 13, 14, 19 and 22). We processed these data by determining the percentage change of each data point to the maximal value obtained in the pain, CD8⁺ T cell exhaustion and tumour size datasets, and then presented these data as percentages of the maximum (100%).

Optogenetic stimulation

Orthotopic B16F10-mCherry-OVA cells (5×10^5 cells, i.d.) were inoculated into the left flank of eight-week-old transgenic male mice expressing the light-sensitive protein channelrhodopsin 2 under the control of the *Nav1.8* promoter (*Nav1.8*^{cre}::*ChR2*^{R/WT}). Optogenetic stimulation (3.5 ms, 10 Hz, 478 nm, 60 mW, in a 0.39-NA fibre placed 5–10 mm from the skin, for 20 min) started either when the tumour was visible (around 20 mm³; 5 days after inoculation) or when it reached a volume of 200 mm³ (8 days after inoculation) and lasted up to 14 days after tumour inoculation. The control mice (*Nav1.8*^{cre}::*ChR2*^{R/WT}) were tumour-injected but

Article

not light-stimulated. Groups of littermate control (*Nav1.8^{WT}::Chr2^{R/WT}*) mice were light-stimulated and showed no response (not shown).

CGRP release from skin explant

Tumour-surrounding skin was collected using 10-mm punch biopsies from nociceptor-intact (*Nav1.8^{WT}::DTA^{R/WT}*), nociceptor-ablated (*Nav1.8^{cre}::DTA^{R/WT}*), light-sensitive nociceptor (*Nav1.8^{cre}::Chr2^{R/WT}*) or wild-type mice 3 h after exposure to vehicle (100 μ l), QX-314 (0.3%, 100 μ l) or BoNT/A (25 μ g μ l⁻¹, 100 μ l). The biopsies were transferred into 24-well plates and cultured in DMEM containing 1 μ l ml⁻¹ of protease inhibitor (Sigma, P1860) and capsaicin (1 μ M, Sigma, M2028). After a 30-min incubation (37 °C), the supernatant was collected and the release of CGRP was analysed using a commercial enzyme-linked immunosorbent assay (ELISA)³⁵ (Cayman Chemical, 589001).

CGRP release triggered by SLPI

1×10^4 naive DRG neurons were cultured for 24 h in complete DMEM (10% FBS, 1% penicillin–streptomycin, 1 μ l ml⁻¹ protease inhibitor) and subsequently stimulated (3 h) with vehicle or SLPI (0.1–5.0 ng ml⁻¹). After stimulation, the supernatant was collected and CGRP levels were measured using a commercial ELISA kit (Cayman Chemical, 589001).

Neuron culture

Mice were euthanized, and dorsal root ganglia were dissected out into DMEM medium (Corning, 10-013-CV), completed with 50 U ml⁻¹ penicillin and 50 μ g ml⁻¹ streptomycin (Corning, MT-3001-CI) and 10% FBS (Seradigm, 3100). Cells were then dissociated in HEPES buffered saline (Sigma, 51558) completed with 1 mg ml⁻¹ collagenase IV (Sigma, C0130) + 2.4 U ml⁻¹ dispase II (Sigma, 04942078001) and incubated for 80 min at 37 °C. Ganglia were triturated with glass Pasteur pipettes of decreasing size in supplemented DMEM medium, then centrifuged over a 10% BSA gradient and plated on laminin (Sigma, L2020)-coated cell-culture dishes. Cells were cultured with Neurobasal-A medium (Gibco, 21103-049) completed with 0.05 ng μ l⁻¹ NGF (Life Technologies, 13257-019), 0.002 ng μ l⁻¹ GDNF (PeproTech, 450-51-10), 0.01 mM AraC (Sigma, C6645) and 200 mM L-glutamine (VWR, 02-0131) and B-27 supplement (Gibco, #17504044).

Calcium imaging

L3–L5 DRG neurons were collected and co-cultured with B16F10, B16F0 or MPEK-BL6 for 24–48 h. The cells were then loaded with 5 mM Fura-2 AM (BioVision, 2243) in complete Neurobasal-A medium for 30 min at 37 °C, washed in Standard Extracellular Solution (SES, 145 mM NaCl, 5 mM KCl, 2 mM CaCl₂, 1 mM MgCl₂, 10 mM glucose and 10 mM HEPES, pH 7.5), and the response to noxious ligands (100 nM capsaicin, 100 μ M AITC or 1 μ M ATP) was analysed at room temperature. Ligands were flowed (15 s) directly onto neurons using perfusion barrels followed by buffer washout (105-s minimum). Cells were illuminated by a UV light source (Xenon lamp, 75 watts, Nikon), 340-nm and 380-nm excitation alternated by an LEP MAC 5000 filter wheel (Spectra services), and fluorescence emission was captured by a Cool SNAP ES camera (Princeton Instruments). The 340/380 ratiometric images were processed, background-corrected and analysed (IPLab software, Scientific Analytics), and Microsoft Excel was used for post-hoc analyses. Responsiveness to a particular ligand was determined by an increase in fluorescence (F_{340}/F_{380}) of at least 5–10% above baseline recording (SES). To test neuronal sensitivity in mice inoculated with B16F10 or non-tumorigenic keratinocytes, the mice were euthanized two weeks after inoculation (left hindpaw, i.d.), and L3–L5 DRG neurons were collected and cultured (3 h). Calcium flux to noxious ligands (1 μ M capsaicin or 10 μ M ATP) was subsequently tested. For SLPI, the DRG neurons were cultured for 24 h, loaded with 5 mM Fura-2AM in complete Neurobasal-A medium for 45 min at 37 °C and washed into SES, and the responses to noxious ligands (0–10 ng ml⁻¹ of mouse recombinant SLPI (LifeSpan BioSciences, LS-G13637-10), 1 μ M capsaicin or 50 mM KCl) were analysed at room temperature.

Immunofluorescence

A total of 2×10^3 DRG neurons were co-cultured with 2×10^4 B16F10-mCherry-OVA cells for 24–48 h. The cells were fixed (4% PFA; 30 min), permeabilized (0.1% Triton X-100; 20 min), and blocked (PBS, 0.1% Triton X-100 and 5% BSA; 30 min). The cells were rinsed (PBS), stained, and mounted with vectashield containing DAPI (Vector Laboratories, H-1000). Images were acquired using a Ti2 Nikon fluorescent microscope (IS-Elements Advanced Research v.4.5).

Neurite length and ramification index

TRPV1⁺ nociceptors (*Trpv1^{cre}::tdTomato^{R/WT}*) were cultured alone (2×10^3 cells) or co-cultured (2×10^4 cells) with B16F10-GFP, B16F0 or non-tumorigenic keratinocytes (MPEK-BL6). After 48 h, cells were fixed (see 'Immunofluorescence'), and images were acquired using a Ti2 Nikon fluorescent microscope. The neurite length of TRPV1⁺ (tdTomato) neurons was measured using a neurite tracer macro in ImageJ (Fiji, v.1.53c) developed by the Fournier laboratory⁶³, and the Schoenen ramification index (SRI) was measured by a Sholl analysis⁶⁴ macro in ImageJ (Fiji, v.1.53c).

Isolation of CD8⁺ T cells

Six-to-eight-week-old male and female mice were euthanized, and their spleens were collected in ice-cold PBS (5% FBS) and mechanically dissociated. The cells were strained (70 μ m), RBC lysed (Life Technologies, A1049201; 2 min), and counted using a haemocytometer. Total CD8⁺ T cells were magnet sorted (Stem Cell, 19853A) and cultured (DMEM + FBS 10%, penicillin–streptomycin 1% + nonessential amino acids (Corning, 25-025-CI) + vitamin + β -mercaptoethanol (Gibco, 21985-023) + L-glutamine (VWR, 02-0131) + sodium pyruvate (Corning, 25-000-CI)). Cell purity was systematically confirmed after magnet sorting and the numbers of CD8⁺CD62L^{hi} were immunophenotyped by flow cytometry.

To generate cytotoxic T lymphocytes, 2×10^5 CD8⁺ T cells were seeded and stimulated for 48 h under T_{cl} inflammatory conditions (2 μ g ml⁻¹ plate bounded anti-CD3 and anti-CD28 (Bio X Cell, BE00011, BE00151) + 10 ng ml⁻¹ rIL-12 (BioLegend, 577008) + 10 μ g ml⁻¹ of anti-IL-4 (Bio X Cell, BE0045).

In vitro stimulation of cytotoxic CD8⁺ T cells with neuron-conditioned medium

Naive or ablated DRG neurons were cultured (48 h) in Neurobasal-A medium supplemented with 0.05 ng μ l⁻¹ NGF (Life Technologies, 13257-019) and 0.002 ng μ l⁻¹ GDNF (PeproTech, 450-51-10). After 48 h, the neurobasal medium was removed, neurons were washed with PBS and 200 μ l per well of T cell medium supplemented with 1 μ l ml⁻¹ peptidase inhibitor (Sigma, P1860) and, in certain cases, capsaicin (1 μ M) or KCl (50 mM) was added to DRG neurons. The conditioned medium or vehicle were collected after 30 min and added to T_{cl} CD8⁺ T cells for another 96 h. The expression of exhaustion markers (PD-1, LAG3 and TIM3) and cytokines (IFN γ , TNF and IL-2) by CD8⁺ T cells was analysed by flow cytometry using an LSRFortessa or a FACSCanto II (Becton Dickinson). Cytokine expression levels were analysed after in vitro stimulation (PMA–ionomycin; see 'Intracellular cytokine staining').

In vitro stimulation of cytotoxic CD8⁺ T cells with CGRP

CD8⁺ T cells were isolated and stimulated under T_{cl} conditions in a 96-well plate. After 48 h, cells were treated with either CGRP (0.1 μ M) or PBS in the presence of peptidase inhibitor (1 μ M) for another 96 h. The expression of PD-1, LAG3 and TIM3, as well as IFN γ , TNF and IL-2, was immunophenotyped by flow cytometry using an LSRFortessa or a FACSCanto II (Becton Dickinson). Cytokine expression levels were analysed after in vitro stimulation (PMA–ionomycin; see 'Intracellular cytokine staining').

In vitro silencing of DRG neurons with BoNT/A

Naive DRG neurons (2×10^4) were seeded in a 96-well plate with neurobasal medium supplemented with NGF and GDNF. Neurons were

pre-treated with 50 pg ml⁻¹ of BoNT/A for 24 h. After 24 h, the culture medium was removed, neurons were washed with PBS and 200 µl per well of T cell medium supplemented with 1 µl ml⁻¹ peptidase inhibitor, and KCl (50 mM) was added to DRG neurons. The conditioned medium or vehicle were collected after 30 min and added to T_{cl} CD8⁺ T cells for another 96 h.

In vitro RAMP1 blockade

CD8⁺ T cells were treated with CGRP₈₋₃₇ (Tocris, 1169) 6 h before being exposed to the neuron-conditioned medium. In other instances, the neuron-conditioned medium was incubated for 1 h with 2 µg ml⁻¹ of CGRP₈₋₃₇ before being added to the CD8⁺ T cells.

Co-culture of CD8⁺ T cells and DRG neurons

Naive DRG neurons (2 × 10⁴) were seeded in a 96-well-plate with T cell medium (supplemented with 0.05 ng µl⁻¹ NGF (Life Technologies, 13257-019) and 0.002 ng µl⁻¹ GDNF (PeproTech, 450-51-10)). One day after, T_{cl} CD8⁺ cells (1 × 10⁵) were added to the neurons in the presence of IL-2 (BioLegend, 575408). In some instances, co-cultures were stimulated with either capsaicin (1 µM) or KCl (50 mM). After 96 h, the cells were collected by centrifugation (5 min at 1,300 rpm), stained and immunophenotyped by flow cytometry using an LSRFortessa or a FACSCanto II (Becton Dickinson). Cytokine expression levels were analysed after in vitro stimulation (PMA–ionomycin; see 'Intracellular cytokine staining').

RNA sequencing of triple co-cultures and data processing

A total of 1 × 10⁴ naive *Trpv1^{cre}::CheRiff-eGFP^{fl/wt}* DRG neurons were co-cultured with 1 × 10⁵ B16F10-mCherry-OVA overnight in T cell medium (supplemented with 0.05 ng µl⁻¹ NGF (Life Technologies, 13257-019), 0.002 ng µl⁻¹ GDNF (PeproTech, 450-51-10)). One day after, 4 × 10⁵ stimulated OVA-specific CD8⁺ T cells under T_{cl} conditions were added to the co-culture. After 48 h, the cells were detached and TRPV1 neurons (CD45⁻eGFP⁺mCherry⁻), B16F10-mCherry-OVA (CD45⁻eGFP⁺mCherry⁺) and OVA-specific CD8⁺ T cells (eGFP⁺mCherry⁻CD45⁺CD3⁺CD8⁺) were FACS purified using a FACSAria IIu cell sorter (Becton Dickinson), and the cell supernatant was collected for ELISAs.

RNA-sequencing libraries were constructed using the Illumina TruSeq Stranded RNA LT Kit (Illumina) following the manufacturer's instructions. Illumina sequencing was performed at Fulgent Genetics. Reads were aligned to the Mouse mm10 (GenBank assembly accession GCA_000001635.2) reference genome using STAR v.2.7 (ref. ⁵⁸). Aligned reads were assigned to genic regions using the featureCounts function from subread v.1.6.4 (ref. ⁶⁵). Gene expression levels were represented by TPM. Hierarchical clustering was computed using the heatmap.2 function (ward.D2 method) from the gplots R package (v.3.1.3). Differential gene expression analysis was performed using DeSeq2 v.1.28.1 (ref. ⁵⁹). These data have been deposited in the NCBI's GEO (ref. ⁶⁰) (GSE205864).

RNA sequencing of cancer and neuron co-cultures and data processing

A total of 1 × 10⁴ naive *Trpv1^{cre}::CheRiff-eGFP^{fl/wt}* DRG neurons were co-cultured with 5 × 10⁴ B16F10-mCherry-OVA cells overnight in complete DMEM (Corning, 10-013-CV) supplemented with 10% FBS (Seradigm, 3100), 1% penicillin–streptomycin (Corning, MT-3001-CI), 0.05 ng µl⁻¹ NGF (Life Technologies, 13257-019), 0.002 ng µl⁻¹ GDNF (PeproTech, 450-51-10). After 48 h, the cells were detached and TRPV1 neurons (eGFP⁺mCherry⁻) and B16F10-mCherry-OVA (eGFP⁺mCherry⁺) were FACS purified using a FACSAria IIu cell sorter (Becton Dickinson), and the cell supernatant was collected for ELISAs.

RNA-sequencing libraries were constructed using the Illumina TruSeq Stranded RNA LT Kit (Illumina) following the manufacturer's instructions. Illumina sequencing was performed at Fulgent Genetics. Reads were aligned to the mouse mm10 reference genome (GenBank assembly accession GCA_000001635.2) using STAR v.2.7 (ref. ⁵⁸). Aligned reads

were assigned to genic regions using the featureCounts function from subread v.1.6.4 (ref. ⁶⁵). Gene expression levels were represented by TPM. Hierarchical clustering was computed using the heatmap.2 function (ward.D2 method) from the gplots R package (v.3.1.3). Differential gene expression analysis was performed using DeSeq2 v.1.28.1⁵⁹. These data have been deposited in the NCBI's GEO (ref. ⁶⁰) (GSE205865).

ELISA on co-cultures of B16F10 cells and DRG neurons

A total of 1 × 10⁴ naive DRG neurons were cultured (96 h) with and without 5 × 10⁴ B16F10 cells in complete DMEM (10% FBS, 1% penicillin–streptomycin, 1 µl ml⁻¹ protease inhibitor). The cells were then challenged (30 min) with sterile PBS or KCl (40 mM) and the supernatant was collected. Neuropeptide releases were measured using commercial ELISAs for VIP (Antibodies Online, ABIN6974414), SP (Cayman Chemical, 583751) and CGRP (Cayman Chemical, 589001).

ELISA on co-cultures of B16F10 cells, CD8⁺ T cells and DRG neurons

Levels of SLPI (R&D Systems, DY1735-05) were measured in the cells' supernatant using a commercial ELISA.

OT-I CD8⁺ T cell-induced B16F10 elimination

A total of 2 × 10⁴ naive *Trpv1^{cre}::CheRiff-eGFP^{fl/wt}* DRG neurons were co-cultured with 1 × 10⁵ B16F10-mCherry-OVA cells overnight in T cell medium (supplemented with 0.05 ng µl⁻¹ NGF (Life Technologies, 13257-019) and 0.002 ng µl⁻¹ GDNF (PeproTech, 450-51-10)). One day after, 4 × 10⁵ stimulated OVA-specific CD8⁺ T cells under T_{cl} conditions were added to the co-culture. After 48 h, the cells were detached by trypsin (Gibco, 2062476) and collected by centrifugation (5 min at 1,300 rpm), stained using anti-Annexin V, 7-AAD (BioLegend, 640930) and anti-CD8 for 20 min at 4 °C, and immunophenotyped by flow cytometry using a FACSCanto II (Becton Dickinson). Cytokine expression levels were analysed after in vitro stimulation (PMA/ionomycin; see 'Intracellular cytokine staining').

Effect of neuron-conditioned medium on OT-I CD8⁺ T cell-induced B16F10 elimination

A total of 4 × 10⁵ stimulated OVA-specific CD8⁺ T cells were added to 1 × 10⁵ B16F10-mCherry-OVA and treated with fresh condition medium (1:2 dilution). After 48 h, cells were stained using anti-Annexin V, 7-AAD (BioLegend, 640930) and anti-CD8 for 20 min at 4 °C, and were immunophenotyped by flow cytometry using an LSRFortessa or a FACSCanto II (Becton Dickinson). For CGRP, 4 × 10⁵ stimulated OVA-specific CD8⁺ T cells were added to 1 × 10⁵ B16F10-mCherry-OVA and treated with CGRP (100 nM). After 24 h, the cells were stained using anti-Annexin V, 7-AAD (BioLegend, 640930) and anti-CD8 for 20 min at 4 °C, and were immunophenotyped by flow cytometry using an LSRFortessa or a FACSCanto II (Becton Dickinson). Cytokine expression levels were analysed after in vitro stimulation (PMA–ionomycin; see 'Intracellular cytokine staining').

Survival of B16F10 cells

A total of 1 × 10⁵ B16F10 cells were cultured in six-well plates and challenged with BoNT/A (0–50 pg µl⁻¹) for 24 h, QX-314 (0–1%) for 72 h, BIBN4096 (1–8 µM) for 24 h or their vehicle. The survival of B16F10 cells was assessed using anti-Annexin V staining and measured by flow cytometry using an LSRFortessa or a FACSCanto II (Becton Dickinson), or counted using a haemocytometer.

Effect of drugs on the function of CD8⁺ T cells

Splenocyte-isolated CD8⁺ T cells from naive C57BL/6J mice were cultured under T_{cl}-stimulating conditions (ex-vivo-activated by CD3 and CD28, IL-12 and anti-IL4) in 24-well plates for 48 h. The cells were then exposed to QX-314 (50–150 µM), BoNT/A (10–50 pg µl⁻¹) or BIBN4096 (1–4 µM) for 24 h. Apoptosis, exhaustion and activation levels were measured by flow cytometry using an LSRFortessa or a FACSCanto II (Becton Dickinson).

In silico analysis of neuronal expression profiles using RNA-sequencing and microarray datasets

Publicly available RNA gene expression data from seven datasets were downloaded from the NCBI GEO portal⁶⁶. RNA gene expression values of genes of interest were extracted. Expression values from single-cell sequencing were averaged for all cells. To be able to compare expression from datasets that were generated using different techniques (single-cell RNA sequencing, bulk RNA sequencing and microarrays) and normalization methods (TPM, RPKM (reads per kilobase per million mapped reads), RMA (robust multiarray analysis) and UMI (unique molecular identifiers)), all genes of interest were ratioed over *TRPV1* expression, then multiplied by 100, and the \log_{10} values of these values were plotted as a heat map⁶⁶. Kupari et al.⁶⁷ used single-cell RNA sequencing of JNC neurons, whereas Usoskin et al.⁶⁸ and Li et al.⁶⁹ used single-cell RNA sequencing of lumbar neurons. Chiu et al.⁷⁰ measured gene expression by microarrays of whole and FACS-sorted $\text{Na}_v1.8^+$ lumbar neurons. Goswami et al.⁷¹ performed RNA sequencing of TRPV1^+ lumbar neurons, whereas Ray et al.⁷² performed RNA sequencing of human lumbar neurons.

In silico analysis of tumour expression profiles of patients with melanoma using single-cell RNA sequencing

Using the publicly available Broad Institute single-cell bioportal, we performed an in silico analysis of single-cell RNA sequencing of human melanoma biopsies. We assessed the gene profile of *RAMP1*-expressing and *RAMP1*-negative T cells in the tumours of patients with metastatic melanoma⁴². Similarly, we assessed the genetic program of *RAMP1*-expressing and *RAMP1*-negative CD8^+ T cells in patients with melanoma⁴¹. The latter dataset was also used to analyse the genetic profile of CD8^+ T cells in patients who were responsive to immune checkpoint blockers or unresponsive to such treatment, as well as the genetic profile of malignant melanoma cells (defined as $\text{CD90}^+\text{CD45}^-$) from the biopsies of ten different patients⁴¹. Individual cell data are shown as a \log_2 -transformed $1 + (\text{TPM}/10)$. Experimental details and cell clustering have been defined in previous studies^{41,42}.

In silico analysis of the expression profiles of human immune cells

Publicly available RNA gene expression data from a previous study⁷³ were downloaded from the NCBI GEO portal. Read counts normalized to transcripts per million protein-coding genes (pTPM) values for genes of interest were extracted. Expression values from single-cell sequencing were averaged for all cells. Experimental details and cell clustering have been defined before⁷³.

In silico analysis of the expression profiles of cultured B16F10 cells

Publicly available RNA gene expression data from a previous study⁷⁴ were downloaded from the NCBI GEO portal. Read counts normalized to TPM for genes of interest were extracted. Experimental details and cell clustering have been defined before⁷⁴.

In silico analysis of the expression profiles of mouse immune cells using the ImmGen database

Using the publicly available ImmGen database, we performed an in silico analysis of RNA-sequencing data (DESeq2 data) of various mouse immune cells. As per ImmGen protocol, RNA-sequencing reads were aligned to the mouse genome GENCODE GRCm38/mm10 primary assembly (GenBank assembly accession GCA_000001635.2) and gene annotations vM16 with STAR 2.5.4a. The ribosomal RNA gene annotations were removed from the general transfer format file. The gene-level quantification was calculated by featureCounts. Raw read count tables were normalized by the median of ratios method with the DESeq2 package from Bioconductor and then converted to GCT and CLS format. Samples with fewer than 1 million uniquely mapped reads were automatically excluded from normalization. Experimental details

can be found at https://www.immgen.org/Protocols/ImmGenULI_RNAseq_methods.pdf.

Oncomine

In silico analysis of the expression profiles of biopsies from patients with melanoma using bulk microarray sequencing. As described previously¹⁹, samples from 45 cutaneous melanomas and 18 benign melanocytic skin nevus biopsies (around 5–20 μm) were collected and amplified, and their transcriptomes were profiled using Affymetrix U133A microarrays. Data were downloaded from the Oncomine database (<https://www.oncomine.com/>) as \log_2 -transformed (median centred intensity) and genes of interest were shown as heat maps. Experimental details and cell clustering have been defined before¹⁹.

Survival analysis of patients with melanoma

OncoLnc (<http://www.oncolnc.org/>) contains survival data for 8,647 patients from 21 cancer studies performed by TCGA⁴⁰. Using OncoLnc, we assessed the transcript expression of a user-defined list of 333 neuronal-enriched genes (neuronal membrane proteins, neural stem cell markers, transcription factors, ion channel receptors and neuro-peptides) in 459 skin cancer (SKCM) tumour biopsies from the TCGA database. Of these genes, 206 were expressed, and 108 were selected on the basis of their negative Cox coefficient value, indicating a link between lower gene expression and improved patient survival. Kaplan–Meier curves show the survival of the patients after segregation into two groups defined by their low or high expression of a gene of interest. Details of patients can be found in TCGA⁴⁰ and computational analyses can be found at <https://doi.org/10.7717/peerj-cs.67>.

Data collection and analysis

GraphPad Prism (v.9.0) and Microsoft Excel (v.2019) were used for data entry, graph construction and data analysis. Image analysis (neurite length and ramification index) was performed using ImageJ macros (Fiji, v.1.53c). Flow cytometry data were analysed using FlowJo (v.10.0.0). Calcium microscopy analysis was performed using a Nikon Eclipse Ti2 microscope (NIS-Elements Advanced Research v.4.5). Patient biopsy images were collected using an Olympus BX51 bright-field microscope and mouse tumour innervation images were acquired using an Olympus FV3000 confocal imaging system. For RNA sequencing, the reads were aligned to the mouse reference genome GRCm38/mm10 (GenBank assembly accession GCA_000001635.2) using STAR (versions used: 2.5.4a, 2.5.1b and 2.7). Aligned reads were assigned to geneic regions using the featureCounts function from Subread (v.1.6.4 22). Hierarchical clustering was computed using the heatmap.2 function (ward.D2 method) from Gplots R package (v.3.1.3). Differential gene expression analysis was carried out by DESeq2 (versions used: 1.18.1 and 1.28.1). TCGA data were accessed using Oncomine (<https://www.oncomine.com/> for gene expression) and OncoLnc (<http://www.oncolnc.org/> for survival). Single-cell RNA sequencing was analysed using the Broad Single-Cell Portal (<https://singlecell.broadinstitute.org/>). Human and mouse immune cell gene profiles were respectively analysed using the Human Protein Atlas (<https://www.proteinatlas.org/humanproteome/immune+cell>) and Immunological Genome Project (<https://www.immgen.org/>).

Sample size

Statistical methods were not used to predetermine sample size. The size of the cohort, based on similar studies in the field, was validated by pilot studies. All sample sizes are indicated in the figures and/or figure legends. All n values are indicated within the figure legends. In the only case in which a range is used (Fig. 2a,b), exact n values are provided in the source data files. For in vivo experiments, we used $n > 8$ mice. For in vitro experiments in which replicate samples were used, we repeated the experiments at least three independent times to confirm the findings. For other mouse experiments a minimum of five mice were used

to ensure that proper statistics could be used. We determined this to be sufficient as per our pilot data, use of internal controls and/or the observed variability between within experimental groups.

Replication

The number of replicates is indicated in the figures, figure legends and/or methods. On the graphs, individual dots represent individual samples or mice used. For each experiment, all attempts at replication were successful and our findings showed comparable results.

Randomization

Breeding pairs and their offspring (nociceptor-intact and -ablated mice) were co-housed and, in respect with the ARRIVE guidelines⁷⁵, were randomly allocated into each experimental group. For in vitro experiments, randomization was used for treatment selection. In some calcium microscopy experiments, the investigators performing the data collection were tasked to select all ligand-responsive cells for downstream analysis. In these rare cases, randomization was not used for cell selection.

Blinding

Double blinding was used for all in vivo treatments. In calcium microscopy experiments involving co-culture (for example, nociceptors and cancer cells), the differences in cell morphology are obvious and, therefore, the investigator performing the experiment was not blind. However, this investigator was always blinded to the treatment being applied to the cells and a second blinded investigator performed the downstream data analysis.

Data exclusions

No data were excluded.

Statistics

Statistical significance was determined using GraphPad Prism (Dot-matics, v.9) and calculated using simple linear regression analysis, Mantel–Cox regression, one-way or two-way ANOVA for multiple comparisons and two-sided unpaired Student's *t*-test for single variable comparison. In calcium imaging experiments, the *P* value is calculated on ligand-responsive neurons (calcium flux ≥ 5 –10%). *P* values < 0.05 were considered significant.

Antibodies

All of the antibodies used in this study are also listed in Supplementary Table 2.

Reporting summary

Further information on research design is available in the Nature Research Reporting Summary linked to this article.

Data availability

All data are readily available online (<https://www.talbotlab.com/nature>) and from the corresponding author. The RNA-sequencing datasets have been deposited in the NCBI's GEO (GSE205863, GSE205864 and GSE205865). Source data are provided with this paper.

43. Hogquist, K. A. et al. T cell receptor antagonist peptides induce positive selection. *Cell* **76**, 17–27 (1994).
44. Crosson, T. et al. FcεR1-expressing nociceptors trigger allergic airway inflammation. *J. Allergy Clin. Immunol.* **147**, 2330–2342 (2021).
45. Madisen, L. et al. A toolbox of Cre-dependent optogenetic transgenic mice for light-induced activation and silencing. *Nat. Neurosci.* **15**, 793–802 (2012).
46. Madisen, L. et al. A robust and high-throughput Cre reporting and characterization system for the whole mouse brain. *Nat. Neurosci.* **13**, 133–140 (2010).
47. Voehringer, D., Liang, H. E. & Locksley, R. M. Homeostasis and effector function of lymphopenia-induced “memory-like” T cells in constitutively T cell-depleted mice. *J. Immunol.* **180**, 4742–4753 (2008).

48. Lou, S. et al. Genetically targeted all-optical electrophysiology with a transgenic cre-dependent optopatch mouse. *J. Neurosci.* **36**, 11059–11073 (2016).
49. Agarwal, N., Offermanns, S. & Kuner, R. Conditional gene deletion in primary nociceptive neurons of trigeminal ganglia and dorsal root ganglia. *Genesis* **38**, 122–129 (2004).
50. Fidler, I. J. Biological behavior of malignant melanoma cells correlated to their survival in vivo. *Cancer Res.* **35**, 218–224 (1975).
51. Fidler, I. J. & Kripke, M. L. Metastasis results from preexisting variant cells within a malignant tumor. *Science* **197**, 893–895 (1977).
52. Headley, M. B. et al. Visualization of immediate immune responses to pioneer metastatic cells in the lung. *Nature* **531**, 513–517 (2016).
53. Twyman-Saint Victor, C. et al. Radiation and dual checkpoint blockade activate non-redundant immune mechanisms in cancer. *Nature* **520**, 373–377 (2015).
54. Huang, S. et al. Lymph nodes are innervated by a unique population of sensory neurons with immunomodulatory potential. *Cell* **184**, 441–459 (2021).
55. Renier, N. et al. iDISCO: a simple, rapid method to immunolabel large tissue samples for volume imaging. *Cell* **159**, 896–910 (2014).
56. Broz, M. L. et al. Dissecting the tumor myeloid compartment reveals rare activating antigen-presenting cells critical for T cell immunity. *Cancer Cell* **26**, 638–652 (2014).
57. Stathopoulou, C. et al. PD-1 inhibitory receptor downregulates asparaginyl endopeptidase and maintains Foxp3 transcription factor stability in induced regulatory T cells. *Immunity* **49**, 247–263 (2018).
58. Dobin, A. et al. STAR: ultrafast universal RNA-seq aligner. *Bioinformatics* **29**, 15–21 (2013).
59. Love, M. I., Huber, W. & Anders, S. Moderated estimation of fold change and dispersion for RNA-seq data with DESeq2. *Genome Biol.* **15**, 550 (2014).
60. Barrett, T. et al. NCBI GEO: archive for functional genomics data sets—update. *Nucleic Acids Res.* **41**, D991–995 (2013).
61. Chaplan, S. R., Bach, F. W., Pogrel, J. W., Chung, J. M. & Yaksh, T. L. Quantitative assessment of tactile allodynia in the rat paw. *J. Neurosci. Methods* **53**, 55–63 (1994).
62. Hargreaves, K., Dubner, R., Brown, F., Flores, C. & Joris, J. A new and sensitive method for measuring thermal nociception in cutaneous hyperalgesia. *Pain* **32**, 77–88 (1988).
63. Pool, M., Thiemann, J., Bar-Or, A. & Fournier, A. E. NeuriteTracer: a novel ImageJ plugin for automated quantification of neurite outgrowth. *J. Neurosci. Methods* **168**, 134–139 (2008).
64. Garcia-Segura, L. M. & Perez-Marquez, J. A new mathematical function to evaluate neuronal morphology using the Sholl analysis. *J. Neurosci. Methods* **226**, 103–109 (2014).
65. Liao, Y., Smyth, G. K. & Shi, W. featureCounts: an efficient general purpose program for assigning sequence reads to genomic features. *Bioinformatics* **30**, 923–930 (2014).
66. Crosson, T. et al. Profiling of how nociceptor neurons detect danger—new and old foes. *J. Intern. Med.* **286**, 268–289 (2019).
67. Kupari, J., Haring, M., Agirre, E., Castelo-Branco, G. & Ernfors, P. An atlas of vagal sensory neurons and their molecular specialization. *Cell Rep.* **27**, 2508–2523 (2019).
68. Usoskin, D. et al. Unbiased classification of sensory neuron types by large-scale single-cell RNA sequencing. *Nat. Neurosci.* **18**, 145–153 (2015).
69. Li, C., Wang, S., Chen, Y. & Zhang, X. Somatosensory neuron typing with high-coverage single-cell RNA sequencing and functional analysis. *Neurosci. Bull.* **34**, 200–207 (2018).
70. Chiu, I. M. et al. Transcriptional profiling at whole population and single cell levels reveals somatosensory neuron molecular diversity. *eLife* **3**, e04660 (2014).
71. Goswami, S. C. et al. Molecular signatures of mouse TRPV1-lineage neurons revealed by RNA-seq transcriptome analysis. *J. Pain* **15**, 1338–1359 (2014).
72. Ray, P. et al. Comparative transcriptome profiling of the human and mouse dorsal root ganglia: an RNA-seq-based resource for pain and sensory neuroscience research. *Pain* **159**, 1325–1345 (2018).
73. Monaco, G. et al. RNA-seq signatures normalized by mRNA abundance allow absolute deconvolution of human immune cell types. *Cell Rep.* **26**, 1627–1640 (2019).
74. Castle, J. C. et al. Exploiting the mutanome for tumor vaccination. *Cancer Res.* **72**, 1081–1091 (2012).
75. Kilkenny, C., Browne, W. J., Cuthill, I. C., Emerson, M. & Altman, D. G. Improving bioscience research reporting: the ARRIVE guidelines for reporting animal research. *J. Pharmacol. Pharmacother.* **1**, 94–99 (2010).
76. Heng, T. S. et al. The Immunological Genome Project: networks of gene expression in immune cells. *Nat. Immunol.* **9**, 1091–1094 (2008).

Acknowledgements S.T. is supported by the Canada Research Chair program (950-231859), the Canadian Institutes of Health Research (407016 (S.T. and M. Rangachari), 461274 and 461275), the Canadian Foundation for Innovation (37439), the Natural Sciences and Engineering Research Council of Canada (RGPIN-2019-06824), the Azrieli Foundation and the Brain Canada Foundation, as well as the Canada Cancer Research Society (840775; S.T., S.D.R., and J.T.). C.J.W. is supported by Dr. Miriam and Sheldon G. Adelson Medical Research Foundation and National Institutes of Health grant R35NS105076. P.D.V. is supported by the University of Pennsylvania Bassler Center for BRCA (Innovation award), and the National Institutes of Health (National Institute of General Medical Science) grants 1U54GM128729-02 (scholar award) and 5P20GM103548-08. J.T. is supported by a Saputo Research Chair, the Canada Foundation for Innovation (30017), and the Canadian Institutes of Health Research (136802). M.B., M.A., and T.E. held a scholarship from the Fonds de Recherche Santé Québec or CAPES/Print (88887.374124/2019-00). We thank the Molecular Pathology and Imaging cores at Sanford Research (supported by National Institutes of Health grants 5P20GM103548 and P20GM103620) for tissue processing. We thank P. B. D. Rosa for graphic design, A. C. Anderson for initial discussions and A. Regev, and L. Jerby-Arnon for discussing the in silico analysis of the single-cell RNA-sequencing datasets.

Author contributions M.B., M.A., T.E., S.H., C.J.S., H.D., K.-C.H., W.C.S., C.S.W., C.R.S., S.L.F., M. Rangachari, J.T., S.D.R., R.D., M. Rafei, N.G., P.D.V., C.J.W. and S.T. designed the study. A.E.T. and N.G. initiated the work on SLPI. E.S., S.C.T., H.M., A.P. and B.D. assisted with experimentation. M.B., M.A., T.E., A.A., A.M., Karine Roversi, Katiane Roversi, C.T.L., A.C.R., S.H., L.J., H.M., D.W.V. and S.T. conducted the experiments. M.B., M.A., P.D.V., C.J.W. and S.T. wrote the manuscript with input from all authors. M.B. performed the experiments in Figs. 1d,e, 2a,b,

Article

3a,b,d,e,h, 4a,b,e and 5a-c and Extended Data Figs. 4e, 5a-e, 6a-g,k,q, 7a-f,h-n, 8a-e,l-r, 9 and 10a-f,h-w. M.A. performed the experiments in Figs. 1d,e, 2a,b, 3a-c, 4a-d and 5a and Extended Data Figs. 4a-c,e, 5a-e,h-j, 6l-n, 7g,o,p, 8g,j,k,s,t and 10e,g. T.E. performed the experiments in Fig. 2c-f and Extended Data Fig. 5f-j and did the in silico analysis for Fig. 5d,e and Extended Data Figs. 1a-d, 3 and 11. A.A. performed the experiments in Fig. 3g,h and Extended Data Figs. 6o and 9. A.M. performed the experiments in Fig. 3f. Karine Roversi performed the experiments in Fig. 3a and Extended Data Fig. 6c-g,p. Katiane Roversi performed the experiments in Fig. 3a. C.T.L. performed the experiments in Extended Data Fig. 2. A.C.R. performed the experiments in Extended Data Fig. 2. S.H. performed the experiments in Fig. 1a. L.J. did the bioinformatic analysis of the experiments in Figs. 1d,e and 2a,b and Extended Data Figs. 4e and 5a-e. D.W.V. performed the experiments in Extended Data Fig. 2. S.T. performed the experiments in Fig. 1b,c and Extended Data Figs. 4d and 8f,h,i.

Competing interests S.T. and C.J.W. have an equity stake in Nocion Therapeutics. S.T. and C.J.W. have deposited a provisional patent (WO 2021/173916) on the use of charged sodium channel blockers to silence nociceptor neurons as a means to safeguard host anti-tumour immunity.

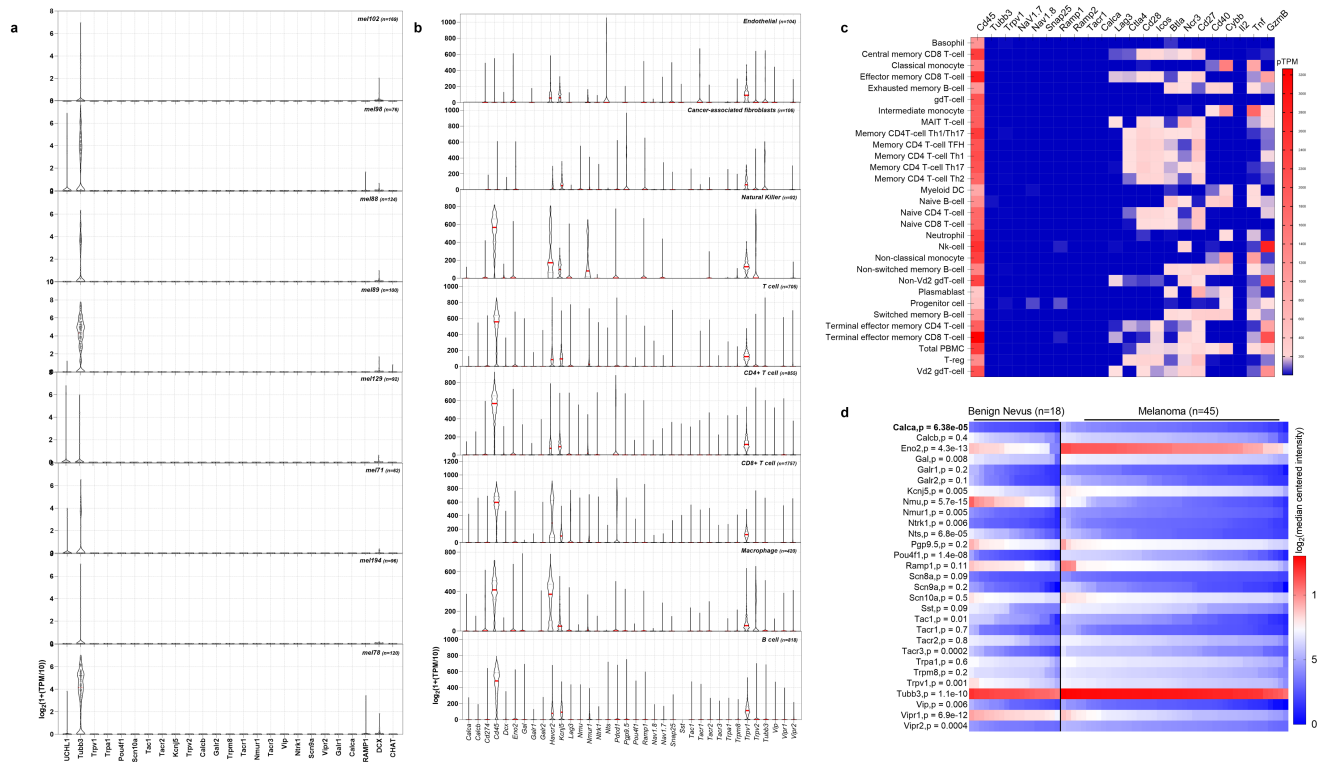
Additional information

Supplementary information The online version contains supplementary material available at <https://doi.org/10.1038/s41586-022-05374-w>.

Correspondence and requests for materials should be addressed to Sebastien Talbot.

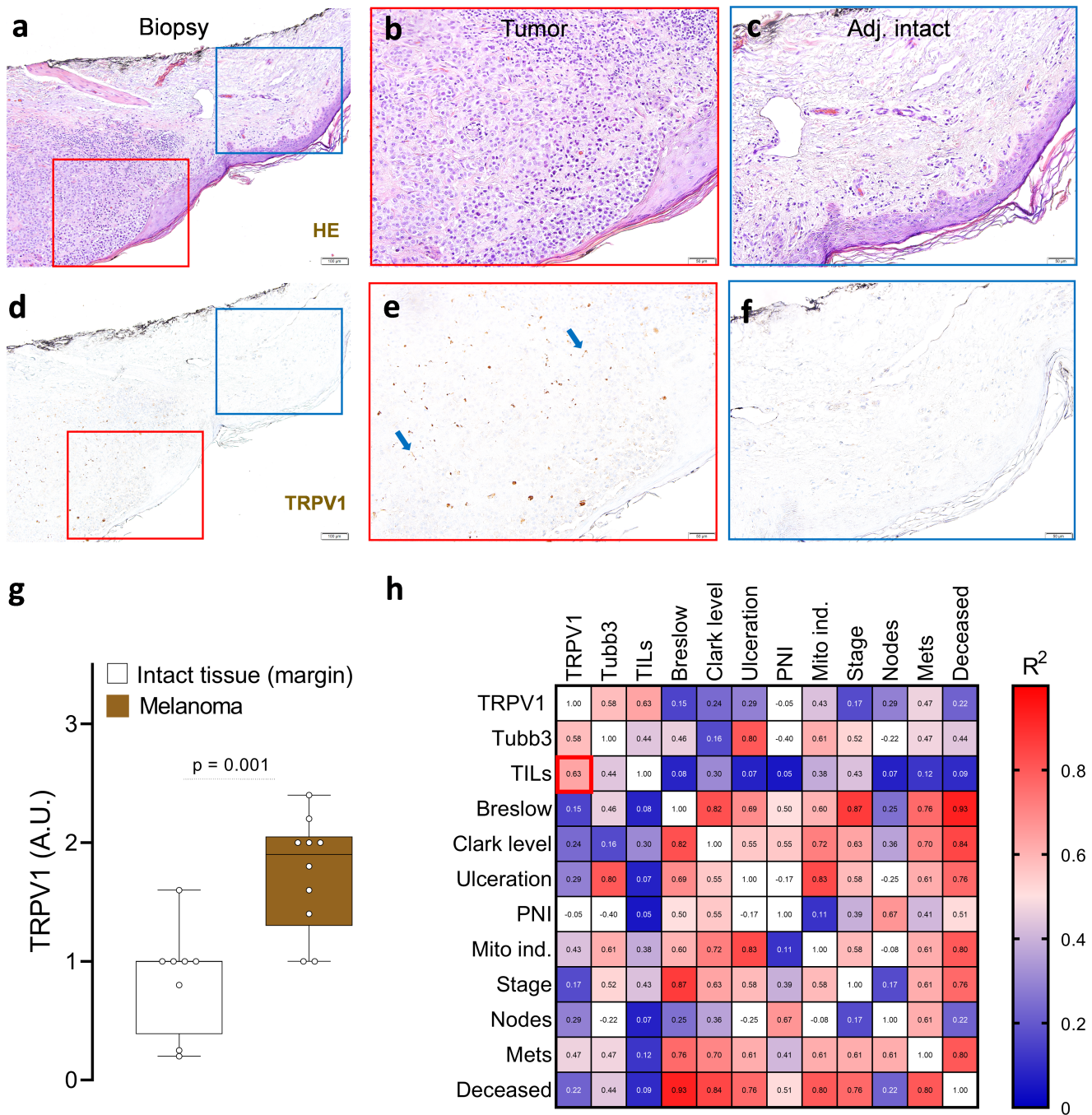
Peer review information *Nature* thanks Meenhard Herlyn and the other, anonymous, reviewer(s) for their contribution to the peer review of this work. Peer reviewer reports are available.

Reprints and permissions information is available at <http://www.nature.com/reprints>.



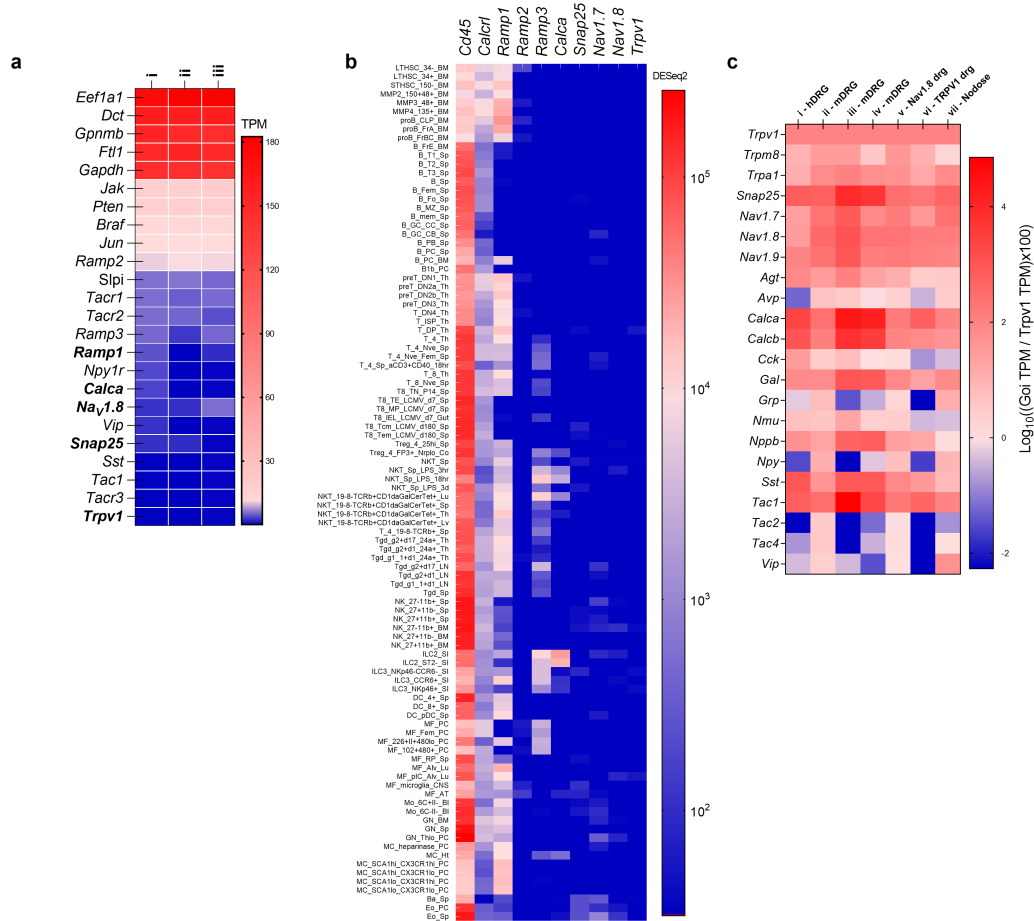
Extended Data Fig. 1 | *TRPV1*, *NAV1.8*, *SNAP25* or *RAMP1* transcripts are expressed in patient melanoma biopsies but are not detected in human immune cells or malignant cells. (a–b) In silico analysis of single-cell RNA sequencing of human melanoma-infiltrating cells revealed that *Trpv1*, *Nav1.8* (*Scn10a*), *Snap25* (the molecular target of BoNT/A), *Calca* (gene encoding for CGRP) transcripts are not detected in malignant melanoma cells (defined as CD90⁺ CD45⁺) from ten different patients' biopsies (a) nor in cancer-associated fibroblasts, macrophage, endothelial, natural killer, T, and B cells (b). Individual cell data are shown as a \log_2 of 1 + (transcript per million/10). Experimental details and cell clustering were defined in Jerby-Arnon et al⁴¹. N are defined in the figures. (c) In silico analysis of human immune cells revealed their basal expression of *Cd45*. Using RNA sequencing approaches, *Calca*, *Snap25*, *Trpv1* or

Nav1.8 are not detected in these cells. Heat maps show the read counts normalized to transcripts per million protein-coding genes (pTPM) for each of the single-cell clusters. Experimental details and cell clustering were defined in Monaco et al⁷³. (d) Forty-five cutaneous melanomas and 18 benign melanocytic skin nevus biopsies transcriptomes were profiled using Affymetrix U133A microarrays¹⁹. In silico analysis of this dataset revealed that cutaneous melanoma heightened expression levels of *Calca* (1.4-fold), *Pou4f1* (2-fold), *Eno2* (1.4-fold), and *Tubb3* (1.1-fold), as well as other neuronal-enriched genes. Heat map data are shown as \log_2 (median centered intensity); two-sided unpaired Student's t-test; p-values and n are shown in the figure. Experimental details were defined in Haqq et al¹⁹.



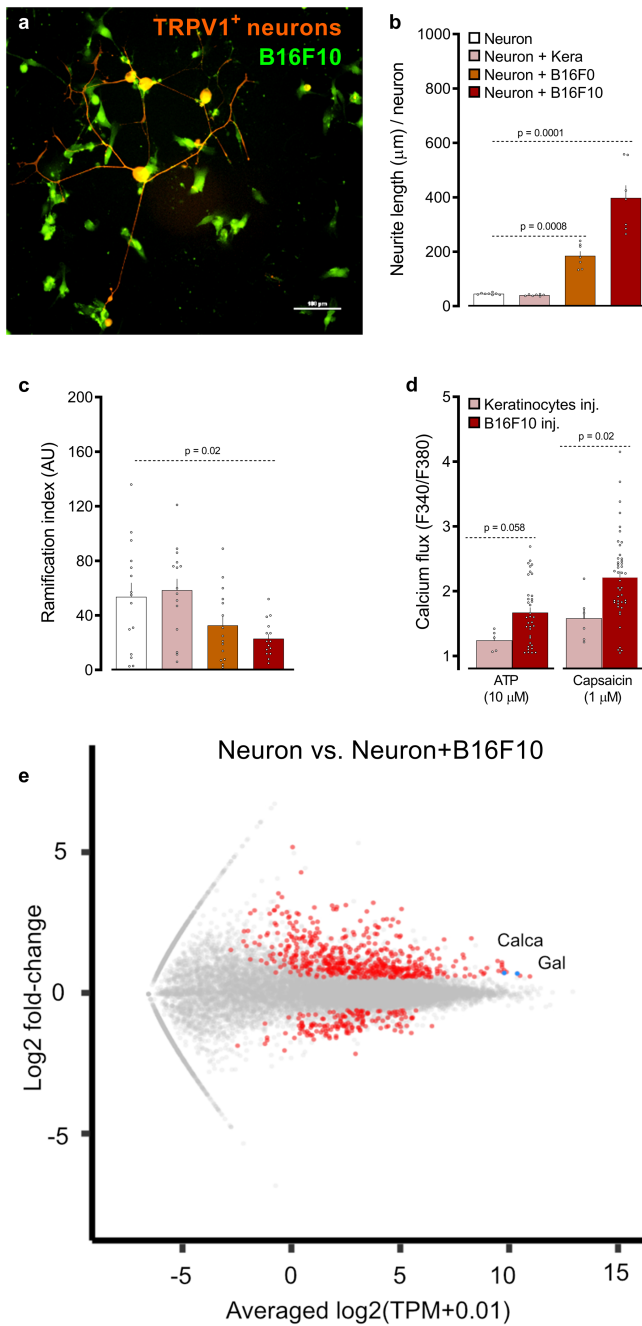
Extended Data Fig. 2 | TRPV1⁺ neurons innervate patient melanomas. Patients' melanoma sections were stained with hematoxylin eosin (a–f), and the presence of TRPV1 (d–f; brown) neurons was analysed by immunohistochemistry. Increased levels of TRPV1⁺ neurons (g) were found in the tumour (delimited by red square; a–b, d–e) compared to adjacent healthy skin (delimited by blue square; a, c, d, f). Increased TRPV1 immunolabelling in tumour sections primarily correlated with enhanced levels of tumour-infiltrating leukocytes (h) as scored from a retrospective correlation analysis performed on the patients' pathology

reports. Data are shown as representative immunohistochemistry images (a–f), box-and-whisker plots (runs from minimal to maximal values; the box extends from 25th to 75th percentile and the middle line indicates the median), for which individual data points are given (g) or as a heat map (h) displaying Pearson's correlation (R^2). N are as follows: a–f: n=10, g: intact (n = 8), tumour (n = 10), h: n = 10. Slides were scored blindly by two experienced medical pathologists. P-values are shown in the figure and determined by two-sided unpaired Student's t-test (g). Scale = 100 μ m (a, d), 50 μ m (b, c, e, f).



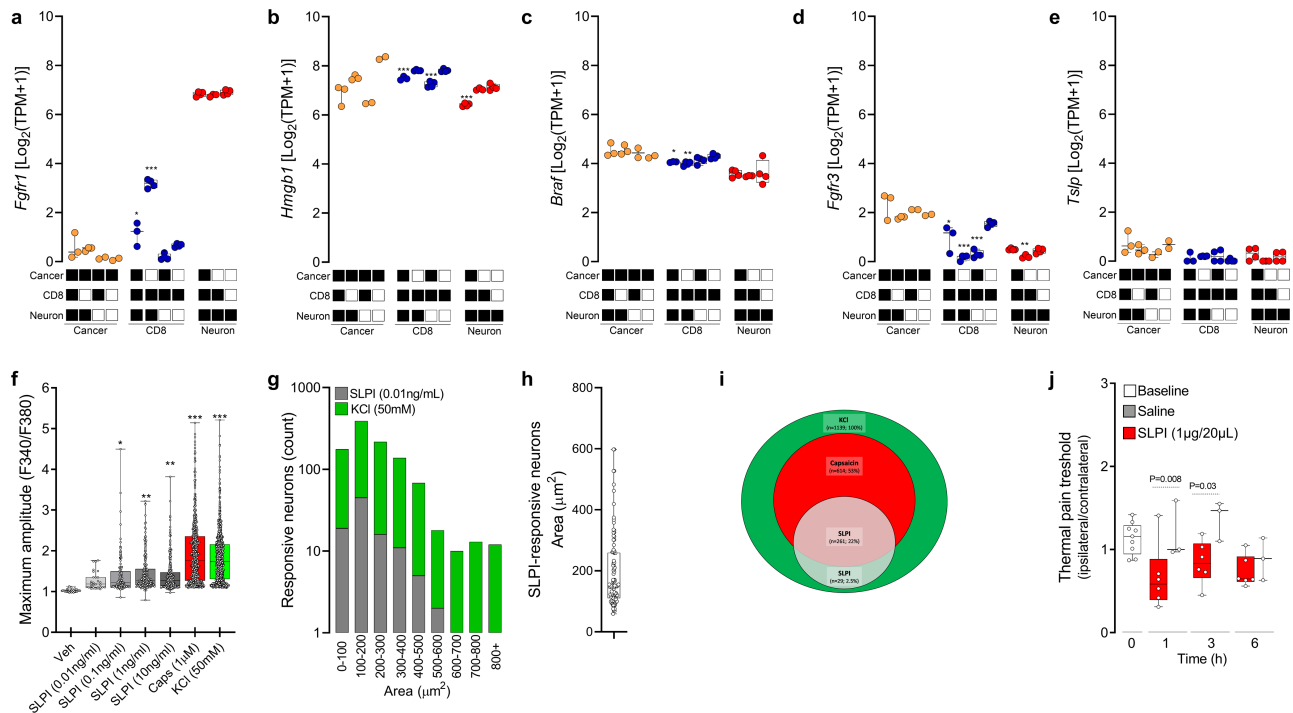
Extended Data Fig. 3 | *Trpv1*, *Nav1.8*, *Snap25* or *Ramp1* transcripts are not detected in B16F10 cancer cells or mouse immune cells. (a) *In silico* analysis of three different B16F10 cells cultures (labelled as i, ii, iii)⁷⁴ revealed their basal expression of *Braf* and *Pten*. In contrast, *Calca*, *Snap25*, *Trpv1* or *Nav1.8* transcripts are not detected in B16F10 cells. Heat map data are shown as transcript per million (TPM) on a linear scale. Experimental details were defined in Castle et al⁷⁴. N=3/group. **(b)** ImmGen RNA sequencing of leukocyte subpopulations⁷⁶ reveals their basal expression of *Cd45* and *Ramp1*. In contrast, *Snap25*, *Trpv1*, or *Nav1.8* transcripts are not detected in mouse immune cells. Heat map data are shown as DESeq₂ on a logarithmic scale. **(c)** A meta-analysis

of seven published nociceptor neuron expression profiling datasets⁶⁶ revealed the basal expression of sensory neuron markers (*Trpv1*, *Trpa1*) and neuropeptides (*Sp*, *Vip*, *Nmu*, *Calca*). Expression across datasets was ratioed over *Trpv1* and multiplied by 100. The \log_{10} of these values is presented as a heat map. i) RNA sequencing of human lumbar neurons;⁷² ii) microarrays of mouse FACS-sorted $\text{Na}_v1.8^+$ neurons;⁷⁰ iii) and iv) single-cell RNA sequencing of mouse lumbar neurons;^{68,69} v) microarray profiling of mouse $\text{Na}_v1.8^+$ DRG neurons;⁷⁰ vi) performed RNA sequencing of mouse TRPV1⁺ neurons;⁷¹ and vii) single-cell RNA sequencing of mouse vagal ganglia⁶⁷.



Extended Data Fig. 4 | B16F10 cells interact with nociceptor neurons. (a–c) When co-cultured with B16F10-eGFP cells (green), TRPV1⁺ nociceptor (*Trpv1^{cre::tdTomato}^{R/WT}*; orange) neurons form neuro-neoplastic contacts (a), show longer neurites (b), and exhibit reduced arborization (c) than when cultured alone or with non-tumorigenic keratinocytes (b–c). (d) L3–L5 DRG neurons were collected from mice 2-weeks after they were inoculated (left hindpaw; i.d.) with B16F10- or non-tumorigenic keratinocytes, cultured and calcium flux to ligands tested (ATP (10 μM), and capsaicin (1 μM)). Compared to neurons from keratinocytes-injected mice, the one from tumour-bearing mice showed increased sensitivity to capsaicin. (e) Naive DRG neurons (*Trpv1^{cre::Cherry}-eGFP^{fl/WT}*) were cultured alone or in combination with B16F10-mCherry-OVA. After 48h, the cells were collected, FACS purified, and RNA sequenced. Hierarchical clustering of sorted neuron DEG show distinct groups of transcripts enriched in TRPV1⁺ neuron vs cancer-exposed TRPV1⁺ neuron

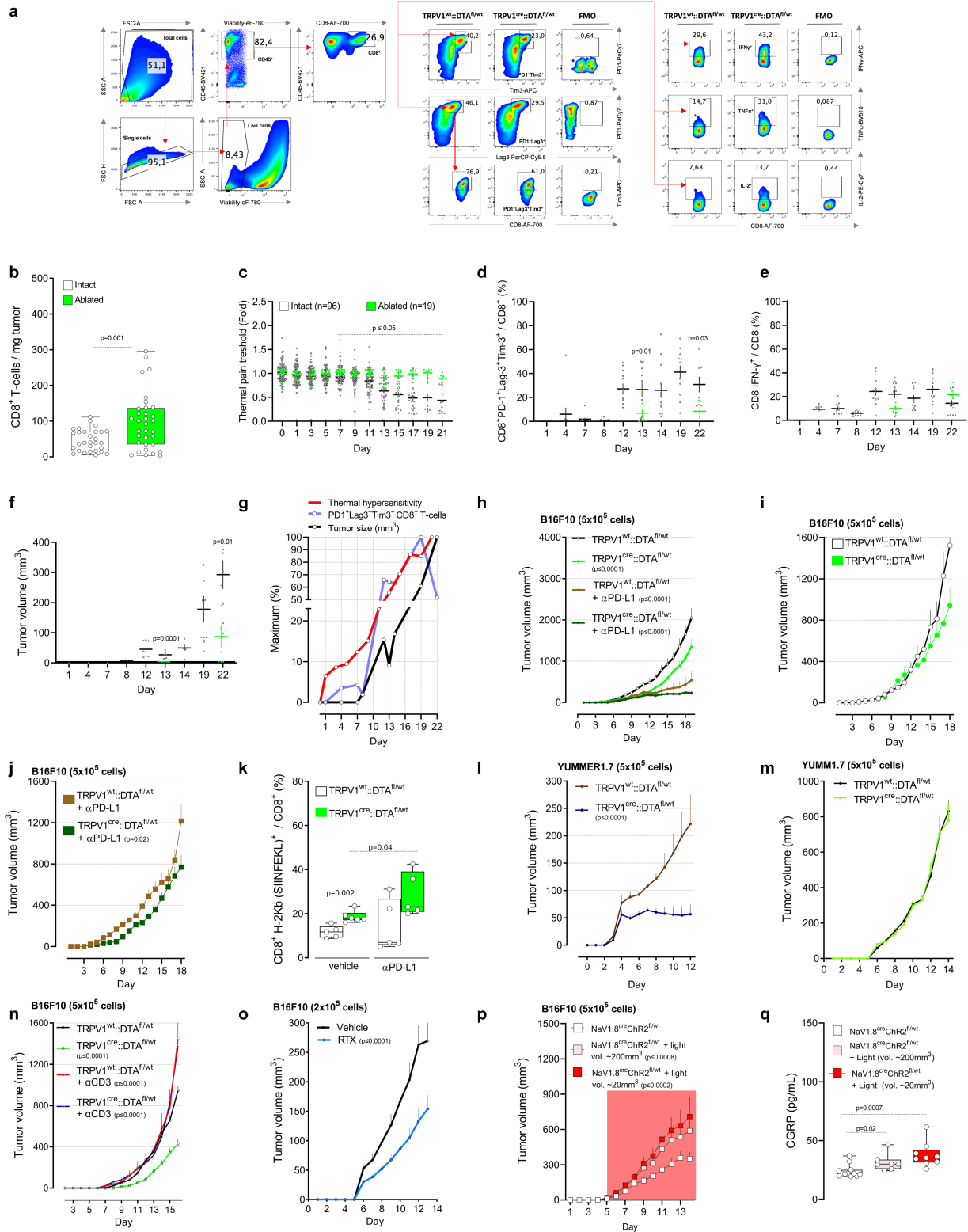
populations. Pairwise comparison of naive TRPV1⁺ neuron vs cancer-exposed TRPV1⁺ neuron populations showing differentially expressed transcripts as a volcano plot ($p < 0.05$). Among others, *Calca* (gene encoding for CGRP) was overexpressed in TRPV1⁺ (FACS-purified eGFP-expressing cells) neurons when co-cultured with B16F10-mCherry-OVA. Data are shown as representative image (a), mean ± S.E.M (b–d), or volcano plot (e). N are as follows: a: n = 4, b: neuron (n=8), neuron + keratinocytes (n = 7), neuron + B16F0 (n = 7), neuron + B16F10 (n = 7), c: n = 15/groups, d: keratinocytes inj. + ATP (n=5), B16F10 inj. + ATP (n=36), Keratinocytes inj. + caps (n = 6), B16F10 inj. + caps (n = 44), e: n = 4/groups. Experiments were independently repeated two (d) or three (a–c) times with similar results. Sequencing experiment was not repeated (e). P-values are shown in the figure and determined by one-way ANOVA post-hoc Bonferroni (b–c) or two-sided unpaired Student’s t-test (d). Scale bar = 100 μm (a).



Extended Data Fig. 5 | B16F10-secreted SLPI activates nociceptor neurons.

(a-e) Naive DRG neurons (*Trpv1^{cre}::CheRiff-eGFP^{fl/wt}*), B16F10-mCherry-OVA, and OVA-specific cytotoxic CD8⁺ T cells were cultured alone or in combination. After 48h, the cells were collected, FACS purified, and RNA sequenced. DEGs were calculated, and *Fgfr1* (fibroblast growth factor receptor 1) was found to be overexpressed in OVA-specific cytotoxic CD8⁺ T cells when co-cultured with cancer cells and DRG neurons (a). Conversely, OVA-specific cytotoxic CD8⁺ T cells downregulates the expression of the pro-nociceptive factor *Hmgb1* (High-mobility group box 1; b), *Braf* (c), as well as *Fgfr3* (d) when co-cultured with B16F10-mCherry-OVA and DRG neurons. *Tslp* expression level was not affected in any of tested groups (e). (f-i) Using calcium microscopy, we probed whether SLPI directly activates cultured DRG neurons. We found that SLPI (0.01-10 ng/mL) induces a significant calcium influx in DRG neurons (f). SLPI-responsive neurons are mostly small-sized neurons (g-h; mean area = 151 μm^2) and largely capsaicin-responsive (i; -42%). (j) The right hindpaw of naive mice was injected with saline (20 μL) or SLPI (i.d., 1 $\mu\text{g}/20 \mu\text{L}$), and the mice's noxious thermal nociceptive threshold was measured (0-6h). The ipsilateral paw injected with SLPI showed thermal hypersensitivity in contrast with the

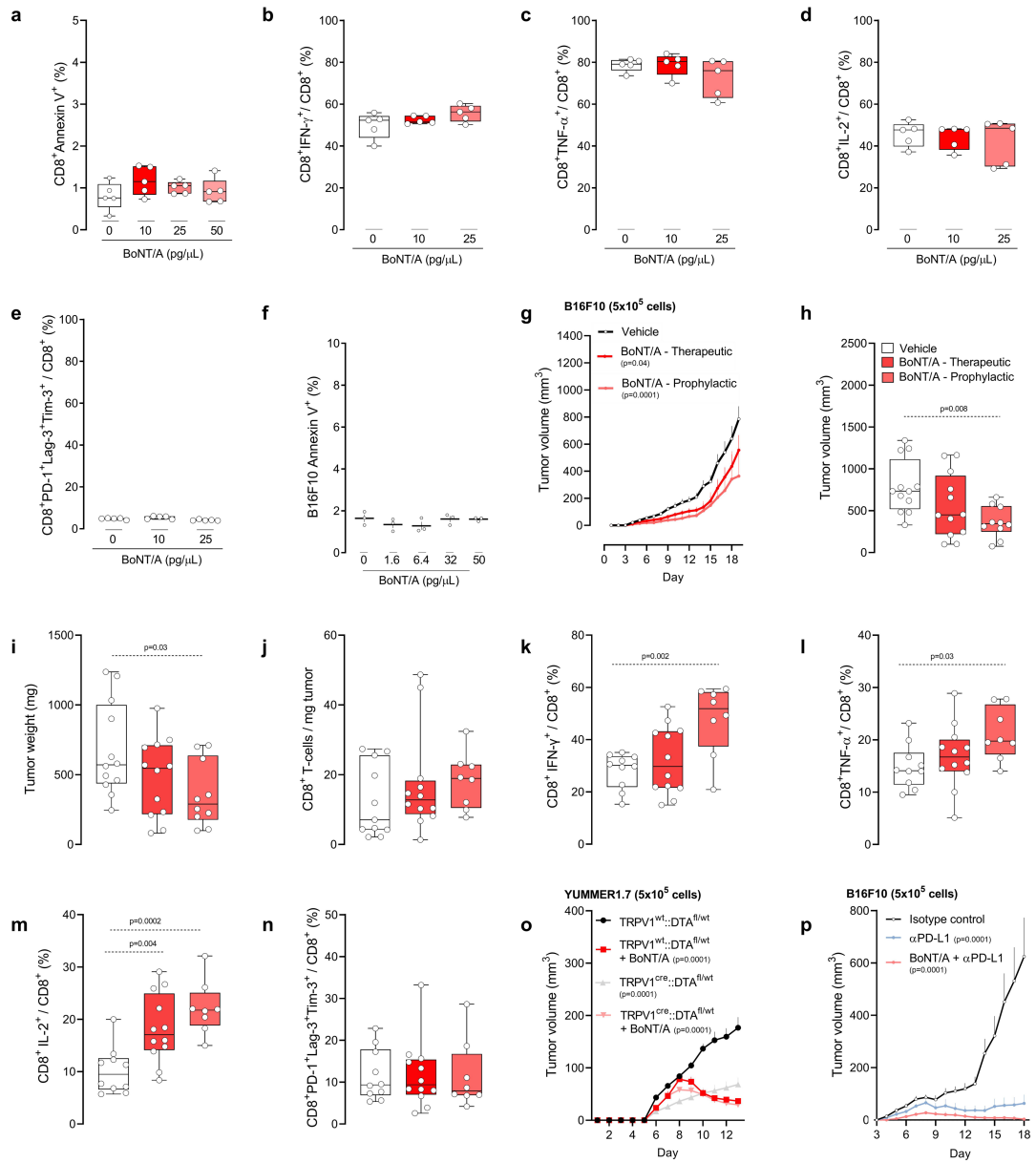
contralateral paw. Saline had no effect on the mice's thermal sensitivity. Data are shown as box-and-whisker plots (runs from minimal to maximal values; the box extends from 25th to 75th percentile and the middle line indicates the median), for which individual data points are given (a-f, h, j), stacked bar graph on a logarithmic scale (g), and Venn Diagram (i). N are as follows: a-e: n = 2-4/groups, f: vehicle (n = 28), 10pg/ml (n = 28), 100 pg/ml (n = 132), 1,000 pg/ml (n = 191), 10 ng/ml (n = 260), capsaicin (n = 613), KCl (n = 1,139), g: 0-100 (SLPI=19; KCl=177), 100-200 (SLPI = 45; KCl = 390), 200-300 (SLPI = 16; KCl = 216), 300-400 (SLPI=11; KCl = 138), 400-500 (SLPI = 5; KCl = 68), 500-600 (SLPI=2, KCl = 18), 600-700 (SLPI = 0; KCl = 10), 700-800 (SLPI=0; KCl=13), 800+ (SLPI = 0; KCl = 12), h: n = 98, i: KCl⁺=1139, KCl⁺Caps⁺=614, KCl⁺Caps⁺SLPI⁺=261, KCl⁺Caps⁺SLPI⁻=29, j: 0h (n = 9), SLPI at 1h (n = 6), saline at 1h (n = 3), SLPI at 3h (n = 6), saline at 3h (n=3), SLPI at 6h (n = 6), saline at 6h (n = 3). Experiments were independently repeated two (j) or three (f-i) times with similar results. Sequencing experiment was not repeated (a-e). P-values were determined by one-way ANOVA post-hoc Bonferroni (a-f); or two-sided unpaired Student's t-test (j). P-values are shown in the figure or indicated by * for $p \leq 0.05$; ** for $p \leq 0.01$; *** for $p \leq 0.001$.



Extended Data Fig. 6 | See next page for caption.

Extended Data Fig. 6 | Nociceptor ablation reduces the exhaustion of intratumoral CD8⁺ T cells. (a-b) Orthotopic B16F10-mCherry-OVA (5x10⁵ cells; i.d.) cells were injected to nociceptor intact (*Trpv1^{WT}::DTA^{fl/WT}*) and ablated (*Trpv1^{cre}::DTA^{fl/WT}*) mice. Sixteen days post-B16F10-mCherry-OVA cells inoculation (5x10⁵ cells; i.d.), tumour-infiltrating CD8⁺ T cells were immunophenotyped (a) and were found to be more numerous in sensory neuron depleted tumours (b). (c-g) Orthotopic B16F10-mCherry-OVA (2x10⁵ cells; i.d.) cells were injected into the left hindpaw paw of nociceptor intact (n = 96; *Trpv1^{WT}::DTA^{fl/WT}*) or ablated (n = 18; *Trpv1^{cre}::DTA^{fl/WT}*) mice. When compared to their baseline threshold, littermate control mice showed significant thermal hypersensitivity on day 7, an effect that peaks on day 21 (c). In these mice, intratumoral frequency of PD-1⁺LAG3⁺TIM3⁺ CD8⁺ T cells (d) and IFN γ (e) CD8⁺ T cells increased 12 days post tumour inoculation, an effect that peaked on day 19. Finally, B16F10 tumour volume peaked on day 22 (f). When compared with littermate control mice, sensory neuron ablated mice inoculated with B16F10 cells showed no thermal pain hypersensitivity (c), reduced intratumoral frequency of PD-1⁺LAG3⁺TIM3⁺ CD8⁺ T cells (d) and tumour volume (f). In littermate control mice, thermal pain hypersensitivity (day 7) precedes the increase in intratumoral frequency of PD-1⁺LAG3⁺TIM3⁺ CD8⁺ T cells (day 12), and significant tumour growth (day 12; g). (h) Orthotopic B16F10-mCherry-OVA cells (5x10⁵ cells; i.d.) were inoculated into 8-week-old male and female sensory neuron intact or ablated mice. The mice were treated with α PD-L1 (6 mg/kg, i.p.; days 7, 10, 13, 16 post tumour inoculation) or its isotype control. On day 19, α PD-L1 potentiated the nociceptor ablation mediated reduction in B16F10-OVA tumour volume. (i-k) Orthotopic B16F10-mCherry-OVA cells (5x10⁵ cells, i.d.) were injected into a cohort of nociceptor neuron-ablated mice 3 days prior to the injection given to nociceptor intact mice. Mice from each group with similar tumour size (~85mm³) were selected and exposed to α PD-L1 (6 mg/kg, i.p.) once every 3 days for a total of 9 days. Eighteen days post tumour inoculation, we found that α PD-L1-reduced tumour growth was higher (~47%) in nociceptor-ablated mice than was observed in nociceptor-intact mice (~32%; i-j). In addition, nociceptor ablation increased the proportion of intratumoral tumour-specific (k; defined as H-2Kb⁺) CD8⁺ T cells. These differences were further enhanced by α PD-L1 treatment (i-k). (l-m) Sensory neurons ablation (*Trpv1^{cre}::DTA^{fl/WT}*) decreased growth of YUMMER1.7 cells (5x10⁵ cells; i.d.) an immunogenic version of a *Braf^{V600E}Cdkn2a^{-/-}Pten^{-/-}* melanoma cell line (l; assessed until day 12). The non-immunogenic YUMML7 cell line (5x10⁵ cells; i.d.; assessed until day 14) cells were injected to nociceptor intact (*Trpv1^{WT}::DTA^{fl/WT}*) and ablated mice

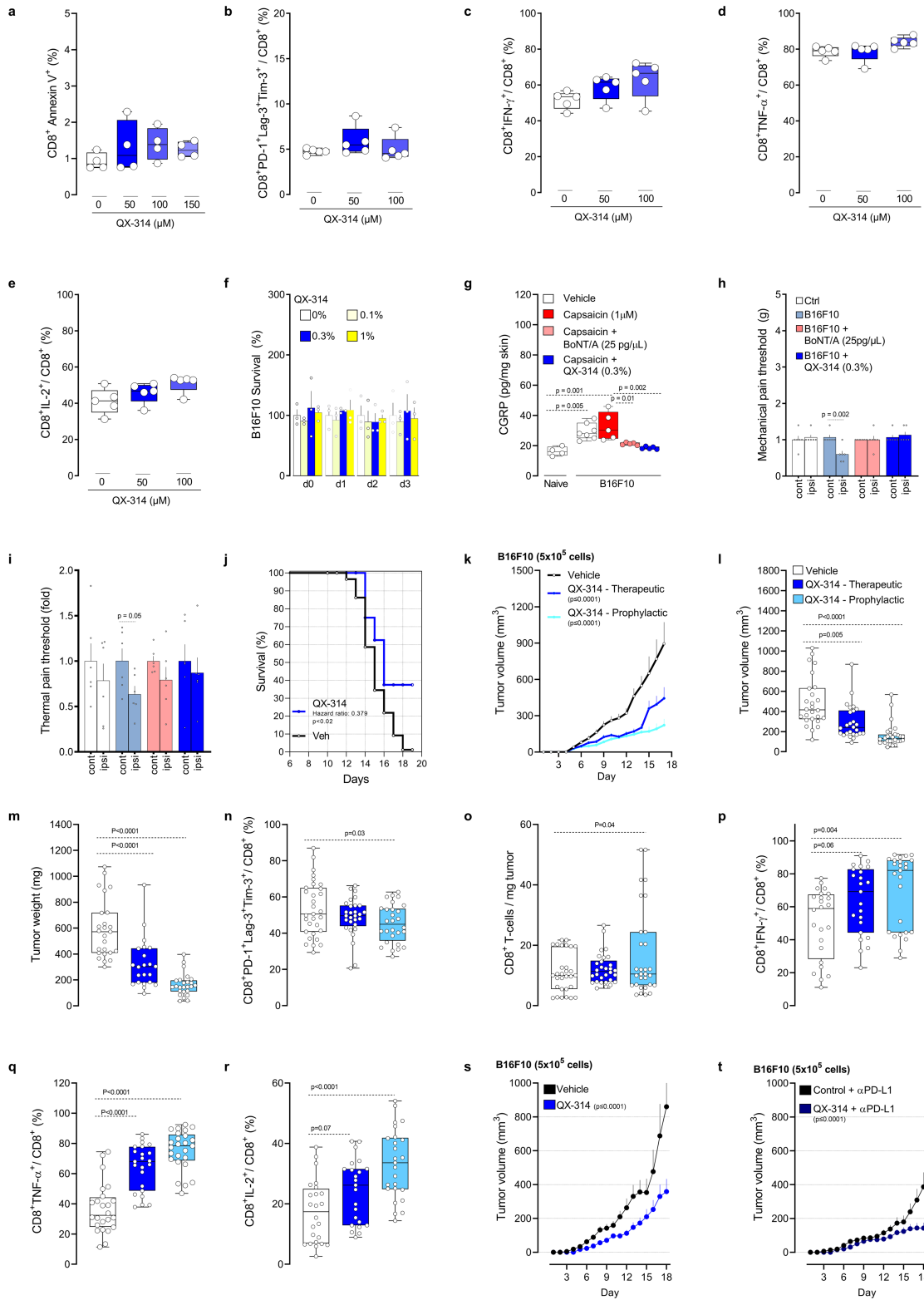
(*Trpv1^{cre}::DTA^{fl/WT}*). Nociceptor ablation had no effect on YUMML7 growth (m). (n) Orthotopic B16F10-mCherry-OVA (5x10⁵ cells; i.d.) cells were injected to nociceptor intact (*Trpv1^{WT}::DTA^{fl/WT}*) and ablated mice (*Trpv1^{cre}::DTA^{fl/WT}*). The reduction in B16F10-mCherry-OVA (5x10⁵ cells; i.d.) tumour growth observed in nociceptors ablated mice was absent following systemic CD3 depletion (assessed until day 15; α CD3, 200 μ g/mouse; i.p.; every 3 days). (o) To deplete their nociceptor neurons, C57BL/6j mice were injected with RTX (s.c., 30, 70, 100 μ g/kg) and were subsequently (28 days later) inoculated with B16F10-mCherry-OVA (2x10⁵ cells). RTX-injected mice showed reduced tumour growth when compared to vehicle-exposed mice (assessed until day 13). (p-q) Orthotopic B16F10-mCherry-OVA (5x10⁵ cells; i.d.) cells were injected to light-sensitive mice (*Nav1.8^{cre}::ChR2^{fl/WT}*). As opposed to unstimulated mice, the optogenetic activation (3.5 ms, 10Hz, 478nm, 60 mW, giving approx. 2-6 mW/mm² with a 0.39-NA fibre placed 5-10 mm from the skin, 20 min) of tumour-innervating nociceptor neurons, when started once B16F10 tumours were visible (~20 mm³) or well established (~200 mm³), resulted in enhanced tumour growth (p, as measured until day 14) and intratumoral CGRP release (q). Data are shown as FACS plot (a; depict the gating strategy used in fig. 3d,e), as box-and-whisker plots (runs from minimal to maximal values; the box extends from 25th to 75th percentile and the middle line indicates the median) for which individual data points are given (b,k,q), scatter dot plot (c-f), percentage change from maximal thermal hypersensitivity, intratumoral frequency of PD-1⁺LAG3⁺TIM3⁺ CD8⁺ T cells and tumour volume (g), or mean \pm S.E.M (h-j, l-p). N are as follows: a-b: intact (n = 29), ablated (n = 33), c: intact (n = 96), ablated (n = 19), d: intact (n = 92), ablated (n = 15), e: intact (n = 96), ablated (n = 15), f: intact (n = 96), ablated (n = 16), g: n=96, h: intact (n = 9), ablated (n = 10), intact+ α PD-L1 (n = 9), ablated+ α PD-L1 (n = 8), i: intact (n = 14), ablated (n = 4), j: intact+ α PD-L1 (n = 12), ablated+ α PD-L1 (n = 12), k: intact (n = 5), ablated (n = 6), intact+ α PD-L1 (n = 5), ablated+ α PD-L1 (n = 5), l: intact (n = 8), ablated (n = 11), m: intact (n = 6), ablated (n = 13), n: intact (n = 5), ablated (n = 5), intact+ α CD3 (n = 6), ablated+ α CD3 (n = 5), o: vehicle (n = 11), RTX (n = 10), p: *Nav1.8^{cre}::ChR2^{fl/WT}* (n = 12), *Nav1.8^{cre}::ChR2^{fl/WT}* + Light (vol. ~200 mm³) (n = 8), *Nav1.8^{cre}::ChR2^{fl/WT}* + Light (vol. ~20 mm³) (n = 8), q: *Nav1.8^{cre}::ChR2^{fl/WT}* (n = 12), *Nav1.8^{cre}::ChR2^{fl/WT}* + Light (vol. ~200 mm³) (n = 7), *Nav1.8^{cre}::ChR2^{fl/WT}* + Light (vol. ~20 mm³) (n = 9). Experiments were independently repeated two (c-g), three (h-q) or six (a,b) times with similar results. P-values are shown in the figure and determined by two-sided unpaired Student's t-test (b-f, k,q), or two-way ANOVA post-hoc Bonferroni (h-j, l-p).



Extended Data Fig. 7 | See next page for caption.

Extended Data Fig. 7 | BoNT/A silencing of B16F10-innervating neurons decreases tumour growth. (a–e) Splenocytes-isolated CD8⁺ T cells from naive C57BL/6 mice were cultured under T_{cl}-stimulating conditions (*ex vivo* activated by CD3 and CD28, IL-12, and anti-IL4) for 48h. The cells were then exposed to BoNT/A (10–50 pg/μL) for 24h; effects on apoptosis, exhaustion, and activation were measured by flow cytometry. When compared to vehicle-exposed cells, BoNT/A did not affect the survival (a) of cultured cytotoxic CD8⁺ T cells, nor their relative expression of IFNγ⁺ (b), TNF⁺ (c), IL-2⁺ (d) and PD-1⁺LAG3⁺TIM3⁺ (e). (f) B16F10 (1x10⁵ cells) were cultured for 24h and subsequently exposed to BoNT/A (1.6-50 pg/μL) or its vehicle for an additional 24h. BoNT/A did not trigger B16F10 cells apoptosis, as measured by the mean fluorescence intensity of Annexin V. (g–n) One and three days prior to tumour inoculation (*defined as prophylactic*), the skin of 8-week-old male and female mice was injected with BoNT/A (25 pg/μL; i.d.) or its vehicle. One day after the last injection, orthotopic B16F10-mCherry-OVA (5x10⁵ cells; i.d.) were inoculated into the area pre-exposed to BoNT/A. In another group of mice, BoNT/A was administered (25 pg/μL; i.d.) one and three days after the tumour reached a volume of ~200mm³ (*defined as therapeutic*). The effect of neuron silencing on tumour size and tumour-infiltrating CD8⁺ T cell exhaustion was measured. Nineteen days post tumour inoculation, we found that the tumour volume (g, h) and weight (i) were reduced in mice treated with BoNT/A (*Prophylactic group*). In parallel, we found that silencing tumour-innervating neurons increased the proportion of IFNγ⁺ (k), TNF⁺ (l), and IL-2⁺ (m) CD8⁺ T cells. BoNT/A had no effect on the total number of intratumoral CD8 T cells (j) or the relative proportion of PD-1⁺LAG3⁺TIM3⁺ (n) CD8⁺ T cells. (o) One and three days prior to tumour inoculation, the skin of 8-week-old male and female sensory neuron-intact or ablated mice was injected with BoNT/A (25 pg/μL; i.d.) or its

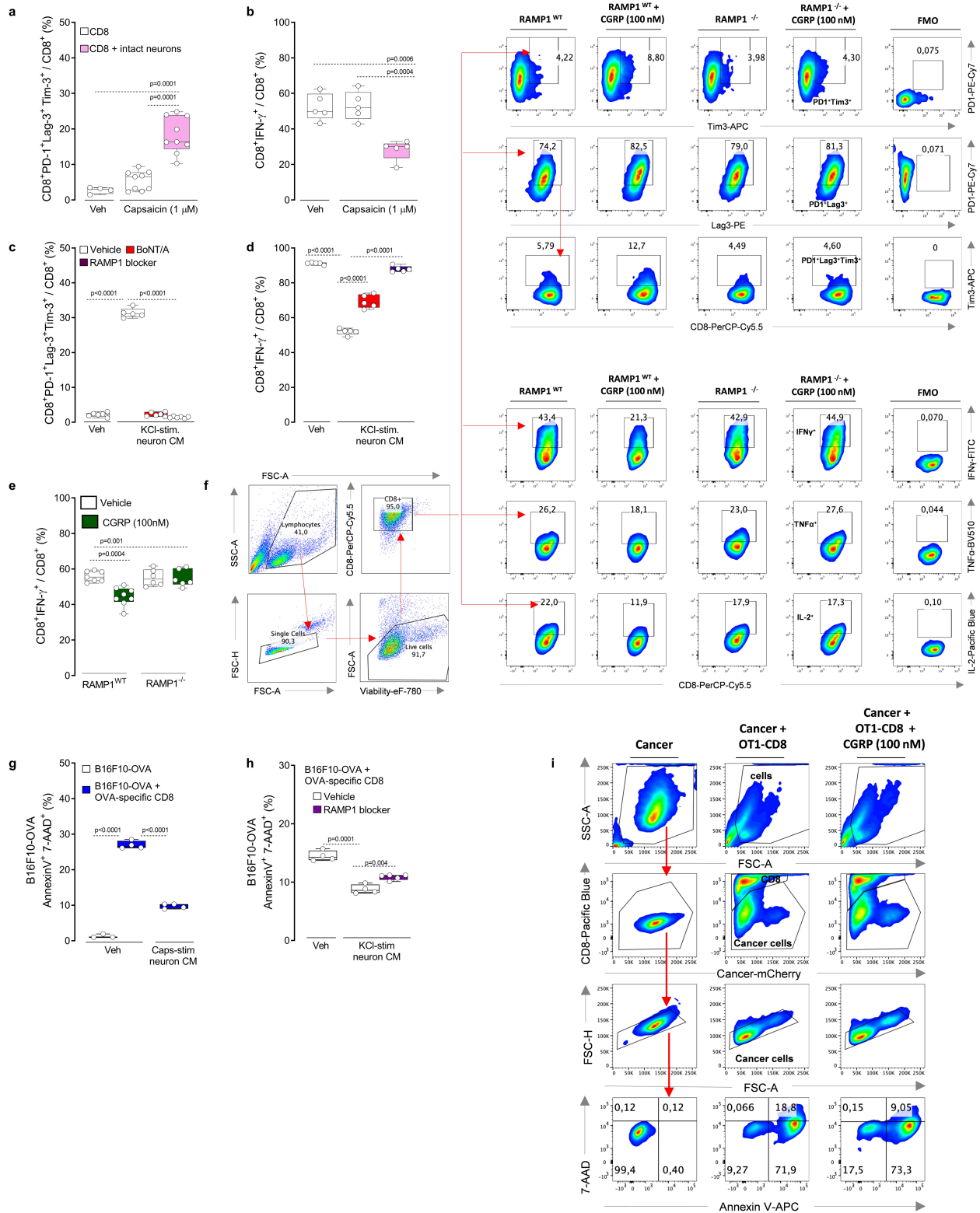
vehicle. One day following the last injection, orthotopic YUMMER1.7 cells (5x10⁵ cells; i.d.) were inoculated into the area pre-exposed to BoNT/A. The effects of nociceptor neuron ablation on tumour size and volume were measured. Thirteen days post tumour inoculation, we found that the tumour growth was lower in mice treated with BoNT/A or in sensory neuron-ablated mice. BoNT/A had no additive effects when administered to sensory neuron-ablated mice. (p) One and three days prior to tumour inoculation, the skin of 8-week-old male and female mice was injected with BoNT/A (25 pg/μL; i.d.) or its vehicle. One day following the last injection, orthotopic B16F10-mCherry-OVA cells (5x10⁵ cells; i.d.) were inoculated into the area pre-exposed to BoNT/A. On days 7, 10, 13 and 16 post tumour inoculation, the mice were exposed to αPD-L1 (6 mg/kg, i.p.) or its isotype control. Eighteen days post tumour inoculation, we found that neuron silencing using BoNT/A potentiated αPD-L1-mediated tumour reduction. Data are shown as box-and-whisker plots (runs from minimal to maximal values; the box extends from 25th to 75th percentile and the middle line indicates the median), for which individual data points are given (a–f; h–n) or as mean ± S.E.M (g, o, p). N are as follows: a–e: n = 5/groups, f: n = 3/groups, g–i: vehicle (n = 12), BoNT/A therapeutic (n = 12), BoNT/A prophylactic (n = 10), j: vehicle (n = 11), BoNT/A therapeutic (n = 12), BoNT/A prophylactic (n = 8), k–n: vehicle (n = 10), BoNT/A therapeutic (n = 12), BoNT/A prophylactic (n = 8), o: intact + vehicle (n = 9), ablated + vehicle (n = 8), intact + BoNT/A (n = 10), ablated + BoNT/A (n = 8), p: vehicle (n = 7), αPD-L1 (n = 8), αPD-L1 + BoNT/A (n = 7). Experiments were independently repeated two (a–f, o–p) or four (g–n) times with similar results. P-values are shown in the figure and determined by one-way ANOVA posthoc Bonferonni (a–f, h–n) or two-way ANOVA post-hoc Bonferonni (g, o, p).



Extended Data Fig. 8 | See next page for caption.

Extended Data Fig. 8 | QX-314 silencing of B16F10-innervating neurons reduces tumour growth. (a–e) Splenocytes-isolated CD8⁺ T cells from naive C57BL/6 mice were cultured under T_{cl}-stimulating conditions (*ex vivo* activated by CD3 and CD28, IL-12, and anti-IL4) for 48h. The cells were then exposed to QX-314 (50–150 μM) for 24h, effects on apoptosis, exhaustion and activation were measured by flow cytometry. When compared to vehicle-exposed cells, QX-314 did not affect the survival of cultured cytotoxic CD8⁺ T cells (a), nor their relative expression of PD-1⁺LAG3⁺TIM3⁺ (b), IFNγ⁺ (c), TNF⁺ (d) and IL-2⁺ (e). (f) B16F10 (1x10⁵ cells) were cultured for 24h. The cells were then exposed or not to QX-314 (0.1-1%) for an additional 24-72h, and cell count was analysed by bright-field microscopy. QX-314 did not affect B16F10 cells' survival, as measured by relative cell count changes (at each time point) in comparison to vehicle-exposed cells. (g–i) One and three days prior to tumour inoculation, 8-week-old male and female wild-type mice's right hindpaws or flanks were injected with BoNT/A (25 pg/μL; i.d.) or its vehicle. On the following day, orthotopic B16F10 cells (g: 5x10⁵ cells; i.d.; h–i: 2x10⁵ cells; i.d.) were inoculated into the area pre-exposed to BoNT/A. Starting one day post inoculation, QX-314 (0.3%) or its vehicle was administered (i.d.) once daily in another group of mice. The effects of sensory neuron silencing were tested on neuropeptide release (g), as well as mechanical (h) and thermal pain hypersensitivity (i). First, CGRP levels were increased in B16F10 tumour surrounding skin explant (assessed on day 15) in comparison to control skin; an effect further enhanced by capsaicin (1 μM; 3h) but was absent in skin pre-treated with BoNT/A (25 pg/μL) or QX-314 (0.3%; g). We also found that B16F10 injection induced mechanical (h) and thermal pain hypersensitivities (i) fourteen days post tumour inoculation. These effects were stopped by sensory neuron silencing with QX-314 or BoNT/A (h–i). (j) Orthotopic B16F10-mCherry-OVA cells (5x10⁵ cells; i.d.) were inoculated into 8-week-old male and female mice. Starting one day post inoculation, QX-314 (0.3%; i.d.; 5 sites) was injected once daily around the tumour. The effect of nociceptor neuron silencing on tumour size and tumour-infiltrating CD8⁺ T cell exhaustion was measured. We found that silencing tumour-innervating neurons increased the mice's median length of survival (-270% Mantel–Haenszel hazard ratio; measured on day 19). (k–r) Orthotopic

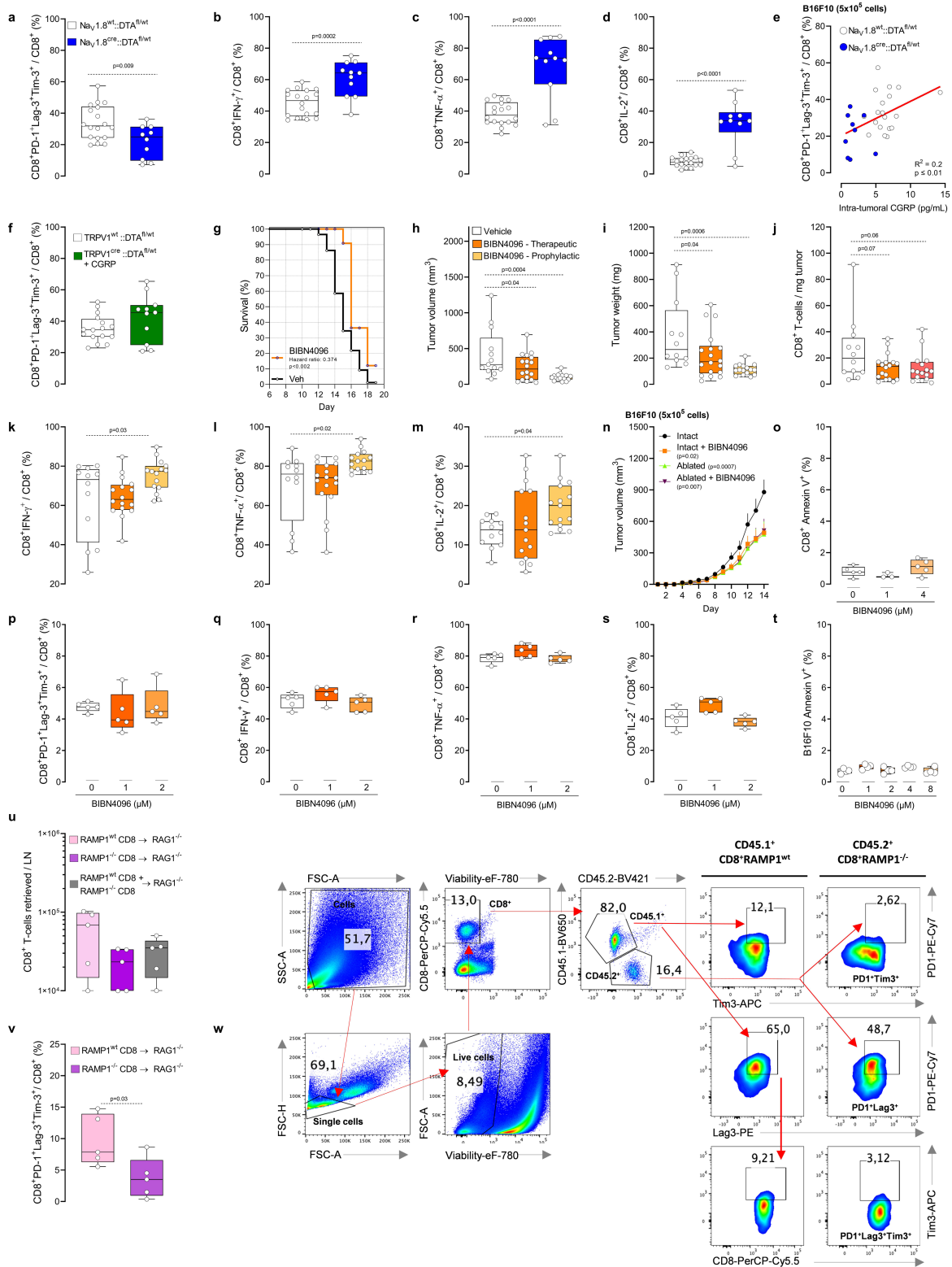
B16F10-mCherry-OVA cells (5x10⁵ cells; i.d.) were inoculated into 8-week-old male and female mice. Starting one day post inoculation (*defined as prophylactic*). In other groups of mice, QX-314 daily injection started once the tumour reached a volume of ~200mm³ (*defined as therapeutic*). As measured seventeen days post tumour inoculation, silencing tumour innervation also decreased tumour volume (k, l) and weight (m), as well as the relative proportion of PD-1⁺LAG3⁺TIM3⁺ (n) CD8⁺ T cells. QX-314 treatment also increased the total number of intratumoral CD8⁺ T cells (o), as well as relative proportion of IFNγ⁺ (p), TNF⁺ (q), and IL-2⁺ (r) CD8⁺ T cells. (s–t) Orthotopic B16F10-mCherry-OVA cells (5x10⁵ cells, i.d.) were injected into mice treated with QX-314 (0.3%; i.d.) 2-3 days prior to being injected into vehicle-exposed mice. Mice from each group with similar tumour size (~100mm³) were selected and exposed to αPD-L1 (6 mg/kg, i.p.) once every 3 days for a total of 9 days. Eighteen days post tumour inoculation, we found that αPD-L1-reduced tumour growth was higher (~61%) in nociceptor silenced mice than was observed in isotype vehicle-exposed mice (~49%; s–t). Data are shown as box-and-whisker plots (runs from minimal to maximal values; the box extends from 25th to 75th percentile and the middle line indicates the median), for which individual data points are given (a–e, g, l–r), as mean ± S.E.M (f, h, i, k, s, t), or as Mantel–Cox regression analysis (j). N are as follows: a: n = 4/groups, b–e: n = 5/groups, f: n = 3/groups, g: naïve (n = 4), vehicle (n = 7), B16F10+vehicle (n = 5), B16F10+BoNT/A (n = 5), B16F10+QX-314 (n = 5), h–i: n = 6/groups, j: vehicle (n = 89), QX-314 (n = 12), k: vehicle (n = 21), QX-314 prophylactic (n = 21), QX-314 therapeutic (n = 17), l: vehicle (n = 26), QX-314 therapeutic (n = 26), QX-314 prophylactic (n = 28), m: vehicle (n = 25), QX-314 therapeutic (n = 22), QX-314 prophylactic (n = 25), n: vehicle (n = 31), QX-314 therapeutic (n = 29), QX-314 prophylactic (n = 28), o: n = 30/groups, p–r: vehicle (n = 24), QX-314 therapeutic (n = 23), QX-314 prophylactic (n = 25), s: vehicle (n = 9), QX-314 (n = 13), t: vehicle + αPD-L1 (n = 18), QX-314 + αPLD1 (n = 13). Experiments were independently repeated two (a–i, s–t) or four (j–r) times with similar results. P-values are shown in the figure and determined by one-way ANOVA posthoc Bonferonni (a–g, l–r), two-sided unpaired Student's t-test (h–i), Mantel–Cox regression (j), or two-way ANOVA posthoc Bonferonni (k, s–t).



Extended Data Fig. 9 | See next page for caption.

Extended Data Fig. 9 | Nociceptor-released CGRP increases cytotoxic CD8⁺ T cell exhaustion. (a–b) Splenocytes-isolated CD8⁺ T cells were cultured under T_{cl}-stimulating condition (*ex vivo* activated by CD3 and CD28, IL-12, and anti-IL4) for 48h. The cells were then cultured or not with wild-type DRG neurons and exposed to capsaicin (1 μM, challenged once every two days) or its vehicle. As measured after 4 days stimulation, capsaicin-stimulated intact neuron increased the proportion of PD-1⁺LAG3⁺TIM3⁺ (a) cytotoxic CD8⁺ T cells, while it decreased the one of IFNγ⁺ (b). (c–d) Splenocytes-isolated CD8⁺ T cells were cultured under T_{cl}-stimulating conditions (*ex vivo* activated by CD3 and CD28, IL-12, and anti-IL4) for 48h. In the presence of peptidase inhibitors (1 μL/mL), naive DRG neurons were cultured in the presence of BoNT/A (50 pg/mL) or its vehicle for 24h. The cells were then washed, stimulated (30 min) with KCl (50mM), and the conditioned medium collected. On alternate days for 4 days, the cytotoxic CD8⁺ T cells were exposed or not to a RAMP1 blocker (CGRP₈₋₃₇; 2 μg/mL) and challenge (1:2 dilution) with fresh KCl-induced conditioned medium from naive, or BoNT/A-silenced neurons. As measured after 4 days stimulation, KCl-stimulated neuron-conditioned medium increased the proportion of PD-1⁺LAG3⁺TIM3⁺ (c) cytotoxic CD8⁺ T cells, while it decreased the one of IFNγ⁺ (d). Such effect was absent when cytotoxic CD8⁺ T cells were co-exposed to the RAMP1 blocker CGRP₈₋₃₇ or challenged with the neuron conditioned medium collected from BoNT/A-silenced neurons (c–d). (e–f) Splenocytes-isolated CD8⁺ T cells from wild-type and *Ramp1*^{-/-} mice were cultured under T_{cl}-stimulating conditions (*ex vivo* activated by CD3 and CD28, IL-12, and anti-IL4) for 48h. On alternate days for 4 days, the cytotoxic CD8⁺ T cells were exposed to CGRP (0.1 μM) or its vehicle. As measured after 4 days stimulation, representative flow cytometry plots (f) show that CGRP decrease *Ramp1*^{WT} cytotoxic CD8⁺ T cells expression of IFNγ⁺ (e,f), TNF⁺ (f), and IL-2⁺ (f) when exposed to CGRP. Inversely, CGRP increase the proportion of PD-1⁺LAG3⁺TIM3⁺ in *Ramp1*^{WT} cytotoxic CD8⁺ T cells (f). *Ramp1*^{-/-} cytotoxic CD8⁺ T cells were protected from the effect of CGRP (e–f). (g–i) Splenocytes-isolated

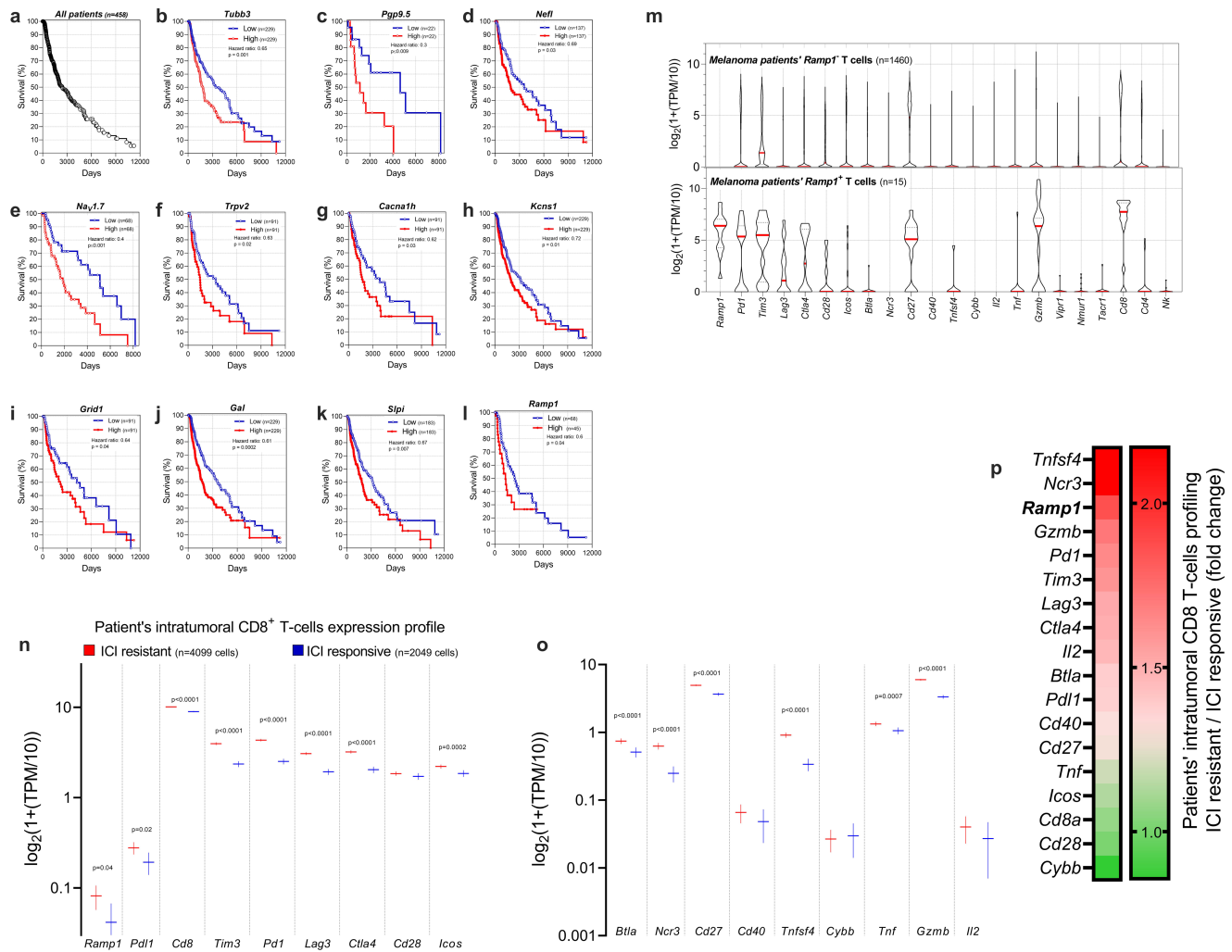
CD8⁺ T cells from naive OT-I mice were cultured under T_{cl}-stimulating conditions (*ex vivo* activated by CD3 and CD28, IL-12, and anti-IL4) for 48h. B16F10-mCherry-OVA cells (1×10⁵ cells) were then cultured with or without OT-I cytotoxic CD8⁺ T cells (4×10⁵ cells). T_{cl}-stimulated OT-I-CD8⁺ T cells lead to B16F10-OVA cell apoptosis (AnnexinV⁺7AAD⁺; g, measured after 48h; h–i, measured after 24h). B16F10-mCherry-OVA cells elimination by cytotoxic CD8⁺ T cells was reduced when the co-cultures were challenged (1:2 dilution; once daily for two consecutive days) with fresh conditioned medium collected from capsaicin (1 μM)-stimulated naive DRG neurons (g; measured after 48h). Similarly, KCl (50mM)-stimulated naive DRG neurons conditioned medium (1:2 dilution) reduced B16F10-mCherry-OVA apoptosis (h; measured after 24h). This effect was blunted when the cells were co-exposed to the RAMP1 blocker CGRP₈₋₃₇ (h; 2 μg/mL; measured after 24h). CGRP (0.1 μM) challenges also reduced OT-I cytotoxic CD8⁺ T cells elimination of B16F10-OVA cell (i; measured after 24h). Data are shown as box-and-whisker plots (runs from minimal to maximal values; the box extends from 25th to 75th percentile and the middle line indicates the median), for which individual data points are given (a–e, g–h), or representative FACS plot (f, i). N are as follows: a: CD8 + vehicle (n = 4), CD8 + capsaicin (n = 9), CD8 + neuron + capsaicin (n = 9), b: n = 5/groups, c: CD8 (n = 6), CD8 + KCl-induced neurons CM (n = 5), CD8 + KCl-induced neurons CM + CGRP₈₋₃₇ (n = 6), CD8 + KCl-induced neurons CM + BoNT/A (n = 6), d: n = 5/groups, e: *Ramp1*^{WT} CD8 + vehicle (n = 7), *Ramp1*^{WT} CD8 + CGRP (n = 8), *Ramp1*^{-/-} CD8 + vehicle (n = 6), *Ramp1*^{-/-} CD8 + CGRP (n = 6), g: B16F10 (n = 3), B16F10 + OT-I CD8 (n = 4), B16F10 + OT-I CD8 + KCl-induced neuron CM (n = 4), h: B16F10 + OT-I CD8 (n = 4), B16F10 + OT-I CD8 + KCl-induced neuron CM (n = 4), B16F10 + OT-I CD8 + KCl-induced neuron CM + CGRP₈₋₃₇ (n = 5). Experiments were repeated a minimum of three independent times with similar results. P-values are shown in the figure and determined by one-way ANOVA posthoc Bonferroni (a–e, g–h).



Extended Data Fig. 10 | See next page for caption.

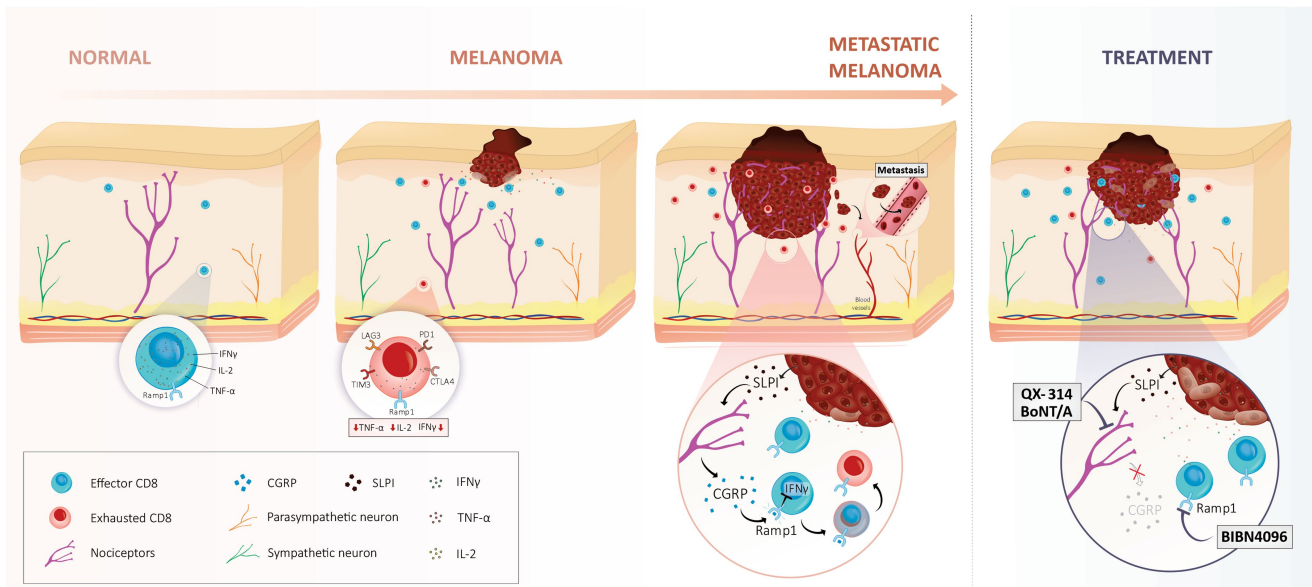
Extended Data Fig. 10 | The CGRP-RAMP1 axis promotes intratumoral CD8⁺ T cell exhaustion. (a-e) Orthotopic B16F10-mCherry-OVA (5x10⁵ cells; i.d.) cells were injected to nociceptor intact (*Nav1.8^{WT}::DTA^{fl/wt}*) and ablated mice (*Nav1.8^{cre}::DTA^{fl/wt}*). As measured fifteen days post inoculation, Na_v1.8⁺ nociceptor-ablated mice had lower proportion of PD-1⁺LAG3⁺TIM3⁺ (a) CD8⁺ T cells, but increased levels of IFN γ ⁺ (b), TNF⁺ (c), IL-2⁺ (d) CD8⁺ T cells. B16F10-mCherry-OVA (5x10⁵ cells; i.d.)-tumour surrounding skin was also collected and capsaicin-induced CGRP release assessed by ELISA. Intratumoral CGRP levels positively correlate with the proportion of PD-1⁺LAG3⁺TIM3⁺ CD8⁺ T cells (e). (f) Orthotopic B16F10-mCherry-OVA cells (5x10⁵ cells; i.d.) were inoculated into 8-week-old female sensory neuron intact or ablated mice. In nociceptor-ablated mice, recombinant CGRP injection (100nM, i.d., once daily) rescues intratumoral CD8⁺ T cells exhaustion (PD-1⁺LAG3⁺TIM3⁺). (g) Orthotopic B16F10-mCherry-OVA cells (5x10⁵ cells; i.d.) were inoculated into 8-week-old male and female mice. Starting one day post inoculation, the RAMP1 antagonist BIBN4096 (5 mg/kg, i.p., every other day) was administered systemically. We found that blocking the action of CGRP on RAMP1-expressing cells, increased the mice's median length of survival (~270% Mantel-Haenszel hazard ratio; measured on day 19). (h-m) Orthotopic B16F10-mCherry-OVA cells (5x10⁵ cells; i.d.) were inoculated into 8-week-old male and female mice. Starting one day post inoculation (defined as prophylactic), the RAMP1 antagonist BIBN4096 (5 mg/kg, i.p., every other day) was administered systemically. In another group of mice, BIBN4096 (5 mg/kg, i.p., every other day) injections were started once the tumour reached a volume of ~200mm³ (defined as therapeutic). The effect of nociceptor neuron-silencing on tumour size and tumour-infiltrating CD8⁺ T cell exhaustion was measured. As assessed thirteen days post tumour inoculation, BIBN4096 decreased tumour volume (h) and weight (i) but increased the relative proportion of IFN γ ⁺ (k), TNF⁺ (l), and IL-2⁺ (m) CD8⁺ T cells. BIBN4096 had no effect on the number of intratumoral CD8⁺ T cells (j). When administered as therapeutic, BIBN4096 reduced tumour volume (h) and weight (i) but had limited effect on CD8⁺ T cells' cytotoxicity (j-m). (n) Orthotopic B16F10-mCherry-OVA cells (5x10⁵ cells; i.d.) were inoculated into 8-week-old male and female sensory neuron-intact (*Trpv1^{WT}::DTA^{fl/wt}*) and ablated (*Trpv1^{cre}::DTA^{fl/wt}*) mice. Starting one day post inoculation, BIBN4096 (5 mg/kg) or its vehicle was administered (i.p.) on alternate days; effects on tumour volume were measured. Fourteen days post tumour inoculation, we found that tumour growth was reduced in sensory neuron-ablated mice and in BIBN4096-treated mice. BIBN4096 had no additive effect when given to sensory neuron-ablated mice. (o-s) Splenocytes-isolated CD8⁺ T cells from

naïve C57BL/6 mice were cultured under Tc1-stimulating conditions (*ex vivo*) activated by CD3 and CD28, IL-12, and anti-IL4) for 48h. The cells were then exposed to BIBN4096 (1-4 μ M) for 24h; effects on apoptosis, exhaustion and activation were measured by flow cytometry. When compared to vehicle-exposed cells, BIBN4096 did not affect the survival (o) of cultured cytotoxic CD8⁺ T cells, nor their relative expression of PD-1⁺LAG3⁺TIM3⁺ (p), IFN γ ⁺ (q), TNF⁺ (r), and IL-2⁺ (s). (t) B16F10 cells (1x10⁵ cells) were cultured for 24h. The cells were then exposed (or not) to BIBN4096 (1-8 μ M) for an additional 24h; effects on apoptosis were measured by flow cytometry. BIBN4096 did not trigger B16F10 cells apoptosis, as measured by the mean fluorescence intensity of Annexin V. (u-w) Naïve splenocyte CD8⁺ T cells were FACS purified from *Ramp1^{WT}* (CD45.1⁺) or *Ramp1^{-/-}* (CD45.2⁺) mice, expanded and stimulated (*CD3 and CD28 + IL-2*) *in vitro*. 8-week-old female *Rag1^{-/-}* mice were transplanted (i.v., 2.5x10⁶ cells) with either *Ramp1^{-/-}* or *Ramp1^{WT}* CD8⁺ T cells or 1:1 mix of *Ramp1^{-/-}* and *Ramp1^{WT}* CD8⁺ T cells. One week post transplantation, the mice were inoculated with B16F10-mCherry-OVA cells (5x10⁵ cells; i.d.). Ten days post tumour inoculation, we retrieved a similar number of tumours draining lymph node CD8⁺ T cells across the three tested groups (u). The relative proportion of intra-tumour PD-1⁺LAG3⁺TIM3⁺ CD8⁺ T cells was lower in *Ramp1^{-/-}* transplanted mice (v). Within the same tumour, intratumoral CD8⁺ T cell exhaustion was immunophenotyped by flow cytometry (representative panel shown in w) and showed that the relative proportion of PD-1⁺LAG3⁺TIM3⁺ CD8⁺ T cells was ~3-fold lower in *Ramp1^{-/-}* CD8⁺ T cells than in *Ramp1^{WT}* CD8⁺ T cells (w). Data are shown as box-and-whisker plots (runs from minimal to maximal values; the box extends from 25th to 75th percentile and the middle line indicates the median), for which individual data points are given (a-d, f, h-m, o-v), linear regression (e), Mantel-Cox regression (g), mean \pm S.E.M (n), or as FACS plot (w). N are as follows a-e: *Nav1.8^{WT}::DTA^{fl/wt}* (n = 18), *Nav1.8^{cre}::DTA^{fl/wt}* (n = 10), f: *Trpv1^{WT}::DTA^{fl/wt}* (n = 16), *Trpv1^{cre}::DTA^{fl/wt}* + CGRP (n = 11), g: vehicle (n = 89), BIBN4096 (n = 16), h-m: Vehicle (n = 13), BIBN4096 therapeutic (n = 18), BIBN4096 prophylactic (n = 16), n: *Trpv1^{WT}::DTA^{fl/wt}* + vehicle (n = 8), *Trpv1^{WT}::DTA^{fl/wt}* + BIBN4096 (n = 9), *Trpv1^{cre}::DTA^{fl/wt}* + vehicle (n = 7), *Trpv1^{cre}::DTA^{fl/wt}* + BIBN4096 (n = 7), o: vehicle (n = 5), 1 μ M BIBN4096 (n = 3), 4 μ M BIBN4096 (n = 5), p-s: n = 5/groups, t: n = 4/groups, u-w: n = 5/groups. Experiments were independently repeated twice (a-f, n-w) or four (g-m) times with similar results. P-values are shown in the figure and determined by two-sided unpaired Student's t-test (a-d, f,v), simple linear regression analysis (e), Mantel-Cox regression (g), by one-way ANOVA posthoc Bonferroni (h-m; o-u), or two-way ANOVA post-hoc Bonferroni (n).



Extended Data Fig. 11 | *RAMP1* expression in patient melanoma-infiltrating T cells correlates with worsened survival and poor responsiveness to ICIs. (a–l) In silico analysis of Cancer Genome Atlas (TCGA) data linked the survival rate among 459 patients with melanoma with their relative expression levels of various genes of interest (determined by bulk RNA sequencing of tumour biopsy). Kaplan–Meier curves show the patients’ survival after segregation in two groups defined by their low or high expression of a gene of interest. Increased gene expression (labelled as high; red curve) of *TUBB3* (b), *PGP9.5* (c), *Nav1.7* (e), *SLPI* (k) and *RAMP1* (l) in biopsy correlate with decreased patient survival ($p \leq 0.05$). The mantel–Haenszel hazard ratio and number of patients included in each analysis are shown in the figure (a–l). Experimental details were defined in Cancer Genome Atlas (TCGA)⁴⁰. (m) In silico analysis of single-cell RNA sequencing of human melanoma-infiltrating T cells revealed that *RAMP1*⁺ T cells downregulated *IL2* expression and strongly overexpressed

several immune checkpoint receptors (*PD-1*, *TIM3*, *LAG3*, *CTLA4*, *CD28*, *ICOS*, *BTLA*, *CD27*) in comparison to *RAMP1*⁺ T cells. Individual cell data are shown as a \log_2 of 1+ (transcript per million / 10). Experimental details and cell clustering were defined in Tirosh et al⁴². N are defined in each panel. (n–p) On the basis of the clinical response of patients with melanoma to immune checkpoint blocker, patients were clustered into two groups defined as ICI-responsive or ICI-resistant⁴¹. In silico analysis of single-cell RNA sequencing of patients’ biopsies revealed that tumour-infiltrating CD8⁺ T cells from patients who were resistant to ICIs significantly overexpressed *RAMP1* (2.0-fold), *PD-1* (1.7-fold), *LAG3* (1.6-fold), *CTLA4* (1.6-fold), and *TIM3* (1.7-fold; n–p). Individual cell data are shown as a $\log_2(1+(transcript\ per\ million/10))$. Experimental details and cell clustering were defined in Jerby-Arnon et al⁴¹. P-values are shown in the figure and determined by two-sided unpaired Student’s t-test. N are defined in each panel (n–o).



Extended Data Fig. 12 | Melanoma-innervating nociceptors attenuate cancer immunosurveillance. Melanoma growth sets off anti-tumour immune responses, including the infiltration of effector CD8 T cells and their subsequent release of cytotoxic cytokines (i.e., IFN γ , TNF, Granzyme B). By acting on tissue-resident nociceptor neurons, melanoma-produced SLPI promotes pain hypersensitivity, tweaks the neurons' transcriptome, and drives neurite outgrowth. These effects culminate in dense melanoma innervation by nociceptors and abundant release of immunomodulatory neuropeptides. CGRP, one such peptide, acts on tumour-infiltrating effector CD8⁺ T cells that express the CGRP receptor RAMP1, increasing their expression of immune

checkpoint receptors (i.e., PD-1, LAG3, TIM3). Therefore, along with the immunosuppressive environment present in the tumour, nociceptor-produced CGRP leads to the functional exhaustion of tumour-infiltrating CD8⁺ T cells, which opens the door to unchecked proliferation of melanoma cells. Genetically ablating (i.e., TRPV1 lineage) or pharmacologically silencing (i.e., QX-314, BoNT/A) nociceptor neurons as well as blocking the action of CGRP on RAMP1 using a selective antagonist (i.e., BIBN4096) prevents effector CD8⁺ T cells from undergoing exhaustion. Therefore, targeting melanoma-innervating nociceptor neurons constitutes a novel strategy to safeguard host anti-tumour immunity and stop tumour growth.

Chapter 3: Discussion

The focus of this study was to unveil the important role of tumor-associated sensory neurons in the development of cancer, which was achieved by the application of *in vitro* and *in vivo* models of melanoma cancer. To uncover the mechanisms associated with sensory neurons, we aimed to answer two main questions: which and how neuronal genes and modulators induce the expression of immune checkpoint receptors on T cells in the tumor microenvironment TME, and what is the overall impact of nerve-cancer crosstalk on anti-tumor immunity?

To address these questions, we designed various *in vitro* experiments, including RNA-sequencing analysis, imaging techniques, tissue staining, neuron-cancer co-culture, neuron-cancer-T cell co-culture, and multiple *in vivo* experiments. Our findings provided novel insights in the cancer research area. This chapter is dedicated to the discussion of our findings, as well as future research studies that can accelerate therapeutic advances in cancer research.

3.1. Tumor cells communicate with sensory neurons

A growing number of studies support the innervation of cancer and its contribution to tumor initiation and progression^{312,313,314,282}. Recent studies have shown that tumor-related neurogenesis and axonogenesis are linked to the progression of several cancer subtypes^{315,288,303,316}. The existence of nerves or neurites within and around the tumors has been visualized using various research approaches, including histological assessments and co-culture studies. For instance, through an advanced histological approach, the presence of nerves was approved in several carcinomas, including bladder, prostate, bone, and breast tumors^{317,318,269}. However, the innervation pattern can be different depending on the cancer type, cancer stage and the level of aggressiveness of tumor model.

In our study, iDISCO imaging technique approved the presence of Nav1.8⁺ nerve fibers within and around melanoma tumor, reflecting melanoma innervation by sensory neurons. We also found that these intra-tumoral sensory fibers contributed to tumor development (**Nature; Figure 1**). In addition, we observed the presence of TRPV1⁺ neurons in melanoma patients biopsies using hematoxylin eosin staining technique (**Nature; extended data Figure 2**).

Furthermore, we performed an *in vitro* co-culture experiment of DRG neurons with B16F10 melanoma cancer cells as an approach to study the interaction of DRG neurons with tumor cells. Several investigations have determined that there is a reciprocal interaction between tumor cells and DRG sensory neurons. Such interaction can influence neurite outgrowth and facilitate tumor cell dissemination along nerves¹². In this study, using an *in vitro* co-culture approach of DRG neurons with B16F10 or B16F0 melanoma cancer cells, we found that cancer cells induce neurite outgrowth and upregulate the expression of various neuropeptides released by DRG neurons. Furthermore, B16F10 cancer cells significantly increased the sensitivity of DRG neurons in the co-culture system as we analyzed changes in calcium flux in response to the noxious ligands (capsaicin, ATP, and AITC).

Importantly, the *in vivo* data also confirmed that the response rate to the noxious ligands is higher in lumbar DRG neurons (L3-L5) extracted from melanoma-bearing mice compared to DRGs harvested from non-tumorigenic keratinocyte injected mice (**Nature; extended data Figure 4**). These data indicate the contribution of tumor cells in the sensitization of nociceptor neurons and mainly reciprocal communication between DRG neurons and tumor cells.

3.2. Cancer cells sensitize sensory neurons

Nerves are able to shape a unique tumor microenvironment. Nerve markers have been detected in many tumors, such as head and neck, prostate, and pancreas. More importantly, these neuronal markers can promote malignancy and are often associated with poor outcomes^{12,319,320,282}. Tumor-nerve communication occurs through the factors secreted by both tumor cells and nerve fibers. Tumor cells can secrete

neurotrophic factors to drive axonogenesis and thereby innervate the tumor cells; nerve fibers reciprocally release neuropeptides and neurotransmitters to modulate tumor cell growth and survival. The important role of several nerve-cancer mediators, such as glutamate, NGF, GDNF, and noradrenaline or acetylcholine has been well understood.

Our RNA sequencing data revealed that the hypersensitivity of DRG neurons by tumor cells allow for the overexpression of several genes by nociceptor neurons. These genes include *Calca* (gene encoding CGRP), *Gal* (gene encoding galanin), several cytokine receptor genes (*IL-13r*, *IL-18r*, *IL-10r*, *IL-4r*), and growth factors such as *Trka* (gene encoding NGF receptor), and fibroblast growth factors (*Fgf*) (**Nature; Figure 1**). Overexpression of CGRP neuropeptide may influence tumor-infiltration lymphocyte activity, and *Trka* might support pain hypersensitivity induced by melanoma cells.

Further, RNA sequencing analysis revealed that, when co-cultured with either nociceptor DRG neurons or CD8⁺ T cells, melanoma tumors increase the expression of Secretory Leukocyte Protease Inhibitor (SLPI). SLPI could directly activate cultured sensory neurons, as we showed by calcium microscopy. Using ELISA, the presence of SLPI was confirmed in the supernatant collected from the co-culture of DRG neuron-B16F10 cancer cells. We also observed that the treatment of DRG neurons with SLPI, induces CGRP release, which supports the idea that SLPI secretion by cancer cells can sensitize tumor-associated sensory neurons (**Nature; Figure 2**).

3.3. Activation of tumor-associated nerves modulates pain

Various types of tumors are identified by moderate to severe pain, which noticeably declines the life quality of patients^{321,322,323}. Despite growing advances, the exact molecular mechanisms underlying pain stay poorly understood. Pancreatic cancer and bone metastasis have been reported as the most painful types of cancer-related pain, which attributes to both neuropathic and nociceptive components³²⁴. Apart from neuropathic and inflammatory mediators (e.g., NGF), reciprocal communication between tumor cells and sensory nerves contributes to pain generation³²⁵.

Perineural invasion of cancer cells along the sensory nerve has also been viewed to damage and activate the nerves, which mediate pain. Oral cancer microenvironment contains various factors released by cancer cells and immune cells. These factors have been reported to sensitize tumor-associated nociceptors and induce cancer-related pain³²². Additionally, the positive correlation between oral cancer-induced pain and the tumor size was reported in this study³²². In the present study, we found that intradermal inoculation of SLPI into the mice enhances the hypersensitivity of sensory neurons, reflecting the important role of SLPI in cancer-associated pain (**Nature; extended data Figure 5**).

Spontaneous activity of nociceptors mediated by SLPI signaling in the tumor microenvironment can contribute to the overexpression of neuropeptides-released nociceptors and pain. Moreover, our data revealed a positive correlation between thermal pain hypersensitivity and tumor growth. Compared to the smaller tumors, the mice with bigger tumors displayed higher pain and higher exhaustion of CD8⁺ T cells.

One feasible mechanism linking to this difference can be due to fewer nociceptors infiltration in smaller tumors and lower levels of pain-related mediators in the tumor microenvironment. Our results also propose that cancer cells release SLPI which directly induce pain and less production of SLPI is associated with higher survival rate (**Nature; extended data Figure 11**). Therefore, SLPI emerged as a key therapeutic target to reduce patient's tumor pain and increase their survival. Thus, tumor pain is considered as a complex condition mediated by neuropathic, inflammatory, and tumor-specific mechanisms.

3.4. Nociceptor neurons modulate CD8⁺ T cell exhaustion

Our findings so far convinced us to design several *in vitro* and *in vivo* experiments to determine the effects of DRG neurons on the activity of the immune system, specifically cytotoxic CD8⁺ T cells. Landmark studies have addressed the fundamental role of cytotoxic CD8⁺ T cells in anti-tumor immunity and

cytotoxic activity in the context of cancer. However, tumors induce T cell exhaustion, a hyperactivation phase characterized by loss of effector functions of T cells, which consequently lead to tumor progression.

Our *in vitro* findings revealed that either co-culture of CD8⁺ T cells with DRG neurons or CD8⁺ T cells treatment with condition media collected from stimulated neurons associated with CD8⁺ T exhaustion. As neuron condition media consist of several neuropeptides, we aimed to examine the influence of nociceptor-released neuropeptides on CD8⁺ T cells activity. Among others, CGRP was found to act as the major driver of T cell exhaustion (**Nature; extended data Figure 9**).

CGRP has been shown to alter the recruitment of T cells and modulate anti-microbial defense in lung³²⁶. CGRP has previously been observed to suppress the proliferation of T cells by inhibiting their IL-2 production³²⁶. A very recent study has shown that nociceptor released CGRP influences the immune cells in the meninges during *S. pneumoniae* infection. Thus, CGRP/RAMP1 axis in meningeal macrophages facilitates the invasion of bacteria into the brain³²⁷.

In addition, we found that CD8⁺ T cells treated with DRG neuron condition media or directly treated with CGRP, failed to eliminate B16F10 melanoma cancer cells, reflecting the immunosuppressive effects of neuropeptide-released nociceptor neurons, specifically CGRP (**Nature; extended data Figure 9**).

Despite the efficacy of our *in vitro* and *in vivo* findings for describing neuro-immune and neuron–cancer communications, we aimed to test the nature of tree-way interaction among cancer, nociceptors and CD8⁺ T cells in a model of melanoma in the absence of sensory neurons.

3.5. Tumor-innervating nociceptors promote cancer progression

Tumor-associated nerves, including sympathetic and sensory fibers, have been reported to promote tumor growth and dissemination in several malignancies. Recently, the cooperation of sensory nerves in *in vivo* metastasis has been demonstrated in triple-negative breast cancer³²⁸. Further study has argued that TRPV1⁺ sensory fibers drive oral and head and neck tumors progression^{329,330}. Another study confirmed that the activation of TRPV1⁺ sensory fibers in sciatic nerve is significantly linked with pain sensitivity and tumor growth³³¹.

However, the exact role of tumor-infiltrating sensory neurons in this context is poorly understood. Our results revealed that neuropeptides released by DRG neurons decline B16F10 elimination by cytotoxic CD8⁺ T cells and induce CD8⁺ T exhaustion (**Nature; Figure 3**). These data suggest that sensory neurons can inhibit anti-tumor responses through the upregulation of immune checkpoint proteins on CD8⁺ T cells. Cytotoxic CD8⁺ T cells are the major immune population in the tumor microenvironment, which target tumor cells³³².

Our findings revealed that genetic ablation of sensory neuron lineages declines tumor growth and increases anti-tumor immune responses. Also, infiltrated CD8⁺ T cells increase the production of cytokines, whereas they decrease the expression of immune checkpoint receptors, reflecting less exhaustion of CD8⁺ T cells. Thus, cytotoxic activity of CD8⁺ T lymphocytes is associated with lower melanoma tumor growth.

According to our findings, we concluded that the presence of inflammatory mediators in the tumor microenvironment can sensitize tumor-associated nociceptors. Activated nociceptors, in turn, secrete a wide variety of neuropeptides that limit the infiltration and cytotoxic function of CD8⁺ T cells in the tumor site.

Since genetic ablation of sensory neurons may lead to some compensatory alterations, we locally silenced tumor-innervated sensory neurons using botulinum toxin A and a membrane-impermeable type of lidocaine (QX-314). Both silencing approaches reduced tumor development and declined the co-expression of immune checkpoint receptors on CD8⁺ T cells (**Nature; extended data Figure 7,8**).

Since our results show that neuropeptides regulate immune responses, we decided to assess intra-tumoral neuropeptide signaling to decipher possible mechanisms that may contribute to their immunosuppressive activity and tumor development.

CGRP neuropeptide can apply different mechanisms to exert tumor progression. CGRP has been observed to increase tumor growth through metabolic reprogramming, abnormal receptor internalization, and prevention of anti-tumor immune responses³³³. Endogenous CGRP released by sensory nerves is considered as a main suppressor of immune responses^{334,335}. In CD4⁺ T cells, CGRP blocks the production of TNF- α and IFN- γ by Th1 cells through increasing intracellular cAMP^{335,334}. CGRP also affects Langerhans cells to impair their capacity to stimulate the proliferation of T cells³³⁶. Similarly, monocytes or dendritic cells exposure to CGRP markedly decrease the proliferation of T cells via the secretion of IL-10³³⁷. Also, CGRP has been shown to limit T cell activity through upregulating the inhibitory genes, including *Pdcd1*, *Tnfrsf18*, and *Tnfrsf9* in T cells^{337,338}.

CD8⁺ T cells express various types of neuropeptide receptors, such as RAMP1, suggesting that CGRP more likely contribute to immunosuppressive activity in tumors. Therefore, to examine whether neuropeptide-released nociceptive neurons can drive CD8⁺ T cell exhaustion, we pharmacologically silenced RAMP1 receptor to block CGRP-RAMP1 axis using its antagonist BIBN4096.

Our results confirmed that targeting CGRP-RAMP1 signaling significantly declines tumor growth and exhaustion of CD8⁺ T cells. Using an *in vivo* adoptive transfer of RAMP1^{-/-} or RAMP1^{wt} CD8⁺ T cells to Rag1^{-/-} mice (mice lacking mature T and B cells), we confirmed the involvement of CGRP-RAMP1 in CD8⁺ T cell exhaustion (**Nature; Figure 4**). We also rescued CGRP level by daily intertumoral injection of CGRP in nociceptor-ablated mice, which led to similar tumor growth and T cell exhaustion to that of sensory neurons intact mice (**Nature; Figure 4**). These data reinforced the idea that neuropeptides, specifically CGRP, released by nociceptor neurons are the major mediators by which sensory neurons attenuate immune responses in tumors.

3.6. Human melanoma tumor biopsies are innervated by TRPV1+ sensory neurons

We observed that melanoma patient samples are highly innervated by TRPV1⁺ neurons. Immunolabeling analysis revealed that the level of TRPV1 in patients' biopsies is around two-fold higher than adjacent healthy skin (**Nature; extended data Figure 2**). In our study, we have shown the importance of nociceptor neurons in regulating melanoma tumor growth *in vivo*. Targeting these neurons in the tumor can enhance host defense and they can potentially be presented as a clinical treatment of cancer. In addition, combination therapy by blocking the activity of TRPV1⁺ neurons as well as other therapeutic approaches, such as immune checkpoint blockade or chemotherapy, can augment the efficacy of treatments.

3.7. Neuropeptides drive carcinogenesis in human

Nociceptive nerve endings have been detected within solid tumors, which is associated with tumor progression and immune suppression via the local release of neuropeptides and growth factors. These outcomes affect the efficacy of clinical treatment and support the invasion of tumors and reduce patient survival. Inhibition of nociceptor neuron activity declines the proliferation of solid tumors, including skin, prostate, pancreatic head and neck, and cervical cancers^{293,290,320}. The neuropeptide substance P (SP), for example, has been indicated to promote the proliferation and migration of tumors after binding to its receptor (NK)-1R^{308,339,340,6}. NK-1R is overexpressed in HER2⁺ primary breast tumors, and SP mediates persistent activation of HER2, resulting in malignant progression³³⁹.

Additionally, high level of CGRP was detected in tumors and serum of patients with thyroid cancer³⁴¹. CGRP also was shown to alter the chemokinetic properties (migration and invasion) of metastatic human breast cancer cells and enhance the expression of its receptors³⁴⁰ (**Nature; extended data Figure 11**). Thus, targeting these neuropeptides or their receptors through antibodies against or blockers can produce efficient cancer-treating strategies. In this study, several silencing approaches were tested to block the activity of nociceptors and consequent neuropeptide release. All approaches confirmed their effects on decreasing tumor progression and rescuing anti-tumor responses. These strategies include botulinum neurotoxin A (botox) with long-lasting effect, QX-314 (sodium-channel blocker), CGRP receptor antagonist (BIBN4096) as well as genetic ablation.

3.8. Combination of nerve and immunotherapy as a therapeutic approach for cancer

The identification of nerves in the tumor microenvironment has opened a novel field in investigation of cancer biology. Thus, unraveling the mechanisms by which nerves attenuate immune cell activity in malignancies can promote host immunity against cancer and improve patient survival. Interestingly, a vast population of immune cells has been observed to express multiple neuropeptide receptors and react to neuropeptides. Neuropeptide-released nociceptive nerves in the inflamed tumor can influence immune cell functions^{342,214}.

For instance, single-cell RNA sequencing of human melanoma identified that intra-tumoral RAMP1⁺CD8⁺ T cells significantly overexpress various immune checkpoint receptors and decline the production of cytokines compared to RAMP1⁺CD8⁺ T cells counterparts (**Nature; extended data Figure 11**). These results suggest that the secretion of CGRP by tumor-associated nociceptive neurons can mediate T-cell exhaustion in patients.

Therapeutic improvements in cancer immunotherapy have rapidly progressed in the past few years. Several cancer immunotherapy approaches, including immune-checkpoint blockade (anti-PD1 and anti-PDL-1) and chimeric antigen receptor (CAR) T cells therapy, have indicated promising responses in different cancer types^{140,343}. Despite the successful outcomes of cancer immunotherapy in a vast range of human cancers, there are still some challenges facing cancer immunotherapy, which require more investigations to modify the TME and find key mechanisms. Neuropeptides and neurotransmitters appear to play a major role in TME.

We studied whether inhibition of neuropeptides, such as CGRP (as a key driver of CD8⁺ T-cell exhaustion) in combination with immune-checkpoint blockade, can improve anti-tumor immunity. We realized that local silencing of sensory neurons by QX-314 or BoNT/A, or genetic ablation of nociceptor neurons combined with anti-PDL-1 therapy effectively elevate the cytotoxicity of CD8⁺ T-cell, decrease CD8⁺ T-cell exhaustion, and reduced tumor growth (**Nature; extended data Figure 6,7 and 8**).

Like previous findings, our results demonstrate that nociceptor neurons directly interact with tumor cells and T cells through neuropeptides, which facilitate tumor development. Thus, targeting this three-way interaction by QX-314 or Botox can control the tumor growth and provide potential therapeutic approaches for cancer treatment.

We propose that targeting tumor-associated sensory neurons (neuropeptide blockade) in combination with immunotherapy can provide an effective approach to improve the efficacy of immune checkpoint blockade or CAR T cell therapies against tumors and boost anti-tumor T cell reactivity. Since the role of neuropeptides in mediating T cell exhaustion, tumor growth, angiogenesis, and neurogenic inflammation has been widely reported, this novel combination therapy is expected to improve the survival and quality of life of cancer patients.

3.9. Similar findings

Kovacs et al. have recently shown that several solid tumor patient samples, including breast, ovarian, lung, liver, pancreatic, and prostate tumors are innervated by TRPV1⁺ sensory nerves. In addition, using IHC staining, they found that compared to healthy ovary and fallopian tissues, which are innervated by sympathetic fibers (TH⁺), high-grade serous ovarian carcinoma (HGSOC) samples are innervated with TRPV1⁺ sensory nerves. The different innervation type between normal ovary and HGSOC tissues suggests that HGSOCs sensory nerve innervation can be the consequence of disease progression. By measuring the electrical activity of both fresh patient and murine HGSOC slices, the authors confirmed the functionality of innervated neuronal fibers in tumor bed. Similar to our findings, the authors showed that the HGSOC tumors in TRPV1 sensory neuron ablated mice is significantly smaller than their control counterparts suggesting that tumor-associated TRPV1 sensory fibers contribute to tumor growth³⁵³.

Zhang et al. have recently demonstrated the high density of TRPV1⁺ nociceptive fibers in both human and murine oral squamous cell carcinoma (OSCC), which assist in tumor progression and poor overall survival in low-glucose environment. The authors pointed out that cancer cells exert ROS-mediated activation of c-Jun pathway to liberate NGF. Cancer cell-derived NGF then induces CGRP production from tumor-infiltrated nociceptors, thereby sustaining tumor growth and survival in poor-nutrient environment. Furthermore, they determined that when co-cultured with OSCC or melanoma cell lines, trigeminal nerves (TGs) overexpressed calca level (gene encoding CGRP)³⁴⁴.

Another study of cancer-nerve interaction determined the presence of CGRP⁺ sensory nerves in head and neck squamous cell carcinoma (HNSCC) patient tissues and oral cancer sections. Based on their findings, tumor development in mice lacking CGRP (CGRP^{KO}) was significantly smaller than sham animals and immune cell infiltration was increased. It proposes that release of CGRP from tumor-associated sensory nerves dampens anti-tumor immune responses¹³.

Ravindranathan et al. have reported that increased level of neuropeptide vasoactive intestinal peptide (VIP) in pancreatic ductal adenocarcinoma (PDAC) environment is positively correlated with T cell exhaustion and resistant to immune checkpoint therapies. The authors revealed that blocking VIP signaling through antagonizing VIP receptor on the surface of T cells limits T cell exhaustion and rescues anti-tumor immunity. As the authors observed, VIP receptor blockade in combination with anti-PD1 therapy effectively declined tumor growth, improved survival rate, boosted T cell priming, and promoted anti-tumor immunological memory in pre-clinical model of PDCA³⁴⁵.

Deficiency of TP53 (tumor suppressor gene) in head and neck tumors has been found to induce the reprogramming of tumor-associated sensory fibers to adrenergic nerves, which results in tumor progression²⁹⁰.

As reported by Saloman et al., in pancreatic ductal adenocarcinoma (PDAC), ablation of tumor-innervated sensory nerves through neonatal capsaicin treatment, limited neurogenic inflammation and slowed tumor progression. This delay in tumor formation explains the modulatory role of sensory nerves in PDAC environment³⁴⁶.

In gastric tumor, vagal denervation or pharmacological silencing (BoNT/A treatment) was associated with the prevention of Wnt signaling, which subsequentially attenuated tumor progression, improved the effects of chemotherapy and enhanced overall survival rate³⁴⁷.

3.10. Limitations

While other immune cell functions may be affected by locally released neuropeptides, we restricted our initial efforts to cytotoxic CD8⁺ T cells since it is one of the main drivers of anti-tumor immunity. Our *in vitro* model of T cell exhaustion has also been validated for this cell type. It would be helpful to repeat our data using *in vivo* human melanoma tumor models in NGS or Nude mice to investigate adaptive immune system.

In the current study, we proposed CGRP-released neuropeptide as the key driver of T cell exhaustion and inhibiting anti-tumor responses. Accordingly, the use of mice lacking CGRP (CGRP knockout mice) can effectively confirm our current data.

3.11. Future Directions

Growing body of evidence identifies that nociceptor neurons are involved in signaling pathways that affect several malignancies and correlate with worse prognosis. Emerging data propose that tumor cells take the advantage of neuropeptide involved pathways to induce uncontrolled proliferation and invasion. However, how intra-tumoral nerves cooperate with cancer progression is still largely undefined.

Most recent findings of mechanisms are related to downstream pathways of neuropeptides and growth factors, which have been identified to be involved in tumor proliferation. More research and clinical

investigations need to be fulfilled to uncover the key mechanisms underlying the role of nerves in the immune regulation in cancer.

In our study, we defined that nociceptors-locally released neuropeptides can directly interact with CD8⁺ T cells and attenuate pro-inflammatory cytokines, reflecting a strong bidirectional communication between tumor-associated nociceptive neurons and adaptive immune cell activity. Since inflamed tumors consist of different adaptive and innate immune subtypes as well as diverse neuron subgroups, it is worth to apply some strategies, including single-cell RNA sequencing on tumor-associated immune cells and sensory neurons. This approach can reveal the most involved immune and sensory nerve populations in TME and target them to promote host defense against cancer.

Afferent sensory neurons release different neuropeptides when they are activated by tumor cells. Several studies have mentioned the contribution of locally released neuropeptides on tumor growth. For example, SP has been shown to cooperate with cancer progression in both oral squamous cell carcinoma and gastric cancer³⁴⁸. In the current study, we limited the scope of our study to CGRP, which is the most impacted neuropeptide by melanoma cancer cells. Identifying the influence of other neuropeptides such as SP and, which their secreted level was confirmed by ELISA technique and their expression level was upregulated in RNA sequencing data on immune cell function may propose another therapeutic target in cancer.

TME innervation by sensory nerves has been shown in several cancer models. These nerves are significantly involved in tumor progression via various mechanisms. Our team is currently investigating the immunosuppressive activity of capsaicin-responsive neurons in breast and prostate cancers.

CAR T cell therapy is a type of immunotherapy that has generated considerable attention among researchers. In addition, this technique has displayed substantial therapeutic potential in both hematological malignancies and solid tumors^{349,350}. However, the application of CAR T cells remains a challenge due to the complexity of TME³⁵¹. Schmidt et al. performed a genome wide CRISPR screens on human T cells to identify the genes controlling the production of main cytokines in T cell activation. Among other genes, *RAMP1* was one of the CRISPR inhibitory genes that regulate cytokine production in human primary T cells³⁵². Therefore, generating CAR T cells of *RAMP1* knocked out CD8 T cells by CRISPR technology and evaluating its efficacy in the immunotherapy treatment can be key experiment to perform.

3.12. Conclusion

In conclusion, interactions between the nervous and immune systems are pivotal for maintaining homeostasis, and impairing these interactions contributes to carcinogenesis and metastasis. In our study, we found that sensory neurons create a synaptic connection with tumor cells as well as cytotoxic T-cells. Tumor cells actively release growth factors to stimulate sensory fibers, which induce tumor innervation. The activation of nociceptor sensory nerves leads to the local secretion of neuropeptides and modulate immune checkpoint expression on cytotoxic lymphocytes, which limits the anti-tumor activity of cytotoxic CD8⁺ T cells. It appears that cancer cells exploit nociceptor interplay with the immune system to blunt cancer immunosurveillance, thereby maintaining tumor growth.

Overall, sensory neurons participate in dampening the host anti-tumor activity by modulating the expression of immune checkpoint receptors. To address the mechanism by which sensory neurons partake in tumor development, we ablated or silenced cancer-innervating nociceptors. This strategy uncovered that blocking the activity of sensory neurons declines tumor growth and increases anti-tumor immunity.

4. Bibliography

- 1 Ferlay, J. *et al.* Cancer incidence and mortality worldwide: sources, methods and major patterns in GLOBOCAN 2012. *Int J Cancer* **136**, E359-386 (2015). <https://doi.org:10.1002/ijc.29210>
- 2 Hanahan, D. & Weinberg, R. A. Hallmarks of cancer: the next generation. *Cell* **144**, 646-674 (2011). <https://doi.org:10.1016/j.cell.2011.02.013>
- 3 Siegel, R. L., Miller, K. D. & Jemal, A. Cancer statistics, 2016. *CA Cancer J Clin* **66**, 7-30 (2016). <https://doi.org:10.3322/caac.21332>
- 4 Hosseini, H. *et al.* Early dissemination seeds metastasis in breast cancer. *Nature* **540**, 552-558 (2016). <https://doi.org:10.1038/nature20785>
- 5 Chambers, A. F. & Werb, Z. Invasion and metastasis--recent advances and future challenges. *J Mol Med (Berl)* **93**, 361-368 (2015). <https://doi.org:10.1007/s00109-015-1269-z>
- 6 Restaino, A. C. & Vermeer, P. D. Neural regulations of the tumor microenvironment. *FASEB Bioadv* **4**, 29-42 (2022). <https://doi.org:10.1096/fba.2021-00066>
- 7 Ferrone, C. & Dranoff, G. Dual roles for immunity in gastrointestinal cancers. *J Clin Oncol* **28**, 4045-4051 (2010). <https://doi.org:10.1200/JCO.2010.27.9992>
- 8 Mundt, S., Greter, M., Flugel, A. & Becher, B. The CNS Immune Landscape from the Viewpoint of a T Cell. *Trends Neurosci* **42**, 667-679 (2019). <https://doi.org:10.1016/j.tins.2019.07.008>
- 9 Mueller, S. N. Neural control of immune cell trafficking. *J Exp Med* **219** (2022). <https://doi.org:10.1084/jem.20211604>
- 10 Steinhoff, M. *et al.* Neuroimmune communication regulating pruritus in atopic dermatitis. *J Allergy Clin Immunol* **149**, 1875-1898 (2022). <https://doi.org:10.1016/j.jaci.2022.03.010>
- 11 Xue, M. *et al.* Schwann cells regulate tumor cells and cancer-associated fibroblasts in the pancreatic ductal adenocarcinoma microenvironment. *Nat Commun* **14**, 4600 (2023). <https://doi.org:10.1038/s41467-023-40314-w>
- 12 Cervantes-Villagrana, R. D., Albores-Garcia, D., Cervantes-Villagrana, A. R. & Garcia-Acevez, S. J. Tumor-induced neurogenesis and immune evasion as targets of innovative anti-cancer therapies. *Signal Transduct Target Ther* **5**, 99 (2020). <https://doi.org:10.1038/s41392-020-0205-z>
- 13 McIlvried, L. A., Atherton, M. A., Horan, N. L., Goch, T. N. & Scheff, N. N. Sensory Neurotransmitter Calcitonin Gene-Related Peptide Modulates Tumor Growth and Lymphocyte Infiltration in Oral Squamous Cell Carcinoma. *Adv Biol (Weinh)* **6**, e2200019 (2022). <https://doi.org:10.1002/adbi.202200019>
- 14 Restaino, A. C. *et al.* Functional neuronal circuits promote disease progression in cancer. *Sci Adv* **9**, eade4443 (2023). <https://doi.org:10.1126/sciadv.ade4443>
- 15 Heistein, J. B., Acharya, U. & Mukkamalla, S. K. R. in *StatPearls* (2022).
- 16 Buja, A. *et al.* Sex Differences in Cutaneous Melanoma: Incidence, Clinicopathological Profile, Survival, and Costs. *J Womens Health (Larchmt)* **31**, 1012-1019 (2022). <https://doi.org:10.1089/jwh.2021.0223>

- 17 Kuphal, S., Schneider, N., Massoumi, R., Hellerbrand, C. & Bosserhoff, A. K. UVB radiation represses CYLD expression in melanocytes. *Oncol Lett* **14**, 7262-7268 (2017). <https://doi.org:10.3892/ol.2017.7120>
- 18 Rowe, C. J. & Khosrotehrani, K. Clinical and biological determinants of melanoma progression: Should all be considered for clinical management? *Australas J Dermatol* **57**, 175-181 (2016). <https://doi.org:10.1111/ajd.12348>
- 19 Nassar, K. W. & Tan, A. C. The mutational landscape of mucosal melanoma. *Semin Cancer Biol* **61**, 139-148 (2020). <https://doi.org:10.1016/j.semcancer.2019.09.013>
- 20 Yeh, I. *et al.* Targeted Genomic Profiling of Acral Melanoma. *J Natl Cancer Inst* **111**, 1068-1077 (2019). <https://doi.org:10.1093/jnci/djz005>
- 21 Randic, T., Kozar, I., Margue, C., Utikal, J. & Kreis, S. NRAS mutant melanoma: Towards better therapies. *Cancer Treat Rev* **99**, 102238 (2021). <https://doi.org:10.1016/j.ctrv.2021.102238>
- 22 Yin, C. *et al.* Pharmacological Targeting of STK19 Inhibits Oncogenic NRAS-Driven Melanomagenesis. *Cell* **176**, 1113-1127 e1116 (2019). <https://doi.org:10.1016/j.cell.2019.01.002>
- 23 Mannavola, F., Tucci, M., Felici, C., Stucci, S. & Silvestris, F. miRNAs in melanoma: a defined role in tumor progression and metastasis. *Expert Rev Clin Immunol* **12**, 79-89 (2016). <https://doi.org:10.1586/1744666X.2016.1100965>
- 24 Bhatia, A. & Kumar, Y. Cancer-immune equilibrium: questions unanswered. *Cancer Microenviron* **4**, 209-217 (2011). <https://doi.org:10.1007/s12307-011-0065-8>
- 25 Swann, J. B. & Smyth, M. J. Immune surveillance of tumors. *J Clin Invest* **117**, 1137-1146 (2007). <https://doi.org:10.1172/JCI31405>
- 26 Corthay, A. Does the immune system naturally protect against cancer? *Front Immunol* **5**, 197 (2014). <https://doi.org:10.3389/fimmu.2014.00197>
- 27 Dunn, G. P., Bruce, A. T., Ikeda, H., Old, L. J. & Schreiber, R. D. Cancer immunoediting: from immunosurveillance to tumor escape. *Nat Immunol* **3**, 991-998 (2002). <https://doi.org:10.1038/ni1102-991>
- 28 Kim, R., Emi, M. & Tanabe, K. Cancer immunoediting from immune surveillance to immune escape. *Immunology* **121**, 1-14 (2007). <https://doi.org:10.1111/j.1365-2567.2007.02587.x>
- 29 O'Donnell, J. S., Teng, M. W. L. & Smyth, M. J. Cancer immunoediting and resistance to T cell-based immunotherapy. *Nat Rev Clin Oncol* **16**, 151-167 (2019). <https://doi.org:10.1038/s41571-018-0142-8>
- 30 Smyth, M. J., Dunn, G. P. & Schreiber, R. D. Cancer immunosurveillance and immunoediting: the roles of immunity in suppressing tumor development and shaping tumor immunogenicity. *Adv Immunol* **90**, 1-50 (2006). [https://doi.org:10.1016/S0065-2776\(06\)90001-7](https://doi.org:10.1016/S0065-2776(06)90001-7)
- 31 Shankaran, V. *et al.* IFN γ and lymphocytes prevent primary tumour development and shape tumour immunogenicity. *Nature* **410**, 1107-1111 (2001). <https://doi.org:10.1038/35074122>
- 32 Seliger, B., Ruiz-Cabello, F. & Garrido, F. IFN inducibility of major histocompatibility antigens in tumors. *Adv Cancer Res* **101**, 249-276 (2008). [https://doi.org:10.1016/S0065-230X\(08\)00407-7](https://doi.org:10.1016/S0065-230X(08)00407-7)

- 33 Street, S. E., Trapani, J. A., MacGregor, D. & Smyth, M. J. Suppression of lymphoma and epithelial malignancies effected by interferon gamma. *J Exp Med* **196**, 129-134 (2002). <https://doi.org:10.1084/jem.20020063>
- 34 Voskoboinik, I., Whisstock, J. C. & Trapani, J. A. Perforin and granzymes: function, dysfunction and human pathology. *Nat Rev Immunol* **15**, 388-400 (2015). <https://doi.org:10.1038/nri3839>
- 35 Girardi, M. *et al.* Regulation of cutaneous malignancy by gammadelta T cells. *Science* **294**, 605-609 (2001). <https://doi.org:10.1126/science.1063916>
- 36 Sheil, A. G. Organ transplantation and malignancy: inevitable linkage. *Transplant Proc* **34**, 2436-2437 (2002). [https://doi.org:10.1016/s0041-1345\(02\)03169-x](https://doi.org:10.1016/s0041-1345(02)03169-x)
- 37 Boshoff, C. & Weiss, R. AIDS-related malignancies. *Nat Rev Cancer* **2**, 373-382 (2002). <https://doi.org:10.1038/nrc797>
- 38 Sheil, A. G. Cancer after transplantation. *World J Surg* **10**, 389-396 (1986). <https://doi.org:10.1007/BF01655298>
- 39 Pham, S. M. *et al.* Solid tumors after heart transplantation: lethality of lung cancer. *Ann Thorac Surg* **60**, 1623-1626 (1995). [https://doi.org:10.1016/0003-4975\(95\)00120-4](https://doi.org:10.1016/0003-4975(95)00120-4)
- 40 Clark, W. H., Jr. *et al.* Model predicting survival in stage I melanoma based on tumor progression. *J Natl Cancer Inst* **81**, 1893-1904 (1989). <https://doi.org:10.1093/jnci/81.24.1893>
- 41 Clemente, C. G., Mihm, M. C., Jr., Bufalino, R., Zurrida, S., Collini, P. & Cascinelli, N. Prognostic value of tumor infiltrating lymphocytes in the vertical growth phase of primary cutaneous melanoma. *Cancer* **77**, 1303-1310 (1996). [https://doi.org:10.1002/\(SICI\)1097-0142\(19960401\)77:7<1303::AID-CNCR12>3.0.CO;2-5](https://doi.org:10.1002/(SICI)1097-0142(19960401)77:7<1303::AID-CNCR12>3.0.CO;2-5)
- 42 Raskov, H., Orhan, A., Christensen, J. P. & Gogenur, I. Cytotoxic CD8(+) T cells in cancer and cancer immunotherapy. *Br J Cancer* **124**, 359-367 (2021). <https://doi.org:10.1038/s41416-020-01048-4>
- 43 Lugli, E., Galletti, G., Boi, S. K. & Youngblood, B. A. Stem, Effector, and Hybrid States of Memory CD8(+) T Cells. *Trends Immunol* **41**, 17-28 (2020). <https://doi.org:10.1016/j.it.2019.11.004>
- 44 Philip, M. & Schietinger, A. CD8(+) T cell differentiation and dysfunction in cancer. *Nat Rev Immunol* **22**, 209-223 (2022). <https://doi.org:10.1038/s41577-021-00574-3>
- 45 Halloran, P. F. Immunosuppressive drugs for kidney transplantation. *N Engl J Med* **351**, 2715-2729 (2004). <https://doi.org:10.1056/NEJMra033540>
- 46 Liu, J., Fu, M., Wang, M., Wan, D., Wei, Y. & Wei, X. Cancer vaccines as promising immuno-therapeutics: platforms and current progress. *J Hematol Oncol* **15**, 28 (2022). <https://doi.org:10.1186/s13045-022-01247-x>
- 47 Borst, J., Ahrends, T., Babala, N., Melief, C. J. M. & Kastenmuller, W. CD4(+) T cell help in cancer immunology and immunotherapy. *Nat Rev Immunol* **18**, 635-647 (2018). <https://doi.org:10.1038/s41577-018-0044-0>
- 48 Tay, R. E., Richardson, E. K. & Toh, H. C. Revisiting the role of CD4(+) T cells in cancer immunotherapy-new insights into old paradigms. *Cancer Gene Ther* **28**, 5-17 (2021). <https://doi.org:10.1038/s41417-020-0183-x>

- 49 Schoenberger, S. P., Toes, R. E., van der Voort, E. I., Offringa, R. & Melief, C. J. T-cell help for cytotoxic T lymphocytes is mediated by CD40-CD40L interactions. *Nature* **393**, 480-483 (1998). <https://doi.org:10.1038/31002>
- 50 Bennett, S. R., Carbone, F. R., Karamalis, F., Flavell, R. A., Miller, J. F. & Heath, W. R. Help for cytotoxic-T-cell responses is mediated by CD40 signalling. *Nature* **393**, 478-480 (1998). <https://doi.org:10.1038/30996>
- 51 Quezada, S. A. *et al.* Tumor-reactive CD4(+) T cells develop cytotoxic activity and eradicate large established melanoma after transfer into lymphopenic hosts. *J Exp Med* **207**, 637-650 (2010). <https://doi.org:10.1084/jem.20091918>
- 52 Xie, Y. *et al.* Naive tumor-specific CD4(+) T cells differentiated in vivo eradicate established melanoma. *J Exp Med* **207**, 651-667 (2010). <https://doi.org:10.1084/jem.20091921>
- 53 Reed, C. M., Cresce, N. D., Mauldin, I. S., Slingluff, C. L., Jr. & Olson, W. C. Vaccination with Melanoma Helper Peptides Induces Antibody Responses Associated with Improved Overall Survival. *Clin Cancer Res* **21**, 3879-3887 (2015). <https://doi.org:10.1158/1078-0432.CCR-15-0233>
- 54 Gnjatic, S. *et al.* Survey of naturally occurring CD4+ T cell responses against NY-ESO-1 in cancer patients: correlation with antibody responses. *Proc Natl Acad Sci U S A* **100**, 8862-8867 (2003). <https://doi.org:10.1073/pnas.1133324100>
- 55 Nelson, B. H. CD20+ B cells: the other tumor-infiltrating lymphocytes. *J Immunol* **185**, 4977-4982 (2010). <https://doi.org:10.4049/jimmunol.1001323>
- 56 Li, Q., Teitz-Tennenbaum, S., Donald, E. J., Li, M. & Chang, A. E. In vivo sensitized and in vitro activated B cells mediate tumor regression in cancer adoptive immunotherapy. *J Immunol* **183**, 3195-3203 (2009). <https://doi.org:10.4049/jimmunol.0803773>
- 57 Martin, F. & Chan, A. C. B cell immunobiology in disease: evolving concepts from the clinic. *Annu Rev Immunol* **24**, 467-496 (2006). <https://doi.org:10.1146/annurev.immunol.24.021605.090517>
- 58 Wang, W. W. *et al.* CD19+CD24hiCD38hiBregs involved in downregulate helper T cells and upregulate regulatory T cells in gastric cancer. *Oncotarget* **6**, 33486-33499 (2015). <https://doi.org:10.18632/oncotarget.5588>
- 59 Sarvaria, A., Madrigal, J. A. & Saudemont, A. B cell regulation in cancer and anti-tumor immunity. *Cell Mol Immunol* **14**, 662-674 (2017). <https://doi.org:10.1038/cmi.2017.35>
- 60 Xiao, X. *et al.* PD-1hi Identifies a Novel Regulatory B-cell Population in Human Hepatoma That Promotes Disease Progression. *Cancer Discov* **6**, 546-559 (2016). <https://doi.org:10.1158/2159-8290.CD-15-1408>
- 61 Carrega, P. & Ferlazzo, G. Natural killer cell distribution and trafficking in human tissues. *Front Immunol* **3**, 347 (2012). <https://doi.org:10.3389/fimmu.2012.00347>
- 62 Lanier, L. L. Up on the tightrope: natural killer cell activation and inhibition. *Nat Immunol* **9**, 495-502 (2008). <https://doi.org:10.1038/ni1581>
- 63 Paul, S. & Lal, G. The Molecular Mechanism of Natural Killer Cells Function and Its Importance in Cancer Immunotherapy. *Front Immunol* **8**, 1124 (2017). <https://doi.org:10.3389/fimmu.2017.01124>

- 64 Zilionis, R. *et al.* Single-Cell Transcriptomics of Human and Mouse Lung Cancers Reveals Conserved Myeloid Populations across Individuals and Species. *Immunity* **50**, 1317-1334 e1310 (2019). <https://doi.org:10.1016/j.immuni.2019.03.009>
- 65 Coffelt, S. B., Wellenstein, M. D. & de Visser, K. E. Neutrophils in cancer: neutral no more. *Nat Rev Cancer* **16**, 431-446 (2016). <https://doi.org:10.1038/nrc.2016.52>
- 66 Fridlender, Z. G. *et al.* Polarization of tumor-associated neutrophil phenotype by TGF-beta: "N1" versus "N2" TAN. *Cancer Cell* **16**, 183-194 (2009). <https://doi.org:10.1016/j.ccr.2009.06.017>
- 67 Andzinski, L. *et al.* Type I IFNs induce anti-tumor polarization of tumor associated neutrophils in mice and human. *Int J Cancer* **138**, 1982-1993 (2016). <https://doi.org:10.1002/ijc.29945>
- 68 Xiao, Y. *et al.* Cathepsin C promotes breast cancer lung metastasis by modulating neutrophil infiltration and neutrophil extracellular trap formation. *Cancer Cell* **39**, 423-437 e427 (2021). <https://doi.org:10.1016/j.ccell.2020.12.012>
- 69 Barber, D. L. *et al.* Restoring function in exhausted CD8 T cells during chronic viral infection. *Nature* **439**, 682-687 (2006). <https://doi.org:10.1038/nature04444>
- 70 Matsushita, H. *et al.* Cytotoxic T lymphocytes block tumor growth both by lytic activity and IFN γ -dependent cell-cycle arrest. *Cancer Immunol Res* **3**, 26-36 (2015). <https://doi.org:10.1158/2326-6066.CIR-14-0098>
- 71 Thommen, D. S. & Schumacher, T. N. T Cell Dysfunction in Cancer. *Cancer Cell* **33**, 547-562 (2018). <https://doi.org:10.1016/j.ccell.2018.03.012>
- 72 Tietscher, S. *et al.* A comprehensive single-cell map of T cell exhaustion-associated immune environments in human breast cancer. *Nat Commun* **14**, 98 (2023). <https://doi.org:10.1038/s41467-022-35238-w>
- 73 Wherry, E. J. T cell exhaustion. *Nat Immunol* **12**, 492-499 (2011). <https://doi.org:10.1038/ni.2035>
- 74 Nolz, J. C. Molecular mechanisms of CD8(+) T cell trafficking and localization. *Cell Mol Life Sci* **72**, 2461-2473 (2015). <https://doi.org:10.1007/s00018-015-1835-0>
- 75 Hanahan, D. & Coussens, L. M. Accessories to the crime: functions of cells recruited to the tumor microenvironment. *Cancer Cell* **21**, 309-322 (2012). <https://doi.org:10.1016/j.ccr.2012.02.022>
- 76 Kohli, K., Pillarisetty, V. G. & Kim, T. S. Key chemokines direct migration of immune cells in solid tumors. *Cancer Gene Ther* **29**, 10-21 (2022). <https://doi.org:10.1038/s41417-021-00303-x>
- 77 Maimela, N. R., Liu, S. & Zhang, Y. Fates of CD8+ T cells in Tumor Microenvironment. *Comput Struct Biotechnol J* **17**, 1-13 (2019). <https://doi.org:10.1016/j.csbj.2018.11.004>
- 78 Lopez de Rodas, M. & Schalper, K. A. Tumour antigen-induced T cell exhaustion - the archenemy of immune-hot malignancies. *Nat Rev Clin Oncol* **18**, 749-750 (2021). <https://doi.org:10.1038/s41571-021-00562-5>
- 79 Zhang, Z., Liu, S., Zhang, B., Qiao, L., Zhang, Y. & Zhang, Y. T Cell Dysfunction and Exhaustion in Cancer. *Front Cell Dev Biol* **8**, 17 (2020). <https://doi.org:10.3389/fcell.2020.00017>

- 80 Yang, Y., Li, C., Liu, T., Dai, X. & Bazhin, A. V. Myeloid-Derived Suppressor Cells in Tumors: From Mechanisms to Antigen Specificity and Microenvironmental Regulation. *Front Immunol* **11**, 1371 (2020). <https://doi.org/10.3389/fimmu.2020.01371>
- 81 Lee, C. R., Lee, W., Cho, S. K. & Park, S. G. Characterization of Multiple Cytokine Combinations and TGF-beta on Differentiation and Functions of Myeloid-Derived Suppressor Cells. *Int J Mol Sci* **19** (2018). <https://doi.org/10.3390/ijms19030869>
- 82 Huang, B. *et al.* Gr-1+CD115+ immature myeloid suppressor cells mediate the development of tumor-induced T regulatory cells and T-cell anergy in tumor-bearing host. *Cancer Res* **66**, 1123-1131 (2006). <https://doi.org/10.1158/0008-5472.CAN-05-1299>
- 83 Yu, J. *et al.* Myeloid-derived suppressor cells suppress antitumor immune responses through IDO expression and correlate with lymph node metastasis in patients with breast cancer. *J Immunol* **190**, 3783-3797 (2013). <https://doi.org/10.4049/jimmunol.1201449>
- 84 Dallavalasa, S. *et al.* The Role of Tumor Associated Macrophages (TAMs) in Cancer Progression, Chemoresistance, Angiogenesis and Metastasis - Current Status. *Curr Med Chem* **28**, 8203-8236 (2021). <https://doi.org/10.2174/0929867328666210720143721>
- 85 Cassetta, L. & Kitamura, T. Macrophage targeting: opening new possibilities for cancer immunotherapy. *Immunology* **155**, 285-293 (2018). <https://doi.org/10.1111/imm.12976>
- 86 Saeed, M., Gao, J., Shi, Y., Lammers, T. & Yu, H. Engineering Nanoparticles to Reprogram the Tumor Immune Microenvironment for Improved Cancer Immunotherapy. *Theranostics* **9**, 7981-8000 (2019). <https://doi.org/10.7150/thno.37568>
- 87 Noy, R. & Pollard, J. W. Tumor-associated macrophages: from mechanisms to therapy. *Immunity* **41**, 49-61 (2014). <https://doi.org/10.1016/j.immuni.2014.06.010>
- 88 Han, S. *et al.* Tumor microenvironment remodeling and tumor therapy based on M2-like tumor associated macrophage-targeting nano-complexes. *Theranostics* **11**, 2892-2916 (2021). <https://doi.org/10.7150/thno.50928>
- 89 Gao, J., Liang, Y. & Wang, L. Shaping Polarization Of Tumor-Associated Macrophages In Cancer Immunotherapy. *Front Immunol* **13**, 888713 (2022). <https://doi.org/10.3389/fimmu.2022.888713>
- 90 Lin, Y., Xu, J. & Lan, H. Tumor-associated macrophages in tumor metastasis: biological roles and clinical therapeutic applications. *J Hematol Oncol* **12**, 76 (2019). <https://doi.org/10.1186/s13045-019-0760-3>
- 91 Jiang, Y., Li, Y. & Zhu, B. T-cell exhaustion in the tumor microenvironment. *Cell Death Dis* **6**, e1792 (2015). <https://doi.org/10.1038/cddis.2015.162>
- 92 Lakins, M. A., Ghorani, E., Munir, H., Martins, C. P. & Shields, J. D. Cancer-associated fibroblasts induce antigen-specific deletion of CD8 (+) T Cells to protect tumour cells. *Nat Commun* **9**, 948 (2018). <https://doi.org/10.1038/s41467-018-03347-0>
- 93 Erez, N., Truitt, M., Olson, P., Arron, S. T. & Hanahan, D. Cancer-Associated Fibroblasts Are Activated in Incipient Neoplasia to Orchestrate Tumor-Promoting Inflammation in an NF-kappaB-Dependent Manner. *Cancer Cell* **17**, 135-147 (2010). <https://doi.org/10.1016/j.ccr.2009.12.041>
- 94 Mao, X. *et al.* Crosstalk between cancer-associated fibroblasts and immune cells in the tumor microenvironment: new findings and future perspectives. *Mol Cancer* **20**, 131 (2021). <https://doi.org/10.1186/s12943-021-01428-1>

- 95 Kuo, I. Y. *et al.* Converged Rab37/IL-6 trafficking and STAT3/PD-1 transcription axes elicit an immunosuppressive lung tumor microenvironment. *Theranostics* **11**, 7029-7044 (2021). <https://doi.org:10.7150/thno.60040>
- 96 Fang, L. *et al.* Tumor accomplice: T cell exhaustion induced by chronic inflammation. *Front Immunol* **13**, 979116 (2022). <https://doi.org:10.3389/fimmu.2022.979116>
- 97 Li, C. & Zuo, W. IL-10 in vitro could enhance IFN γ expression and suppress PD-1 expression in CD8 T cells from esophageal cancer patients. *Exp Cell Res* **379**, 159-165 (2019). <https://doi.org:10.1016/j.yexcr.2019.03.038>
- 98 Jimbu, L. *et al.* The Potential Advantage of Targeting Both PD-L1/PD-L2/PD-1 and IL-10-IL-10R Pathways in Acute Myeloid Leukemia. *Pharmaceuticals (Basel)* **14** (2021). <https://doi.org:10.3390/ph14111105>
- 99 Tauriello, D. V. F. *et al.* TGF β drives immune evasion in genetically reconstituted colon cancer metastasis. *Nature* **554**, 538-543 (2018). <https://doi.org:10.1038/nature25492>
- 100 Mathieu, M., Cotta-Grand, N., Daudelin, J. F., Thebault, P. & Labrecque, N. Notch signaling regulates PD-1 expression during CD8(+) T-cell activation. *Immunol Cell Biol* **91**, 82-88 (2013). <https://doi.org:10.1038/icb.2012.53>
- 101 Wang, R. X., Li, Y. F., Hao, C. H. & Fang, W. [Increased Notch receptors induces CD8(+) T cell exhaustion in patients with prostate cancer]. *Zhonghua Yi Xue Za Zhi* **100**, 2669-2674 (2020). <https://doi.org:10.3760/cma.j.cn112137-20200509-01468>
- 102 Wang, C., Singer, M. & Anderson, A. C. Molecular Dissection of CD8(+) T-Cell Dysfunction. *Trends Immunol* **38**, 567-576 (2017). <https://doi.org:10.1016/j.it.2017.05.008>
- 103 Liu, X. *et al.* Genome-wide analysis identifies NR4A1 as a key mediator of T cell dysfunction. *Nature* **567**, 525-529 (2019). <https://doi.org:10.1038/s41586-019-0979-8>
- 104 Alfei, F. *et al.* TOX reinforces the phenotype and longevity of exhausted T cells in chronic viral infection. *Nature* **571**, 265-269 (2019). <https://doi.org:10.1038/s41586-019-1326-9>
- 105 Quigley, M. *et al.* Transcriptional analysis of HIV-specific CD8+ T cells shows that PD-1 inhibits T cell function by upregulating BATF. *Nat Med* **16**, 1147-1151 (2010). <https://doi.org:10.1038/nm.2232>
- 106 Huang, Q., Lei, Y., Li, X., Guo, F. & Liu, M. A Highlight of the Mechanisms of Immune Checkpoint Blocker Resistance. *Front Cell Dev Biol* **8**, 580140 (2020). <https://doi.org:10.3389/fcell.2020.580140>
- 107 Laba, S., Mallett, G. & Amarnath, S. The depths of PD-1 function within the tumor microenvironment beyond CD8(+) T cells. *Semin Cancer Biol* **86**, 1045-1055 (2022). <https://doi.org:10.1016/j.semcancer.2021.05.022>
- 108 Ahmadzadeh, M. *et al.* Tumor antigen-specific CD8 T cells infiltrating the tumor express high levels of PD-1 and are functionally impaired. *Blood* **114**, 1537-1544 (2009). <https://doi.org:10.1182/blood-2008-12-195792>
- 109 Jubel, J. M., Barbati, Z. R., Burger, C., Wirtz, D. C. & Schildberg, F. A. The Role of PD-1 in Acute and Chronic Infection. *Front Immunol* **11**, 487 (2020). <https://doi.org:10.3389/fimmu.2020.00487>
- 110 Zuazo, M. *et al.* Molecular mechanisms of programmed cell death-1 dependent T cell suppression: relevance for immunotherapy. *Ann Transl Med* **5**, 385 (2017). <https://doi.org:10.21037/atm.2017.06.11>

- 111 Bardhan, K., Anagnostou, T. & Boussiotis, V. A. The PD1:PD-L1/2 Pathway from Discovery to Clinical Implementation. *Front Immunol* **7**, 550 (2016). <https://doi.org/10.3389/fimmu.2016.00550>
- 112 Patsoukis, N., Brown, J., Petkova, V., Liu, F., Li, L. & Boussiotis, V. A. Selective effects of PD-1 on Akt and Ras pathways regulate molecular components of the cell cycle and inhibit T cell proliferation. *Sci Signal* **5**, ra46 (2012). <https://doi.org/10.1126/scisignal.2002796>
- 113 Youngblood, B. *et al.* Chronic virus infection enforces demethylation of the locus that encodes PD-1 in antigen-specific CD8(+) T cells. *Immunity* **35**, 400-412 (2011). <https://doi.org/10.1016/j.immuni.2011.06.015>
- 114 Oestreich, K. J., Yoon, H., Ahmed, R. & Boss, J. M. NFATc1 regulates PD-1 expression upon T cell activation. *J Immunol* **181**, 4832-4839 (2008). <https://doi.org/10.4049/jimmunol.181.7.4832>
- 115 Blackburn, S. D. *et al.* Coregulation of CD8+ T cell exhaustion by multiple inhibitory receptors during chronic viral infection. *Nat Immunol* **10**, 29-37 (2009). <https://doi.org/10.1038/ni.1679>
- 116 Wherry, E. J. & Kurachi, M. Molecular and cellular insights into T cell exhaustion. *Nat Rev Immunol* **15**, 486-499 (2015). <https://doi.org/10.1038/nri3862>
- 117 Zhang, Q. *et al.* LAG3 limits regulatory T cell proliferation and function in autoimmune diabetes. *Sci Immunol* **2** (2017). <https://doi.org/10.1126/sciimmunol.aah4569>
- 118 Burnell, S. E. A., Capitani, L., MacLachlan, B. J., Mason, G. H., Gallimore, A. M. & Godkin, A. Seven mysteries of LAG-3: a multi-faceted immune receptor of increasing complexity. *Immunother Adv* **2**, ltab025 (2022). <https://doi.org/10.1093/immadv/ltab025>
- 119 Fleury, S. *et al.* Mutational analysis of the interaction between CD4 and class II MHC: class II antigens contact CD4 on a surface opposite the gp120-binding site. *Cell* **66**, 1037-1049 (1991). [https://doi.org/10.1016/0092-8674\(91\)90447-7](https://doi.org/10.1016/0092-8674(91)90447-7)
- 120 Grebinoski, S. *et al.* Autoreactive CD8(+) T cells are restrained by an exhaustion-like program that is maintained by LAG3. *Nat Immunol* **23**, 868-877 (2022). <https://doi.org/10.1038/s41590-022-01210-5>
- 121 Sun, H., Sun, C. & Xiao, W. Expression regulation of co-inhibitory molecules on human natural killer cells in response to cytokine stimulations. *Cytokine* **65**, 33-41 (2014). <https://doi.org/10.1016/j.cyto.2013.09.016>
- 122 Anderson, A. C., Joller, N. & Kuchroo, V. K. Lag-3, Tim-3, and TIGIT: Co-inhibitory Receptors with Specialized Functions in Immune Regulation. *Immunity* **44**, 989-1004 (2016). <https://doi.org/10.1016/j.immuni.2016.05.001>
- 123 Anderson, A. C. Tim-3, a negative regulator of anti-tumor immunity. *Curr Opin Immunol* **24**, 213-216 (2012). <https://doi.org/10.1016/j.coi.2011.12.005>
- 124 Monney, L. *et al.* Th1-specific cell surface protein Tim-3 regulates macrophage activation and severity of an autoimmune disease. *Nature* **415**, 536-541 (2002). <https://doi.org/10.1038/415536a>
- 125 Zhu, C. *et al.* The Tim-3 ligand galectin-9 negatively regulates T helper type 1 immunity. *Nat Immunol* **6**, 1245-1252 (2005). <https://doi.org/10.1038/ni1271>
- 126 Dolina, J. S., Braciale, T. J. & Hahn, Y. S. Liver-primed CD8+ T cells suppress antiviral adaptive immunity through galectin-9-independent T-cell immunoglobulin and mucin 3

- engagement of high-mobility group box 1 in mice. *Hepatology* **59**, 1351-1365 (2014). <https://doi.org/10.1002/hep.26938>
- 127 van de Weyer, P. S., Muehlfeit, M., Klose, C., Bonventre, J. V., Walz, G. & Kuehn, E. W. A highly conserved tyrosine of Tim-3 is phosphorylated upon stimulation by its ligand galectin-9. *Biochem Biophys Res Commun* **351**, 571-576 (2006). <https://doi.org/10.1016/j.bbrc.2006.10.079>
- 128 Cong, Y., Liu, J., Chen, G. & Qiao, G. The Emerging Role of T-Cell Immunoglobulin Mucin-3 in Breast Cancer: A Promising Target For Immunotherapy. *Front Oncol* **11**, 723238 (2021). <https://doi.org/10.3389/fonc.2021.723238>
- 129 Greenwald, R. J., Freeman, G. J. & Sharpe, A. H. The B7 family revisited. *Annu Rev Immunol* **23**, 515-548 (2005). <https://doi.org/10.1146/annurev.immunol.23.021704.115611>
- 130 Chen, L. Co-inhibitory molecules of the B7-CD28 family in the control of T-cell immunity. *Nat Rev Immunol* **4**, 336-347 (2004). <https://doi.org/10.1038/nri1349>
- 131 Chen, L. & Flies, D. B. Molecular mechanisms of T cell co-stimulation and co-inhibition. *Nat Rev Immunol* **13**, 227-242 (2013). <https://doi.org/10.1038/nri3405>
- 132 Yu, X. *et al.* The surface protein TIGIT suppresses T cell activation by promoting the generation of mature immunoregulatory dendritic cells. *Nat Immunol* **10**, 48-57 (2009). <https://doi.org/10.1038/ni.1674>
- 133 Boles, K. S. *et al.* A novel molecular interaction for the adhesion of follicular CD4 T cells to follicular DC. *Eur J Immunol* **39**, 695-703 (2009). <https://doi.org/10.1002/eji.200839116>
- 134 Joller, N. *et al.* Treg cells expressing the coinhibitory molecule TIGIT selectively inhibit proinflammatory Th1 and Th17 cell responses. *Immunity* **40**, 569-581 (2014). <https://doi.org/10.1016/j.immuni.2014.02.012>
- 135 Fuhrman, C. A. *et al.* Divergent Phenotypes of Human Regulatory T Cells Expressing the Receptors TIGIT and CD226. *J Immunol* **195**, 145-155 (2015). <https://doi.org/10.4049/jimmunol.1402381>
- 136 Zhang, Y. & Zhang, Z. The history and advances in cancer immunotherapy: understanding the characteristics of tumor-infiltrating immune cells and their therapeutic implications. *Cell Mol Immunol* **17**, 807-821 (2020). <https://doi.org/10.1038/s41423-020-0488-6>
- 137 Xin Yu, J., Hubbard-Lucey, V. M. & Tang, J. Immuno-oncology drug development goes global. *Nat Rev Drug Discov* **18**, 899-900 (2019). <https://doi.org/10.1038/d41573-019-00167-9>
- 138 Rowshanravan, B., Halliday, N. & Sansom, D. M. CTLA-4: a moving target in immunotherapy. *Blood* **131**, 58-67 (2018). <https://doi.org/10.1182/blood-2017-06-741033>
- 139 Leach, D. R., Krummel, M. F. & Allison, J. P. Enhancement of antitumor immunity by CTLA-4 blockade. *Science* **271**, 1734-1736 (1996). <https://doi.org/10.1126/science.271.5256.1734>
- 140 Robert, C. A decade of immune-checkpoint inhibitors in cancer therapy. *Nat Commun* **11**, 3801 (2020). <https://doi.org/10.1038/s41467-020-17670-y>

- 141 Waldman, A. D., Fritz, J. M. & Lenardo, M. J. A guide to cancer immunotherapy: from T cell basic science to clinical practice. *Nat Rev Immunol* **20**, 651-668 (2020). <https://doi.org:10.1038/s41577-020-0306-5>
- 142 Stanietsky, N. *et al.* The interaction of TIGIT with PVR and PVRL2 inhibits human NK cell cytotoxicity. *Proc Natl Acad Sci U S A* **106**, 17858-17863 (2009). <https://doi.org:10.1073/pnas.0903474106>
- 143 Yu, B. M., Cunningham, J. P., Santhanam, G., Ryu, S. I., Shenoy, K. V. & Sahani, M. Gaussian-process factor analysis for low-dimensional single-trial analysis of neural population activity. *J Neurophysiol* **102**, 614-635 (2009). <https://doi.org:10.1152/jn.90941.2008>
- 144 Talmadge, J. E. & Gaborilovich, D. I. History of myeloid-derived suppressor cells. *Nat Rev Cancer* **13**, 739-752 (2013). <https://doi.org:10.1038/nrc3581>
- 145 Lathers, D. M., Clark, J. I., Achille, N. J. & Young, M. R. Phase 1B study to improve immune responses in head and neck cancer patients using escalating doses of 25-hydroxyvitamin D3. *Cancer Immunol Immunother* **53**, 422-430 (2004). <https://doi.org:10.1007/s00262-003-0459-7>
- 146 Mirza, N. *et al.* All-trans-retinoic acid improves differentiation of myeloid cells and immune response in cancer patients. *Cancer Res* **66**, 9299-9307 (2006). <https://doi.org:10.1158/0008-5472.CAN-06-1690>
- 147 Li, K. *et al.* Myeloid-derived suppressor cells as immunosuppressive regulators and therapeutic targets in cancer. *Signal Transduct Target Ther* **6**, 362 (2021). <https://doi.org:10.1038/s41392-021-00670-9>
- 148 Kolb, H. R., Borchering, N. & Zhang, W. Understanding and Targeting Human Cancer Regulatory T Cells to Improve Therapy. *Adv Exp Med Biol* **1278**, 229-256 (2021). https://doi.org:10.1007/978-981-15-6407-9_12
- 149 Huang, L. *et al.* Targeting regulatory T cells for immunotherapy in melanoma. *Mol Biomed* **2**, 11 (2021). <https://doi.org:10.1186/s43556-021-00038-z>
- 150 Rafiq, S., Hackett, C. S. & Brentjens, R. J. Engineering strategies to overcome the current roadblocks in CAR T cell therapy. *Nat Rev Clin Oncol* **17**, 147-167 (2020). <https://doi.org:10.1038/s41571-019-0297-y>
- 151 Sadelain, M., Riviere, I. & Riddell, S. Therapeutic T cell engineering. *Nature* **545**, 423-431 (2017). <https://doi.org:10.1038/nature22395>
- 152 Labanieh, L., Majzner, R. G. & Mackall, C. L. Programming CAR-T cells to kill cancer. *Nat Biomed Eng* **2**, 377-391 (2018). <https://doi.org:10.1038/s41551-018-0235-9>
- 153 Lin, H., Cheng, J., Mu, W., Zhou, J. & Zhu, L. Advances in Universal CAR-T Cell Therapy. *Front Immunol* **12**, 744823 (2021). <https://doi.org:10.3389/fimmu.2021.744823>
- 154 Sadelain, M., Brentjens, R. & Riviere, I. The promise and potential pitfalls of chimeric antigen receptors. *Curr Opin Immunol* **21**, 215-223 (2009). <https://doi.org:10.1016/j.coi.2009.02.009>
- 155 Huang, R. *et al.* Recent advances in CAR-T cell engineering. *J Hematol Oncol* **13**, 86 (2020). <https://doi.org:10.1186/s13045-020-00910-5>
- 156 Brown, C. E. *et al.* Regression of Glioblastoma after Chimeric Antigen Receptor T-Cell Therapy. *N Engl J Med* **375**, 2561-2569 (2016). <https://doi.org:10.1056/NEJMoa1610497>

- 157 Ahmed, N. *et al.* Human Epidermal Growth Factor Receptor 2 (HER2) -Specific Chimeric Antigen Receptor-Modified T Cells for the Immunotherapy of HER2-Positive Sarcoma. *J Clin Oncol* **33**, 1688-1696 (2015). <https://doi.org:10.1200/JCO.2014.58.0225>
- 158 Qi, C. *et al.* Claudin18.2-specific CAR T cells in gastrointestinal cancers: phase 1 trial interim results. *Nat Med* **28**, 1189-1198 (2022). <https://doi.org:10.1038/s41591-022-01800-8>
- 159 Maude, S. L. *et al.* Chimeric antigen receptor T cells for sustained remissions in leukemia. *N Engl J Med* **371**, 1507-1517 (2014). <https://doi.org:10.1056/NEJMoa1407222>
- 160 Schuster, S. J. *et al.* Chimeric Antigen Receptor T Cells in Refractory B-Cell Lymphomas. *N Engl J Med* **377**, 2545-2554 (2017). <https://doi.org:10.1056/NEJMoa1708566>
- 161 Yang, J., Chen, Y., Jing, Y., Green, M. R. & Han, L. Advancing CAR T cell therapy through the use of multidimensional omics data. *Nat Rev Clin Oncol* (2023). <https://doi.org:10.1038/s41571-023-00729-2>
- 162 June, C. H. & Sadelain, M. Chimeric Antigen Receptor Therapy. *N Engl J Med* **379**, 64-73 (2018). <https://doi.org:10.1056/NEJMra1706169>
- 163 Zhao, J., Lin, Q., Song, Y. & Liu, D. Universal CARs, universal T cells, and universal CAR T cells. *J Hematol Oncol* **11**, 132 (2018). <https://doi.org:10.1186/s13045-018-0677-2>
- 164 Yin, Y. *et al.* Checkpoint Blockade Reverses Anergy in IL-13Ralpha2 Humanized scFv-Based CAR T Cells to Treat Murine and Canine Gliomas. *Mol Ther Oncolytics* **11**, 20-38 (2018). <https://doi.org:10.1016/j.omto.2018.08.002>
- 165 Ren, J. *et al.* A versatile system for rapid multiplex genome-edited CAR T cell generation. *Oncotarget* **8**, 17002-17011 (2017). <https://doi.org:10.18632/oncotarget.15218>
- 166 Seo, H. *et al.* TOX and TOX2 transcription factors cooperate with NR4A transcription factors to impose CD8(+) T cell exhaustion. *Proc Natl Acad Sci U S A* **116**, 12410-12415 (2019). <https://doi.org:10.1073/pnas.1905675116>
- 167 Poorebrahim, M., Melief, J., Pico de Coana, Y., S, L. W., Cid-Arregui, A. & Kiessling, R. Counteracting CAR T cell dysfunction. *Oncogene* **40**, 421-435 (2021). <https://doi.org:10.1038/s41388-020-01501-x>
- 168 Zhu, Y. & Liu, J. The Role of Neoantigens in Cancer Immunotherapy. *Front Oncol* **11**, 682325 (2021). <https://doi.org:10.3389/fonc.2021.682325>
- 169 Carreno, B. M. *et al.* Cancer immunotherapy. A dendritic cell vaccine increases the breadth and diversity of melanoma neoantigen-specific T cells. *Science* **348**, 803-808 (2015). <https://doi.org:10.1126/science.aaa3828>
- 170 Chan, T. A., Wolchok, J. D. & Snyder, A. Genetic Basis for Clinical Response to CTLA-4 Blockade in Melanoma. *N Engl J Med* **373**, 1984 (2015). <https://doi.org:10.1056/NEJMc1508163>
- 171 Rizvi, N. A. *et al.* Cancer immunology. Mutational landscape determines sensitivity to PD-1 blockade in non-small cell lung cancer. *Science* **348**, 124-128 (2015). <https://doi.org:10.1126/science.aaa1348>
- 172 McGranahan, N. *et al.* Clonal neoantigens elicit T cell immunoreactivity and sensitivity to immune checkpoint blockade. *Science* **351**, 1463-1469 (2016). <https://doi.org:10.1126/science.aaf1490>

- 173 Klener, P., Jr., Otahal, P., Lateckova, L. & Klener, P. Immunotherapy Approaches in Cancer Treatment. *Curr Pharm Biotechnol* **16**, 771-781 (2015). <https://doi.org:10.2174/1389201016666150619114554>
- 174 Alatrash, G., Jakher, H., Stafford, P. D. & Mittendorf, E. A. Cancer immunotherapies, their safety and toxicity. *Expert Opin Drug Saf* **12**, 631-645 (2013). <https://doi.org:10.1517/14740338.2013.795944>
- 175 Sambhi, M., Bagheri, L. & Szewczuk, M. R. Current Challenges in Cancer Immunotherapy: Multimodal Approaches to Improve Efficacy and Patient Response Rates. *J Oncol* **2019**, 4508794 (2019). <https://doi.org:10.1155/2019/4508794>
- 176 Peterson, C., Denlinger, N. & Yang, Y. Recent Advances and Challenges in Cancer Immunotherapy. *Cancers (Basel)* **14** (2022). <https://doi.org:10.3390/cancers14163972>
- 177 Hegde, P. S. & Chen, D. S. Top 10 Challenges in Cancer Immunotherapy. *Immunity* **52**, 17-35 (2020). <https://doi.org:10.1016/j.immuni.2019.12.011>
- 178 Schandendorf, D. *et al.* Health-related quality of life results from the phase III CheckMate 067 study. *Eur J Cancer* **82**, 80-91 (2017). <https://doi.org:10.1016/j.ejca.2017.05.031>
- 179 Weber, J. S. *et al.* Nivolumab versus chemotherapy in patients with advanced melanoma who progressed after anti-CTLA-4 treatment (CheckMate 037): a randomised, controlled, open-label, phase 3 trial. *Lancet Oncol* **16**, 375-384 (2015). [https://doi.org:10.1016/S1470-2045\(15\)70076-8](https://doi.org:10.1016/S1470-2045(15)70076-8)
- 180 Zahalka, A. H. & Frenette, P. S. Nerves in cancer. *Nat Rev Cancer* **20**, 143-157 (2020). <https://doi.org:10.1038/s41568-019-0237-2>
- 181 Rotthier, A., Baets, J., Timmerman, V. & Janssens, K. Mechanisms of disease in hereditary sensory and autonomic neuropathies. *Nat Rev Neurol* **8**, 73-85 (2012). <https://doi.org:10.1038/nrneurol.2011.227>
- 182 Akinrodoye, M. A. & Lui, F. in *StatPearls* (2022).
- 183 Malet, M. & Brumovsky, P. R. VGLUTs and Glutamate Synthesis-Focus on DRG Neurons and Pain. *Biomolecules* **5**, 3416-3437 (2015). <https://doi.org:10.3390/biom5043416>
- 184 Jeftinija, S., Jeftinija, K., Liu, F., Skilling, S. R., Smullin, D. H. & Larson, A. A. Excitatory amino acids are released from rat primary afferent neurons in vitro. *Neurosci Lett* **125**, 191-194 (1991). [https://doi.org:10.1016/0304-3940\(91\)90025-o](https://doi.org:10.1016/0304-3940(91)90025-o)
- 185 Crawford, L. K. & Caterina, M. J. Functional Anatomy of the Sensory Nervous System: Updates From the Neuroscience Bench. *Toxicol Pathol* **48**, 174-189 (2020). <https://doi.org:10.1177/0192623319869011>
- 186 Le Pichon, C. E. & Chesler, A. T. The functional and anatomical dissection of somatosensory subpopulations using mouse genetics. *Front Neuroanat* **8**, 21 (2014). <https://doi.org:10.3389/fnana.2014.00021>
- 187 Zimmerman, A., Bai, L. & Ginty, D. D. The gentle touch receptors of mammalian skin. *Science* **346**, 950-954 (2014). <https://doi.org:10.1126/science.1254229>
- 188 Qi, J. *et al.* Painful pathways induced by TLR stimulation of dorsal root ganglion neurons. *J Immunol* **186**, 6417-6426 (2011). <https://doi.org:10.4049/jimmunol.1001241>
- 189 Molliver, D. C., Radeke, M. J., Feinstein, S. C. & Snider, W. D. Presence or absence of TrkA protein distinguishes subsets of small sensory neurons with unique cytochemical characteristics and dorsal horn projections. *J Comp Neurol* **361**, 404-416 (1995). <https://doi.org:10.1002/cne.903610305>

- 190 Molliver, D. C. *et al.* IB4-binding DRG neurons switch from NGF to GDNF dependence in early postnatal life. *Neuron* **19**, 849-861 (1997). [https://doi.org:10.1016/s0896-6273\(00\)80966-6](https://doi.org:10.1016/s0896-6273(00)80966-6)
- 191 Bennett, D. L. *et al.* A distinct subgroup of small DRG cells express GDNF receptor components and GDNF is protective for these neurons after nerve injury. *J Neurosci* **18**, 3059-3072 (1998). <https://doi.org:10.1523/JNEUROSCI.18-08-03059.1998>
- 192 Dib-Hajj, S. D. & Waxman, S. G. Translational pain research: Lessons from genetics and genomics. *Sci Transl Med* **6**, 249sr244 (2014). <https://doi.org:10.1126/scitranslmed.3007017>
- 193 von Hehn, C. A., Baron, R. & Woolf, C. J. Deconstructing the neuropathic pain phenotype to reveal neural mechanisms. *Neuron* **73**, 638-652 (2012). <https://doi.org:10.1016/j.neuron.2012.02.008>
- 194 Ranade, S. S., Syeda, R. & Patapoutian, A. Mechanically Activated Ion Channels. *Neuron* **87**, 1162-1179 (2015). <https://doi.org:10.1016/j.neuron.2015.08.032>
- 195 Pinho-Ribeiro, F. A., Verri, W. A., Jr. & Chiu, I. M. Nociceptor Sensory Neuron-Immune Interactions in Pain and Inflammation. *Trends Immunol* **38**, 5-19 (2017). <https://doi.org:10.1016/j.it.2016.10.001>
- 196 Julius, D. TRP channels and pain. *Annu Rev Cell Dev Biol* **29**, 355-384 (2013). <https://doi.org:10.1146/annurev-cellbio-101011-155833>
- 197 Cunha, T. M. *et al.* Crucial role of neutrophils in the development of mechanical inflammatory hypernociception. *J Leukoc Biol* **83**, 824-832 (2008). <https://doi.org:10.1189/jlb.0907654>
- 198 Wood, J. N., Boorman, J. P., Okuse, K. & Baker, M. D. Voltage-gated sodium channels and pain pathways. *J Neurobiol* **61**, 55-71 (2004). <https://doi.org:10.1002/neu.20094>
- 199 Shuba, Y. M. Beyond Neuronal Heat Sensing: Diversity of TRPV1 Heat-Capsaicin Receptor-Channel Functions. *Front Cell Neurosci* **14**, 612480 (2020). <https://doi.org:10.3389/fncel.2020.612480>
- 200 Koivisto, A. P., Belvisi, M. G., Gaudet, R. & Szallasi, A. Advances in TRP channel drug discovery: from target validation to clinical studies. *Nat Rev Drug Discov* **21**, 41-59 (2022). <https://doi.org:10.1038/s41573-021-00268-4>
- 201 Oliveira, S. M. *et al.* Involvement of mast cells in a mouse model of postoperative pain. *Eur J Pharmacol* **672**, 88-95 (2011). <https://doi.org:10.1016/j.ejphar.2011.10.001>
- 202 Shutov, L. P. *et al.* The Complement System Component C5a Produces Thermal Hyperalgesia via Macrophage-to-Nociceptor Signaling That Requires NGF and TRPV1. *J Neurosci* **36**, 5055-5070 (2016). <https://doi.org:10.1523/JNEUROSCI.3249-15.2016>
- 203 Kobayashi, Y., Kiguchi, N., Fukazawa, Y., Saika, F., Maeda, T. & Kishioka, S. Macrophage-T cell interactions mediate neuropathic pain through the glucocorticoid-induced tumor necrosis factor ligand system. *J Biol Chem* **290**, 12603-12613 (2015). <https://doi.org:10.1074/jbc.M115.636506>
- 204 Woolf, C. J., Allchorne, A., Safieh-Garabedian, B. & Poole, S. Cytokines, nerve growth factor and inflammatory hyperalgesia: the contribution of tumour necrosis factor alpha. *Br J Pharmacol* **121**, 417-424 (1997). <https://doi.org:10.1038/sj.bjp.0701148>

- 205 Nieto-Posadas, A. *et al.* Lysophosphatidic acid directly activates TRPV1 through a C-terminal binding site. *Nat Chem Biol* **8**, 78-85 (2011). <https://doi.org:10.1038/nchembio.712>
- 206 Xiao, T., Sun, M., Kang, J. & Zhao, C. Transient Receptor Potential Vanilloid1 (TRPV1) Channel Opens Sesame of T Cell Responses and T Cell-Mediated Inflammatory Diseases. *Front Immunol* **13**, 870952 (2022). <https://doi.org:10.3389/fimmu.2022.870952>
- 207 Sousa-Valente, J. & Brain, S. D. A historical perspective on the role of sensory nerves in neurogenic inflammation. *Semin Immunopathol* **40**, 229-236 (2018). <https://doi.org:10.1007/s00281-018-0673-1>
- 208 Sapio, M. R. *et al.* Pain control through selective chemo-axotomy of centrally projecting TRPV1+ sensory neurons. *J Clin Invest* **128**, 1657-1670 (2018). <https://doi.org:10.1172/JCI94331>
- 209 Jancso, N., Jancso-Gabor, A. & Szolcsanyi, J. Direct evidence for neurogenic inflammation and its prevention by denervation and by pretreatment with capsaicin. *Br J Pharmacol Chemother* **31**, 138-151 (1967). <https://doi.org:10.1111/j.1476-5381.1967.tb01984.x>
- 210 Crosson, T. *et al.* Profiling of how nociceptor neurons detect danger - new and old foes. *J Intern Med* **286**, 268-289 (2019). <https://doi.org:10.1111/joim.12957>
- 211 Talbot, S., Foster, S. L. & Woolf, C. J. Neuroimmunity: Physiology and Pathology. *Annu Rev Immunol* **34**, 421-447 (2016). <https://doi.org:10.1146/annurev-immunol-041015-055340>
- 212 Staurengo-Ferrari, L., Deng, L. & Chiu, I. M. Interactions between nociceptor sensory neurons and microbial pathogens in pain. *Pain* **163**, S57-S68 (2022). <https://doi.org:10.1097/j.pain.0000000000002721>
- 213 Steinman, L. Elaborate interactions between the immune and nervous systems. *Nat Immunol* **5**, 575-581 (2004). <https://doi.org:10.1038/ni1078>
- 214 Chu, C., Artis, D. & Chiu, I. M. Neuro-immune Interactions in the Tissues. *Immunity* **52**, 464-474 (2020). <https://doi.org:10.1016/j.immuni.2020.02.017>
- 215 Godinho-Silva, C., Cardoso, F. & Veiga-Fernandes, H. Neuro-Immune Cell Units: A New Paradigm in Physiology. *Annu Rev Immunol* **37**, 19-46 (2019). <https://doi.org:10.1146/annurev-immunol-042718-041812>
- 216 Abaira, V. E. & Ginty, D. D. The sensory neurons of touch. *Neuron* **79**, 618-639 (2013). <https://doi.org:10.1016/j.neuron.2013.07.051>
- 217 Brierley, S. M., Jones, R. C., 3rd, Gebhart, G. F. & Blackshaw, L. A. Splanchnic and pelvic mechanosensory afferents signal different qualities of colonic stimuli in mice. *Gastroenterology* **127**, 166-178 (2004). <https://doi.org:10.1053/j.gastro.2004.04.008>
- 218 Felten, D. L., Felten, S. Y., Carlson, S. L., Olschowka, J. A. & Livnat, S. Noradrenergic and peptidergic innervation of lymphoid tissue. *J Immunol* **135**, 755s-765s (1985).
- 219 Fink, T. & Weihe, E. Multiple neuropeptides in nerves supplying mammalian lymph nodes: messenger candidates for sensory and autonomic neuroimmunomodulation? *Neurosci Lett* **90**, 39-44 (1988). [https://doi.org:10.1016/0304-3940\(88\)90783-5](https://doi.org:10.1016/0304-3940(88)90783-5)
- 220 Huang, S. *et al.* Lymph nodes are innervated by a unique population of sensory neurons with immunomodulatory potential. *Cell* **184**, 441-459 e425 (2021). <https://doi.org:10.1016/j.cell.2020.11.028>

- 221 Baral, P., Udit, S. & Chiu, I. M. Pain and immunity: implications for host defence. *Nat Rev Immunol* **19**, 433-447 (2019). <https://doi.org:10.1038/s41577-019-0147-2>
- 222 Suvas, S. Role of Substance P Neuropeptide in Inflammation, Wound Healing, and Tissue Homeostasis. *J Immunol* **199**, 1543-1552 (2017). <https://doi.org:10.4049/jimmunol.1601751>
- 223 Jagannathan-Bogdan, M. & Zon, L. I. Hematopoiesis. *Development* **140**, 2463-2467 (2013). <https://doi.org:10.1242/dev.083147>
- 224 Warr, M. R., Pietras, E. M. & Passegue, E. Mechanisms controlling hematopoietic stem cell functions during normal hematopoiesis and hematological malignancies. *Wiley Interdiscip Rev Syst Biol Med* **3**, 681-701 (2011). <https://doi.org:10.1002/wsbm.145>
- 225 Calvo, W. The innervation of the bone marrow in laboratory animals. *Am J Anat* **123**, 315-328 (1968). <https://doi.org:10.1002/aja.1001230206>
- 226 Mach, D. B. *et al.* Origins of skeletal pain: sensory and sympathetic innervation of the mouse femur. *Neuroscience* **113**, 155-166 (2002). [https://doi.org:10.1016/s0306-4522\(02\)00165-3](https://doi.org:10.1016/s0306-4522(02)00165-3)
- 227 Robles, H., Park, S., Joens, M. S., Fitzpatrick, J. A. J., Craft, C. S. & Scheller, E. L. Characterization of the bone marrow adipocyte niche with three-dimensional electron microscopy. *Bone* **118**, 89-98 (2019). <https://doi.org:10.1016/j.bone.2018.01.020>
- 228 Nencini, S. & Ivanusic, J. J. The Physiology of Bone Pain. How Much Do We Really Know? *Front Physiol* **7**, 157 (2016). <https://doi.org:10.3389/fphys.2016.00157>
- 229 Wee, N. K. Y., Lorenz, M. R., Bekirov, Y., Jacquin, M. F. & Scheller, E. L. Shared Autonomic Pathways Connect Bone Marrow and Peripheral Adipose Tissues Across the Central Neuraxis. *Front Endocrinol (Lausanne)* **10**, 668 (2019). <https://doi.org:10.3389/fendo.2019.00668>
- 230 Lorenz, M. R., Brazill, J. M., Beeve, A. T., Shen, I. & Scheller, E. L. A Neuroskeletal Atlas: Spatial Mapping and Contextualization of Axon Subtypes Innervating the Long Bones of C3H and B6 Mice. *J Bone Miner Res* **36**, 1012-1025 (2021). <https://doi.org:10.1002/jbmr.4273>
- 231 Zhang, X., Hassan, M. G. & Scheller, E. L. Neural regulation of bone marrow adipose tissue. *Best Pract Res Clin Endocrinol Metab* **35**, 101522 (2021). <https://doi.org:10.1016/j.beem.2021.101522>
- 232 Rampton, D. S. The influence of stress on the development and severity of immune-mediated diseases. *J Rheumatol Suppl* **88**, 43-47 (2011). <https://doi.org:10.3899/jrheum.110904>
- 233 Sun, Y. & Smith, L. E. H. Notice of Withdrawal: Retinal Vasculature in Development and Diseases. *Annu Rev Vis Sci* **0** (2020). <https://doi.org:10.1146/annurev-vs-04-091720-200001>
- 234 Kin, N. W. & Sanders, V. M. It takes nerve to tell T and B cells what to do. *J Leukoc Biol* **79**, 1093-1104 (2006). <https://doi.org:10.1189/jlb.1105625>
- 235 Kouassi, E., Li, Y. S., Boukhris, W., Millet, I. & Revillard, J. P. Opposite effects of the catecholamines dopamine and norepinephrine on murine polyclonal B-cell activation. *Immunopharmacology* **16**, 125-137 (1988). [https://doi.org:10.1016/0162-3109\(88\)90001-x](https://doi.org:10.1016/0162-3109(88)90001-x)

- 236 ThyagaRajan, S. & Priyanka, H. P. Bidirectional communication between the neuroendocrine system and the immune system: relevance to health and diseases. *Ann Neurosci* **19**, 40-46 (2012). <https://doi.org:10.5214/ans.0972.7531.180410>
- 237 Hanes, W. M. *et al.* Neuronal Circuits Modulate Antigen Flow Through Lymph Nodes. *Bioelectron Med* **3**, 18-28 (2016). <https://doi.org:10.15424/bioelectronmed.2016.00001>
- 238 Bellinger, D. L., Lorton, D., Hamill, R. W., Felten, S. Y. & Felten, D. L. Acetylcholinesterase staining and choline acetyltransferase activity in the young adult rat spleen: lack of evidence for cholinergic innervation. *Brain Behav Immun* **7**, 191-204 (1993). <https://doi.org:10.1006/brbi.1993.1021>
- 239 Bellinger, D. L. & Lorton, D. Autonomic regulation of cellular immune function. *Auton Neurosci* **182**, 15-41 (2014). <https://doi.org:10.1016/j.autneu.2014.01.006>
- 240 Bellinger, D. L., Felten, S. Y., Lorton, D. & Felten, D. L. Origin of noradrenergic innervation of the spleen in rats. *Brain Behav Immun* **3**, 291-311 (1989). [https://doi.org:10.1016/0889-1591\(89\)90029-9](https://doi.org:10.1016/0889-1591(89)90029-9)
- 241 Bratton, B. O., Martelli, D., McKinley, M. J., Trevaks, D., Anderson, C. R. & McAllen, R. M. Neural regulation of inflammation: no neural connection from the vagus to splenic sympathetic neurons. *Exp Physiol* **97**, 1180-1185 (2012). <https://doi.org:10.1113/expphysiol.2011.061531>
- 242 Wheway, J. *et al.* A fundamental bimodal role for neuropeptide Y1 receptor in the immune system. *J Exp Med* **202**, 1527-1538 (2005). <https://doi.org:10.1084/jem.20051971>
- 243 Gonzalez-Rey, E., Chorny, A., Fernandez-Martin, A., Ganea, D. & Delgado, M. Vasoactive intestinal peptide generates human tolerogenic dendritic cells that induce CD4 and CD8 regulatory T cells. *Blood* **107**, 3632-3638 (2006). <https://doi.org:10.1182/blood-2005-11-4497>
- 244 Gonzalez-Rey, E. & Delgado, M. Vasoactive intestinal peptide and regulatory T-cell induction: a new mechanism and therapeutic potential for immune homeostasis. *Trends Mol Med* **13**, 241-251 (2007). <https://doi.org:10.1016/j.molmed.2007.04.003>
- 245 Rochlitzer, S. *et al.* The neuropeptide calcitonin gene-related peptide affects allergic airway inflammation by modulating dendritic cell function. *Clin Exp Allergy* **41**, 1609-1621 (2011). <https://doi.org:10.1111/j.1365-2222.2011.03822.x>
- 246 Gomes, R. N. *et al.* Calcitonin gene-related peptide inhibits local acute inflammation and protects mice against lethal endotoxemia. *Shock* **24**, 590-594 (2005). <https://doi.org:10.1097/01.shk.0000183395.29014.7c>
- 247 Bellinger, D. L. & Lorton, D. Sympathetic Nerve Hyperactivity in the Spleen: Causal for Nonpathogenic-Driven Chronic Immune-Mediated Inflammatory Diseases (IMIDs)? *Int J Mol Sci* **19** (2018). <https://doi.org:10.3390/ijms19041188>
- 248 Elenkov, I. J., Wilder, R. L., Chrousos, G. P. & Vizi, E. S. The sympathetic nerve--an integrative interface between two supersystems: the brain and the immune system. *Pharmacol Rev* **52**, 595-638 (2000).
- 249 Hodo, T. W., de Aquino, M. T. P., Shimamoto, A. & Shanker, A. Critical Neurotransmitters in the Neuroimmune Network. *Front Immunol* **11**, 1869 (2020). <https://doi.org:10.3389/fimmu.2020.01869>

- 250 Wong, C. H., Jenne, C. N., Lee, W. Y., Leger, C. & Kubes, P. Functional innervation of hepatic iNKT cells is immunosuppressive following stroke. *Science* **334**, 101-105 (2011). <https://doi.org:10.1126/science.1210301>
- 251 Moriyama, S. *et al.* beta(2)-adrenergic receptor-mediated negative regulation of group 2 innate lymphoid cell responses. *Science* **359**, 1056-1061 (2018). <https://doi.org:10.1126/science.aan4829>
- 252 Diaz-Salazar, C. *et al.* Cell-intrinsic adrenergic signaling controls the adaptive NK cell response to viral infection. *J Exp Med* **217** (2020). <https://doi.org:10.1084/jem.20190549>
- 253 Mohammadpour, H. *et al.* beta2 adrenergic receptor-mediated signaling regulates the immunosuppressive potential of myeloid-derived suppressor cells. *J Clin Invest* **129**, 5537-5552 (2019). <https://doi.org:10.1172/JCI129502>
- 254 Ben-Shaanan, T. L. *et al.* Activation of the reward system boosts innate and adaptive immunity. *Nat Med* **22**, 940-944 (2016). <https://doi.org:10.1038/nm.4133>
- 255 Zhang, X. *et al.* Brain control of humoral immune responses amenable to behavioural modulation. *Nature* **581**, 204-208 (2020). <https://doi.org:10.1038/s41586-020-2235-7>
- 256 Guggilam, A., Patel, K. P., Haque, M., Ebenezer, P. J., Kapusta, D. R. & Francis, J. Cytokine blockade attenuates sympathoexcitation in heart failure: cross-talk between nNOS, AT-1R and cytokines in the hypothalamic paraventricular nucleus. *Eur J Heart Fail* **10**, 625-634 (2008). <https://doi.org:10.1016/j.ejheart.2008.05.004>
- 257 Baral, P. *et al.* Nociceptor sensory neurons suppress neutrophil and gammadelta T cell responses in bacterial lung infections and lethal pneumonia. *Nat Med* **24**, 417-426 (2018). <https://doi.org:10.1038/nm.4501>
- 258 Holzmann, B. Modulation of immune responses by the neuropeptide CGRP. *Amino Acids* **45**, 1-7 (2013). <https://doi.org:10.1007/s00726-011-1161-2>
- 259 Andreeva, L. & Rang, H. P. Effect of bradykinin and prostaglandins on the release of calcitonin gene-related peptide-like immunoreactivity from the rat spinal cord in vitro. *Br J Pharmacol* **108**, 185-190 (1993). <https://doi.org:10.1111/j.1476-5381.1993.tb13460.x>
- 260 Haensel, A., Mills, P. J., Nelesen, R. A., Ziegler, M. G. & Dimsdale, J. E. The relationship between heart rate variability and inflammatory markers in cardiovascular diseases. *Psychoneuroendocrinology* **33**, 1305-1312 (2008). <https://doi.org:10.1016/j.psyneuen.2008.08.007>
- 261 Tokoyoda, K. *et al.* Up-regulation of IL-4 production by the activated cAMP/cAMP-dependent protein kinase (protein kinase A) pathway in CD3/CD28-stimulated naive T cells. *Int Immunol* **16**, 643-653 (2004). <https://doi.org:10.1093/intimm/dxh072>
- 262 Chhatar, S. & Lal, G. Role of adrenergic receptor signalling in neuroimmune communication. *Curr Res Immunol* **2**, 202-217 (2021). <https://doi.org:10.1016/j.crimmu.2021.11.001>
- 263 Serhan, N. *et al.* House dust mites activate nociceptor-mast cell clusters to drive type 2 skin inflammation. *Nat Immunol* **20**, 1435-1443 (2019). <https://doi.org:10.1038/s41590-019-0493-z>
- 264 Yissachar, N. *et al.* An Intestinal Organ Culture System Uncovers a Role for the Nervous System in Microbe-Immune Crosstalk. *Cell* **168**, 1135-1148 e1112 (2017). <https://doi.org:10.1016/j.cell.2017.02.009>

- 265 Klein Wolterink, R. G. J., Wu, G. S., Chiu, I. M. & Veiga-Fernandes, H. Neuroimmune Interactions in Peripheral Organs. *Annu Rev Neurosci* **45**, 339-360 (2022). <https://doi.org:10.1146/annurev-neuro-111020-105359>
- 266 Shao, J. X., Wang, B., Yao, Y. N., Pan, Z. J., Shen, Q. & Zhou, J. Y. Autonomic nervous infiltration positively correlates with pathological risk grading and poor prognosis in patients with lung adenocarcinoma. *Thorac Cancer* **7**, 588-598 (2016). <https://doi.org:10.1111/1759-7714.12374>
- 267 Wang, W. *et al.* Nerves in the Tumor Microenvironment: Origin and Effects. *Front Cell Dev Biol* **8**, 601738 (2020). <https://doi.org:10.3389/fcell.2020.601738>
- 268 Mauffrey, P. *et al.* Progenitors from the central nervous system drive neurogenesis in cancer. *Nature* **569**, 672-678 (2019). <https://doi.org:10.1038/s41586-019-1219-y>
- 269 Ayala, G. E. *et al.* In vitro dorsal root ganglia and human prostate cell line interaction: redefining perineural invasion in prostate cancer. *Prostate* **49**, 213-223 (2001). <https://doi.org:10.1002/pros.1137>
- 270 Madeo, M. *et al.* Cancer exosomes induce tumor innervation. *Nat Commun* **9**, 4284 (2018). <https://doi.org:10.1038/s41467-018-06640-0>
- 271 Sharawy, I. Neuroimmune crosstalk and its impact on cancer therapy and research. *Discov Oncol* **13**, 80 (2022). <https://doi.org:10.1007/s12672-022-00547-5>
- 272 Wang, L., Zeng, H., Wang, P., Soker, S. & Mukhopadhyay, D. Neuropilin-1-mediated vascular permeability factor/vascular endothelial growth factor-dependent endothelial cell migration. *J Biol Chem* **278**, 48848-48860 (2003). <https://doi.org:10.1074/jbc.M310047200>
- 273 Saloman, J. L., Albers, K. M., Rhim, A. D. & Davis, B. M. Can Stopping Nerves, Stop Cancer? *Trends Neurosci* **39**, 880-889 (2016). <https://doi.org:10.1016/j.tins.2016.10.002>
- 274 Kuol, N., Stojanovska, L., Apostolopoulos, V. & Nurgali, K. Role of the Nervous System in Tumor Angiogenesis. *Cancer Microenviron* **11**, 1-11 (2018). <https://doi.org:10.1007/s12307-018-0207-3>
- 275 Wang, H. *et al.* Role of the nervous system in cancers: a review. *Cell Death Discov* **7**, 76 (2021). <https://doi.org:10.1038/s41420-021-00450-y>
- 276 Song, P. *et al.* Activated cholinergic signaling provides a target in squamous cell lung carcinoma. *Cancer Res* **68**, 4693-4700 (2008). <https://doi.org:10.1158/0008-5472.CAN-08-0183>
- 277 Lin, G., Sun, L., Wang, R., Guo, Y. & Xie, C. Overexpression of muscarinic receptor 3 promotes metastasis and predicts poor prognosis in non-small-cell lung cancer. *J Thorac Oncol* **9**, 170-178 (2014). <https://doi.org:10.1097/JTO.0000000000000066>
- 278 Choquet, D. & Triller, A. The dynamic synapse. *Neuron* **80**, 691-703 (2013). <https://doi.org:10.1016/j.neuron.2013.10.013>
- 279 Venkatesh, H. S. *et al.* Electrical and synaptic integration of glioma into neural circuits. *Nature* **573**, 539-545 (2019). <https://doi.org:10.1038/s41586-019-1563-y>
- 280 Venkataramani, V. *et al.* Glutamatergic synaptic input to glioma cells drives brain tumour progression. *Nature* **573**, 532-538 (2019). <https://doi.org:10.1038/s41586-019-1564-x>
- 281 Cheshire, W. P. *et al.* Electrodiagnostic assessment of the autonomic nervous system: A consensus statement endorsed by the American Autonomic Society, American Academy

- of Neurology, and the International Federation of Clinical Neurophysiology. *Clin Neurophysiol* **132**, 666-682 (2021). <https://doi.org:10.1016/j.clinph.2020.11.024>
- 282 Ayala, G. E. *et al.* Cancer-related axonogenesis and neurogenesis in prostate cancer. *Clin Cancer Res* **14**, 7593-7603 (2008). <https://doi.org:10.1158/1078-0432.CCR-08-1164>
- 283 Kobayashi, T., Kihara, K., Hyochi, N., Masuda, H. & Sato, K. Spontaneous regeneration of the seriously injured sympathetic pathway projecting to the prostate over a long period in the dog. *BJU Int* **91**, 868-872 (2003). <https://doi.org:10.1046/j.1464-410x.2003.04222.x>
- 284 Magnon, C. *et al.* Autonomic nerve development contributes to prostate cancer progression. *Science* **341**, 1236361 (2013). <https://doi.org:10.1126/science.1236361>
- 285 Li, X. *et al.* Targeting tumor innervation: premises, promises, and challenges. *Cell Death Discov* **8**, 131 (2022). <https://doi.org:10.1038/s41420-022-00930-9>
- 286 Lu, R. *et al.* Neurons generated from carcinoma stem cells support cancer progression. *Signal Transduct Target Ther* **2**, 16036 (2017). <https://doi.org:10.1038/sigtrans.2016.36>
- 287 Schwartz, E. S. *et al.* Synergistic role of TRPV1 and TRPA1 in pancreatic pain and inflammation. *Gastroenterology* **140**, 1283-1291 e1281-1282 (2011). <https://doi.org:10.1053/j.gastro.2010.12.033>
- 288 Stopczynski, R. E. *et al.* Neuroplastic changes occur early in the development of pancreatic ductal adenocarcinoma. *Cancer Res* **74**, 1718-1727 (2014). <https://doi.org:10.1158/0008-5472.CAN-13-2050>
- 289 March, B. *et al.* Tumour innervation and neurosignalling in prostate cancer. *Nat Rev Urol* **17**, 119-130 (2020). <https://doi.org:10.1038/s41585-019-0274-3>
- 290 Amit, M. *et al.* Loss of p53 drives neuron reprogramming in head and neck cancer. *Nature* **578**, 449-454 (2020). <https://doi.org:10.1038/s41586-020-1996-3>
- 291 Ostrowski, M. *et al.* Rab27a and Rab27b control different steps of the exosome secretion pathway. *Nat Cell Biol* **12**, 19-30; sup pp 11-13 (2010). <https://doi.org:10.1038/ncb2000>
- 292 Hessvik, N. P. & Llorente, A. Current knowledge on exosome biogenesis and release. *Cell Mol Life Sci* **75**, 193-208 (2018). <https://doi.org:10.1007/s00018-017-2595-9>
- 293 Lucido, C. T. *et al.* Innervation of cervical carcinoma is mediated by cancer-derived exosomes. *Gynecol Oncol* **154**, 228-235 (2019). <https://doi.org:10.1016/j.ygyno.2019.04.651>
- 294 Silverman, D. A., Martinez, V. K., Dougherty, P. M., Myers, J. N., Calin, G. A. & Amit, M. Cancer-Associated Neurogenesis and Nerve-Cancer Cross-talk. *Cancer Res* **81**, 1431-1440 (2021). <https://doi.org:10.1158/0008-5472.CAN-20-2793>
- 295 Liebig, C., Ayala, G., Wilks, J. A., Berger, D. H. & Albo, D. Perineural invasion in cancer: a review of the literature. *Cancer* **115**, 3379-3391 (2009). <https://doi.org:10.1002/cncr.24396>
- 296 Amit, M., Na'ara, S. & Gil, Z. Mechanisms of cancer dissemination along nerves. *Nat Rev Cancer* **16**, 399-408 (2016). <https://doi.org:10.1038/nrc.2016.38>
- 297 Tuxhorn, J. A., Ayala, G. E., Smith, M. J., Smith, V. C., Dang, T. D. & Rowley, D. R. Reactive stroma in human prostate cancer: induction of myofibroblast phenotype and extracellular matrix remodeling. *Clin Cancer Res* **8**, 2912-2923 (2002).

- 298 Ayala, G. E. *et al.* Stromal antiapoptotic paracrine loop in perineural invasion of prostatic carcinoma. *Cancer Res* **66**, 5159-5164 (2006). <https://doi.org:10.1158/0008-5472.CAN-05-1847>
- 299 Cavel, O. *et al.* Endoneurial macrophages induce perineural invasion of pancreatic cancer cells by secretion of GDNF and activation of RET tyrosine kinase receptor. *Cancer Res* **72**, 5733-5743 (2012). <https://doi.org:10.1158/0008-5472.CAN-12-0764>
- 300 Gil, Z. *et al.* Paracrine regulation of pancreatic cancer cell invasion by peripheral nerves. *J Natl Cancer Inst* **102**, 107-118 (2010). <https://doi.org:10.1093/jnci/djp456>
- 301 Salmon, H., Remark, R., Gnjjatic, S. & Merad, M. Host tissue determinants of tumour immunity. *Nat Rev Cancer* **19**, 215-227 (2019). <https://doi.org:10.1038/s41568-019-0125-9>
- 302 Wrona, D. Neural-immune interactions: an integrative view of the bidirectional relationship between the brain and immune systems. *J Neuroimmunol* **172**, 38-58 (2006). <https://doi.org:10.1016/j.jneuroim.2005.10.017>
- 303 Kamiya, A. *et al.* Genetic manipulation of autonomic nerve fiber innervation and activity and its effect on breast cancer progression. *Nat Neurosci* **22**, 1289-1305 (2019). <https://doi.org:10.1038/s41593-019-0430-3>
- 304 Jiang, S. H., Hu, L. P., Wang, X., Li, J. & Zhang, Z. G. Neurotransmitters: emerging targets in cancer. *Oncogene* **39**, 503-515 (2020). <https://doi.org:10.1038/s41388-019-1006-0>
- 305 Zahalka, A. H. *et al.* Adrenergic nerves activate an angio-metabolic switch in prostate cancer. *Science* **358**, 321-326 (2017). <https://doi.org:10.1126/science.aah5072>
- 306 Hondermarck, H. & Jobling, P. The Sympathetic Nervous System Drives Tumor Angiogenesis. *Trends Cancer* **4**, 93-94 (2018). <https://doi.org:10.1016/j.trecan.2017.11.008>
- 307 Thaker, P. H. *et al.* Chronic stress promotes tumor growth and angiogenesis in a mouse model of ovarian carcinoma. *Nat Med* **12**, 939-944 (2006). <https://doi.org:10.1038/nm1447>
- 308 Covenas, R. & Munoz, M. Cancer progression and substance P. *Histol Histopathol* **29**, 881-890 (2014). <https://doi.org:10.14670/HH-29.881>
- 309 Munoz, M., Rosso, M. & Covenas, R. The NK-1 receptor: a new target in cancer therapy. *Curr Drug Targets* **12**, 909-921 (2011). <https://doi.org:10.2174/138945011795528796>
- 310 Munoz, M. & Covenas, R. Neurokinin-1 receptor antagonists as antitumor drugs in gastrointestinal cancer: A new approach. *Saudi J Gastroenterol* **22**, 260-268 (2016). <https://doi.org:10.4103/1319-3767.187601>
- 311 Tilan, J. & Kitlinska, J. Neuropeptide Y (NPY) in tumor growth and progression: Lessons learned from pediatric oncology. *Neuropeptides* **55**, 55-66 (2016). <https://doi.org:10.1016/j.npep.2015.10.005>
- 312 Reiche, E. M., Nunes, S. O. & Morimoto, H. K. Stress, depression, the immune system, and cancer. *Lancet Oncol* **5**, 617-625 (2004). [https://doi.org:10.1016/S1470-2045\(04\)01597-9](https://doi.org:10.1016/S1470-2045(04)01597-9)
- 313 Huang, D. *et al.* Nerve fibers in breast cancer tissues indicate aggressive tumor progression. *Medicine (Baltimore)* **93**, e172 (2014). <https://doi.org:10.1097/MD.000000000000172>

- 314 Tan, X. *et al.* Nerve fibers in the tumor microenvironment in neurotropic cancer-pancreatic cancer and cholangiocarcinoma. *Oncogene* **40**, 899-908 (2021). <https://doi.org:10.1038/s41388-020-01578-4>
- 315 Dobrenis, K., Gauthier, L. R., Barroca, V. & Magnon, C. Granulocyte colony-stimulating factor off-target effect on nerve outgrowth promotes prostate cancer development. *Int J Cancer* **136**, 982-988 (2015). <https://doi.org:10.1002/ijc.29046>
- 316 Gillespie, S. & Monje, M. An active role for neurons in glioma progression: making sense of Scherer's structures. *Neuro Oncol* **20**, 1292-1299 (2018). <https://doi.org:10.1093/neuonc/nyo083>
- 317 Seifert, P. & Spitznas, M. Tumours may be innervated. *Virchows Arch* **438**, 228-231 (2001). <https://doi.org:10.1007/s004280000306>
- 318 Seifert, P., Benedic, M. & Effert, P. Nerve fibers in tumors of the human urinary bladder. *Virchows Arch* **440**, 291-297 (2002). <https://doi.org:10.1007/s004280100496>
- 319 Hibi, T. *et al.* Synuclein-gamma is closely involved in perineural invasion and distant metastasis in mouse models and is a novel prognostic factor in pancreatic cancer. *Clin Cancer Res* **15**, 2864-2871 (2009). <https://doi.org:10.1158/1078-0432.CCR-08-2946>
- 320 Chatterjee, D. *et al.* Perineural and intraneural invasion in posttherapy pancreaticoduodenectomy specimens predicts poor prognosis in patients with pancreatic ductal adenocarcinoma. *Am J Surg Pathol* **36**, 409-417 (2012). <https://doi.org:10.1097/PAS.0b013e31824104c5>
- 321 Tanaka, K. *et al.* Cancer aggravation due to persistent pain signals with the increased expression of pain-related mediators in sensory neurons of tumor-bearing mice. *Mol Brain* **16**, 19 (2023). <https://doi.org:10.1186/s13041-023-01001-5>
- 322 Haroun, R., Wood, J. N. & Sikandar, S. Mechanisms of cancer pain. *Front Pain Res (Lausanne)* **3**, 1030899 (2022). <https://doi.org:10.3389/fpain.2022.1030899>
- 323 Zhu, Y. F. *et al.* Cancer pain and neuropathic pain are associated with A beta sensory neuronal plasticity in dorsal root ganglia and abnormal sprouting in lumbar spinal cord. *Mol Pain* **14**, 1744806918810099 (2018). <https://doi.org:10.1177/1744806918810099>
- 324 Erin, N., Shurin, G. V., Baraldi, J. H. & Shurin, M. R. Regulation of Carcinogenesis by Sensory Neurons and Neuromediators. *Cancers (Basel)* **14** (2022). <https://doi.org:10.3390/cancers14092333>
- 325 Mantyh, P. Bone cancer pain: causes, consequences, and therapeutic opportunities. *Pain* **154 Suppl 1**, S54-S62 (2013). <https://doi.org:10.1016/j.pain.2013.07.044>
- 326 Mikami, N. *et al.* Calcitonin gene-related peptide is an important regulator of cutaneous immunity: effect on dendritic cell and T cell functions. *J Immunol* **186**, 6886-6893 (2011). <https://doi.org:10.4049/jimmunol.1100028>
- 327 Pinho-Ribeiro, F. A. *et al.* Bacteria hijack a meningeal neuroimmune axis to facilitate brain invasion. *Nature* **615**, 472-481 (2023). <https://doi.org:10.1038/s41586-023-05753-x>
- 328 Le, T. T. *et al.* Sensory nerves enhance triple-negative breast cancer invasion and metastasis via the axon guidance molecule PlexinB3. *NPJ Breast Cancer* **8**, 116 (2022). <https://doi.org:10.1038/s41523-022-00485-z>

- 329 Scheff, N. N. *et al.* Oral cancer induced TRPV1 sensitization is mediated by PAR(2) signaling in primary afferent neurons innervating the cancer microenvironment. *Sci Rep* **12**, 4121 (2022). <https://doi.org:10.1038/s41598-022-08005-6>
- 330 Barr, J. L. *et al.* Intra-Tumoral Nerve-Tracing in a Novel Syngeneic Model of High-Grade Serous Ovarian Carcinoma. *Cells* **10** (2021). <https://doi.org:10.3390/cells10123491>
- 331 Tanaka, K. *et al.* Repeated activation of Trpv1-positive sensory neurons facilitates tumor growth associated with changes in tumor-infiltrating immune cells. *Biochem Biophys Res Commun* **648**, 36-43 (2023). <https://doi.org:10.1016/j.bbrc.2023.01.075>
- 332 Overgaard, N. H., Jung, J. W., Steptoe, R. J. & Wells, J. W. CD4+/CD8+ double-positive T cells: more than just a developmental stage? *J Leukoc Biol* **97**, 31-38 (2015). <https://doi.org:10.1189/jlb.1RU0814-382>
- 333 Zhang, Y., Lin, C., Wang, X. & Ji, T. Calcitonin gene-related peptide: A promising bridge between cancer development and cancer-associated pain in oral squamous cell carcinoma. *Oncol Lett* **20**, 253 (2020). <https://doi.org:10.3892/ol.2020.12116>
- 334 Wang, F., Millet, I., Bottomly, K. & Vignery, A. Calcitonin gene-related peptide inhibits interleukin 2 production by murine T lymphocytes. *J Biol Chem* **267**, 21052-21057 (1992).
- 335 Kawamura, N. *et al.* Differential effects of neuropeptides on cytokine production by mouse helper T cell subsets. *Neuroimmunomodulation* **5**, 9-15 (1998). <https://doi.org:10.1159/000026321>
- 336 Hosoi, J. *et al.* Regulation of Langerhans cell function by nerves containing calcitonin gene-related peptide. *Nature* **363**, 159-163 (1993). <https://doi.org:10.1038/363159a0>
- 337 Carucci, J. A. *et al.* Calcitonin gene-related peptide decreases expression of HLA-DR and CD86 by human dendritic cells and dampens dendritic cell-driven T cell-proliferative responses via the type I calcitonin gene-related peptide receptor. *J Immunol* **164**, 3494-3499 (2000). <https://doi.org:10.4049/jimmunol.164.7.3494>
- 338 Chihara, N. *et al.* Induction and transcriptional regulation of the co-inhibitory gene module in T cells. *Nature* **558**, 454-459 (2018). <https://doi.org:10.1038/s41586-018-0206-z>
- 339 Garcia-Roman, J. & Zentella-Dehesa, A. Vascular permeability changes involved in tumor metastasis. *Cancer Lett* **335**, 259-269 (2013). <https://doi.org:10.1016/j.canlet.2013.03.005>
- 340 Gutierrez, S. & Boada, M. D. Neuropeptide-induced modulation of carcinogenesis in a metastatic breast cancer cell line (MDA-MB-231(LUC+)). *Cancer Cell Int* **18**, 216 (2018). <https://doi.org:10.1186/s12935-018-0707-8>
- 341 Dottorini, M. E., Assi, A., Sironi, M., Sangalli, G., Spreafico, G. & Colombo, L. Multivariate analysis of patients with medullary thyroid carcinoma. Prognostic significance and impact on treatment of clinical and pathologic variables. *Cancer* **77**, 1556-1565 (1996). [https://doi.org:10.1002/\(SICI\)1097-0142\(19960415\)77:8<1556::AID-CNCR20>3.0.CO;2-Y](https://doi.org:10.1002/(SICI)1097-0142(19960415)77:8<1556::AID-CNCR20>3.0.CO;2-Y)
- 342 Murray, K., Barboza, M., Rude, K. M., Brust-Mascher, I. & Reardon, C. Functional circuitry of neuro-immune communication in the mesenteric lymph node and spleen. *Brain Behav Immun* **82**, 214-223 (2019). <https://doi.org:10.1016/j.bbi.2019.08.188>
- 343 Nanda, V. G. Y. *et al.* Melanoma and immunotherapy bridge 2015 : Naples, Italy. 1-5 December 2015. *J Transl Med* **14**, 65 (2016). <https://doi.org:10.1186/s12967-016-0791-2>

- 344 Zhang, Y. *et al.* Cancer cells co-opt nociceptive nerves to thrive in nutrient-poor environments and upon nutrient-starvation therapies. *Cell Metab* **34**, 1999-2017 e1910 (2022). <https://doi.org:10.1016/j.cmet.2022.10.012>
- 345 Ravindranathan, S. *et al.* Targeting vasoactive intestinal peptide-mediated signaling enhances response to immune checkpoint therapy in pancreatic ductal adenocarcinoma. *Nat Commun* **13**, 6418 (2022). <https://doi.org:10.1038/s41467-022-34242-4>
- 346 Saloman, J. L. *et al.* Ablation of sensory neurons in a genetic model of pancreatic ductal adenocarcinoma slows initiation and progression of cancer. *Proc Natl Acad Sci U S A* **113**, 3078-3083 (2016). <https://doi.org:10.1073/pnas.1512603113>
- 347 Zhao, C. M. *et al.* Denervation suppresses gastric tumorigenesis. *Sci Transl Med* **6**, 250ra115 (2014). <https://doi.org:10.1126/scitranslmed.3009569>
- 348 Mehboob, R., Tanvir, I., Warraich, R. A., Perveen, S., Yasmeen, S. & Ahmad, F. J. Role of neurotransmitter Substance P in progression of oral squamous cell carcinoma. *Pathol Res Pract* **211**, 203-207 (2015). <https://doi.org:10.1016/j.prp.2014.09.016>
- 349 Lee, D. W. *et al.* T cells expressing CD19 chimeric antigen receptors for acute lymphoblastic leukaemia in children and young adults: a phase 1 dose-escalation trial. *Lancet* **385**, 517-528 (2015). [https://doi.org:10.1016/S0140-6736\(14\)61403-3](https://doi.org:10.1016/S0140-6736(14)61403-3)
- 350 Melenhorst, J. J. *et al.* Decade-long leukaemia remissions with persistence of CD4(+) CAR T cells. *Nature* **602**, 503-509 (2022). <https://doi.org:10.1038/s41586-021-04390-6>
- 351 Guerra, E., Di Pietro, R., Basile, M., Trerotola, M. & Alberti, S. Cancer-Homing CAR-T Cells and Endogenous Immune Population Dynamics. *Int J Mol Sci* **23** (2021). <https://doi.org:10.3390/ijms23010405>
- 352 Schmidt, R. *et al.* CRISPR activation and interference screens decode stimulation responses in primary human T cells. *Science* **375**, eabj4008 (2022). <https://doi.org:10.1126/science.abj4008>
- 353 Covacs, A. *et al.* Tumor-infiltrating nerves create an electro-physiologically active microenvironment and contribute to treatment resistance. *BioRxiv*, doi: <https://doi.org/10.1101/2020.04.24.058594> (2020).